RCA Review

Satellite Communications

September 1980 **Volume 41 No. 3**

RCARCI 41 (3) 373–514 (1980)

RCA Review, published quarterly in March, June, September and December by RCA Research and Engineering, RCA Corporation, Princeton, New Jersey 08540. Entered as second class matter July 3, 1950 under the Act of March 3, 1879. Second-class postage paid at Princeton, New Jersey, and at additional mailing offices. Effective January 1, 1978, subscription rates as follows: United States and Canada: one year $8.00, two years $14.00, three years $18.00; in other countries, one year $8.60, two years $15.20, three years $19.80. Single copies (except for special issues) up to five years old $3.00.

RCA Review

RCA Review (ISSN 0033-6831) is a technical journal published quarterly by RCA Research and Engineering in cooperation with the subsidiaries and divisions of RCA.

Contents

September 1980 Volume 41 Number 3 ISSN 0033-6831

Foreword

The age of satellite communications is now in full flower. From very modest beginnings fifteen years ago when the first Intelsat satellite (with a capacity of only 240 two-way voice circuits) was launched, to today when each of approximately two dozen satellites has an equivalent capacity of at least 12,000 two-way voice circuits, satellite communications has grown not only in the amount of traffic carried but also in geographic coverage and scope of services offered. The prospects for the next fifteen years are even more glowing.

The earliest satellite communication service offered was primarily telephone trunking, but now TV distribution is equally prominent. In fact, many believe that satellites are responsible for the recent explosive growth in CATV. Shortly, it is expected that Direct Broadcast Satellites, electronic mail and video conferencing networks will become regular features of our everyday lives. The growth has been so dramatic that new technology and new techniques had to be developed to "shoehorn" more traffic into a given bandwidth. These cover a wide range of different approaches from the most obvious to the quite esoteric, from utilizing ever higher frequency bands to the development of innovative techniques that permit accommodating several TV programs per channel where only one program was possible before. In between lie such techniques as frequency reuse by polarization diversity, syllabic companding, and overdeviation.

RCA has participated actively in the growth of satellite communications and in the development of the new technology that helped make satellite communications what it is today—a vital public service and a viable economic enterprise. The RCA Satcom system operated by RCA Americom employing satellites designed and produced by Astro Electronics incorporates numerous firsts in the industry both in the communications subsystem and the spacecraft bus.

Now that almost ten years have passed since RCA first began planning for its own satellite communication system, it was felt that a special issue of RCA REVIEW, devoted to satellite communications, would be appropriate. This issue is the result. There are papers here covering a variety of topics related to satellite communications—papers on techniques for increasing the traffic capacity on existing satellites, a paper on a new solid-state power amplifier that will replace TWT amplifiers for lighter weight and better performance on board future satellites, a paper on scrambling of TV pictures for use in pay TV distribution, and two papers relating to doubling the TV carrying capacity of terrestrial microwave

links that interface with the satellite communication link. In this connection, it is of interest to note that RCA was the first, and so far the only carrier, to put such a system into operation.

The papers represented in this issue range over the whole spectrum of studies conducted at RCA during the past decade or so and the authors come from various divisions of the Company. The first six papers deal with various techniques for increasing the standard traffic that can be carried by a satellite transponder, where "standard" refers to telephone, TV, and low data rate digital traffic. The techniques include reducing intermodulation products, introducing syllabic companding for telephone circuits and specialized cross-talk cancellation procedures for video channels. The next two papers, one by Klensch and Kelly and the other by Kaplan, describe the design and test of the first operational system that carries two TV channels in one terrestrial microwave channel. The next paper, by Dr. Mangulis, describes and presents pictorial results of a scheme for scrambling TV pictures in order to protect privacy on satellite transmissions. The paper by Acampora and Saulnier discusses still another technique for doubling the satellite transponder capacity for carrying video signals, but this time the constraint that the signal sources be co-located is removed.

The last two papers are different in tone and purpose but still vital to the effective performance of a satellite communication system. The paper by Carl Hubert describes some mechanical problems and solutions associated with geosynchronous satellites, and the last paper, by Dornan et al, describes an FET solid-state power amplifier that is expected to replace the TWT power amplifier currently in use on all communication satellites.

Dr. Harold Staras
RCA Laboratories, Princeton, New Jersey

Syllabic Companding and Voice Capacity of a Transponder

Krishnamurthy Jonnalagadda

RCA Laboratories, Princeton, NJ 08540

Abstract—A novel use of syllabic compandors in satellite communications is to increase the capacity of FDM/FM carrying voice channels. In the RCA SATCOM, the capacity of the carriers is doubled economically using compandors. This paper describes how to design such systems. Equations standardized by the CCIR are modified and a set of design rules are developed that incorporate the companding advantage and changes in the rms deviation. We also show that by allowing the carriers to deviate beyond their Carson's bandwidths, the capacity can be increased even further.

1. Introduction

Syllabic compandors in analog voice communication over telephone channels provide an economical way of improving the performance of the communication link. In FDM/FM the compandors can be used to improve the noise performance, or this noise advantage can be traded to increase the capacity of the link. In satellite applications this can lead to nearly doubling the capacity of a transponder. A single carrier designed to occupy a single transponder of 36 MHz bandwidth and carrying 1092 uncompanded channels can be used to carry 2074 companded channels with no loss in quality. Some transponders of RCA SATCOM now carry FDM/FM traffic with companded baseband channels. The experience with these companded carriers shows that the doubling of the capacity is realizable in practice.

This paper discusses how FDM/FM systems are to be designed when

some or all of the baseband channels are companded. The approach taken is to modify the CCIR equations commonly used in designing standard systems with uncompanded channels. In terms of the approximations made, the results are in the same spirit as those of the CCIR.

A compandor actually contains two devices: a *compressor*, which reduces the dynamic range of speech at syllabic rate and is located in the transmitter, and an *expandor*, which re-expands the speech to its normal range and is located in the receiver. The properties of these devices relevant to the design equations are described in Sec. 2. In Secs. 3 and 4, the link equations are derived for the case where some or all of the channels are companded. These equations are used to determine the capacities of companded channel carriers when they are designed to occupy a given bandwidth. It is also shown that if the capacities are unchanged, the companded channel carrier occupies only half the bandwidth of the uncompanded carrier.

The Carson's bandwidth (usually referred to as the occupied bandwidth) of a carrier is traditionally made to nearly equal the allocated bandwidth. The main reason for this is that the distortion in the baseband, due to the bandlimiting action of channel filters in the link, will be negligible. The margin between this distortion and thermal noise increases on companding the channels. This extra margin can be used to increase the capacity beyond the doubling of the capacity mentioned earlier. This topic, referred to as design with overdeviation, is described in Sec. 5. With companding and overdeviation, the capacity of a single FDM/FM carrier occupying a full transponder is 2892 companded channels, when the satellite input filter is group delay equalized. This capacity is an increase of 265% over that of the 1092 uncompanded channels.

2. Properties of Compandors

A detailed discussion on the characteristics of compressors and expandors is given in Refs. [1]–[3]. Here we are interested in those quantities relevant to FDM/FM design.

2.1 Unaffected level

Input–output characteristics of a compressor are shown in Fig. 1. Unaffected level is defined as the input signal level at which the compressor introduces no gain or loss on the input signal. Let P_i and P_o denote the compressor input and output signal levels, respectively. These are related by the equation

$$P_o = (P_i/K_c) + A$$

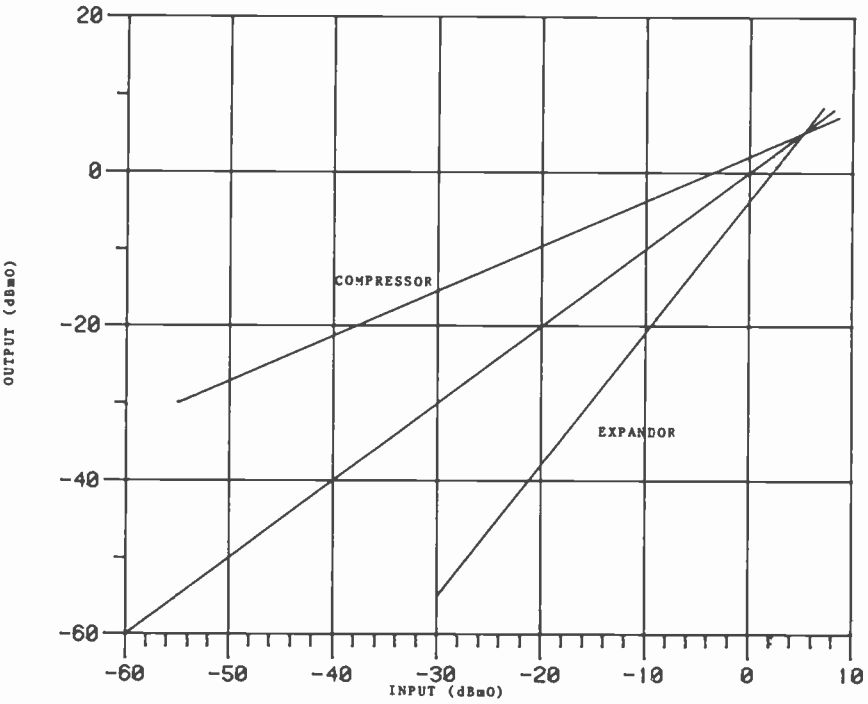

Fig. 1—Input–output characteristics of compressor and expandor.

where K_c and A are constants. The compression ratio K_c usually has the value $K_c = 2$. With this value the above equation can be written as

$$P_o = (P_i + U)/2 \qquad [1]$$

where U is the unaffected level. Such a compandor is equivalent to a 0 dBmO unaffected level compandor followed by an attenuator of value $U/2$.

2.2 Companding advantage

When a compandor is used over a channel with a given noise, the subjective effect is the same as for a channel with lower value of noise. This subjectively perceived drop in noise is called the companding advantage, C, in dB. This advantage depends on the listener, the volume and nature of the speech source, and the amount of noise in the uncompanded situation. Experiments done by RCA at the Rensselaer Polytechnic Institute using compandors with 0 dBmO unaffected levels reveal that the companding advantage can be thought of as a random variable with a distribution. Based on the cumulative distribution functions obtained

for the companding advantage, a value of $C = 16$ dB was chosen for design purposes. At this value of C, there is a 90% probability that the actual companding advantage is equal to or better than 16 dB.

2.3 Compressor power increase

The average speech power out of a compressor (with 0 dBmO unaffected level) is higher than the average speech power into it. This follows from Eq. [1] which shows that the mean speech power (about −15 dBmO) as well as the standard deviation are multiplied by a factor of 1/2. Thus the compressor changes the average level and the statistics of the speech, resulting in new talker distribution. Experiments reported in Ref. [1] show that the increase in the average power, X dB, is about 3 to 4 dB when the unaffected level is 0 dBmO. For the purpose of design the assumed value of X is 4 dB.

2.4 Multiplexed load with compressors

The multichannel speech power recommended by the CCIR for design purposes is (when N uncompanded channels are used)

$$\begin{aligned} G(N) &= -15 + 10 \log N \qquad \text{dBmO if } N \geq 240 \\ &= -1 + 4 \log N \qquad \text{dBmO if } N < 240, \end{aligned} \tag{2}$$

where the log function is to the base 10. When the N channels are companded, the analogous load factor, $G_c(N)$, is different for two distinct reasons. The first is the increase in the compressor power output (X dB) compared to its input. The second reason is that the compressor output has less fluctuation than its input. Consequently, the statistics (in particular the power level exceeded only 1% of the time) of the multiplexed compressed channels are different than for uncompressed channels (over and above the fact that the average power is X dB higher). We can thus define

$$G_c(N) = X + G'(N) \qquad \text{dBmO}, \tag{3}$$

where antilog $[G'(N)/20]$ is a ratio equal to the quotient of the voltage corresponding to the 1% power of a multiplexed group of compressors and the voltage corresponding to the power produced by a single 0 dBmO test tone at the same point.

If N is large ($N \geq 240$), $G'(N)$ equals $G(N)$ of Eq. [2]. This is observed from the experimental results* of Ref. [1]. In Fig. 2, $G'(N)$ and $G(N)$ are

* In Ref. [1], curves with zero unaffected levels in Figs. 9 and 12 should be moved up by 3 dB. This is because the measurements made with modern compandors do not show the 3 dB difference in output power from the compressor between a sine wave and speech as reported in that paper.

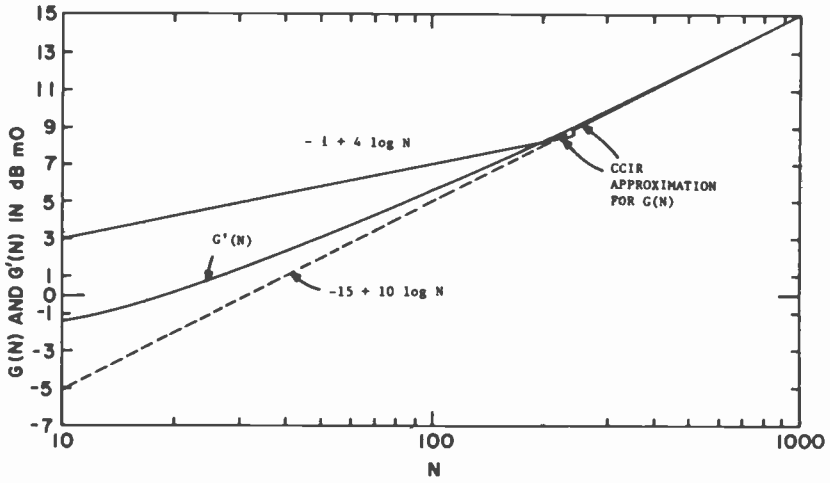

Fig. 2—Multichannel loads, $G(N)$ and $G'(N)$.

compared, $G'(N)$ being obtained from Fig. 9 of Ref. [1]. If $N < 240$, $G'(N)$ can be considerably lower than $G(N)$.

The other factor that enters the multiplexed load calculations is the peaking factor, P dB. If $N \geq 240$, the peaking factors P (for N uncompanded channels) and P_c (for companded channels) can both be made equal to 10 dB (see Fig. 11 of Ref. [1]). If $N < 240$, P and P_c are larger, with P_c being smaller than P. In this paper we assume that P is 10 dB whether $N \geq 240$ or $N < 240$ and use $G(N)$ of Eq. [2] for multichannel load. With N companded channels, if we use $G'(N)$ when $N < 240$, then P_c is obtained from the graphs of Ref. [1]. However, a slightly conservative way of doing the computations is to assume that when $N < 240$, $G'(N)$ equals $G(N)$ and P_c is 10 dB. With this conservative approach,

$$P_c + G_c(N) = 10 + X + [-1 + 4 \log N], N \leq 240. \quad [4]$$

The multichannel peak load is characterized in greater detail in Ref. [2], where various activity factors and experimentally obtained peaking factors are included. These equations can be modified taking into account companding. In the Appendix we will show that when $N \leq 240$, the results obtained by using Eq. [4] are only slightly conservative.

3. Link Equations When All Channels Are Companded

Let

N = number of uncompanded channels
f_m = maximum baseband frequency
f_r = rms deviation per channel

b = bandwidth per channel (3.1 kHz)
B = allocated bandwidth
C/N = carrier-to-noise ratio
w = psophometric weighting factor (2.5 dB)
$P(f)$ = pre-emphasis function
$= |H(f)|^2$
$H(f)$ = transfer function of the pre-emphasis filter
$G(N)$ = multichannel load given by Eq. [2]
P = peaking factor (10 dB)
$g(N) = 10^{G(N)/20}$
$p = 10^{P/20}$

With reference to the hypothetical FDM/FM system shown in Fig. 3, a 0 dBmO test tone introduced in the top channel before the multiplexer produces an rms deviation of $f_r\sqrt{P(f_m)}$. The resulting test-tone-to-noise ratio is given by the CCIR equation

$$\mathrm{TT/N} = (C/N)(B/b)(f_r/f_m)^2 P(f_m) w. \tag{5}$$

An ideal pre-emphasis of $P(f) = f^2$ gives the same TT/N at all channels. However, because the demodulation process introduces excessive noise at low frequencies, we use the following form of pre-emphasis (which is an approximation to the CCIR recommended form of $P(f)$):

$$P(f) = [1 + (f/f_0)^2]/K \tag{6}$$

where f_o and K are two constants determined by imposing the two following constraints on $P(f)$:

$$P(f_m) = 4 \text{ dB} \doteq 2.5 \tag{7}$$

$$\int_0^{f_m} P(f)df = f_m. \tag{8}$$

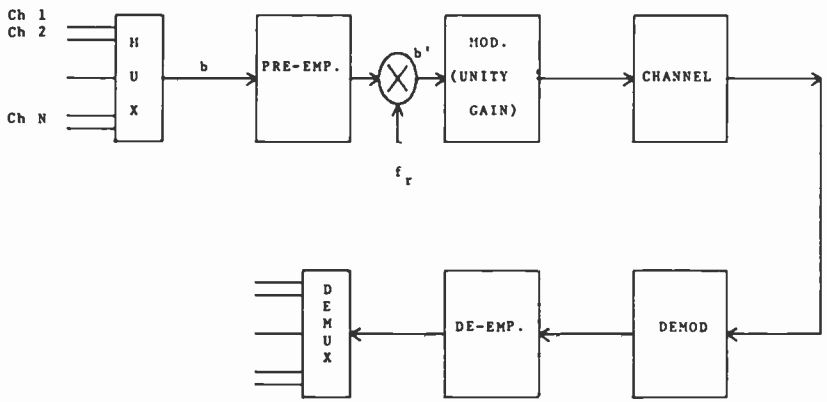

Fig. 3—FDM/FM communication system.

The second of the two constraints merely implies that if the input to the pre-emphasis is a random process with flat power spectral density, the input and output powers are the same. These two constraints give

$$K = 4.1,$$

$$(f_m/f_o)^2 = 9.3.$$

The second CCIR equation is for the occupied bandwidth B. This is the Carson's bandwidth

$$B = 2(f_m + f_{peak}), \qquad [9]$$

where f_{peak} is a "peak" deviation. The output of the multiplexer is assumed to be a Gaussian process (for large N) with flat power spectral density (Ref. [7]). This process continues to be Gaussian with the same power as it goes through the pre-emphasis filter. If $g(N)$ is the ratio of the rms voltage produced at point b of Fig. 3 (by the N channels multiplexed together) to the rms voltage produced at b by a 0 dBmO test tone, the rms frequency deviation produced at the point b′ of Fig. 3 would be $g(N)f_r$. The "peak" deviation used in Eq. (9) is at P dB above this value, with the CCIR recommending that P be 10 dB. In other words, the peak value is considered to be at the 3.16σ point of the Gaussian distribution where σ equals $g(N)f_r$. The CCIR also recommends that $g(N)$ be the power level exceeded only 1% of the time, with 20 log $g(N)$ being given by Eq. [2]. Thus, Eq. [9] can be written as

$$B = 2[f_m + pg(N)f_r]. \qquad [10]$$

Eqs. [5] and [10] are valid when none of the channels are companded. When all the channels are companded the capacity can be increased. Let the number of companded channels be N_c with maximum baseband frequency f_{mc}. The parameters f_r, B, $g(N)$, $G(N)$, P, p, and TT/N are all now different and we will denote them by f_{rc}, B_c, $g_c(N)$, $G_c(N)$, P_c, p_c, and $(\mathrm{TT/N})_c$. Here $G_c(N)$ is

$$G_c(N) = X + G'(N) \qquad (11)$$

where $G'(N) = G(N)$ if $N \geq 240$ and is determined from Fig. 2 if $N < 240$.

When $N \geq 240$, the peaking factor P_c will be assumed to be 10 dB, which is the same as when the channels are uncompanded. If we use Fig. 2 to determine $G'(N)$ when $N < 240$, we must determine the corresponding P_c from Fig. 11 of Ref. [1]; this P_c will be larger than 10 dB. However, we can replace the value of $G'(N)$ by the larger value $G(N)$ when $N < 240$ and continue to assume that P_c equals 10 dB. This leads to slightly conservative results, as will be shown in the Appendix. The results of this and the next sections are developed with $G'(N) = G(N) = -1 + 4 \log N$ and $P_c = 10$ dB, whenever $N < 240$.

The companding advantage of C dB was obtained by increasing the channel noise by C, which results in the same subjective quality of speech as when no companding was done. In reality the channel noise remains the same, and the companding advantage can be effectively obtained by decreasing the test tone power by C (C = 16 dB), as shown in Fig. 4. This attenuation of C at the output of the compressor will make the multichannel load $g_c(N_c)10^{-C/20}$. The pre-emphasis will not change this load, and the Carson's bandwidth now becomes

$$B_c = 2[f_{mc} + p_c g_c(N_c)10^{-C/20} f_{rc}]. \quad [12]$$

On introducing a 0 dBmO tone at the top companded channel, we achieve

$$(\mathrm{TT/N})_c = (C/N)(B_c/b)(f_{rc}/f_{mc})^2 P(f_{mc}) w 10^{-C/10} \quad [13]$$

since the rms deviation now is $f_{rc}10^{-C/20}$. Due to companding advantage the listener perceives the test tones to be C dB higher, so that the subjective $(\mathrm{TT/N})_c$ is

$$(\mathrm{TT/N})_c = (C/N)(B_c/b)(f_{rc}/f_{mc})^2 P(f_{mc}) w. \quad [14]$$

In the present application of companding, this subjective $(\mathrm{TT/N})_c$ is made equal to the TT/N obtained by N uncompanded channels, which is given by Eq. [5]. This results in

$$B_c(f_{rc}/f_{mc})^2 = B(f_r/f_m)^2 \quad [15]$$

Eqs. [12] and [15] can be used in two ways, depending on the purpose of companding (i.e., to increase the capacity or to reduce the occupied bandwidth). If B and B_c are the same, Eq. [15] reduces to

$$f_{rc}/f_{mc} = f_r/f_m, \quad [16]$$

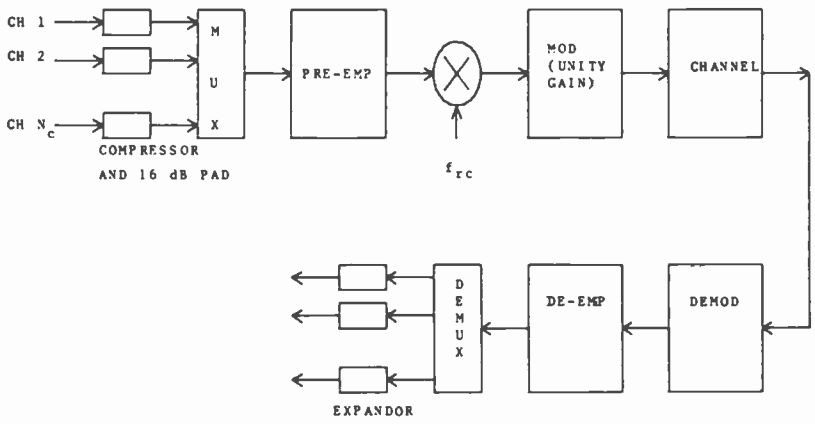

Fig. 4—Companded FDM/FM system.

which can be substituted in Eq. [12]. This, along with

$$f_{mc} = N_c f_m / N, \tag{17}$$

gives

$$B = 2N_c(f_m/N)[1 + p_c g_c(N_c)10^{-C/20}(f_r/f_m)], \tag{18}$$

where

$$20 \log [p_c g_c(N_c)10^{-C/20}] = -17 + 10 \log N_c, \; N_c \geq 240$$
$$= -3 + 4 \log N_c, \; N_c < 240. \tag{19}$$

Thus we can solve for N_c, given the parameters N, f_r, and f_m of a standard uncompanded situation. In Table 1 we give the values of N_c for several standard SATCOM carriers. The corresponding values of f_{rc} to be used are obtained from the equation

$$f_{rc} = N_c f_r / N, \tag{20}$$

which is obtained by using Eqs. [16] and [17]. It is seen in this table that when N is large, companding can double the capacity. When N is small, companding can increase the capacity by an even larger percentage.

The other use of companding is to decrease the occupied bandwidth B_c without changing the capacity. Eq. [15] then becomes

$$B_c f_{rc}^2 = B f_r^2, \tag{21}$$

and Eq. [10] becomes

$$B = 2[f_m + p_c g_c(N)10^{-C/20} f_r \sqrt{B/B_c}](B/B_c),$$

which can now be solved for B_c. Using Eq. [21] we can now obtain the corresponding value of f_{rc} that should be used in the system. To avoid any confusion, we denote the occupied bandwidth B_c by B_c' and f_{rc} by f_{rc}', and show these values in Table 1 for several SATCOM standard carriers. Clearly, the saving in the bandwidth (from B to B_c') can be converted, fully or in part, to reduction in the carrier-to-noise ratio.

In Eqs. [12] and [13] we observe that it is the product $10^{-C/20} f_{rc}$ that controls the occupied bandwidth and TT/N. Here C is the attenuation introduced after the 0 dBmO unaffected level compressor. Clearly one need not introduce this attenuation, but can change the rms deviation f_{rc} to a value of $f_{rc}10^{-C/20}$. Similarly, one can put only an attenuation of X dB ($X = 4$) at the output of the 0 dBmO unaffected level compressor, but change f_{rc} to a value $f_{rc}\ 10^{-(C-X)/20}$. These three situations are equivalent and will give either the same improvement in capacity due to companding, or the same reduction in the occupied bandwidth.

When all the channels are companded, there is an alternative to using the above CCIR type of equations. These alternative equations, based

Table 1—Companded Carrier Parameters: N, f_r, f_m, B are standard carrier (uncompanded) parameters; N_c, f_{rc} are the companded carrier capacity and the required rms deviation; B_c' and f_{rc}' are the companded carrier bandwidth and rms deviation when the capacity is unchanged; $G_c(N_c)$ is the multiplexed load of N_c companded channels, in dBmO.

N (channels)	f_r (MHz)	f_m (MHz)	B (MHz)	N_c (channels)	f_{rc} (MHz)	$G_c(N_c)$ (dBmO)	B_c' (MHz)	f_{rc}' (MHz)
24	0.164	0.108	2.00	64	0.437	10.2	0.873	0.246
36	0.168	0.156	2.25	90	0.420	10.8	1.025	0.247
60	0.270	0.252	4.00	154	0.693	11.7	1.791	0.402
72	0.294	0.300	4.50	182	0.743	12.0	2.037	0.435
96	0.360	0.408	5.90	240	0.900	12.5	2.684	0.532
132	0.430	0.552	7.50	306	0.997	13.8	3.474	0.631
192	0.457	0.804	9.00	409	0.973	15.1	4.288	0.661
252	0.577	1.052	12.40	532	1.218	16.2	5.862	0.838
312	0.546	1.300	13.50	645	1.128	17.1	6.520	0.785
432	0.729	1.796	20.70	911	1.537	18.6	9.805	1.059
612	0.622	2.540	22.40	1221	1.241	19.9	11.22	0.878
792	0.930	3.284	36.00	1652	1.939	21.2	17.25	1.343
972	0.802	4.028	36.00	1940	1.600	21.9	18.03	1.133
1092	0.674	5.140	36.00	2074	1.280	22.2	18.94	0.929

on Ref. [2] are more difficult to apply and are briefly derived in the Appendix.

4. Link Equations When Only Some of the Channels Are Companded

To develop link equations for this mixed situation, we use the idea of compensatory pre-emphasis developed in Ref. [4]. Let N_1 of the total N channels be uncompanded and N_2 channels be companded, where $N = N_1 + N_2$. The N_2 channels should occupy the top portion of the baseband (the reasons for this will be mentioned later). As the compressors increase the power by X dB, we will attenuate them by X dB as shown in Fig. 5, so that the spectral density at the output of these attenuators will be the same as on the uncompanded channels. The multiplexed signal is passed through a pre-emphasis whose characteristics are

$$\begin{aligned} P_m(f) &= b_1[1 + (f/f_0)^2]/K,\ 0 \leqslant f \leqslant N_1 f_m/N \\ &= b_2[1 + (f/f_0)^2]/K,\ N_1 f_m/N < f \leqslant f_m. \end{aligned} \qquad [22]$$

The purpose of this pre-emphasis is to give a total of C dB attenuation at the output of the 0 dBmO unaffected level compandors in comparison to the uncompanded channels. The TT/N in these companded channels will then be C dB lower than that in the uncompanded channels. However, due to the C dB companding advantage, the subjectively perceived TT/N will be the same as those on the uncompanded channels.

As X dB attenuation is provided in the compressed channels *before* the multiplexer, the additional required $-C + X$ dB attenuation is provided by choosing

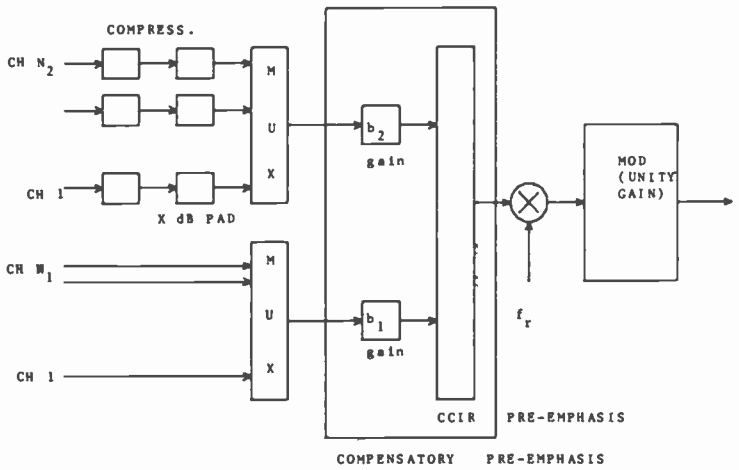

Fig. 5—FDM/FM with mixed channels and compensatory pre-emphasis.

$$b_2/b_1 = 10^{-D/10}, \qquad [23]$$

where $D = C - X = 12$ dB.

Use of Eq. [23] and the constraint (Eq. [8]) on $P_m(f)$ will result in $b_1 = 1/\delta$, where

$$\delta = \left(1 - \frac{1}{d}\right)\left[\frac{N_1}{N} + \left(\frac{N_1}{N}\right)^3 \frac{(f_m/f_o)^2}{3}\right]\left[1 + \frac{(f_m/f_o)^2}{3}\right]^{-1} + \frac{1}{d} \qquad [24]$$

$$d = 10^{D/10}$$

$$(f_m/f_o)^2 = 9.3.$$

The multiplexed load at the output of N_2 compressors is $G_c(N_2)$ dBmO. At the output of the X-dB attenuators, this becomes $G_c(N_2) - X$, i.e., $G'(N_2)$ dBmO. The multiplexed load due to the N_1 standard channels is $G(N_1)$ dBmO, so that the combined load is 10 log [antilog $\{G'(N_2)/10\}$ + antilog $\{G(N_1)/10\}$]. Considering the accuracy needed, the combined load can be approximated by the weighted sum

$$L(N) = (N_1/N)G(N) + (N_2/N)G'(N) \text{ dBmO}. \qquad [25]$$

As seen from Fig. 2, $L(N)$ equals $G(N)$ if N_1 and N_2 are larger than 240. If $N < 240$, we conservatively assume that multiplexed load $G'(N)$ can be replaced by $G(N)$. Thus

$$\begin{aligned} L(N) &= -15 + 10 \log N, \; N \geq 240, \\ &= -1 + 4 \log N, \; N < 240, \end{aligned} \qquad [26]$$

which is simply the multiplexed load obtained as if none of the channels are companded. We will assume in this section that the total of N channels occupy the same Carson's bandwidth as N uncompanded channels. Thus the rms deviation required for this mixed situation is the same as when no channels are companded, due to the fact that the mixed load is the same as the uncompanded load. The occupied bandwidth thus is

$$B = 2[f_m + pl(N)f_r] \qquad [27]$$

where $l(N) \triangleq 10^{L(N)/20}$. We assume that the peaking factor p or p_c is always 10 dB.

The TT/N obtained by introducing a 0 dBmO tone at the input of a compressed channel is given by

$$\text{TT/N} = 10^{-X/10}(C/N)(B/b)(f_r/f)^2 P_m(f)w, \; N_1 f_m/N \leq f \leq f_m, \qquad [28]$$

where the $10^{-X/10}$ factor is due to the fact that the compressors have 0 dBmO unaffected levels. The TT/N in the uncompressed channels is

$$\text{TT/N} = (C/N)(B/b)(f_r/f)^2 P_m(f)w, \; 0 \leq f \leq N_1 f_m/N. \qquad [29]$$

The above equations use the mathematical notion of compensatory pre-emphasis. In reality one uses standard pre-emphasis and absorbs the multiplying constants b_1 and b_2 into new values for f_r and the attenuators used in the compressor outputs. Thus, by defining

$$f_{rc} \triangleq f_r\sqrt{b_1} = f_r/\sqrt{\delta} \qquad [30]$$

and changing the X dB attenuation to $X + D$ (i.e., C dB), we get the equivalent representation, as shown in Fig. 6. Using Eqs. [22], [23] and [24], we can write Eqs. [27], [28], and [29] as

$$\begin{aligned} \mathrm{TT/N} &= (C/N)(B/b)(f_{rc}/f)^2P(f)w,\ 0 \leqslant f \leqslant N_1f_m/N \\ &= (C/N)(B/b)(f_{rc}/f)^2P(f)w10^{-C/10},\ N_1f_m/N < f \leqslant f_m, \end{aligned} \qquad [31]$$

$$B = 2[f_m + pl(N)f_{rc}\sqrt{\delta}]. \qquad [32]$$

Due to the C dB companding advantage, the subjective TT/N is

$$\mathrm{TT/N} = (C/N)(B/b)(f_{rc}/f)^2P(f)w,\ 0 \leqslant f \leqslant f_m, \qquad (33)$$

which is the same for all channels, whether they are companded or not (ignoring that $P(f)$ is not ideally parabolic).

If none of the channels are companded, δ equals unity; and if all the channels are companded, δ equals $1/d$, i.e., 20 log $[pl(N)\sqrt{\delta}]$ equals $P + G_c(N) - 16$ dB. Thus, Eq. [32] for B is the same as Eq. [12].

The above equations were derived to show that the subjective TT/N increases (by $-20\log\delta$ dB) on companding the N_2/N fraction of the total N channels. We can now increase the capacity to N_c total channels in

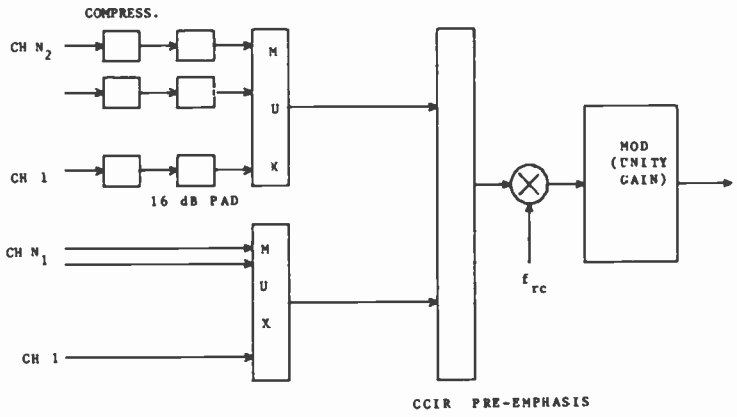

Fig. 6—FDM/FM with mixed channels. This system is exactly equivalent to that of Fig. 5.

which N_1 channels are uncompanded and N_2 are companded ($N_c = N_1 + N_2$) in such a way that the subjective TT/N equals, say, 51.0 dB and the N_c channels occupy the same Carson's bandwidth as the N uncompanded channel carrier.

Consider a standard uncompanded situation of N baseband channels that, with an rms deviation of f_r, requires a Carson's bandwidth of B and yields the desired TT/N. If we assume that N_1 channels cannot be companded, the new capacity of N_c channels (in which the N_1/N_c fraction is uncompanded) will yield the same subjective $(TT/N)_c$ as the standard TT/N and occupies the same Carson bandwidth as the standard situation if

$$B = 2[f_{mc} + pl(N_c)f_{rc}\sqrt{\delta}] \quad [34]$$

$$f_{rc}/f_{mc} = f_r/f_m, \quad [35]$$

where

$$\delta = \frac{[1 - (1/d)]\{(N_1/N_c) + (N_1/N_c)^3[(f_m/f_o)^2/3]\}}{1 + [(f_m/f_o)^2/3]} + \frac{1}{d}$$

$$(f_m/f_o)^2 = 9.3$$

$$d = 10^{12/10}$$

and

$$l(N_c) = -15 + 10 \log N_c, \; N_c \geq 240$$
$$-1 + 4 \log N_c, \; N_c < 240.$$

In arriving at these equations we assumed, conservatively, that if $N_c \leq 240$, the multiplexed load $G'(N_c)$ can be replaced by $G(N_c)$. Using the values N, f_r, and f_m from the standard uncompanded situation and assuming

$$f_{mc} = N_c(f_m/N), \quad [36]$$

we can solve for N_c by specifying a pre-assigned value of N_1. In Table 2 we give the values of N_c for several combinations of (N, N_1). The standard values of f_r and f_m for a given N are given in Table 1. The value of f_{rc} required when N_c channels are used is simply given by $f_r(N_c/N)$.

We can now state the reasons why the N_1 uncompanded channels must occupy the bottom part of the baseband spectrum. It is seen from Eq. [32] that it is the value of δ that controls how much increase in capacity or TT/N is possihle due to the companding of the N_2 channels, where $N = N_1 + N_2$. The smaller the value of δ, the better the increase in capacity, or TT/N.

In terms of the baseband frequency assignment, consider the other extreme of assigning N_2 companded channels the bottom frequencies. These bottom channels have the X dB attenuation, and the compensatory pre-emphasis gains b_1 and b_2 now should be set such that

Table 2—Capacities of Mixed Carriers (N_c Channels): N = number of channels in a standard (uncompanded) carrier; N_1 = number of channels which cannot be companded; N_c = number of channels in the mixed carrier in which N_1 are uncompanded and $N_c - N_1$ are companded.

	N_1														
N	0	24	36	60	72	96	132	192	252	312	432	612	792	972	1092
36	90	65	36	—	—	—	—	—	—	—	—	—	—	—	—
60	154	130	116	60	—	—	—	—	—	—	—	—	—	—	—
72	182	158	145	110	72	—	—	—	—	—	—	—	—	—	—
96	240	218	206	179	162	96	—	—	—	—	—	—	—	—	—
132	306	286	276	257	246	222	132	—	—	—	—	—	—	—	—
192	409	390	380	362	353	332	296	192	—	—	—	—	—	—	—
252	532	512	502	484	474	455	423	355	252	—	—	—	—	—	—
312	645	626	617	599	590	572	544	489	417	312	—	—	—	—	
432	911	891	881	862	853	834	806	757	701	633	432	—	—	—	—
612	1221	1203	1194	1177	1168	1151	1126	1085	1040	992	875	612	—	—	—
792	1652	1632	1622	1603	1593	1575	1547	1502	1456	1408	1302	1098	792	—	—
972	1940	1921	1912	1894	1885	1868	1842	1800	1758	1716	1625	1465	1254	972	—
1092	2074	2058	2050	2035	2027	2012	1990	1953	1917	1881	1804	1673	1511	1303	1092

$$b_1/b_2 = 10^{-D/10} \qquad [37]$$

instead of Eq. [23]. The equation analogous to Eq. [24] is now

$$\delta' = d + (1 - d)\frac{(N_2/N) + (N_2/N)^3 3.1}{4.1}. \qquad [38]$$

The TT/N in a channel of frequency f is now given by

$$\begin{aligned} \text{TT/N} &= (C/N)(B/b)(f_r/f)^2 P_m(f) w, \ (N_2/N) f_m \leqslant f \leqslant f_m \\ &= (C/N)(B/b)(f_r/f)^2 P_m(f) w \ 10^{-X/10}, \ 0 \leqslant f < N_2 f_m/N. \end{aligned} \qquad [39]$$

The subjective TT/N at any f now equals

$$\text{TT/N} = (C/N)(B/b)(f_r^*/f)^2 P(f) w, \qquad [40]$$

where

$$f_r^* \triangleq (10^{D/10}/\sqrt{\delta'}) f_r. \qquad [41]$$

The accompanying equation for the bandwidth is

$$B = 2[f_m + pl(N) f_r^* \sqrt{\delta''}] \qquad [42]$$

where $\delta'' = 10^{-D/10}\delta'$.

We can now compare δ'' to δ, because all other terms in Eqs. [40] and [42] are the same as in Eqs. [33] and [32]. The ratio δ/δ'' equals

$$\delta/\delta'' = [1 + (d - 1)\theta]/[d - (d - 1)\theta'']$$

where

$$\theta = \frac{(N_1/N) + (N_1/N)^3 3.1}{4.1},$$

$$\theta'' = \frac{1 - (N_1/N) + [1 - (N_1/N)]^3 3.1}{4.1}.$$

It can now be shown that $\delta/\delta'' < 1$ for any value of N_1/N where $0 < N_1/N < 1$. Thus, putting the N_2 companded channels in the bottom part of the baseband will not give as much improvement in capacity of TT/N as putting them in the top region of the baseband spectrum.

5. Design with Overdeviation

In Secs. 3 and 4 we assumed that the allocated bandwidths of the carriers are equal to or larger than their Carson's bandwidth. This led to doubling of the capacity when companded channels are used. The designs were based on the fact that the companded channels need lower TT/N, but the subjectively perceived TT/N is equal to the uncompanded TT/N.

If the desired subjective TT/N is, e.g., 51dB, the actual TT/N is only 35 dB. With this design, the distortion in the baseband channels due to the channel filters and satellite amplifier nonlinearities is negligible. The effect of these distortions can be quantified by obtaining the test tone-to-distortion ratio (TT/D). Suppose that the TT/D is 60 dB in a standard uncompanded situation. This is 9 dB above the TT/N, which is 51 dB. Now if the channels are companded and the capacity increased to the limit of the companded carrier occupying the same Carson's bandwidth as the uncompanded carrier, the TT/N is 35 dB but TT/D continues to be at 60 dB due to the design constraint that the carrier deviation remain the same. Thus the TT/D is 25 dB above TT/N. This margin can be decreased by increasing the capacity in such a way that the TT/N continues to remain at 35 dB but the TT/D is decreased.

As the number of channels increases beyond the limit imposed by the Carson's bandwidth restriction, f_m increases; but if we also increase f_r proportionately, the TT/N continues to be at 35 dB. The distortion, however, increases and one can keep on adding more channels till TT/D reaches a specified lower limit. At this limit the carrier deviates beyond the Carson's bandwidth; this is referred to as overdeviation.

To determine the capacity with overdeviation, the TT/D must be estimated accurately. Exhaustive computer simulation techniques were used in estimating the TT/D in a single carrier occupying one full transponder. It was seen that most of the distortion is due to the satellite input filter, whose characteristics are dependent on the type of filter, multipath effects (see Ref. [5]), and the type of nonlinearity of the satellite amplifier. It was also observed that the amount of group delay of the input filter near the band edges has substantial effect on the distortion as the carrier deviates beyond its Carson's bandwidth.

In Fig. 7, TT/D is plotted as a function of the number of baseband channels. The value of f_{rc} is 1.35 MHz when the number of channels is 2071, and f_{rc} increases linearly with the capacity. It was established that TT/D should be at least 41 dB, which is 6 dB above the TT/N of 35 dB. This will make the subjective test tone-to-noise plus distortion TT/(N + D) be at 50.2 dB; this is considered to be an acceptable level of performance of the system. From Fig. 7 it is seen that TT/D reaches a value of 41 dB when the number of companded channels is 2600. This can be further improved by group delay equalization of the satellite input filter. Such equalization is not done in the RCA SATCOM spacecrafts. Consequently, the equalization was done at the transmit earth station i-f stage. When the equalizer parameters (amount of linear and parabolic delay compensation) were chosen optimally, the new capacity was estimated to be 2892 channels. The estimated TT/(N + D) obtained by computer simulation was found to be within 0.5 dB of the experimental

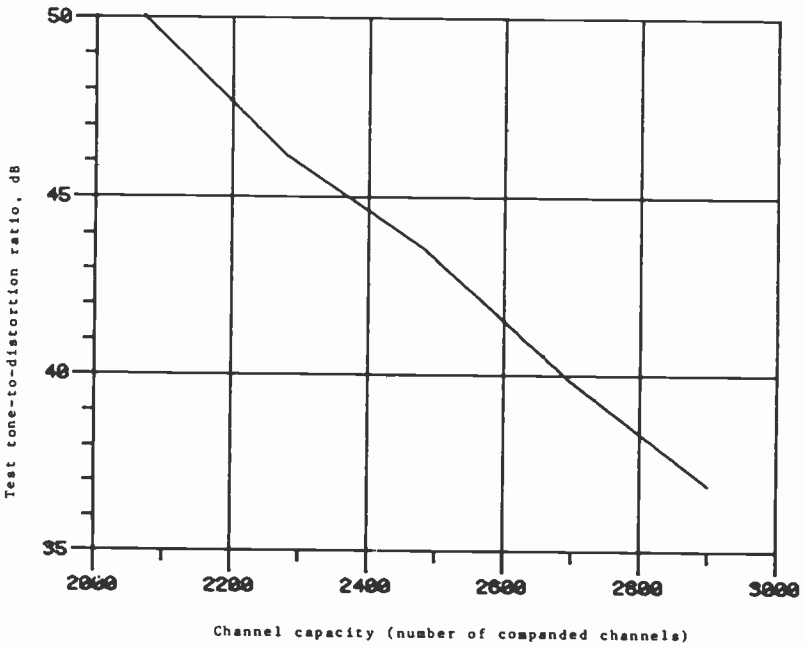

Fig. 7—Variation of TT/D with channel capacity (satellite input filter unequalized).

value obtained by using the satellite in orbit. This increase in capacity to 2892 channels is 40% more than the capacity of 2071 channels obtained by non-overdeviation and is 265% above the capacity of 1092 uncompanded channels.

6. Conclusions

Equations standardized by the CCIR for designing FDM/FM systems are modified in this paper to design companded systems. The design equations can be used in computing the capacities, required rms deviation, and the occupied bandwidth. It is shown that the capacity can be doubled by companding the channels, the occupied bandwidth being the same as that of the uncompanded carrier. Acceptable performance can be obtained by overdeviating the carrier beyond its Carson's bandwidth, but restricting the capacity till the bandlimiting distortion reaches a specified lower limit. By use of this technique, the capacity of a single carrier occupying a full transponder can be increased further; an RCA SATCOM transponder can carry up to 2892 companded channels.

Acknowledgments

Theoretical and experimental contributions to the work reported in this paper were made by many members of the Communication Systems Research Laboratory. Notable among them are E. S. Rogers, R. Craig Skevington, L. Schiff, H. Staras, L. L. Stetz, and J. A. Zenel.

Appendix

The results of Sec. 2 on multichannel loading were developed primarily to modify the standard CCIR methods in a simple way that makes the design procedures easy. The experimental results of Ref. [1] were also used in developing some of the equations. A different point of view can be obtained by using the results of Ref. [2]. The maximum peak load in a standard (i.e., uncompanded) situation can be written as equal to the peak sine wave power of $P_s + 3$, where

$$P_s = V_o - 1.4 + 0.115\,\sigma^2 + 10 \log T + 10 \log N + \Delta C \qquad [43]$$

and

V_o = mean speaker volume in VU, −14.5 VU,
1.4 = correction from VU to dBm for V_o,
σ^2 = variance of normal distribution of speakers, $\sigma = 5.4$,
T = activity factor, 0.25
N = number of channels
ΔC = multichannel load factor,
$= 10.5 + 40\,\sigma/[N\tau_i + 5\sqrt{2\sigma}]$,
τ_i = talker load activity, 0.25.

On using 0 dBmO unaffected level compandors, V_o becomes $V_o/2$ and σ becomes $\sigma/2$. Suppose that the maximum peak load for N_c companded channels be denoted by P_{sc}, assuming that all the channels are companded. Assuming that the Carson's bandwidth be the same in both the cases we arrive at*

$$B = 2(f_m + f_r p_s) \qquad [44]$$

and

$$B = 2(f_{mc} + f_{rc} p_{sc}), \qquad [45]$$

where $p_s = 10^{P_s/20}$ and $p_{sc} = 10^{P_{sc}/20}$. The consequent TT/N in the top channels are

$$\mathrm{TT/N} = (C/N)(B/b)(f_r/f_m)^2 P(f_m) w,$$

* In Eqs. [44] and [45], the peak sinewave power is $P_s + 3$ dB. However, we will substract a 3 dB factor from this to make the peaking factor $\Delta C + 3$ dB equal 10.5 for large N; this is nearly equal to the CCIR peaking factor of 10 dB.

$$(\mathrm{TT/N})_c = (C/N)(B/b)(f_{rc}/f_{mc})^2 P(f_{mc}) w.$$

Now let $(\mathrm{TT/N})_c$ be C dB lower than TT/N. Then

$$f_{rc}/f_{mc} = 10^{-C/20} f_r/f_m. \qquad [46]$$

Solving Eqs. [44] and [45] for f_r and f_{rc}, substituting them into Eq. [46], and finally using the expressions for P_s and P_{sc}, we arrive at (see Ref. [6])

$$\begin{aligned}(V_o/2) + 0.115\sigma^2 \times 0.75 + C + \Delta C - \Delta C_c \\ = 10 \log [n^3 (B - 2f_m)^2/(B - 2nf_m)^2],\end{aligned} \qquad [47]$$

where $n = N_c/N$ and

$$\Delta C - \Delta C_c = \frac{40\sigma}{N \times 0.25 + 5\sqrt{2\sigma}} - \frac{20\sigma}{N_c \times 0.25 + 5\sqrt{\sigma}}.$$

We can now solve for N_c, on specifying a standard set of values for N and f_m. In Table 3 we give the values of N_c for several standard SATCOM carriers. It is seen that the CCIR equations yield capacities that are only slightly conservative compared to the capacities obtained by solving Eq. (18).

The other use of the equations is to compute the saving in bandwidth by companding all the channels but without changing the number of channels. The equation analogous to Eq. [47] can be derived and is given by

$$\begin{aligned}(V_o/2) + 0.115\sigma^2 \times 0.75 + C + \Delta C - \Delta C_c \\ = 10 \log [(B/B_c)^3 (B - 2f_m)^2/(B - 2f_m B/B_c)^2]\end{aligned} \qquad [48]$$

where

Table 3—Capacities and Bandwidths of Companded Carrier: N_c = number of companded channels in the carrier that occupies the same bandwidth as that of N uncompanded channels; B_c = bandwidth of the carrier with N companded channels.

N	N_c Obtained by using the Appendix	N_c Obtained by using CCIR Method	B_c Obtained by using the Appendix (MHz)	B_c Obtained by using CCIR Method (MHz)
24	76	64	0.63	0.87
36	105	90	0.77	1.03
60	173	154	1.39	1.79
72	201	182	1.61	2.04
96	257	240	2.20	2.68
132	336	306	2.95	3.47
192	451	409	3.83	4.29
252	586	532	5.87	5.85
312	692	645	6.09	6.52
432	959	911	9.32	9.80
612	1258	1221	10.90	11.22
792	1691	1652	16.86	17.25
972	1973	1940	17.74	18.02
1092	2072	2071	18.97	18.95

$$\Delta C - \Delta C_c = \frac{40\sigma}{N \times 0.25 + 5\sqrt{2\sigma}} - \frac{20\sigma}{N \times 0.25 + 5\sqrt{\sigma}}.$$

The occupied bandwidth B_c can now be obtained solving Eq. [48] for B/B_c. In Table 3 we give the values of B_c and see that these are slightly lower than those obtained by the modified CCIR equations.

Although the results of this Appendix are somewhat more accurate than those obtained by using the modified CCIR equations, it is difficult to apply them for the mixed channel situations of Sec. 4. Further, the modified CCIR equations are also easier to apply for the all-companded situation.

References:

[1] E. M. Rizzoni, "Compandor Loading and Noise Improvement in Frequency Division Multiplex Radio-Relay Systems," *Proc. IRE*, **49**, p. 208, Feb. 1960.

[2] *Transmission Systems for Communications*, Members of Technical Staff, Bell Telephone Laboratories, Revised Fourth Edition, pp. 677–682, 1971.

[3] CCITT, Orange Book, Vol. III-1, G-162, pp. 103–109.

[4] L. Schiff, "Compensatory Pre-emphasis," *RCA Review*, **37**, p. 515, Dec. 1976.

[5] M. V. O'Donovan, et al., "Design of a Light-Weight Microwave Repeater for a 24-Channel Domestic Satellite System," *RCA Review*, **34**, p. 506, Sep. 1973.

[6] R. Craig Skevington, "Compandors for FDM/FM Voice Traffic," *National Telecommunications Conf.*, Nov. 27–29, 1979, pp. 12.5.1–12.5.5

[7] P. F. Panter, *Communication Systems Design*, McGraw-Hill Book Company, N.Y. (1972).

Maximizing Satellite Transponder Utilization

Allan Guida

RCA Laboratories, Princeton, NJ 08540

Abstract—A major objective in satellite communications is to fully utilize the satellite transponders. This means that (1) the satellite transponder should be fully occupied (in terms of the frequency spectrum) and (2) that carrier amplitudes should be adjusted so that each earth station receives a carrier-to-noise power ratio greater than or equal to the minimum C/N required for satisfactory signal detection. The present procedure for solving this problem in the RCA Satcom system is described in this paper.

1. Introduction

To determine the best transmission arrangement for the many signals that must to through the RCA satellite, a method for simulating any given transmission arrangement had to be developed. While a direct simulation of the system in the laboratory would be the most accurate approach, the equipment would be costly and the experiments time consuming. A digital computer simulation turns out to be much less expensive and each new arrangement can be set up quickly. However, the accuracy is only moderate. Various special interference effects that would show up in a laboratory simulation do not show up in a computer calculation, where a number of approximations have been made to keep the program reasonably simple and to keep the execution time down. The result is a computer program that can tell the user the C/N ratios achievable with a particular arrangement of carriers in a transponder. However, it is important for the user to know the limitations of the program in order to make a final decision.

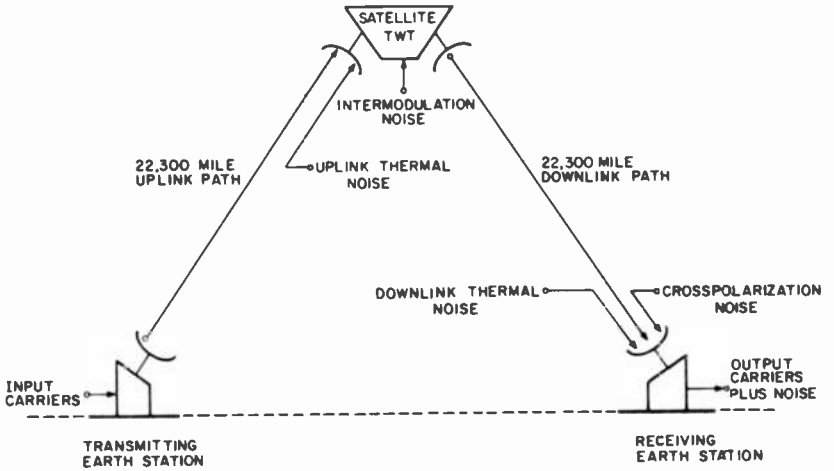

Fig. 1—Satellite Transmission System.

2. Transmission System Description

The transmission system under consideration consists of (1) a transmitting earth station, (2) a 22,300 mile uplink path, (3) a satellite TWT (one transponder), (4) a 22,300 mile downlink path, and (5) a receiving earth station (see Fig. 1). The input to this system is a set of two or more carriers that enter the uplink path from the transmitting earth station. In the uplink path, gaussian thermal noise is added to the carriers. In the TWT, the carriers undergo gain changes, and intermodulation distortion carriers (nonlinear product terms) are added. In the downlink path, more gaussian thermal noise and some cross-polarization noise (signals from adjacent cross-polarized transponders) are added to the carriers. Note that, in some cases, the input carriers may originate from more than one earth station and may also terminate at more than one earth station. As a result, the uplink and downlink path losses for all the carriers may be unequal.

3. Types of Carriers

At the present time, the satellite transmission of five types of carriers can be analyzed with the OPTX program:

(a) FDM/FM (voice/data channel carrier)
(b) TV/FM (TV carrier)
(c) BPSK (digital data carrier—2 phase)
(d) SCPC (single channel per carrier—many small carriers)
(e) QPSK (digital data carrier—4 phase)

Carrier combinations that include SCPC are analyzed with a separate

program called SCPCX. This program is limited to 3rd order intermodulation effects at present.

A sixth category, the overdeviated FDM/FM carrier, has not as yet been included.

4. Description of the Program (OPTX)

4.1 Calculation of Carrier-to-Noise Ratio

The computer program calculates all power levels relative to the saturation power of the satellite TWT (set to unity). On this basis, the system output carrier power of any carrier is simply the TWT output power for that carrier. TWT output signals (carriers plus intermodulation distortion terms) are calculated by using Shimbo's method.[1] Originally, Lyons' method[2] was used, but the program was changed because Shimbo's method requires much less computation time.

The noise powers for a particular carrier are obtained by calculating the thermal noises (uplink and downlink), the intermodulation distortion, and the cross-polarization noise falling in the bandwidth of that carrier. Since uplink thermal noise goes through the TWT and is amplified, the output uplink noise is calculated by multiplying the input uplink noise by the gain of the corresponding input carrier.

The actual received thermal noise depends on the parameters of the transmitting and receiving earth stations. Some earth stations send a noisier signal to the transponder because they are located at a place where the satellite is very low on the horizon. (They also received a noisier signal.) Other transmitting earth stations have a range of G/T and EIRP values depending on the antenna size, location, and low-noise amplifier in use.

Once the output carrier power and noise powers are known for each carrier, the C/N ratios are readily obtained for each carrier by using the formula

$$\frac{C}{N} = \frac{P_s}{N_U G_c + N_D + P_I + P_c}, \qquad [1]$$

where

P_s = TWT output carrier power,
N_U = Uplink thermal noise power,
G_c = TWT carrier gain,
N_D = downlink thermal noise power,
P_I = TWT intermodulation power,
P_c = cross-polarization noise power.

4.2 Margin

The margin for each carrier is obtained by subtracting the desired carrier-to-noise ratio $(C/N)_D$ in dB from the C/N ratio (dB) calculated using the given input power levels. If the optimization routine in the program is requested, the computer then tries to maximize the minimum margin for all of the carriers by varying the input carrier power levels. Because of the nature of the TWT, the optimum point is reached when all of the margins are equal and as large as possible. If the calculated margin is above some arbitrary level (usually 0 to 2 dB), the arrangement is deemed feasible assuming other limitations (see Sec. 6) are not involved.

4.3 Permutation

Because intermodulation power in a TWT transponder is not uniformly distributed but, in fact, tends to concentrate at the center of the transponder, the arrangement (or sequence) of the carriers can affect the optimum margin point. Generally speaking, the big carriers (wide bandwidth, high power) should be at one end of the transponder frequency band and the small carriers should be at the other end (see Table 2). To some small extent, the desired C/N ratio and wide ranging uplink–downlink parameters also play a role; consequently, it is worthwhile to permute the order of the carriers and optimize each permutation to find the best arrangement. A subroutine in OPTX provides a list of the permutations and the average margin obtained for each permutation. This is not the optimized margin; however, by selecting from the list those permutations with the best margins, one can select a few of the most likely candidates for further optimization. In most cases, this procedure should lead to the true optimum margin point.

4.4 Frequency Sliding

When the transponder is not completely full (i.e., when some left over bandwidth remains other than that required for guard bands), it is possible to shift the carriers about (without permuting their order) to try to reach a higher optimum point. A subroutine can be called that randomly changes the sizes of the frequency separations between the carriers and calculates the margin for each arrangement. The routine prints out the best set of separations and, at the request of the user, optimizes the carriers for that particular arrangement. Several runs of the permutation and slide routines must be employed to optimize a case where both types of adjustment are permitted.

4.5 Optimization

The maximization of a scalar function (minimum margin) of n variables (n input carrier power levels) could ordinarily be done by any one of the well known methods of optimization. Since the individual margins are available, however, they can be used in the process to cut down on the number of calculations needed. For example, if we have the margins of the n carriers and these margins are unequal, then the carriers with the lower margins must have their input power levels raised compared to those with the higher margins. Hence, a formula for the input carrier powers in an iterative optimization scheme is

$$P_{i(new)} = A \frac{P_{i(old)}}{M_{i(old)}}, \; i = 1 \text{ to } n$$

and

$$T_{(new)} = \sum P_{i(new)},$$

where

P_i = input carrier power in the ith carrier,
M_i = margin in the ith carrier,
T = total input carrier power (backoff) (TIBO)

and A is adjusted to set the total input power in the new carrier levels to the particular value $T_{(new)}$. This value of $T_{(new)}$ is determined by a linear search process[3] for the value of T (in the range 0 to 1) that produces the best margin. When the optimum margin point is reached, all of the carriers have the same margin. However, this is not the only point where all of the carriers have equal margin; there are many equal margin points. Therefore, the optimization routine is constructed so that the optimum point will be reached several times from different directions. When the same optimum point is reached more than once, the user can safely conclude that it is the actual optimum point.

The above procedure describes the last of four optimization routines available to the user. If there is still some doubt as to whether the optimum point reached is the true optimum point, the user can select one of the other routines and try again.

4.6 Data Entry

Data is entered into the program by creating a data file that includes the following:

(a) Number of carriers (n)
(b) Highest order intermod to be calculated (usually 3, 5, or 7)
(c) Type of carrier (see list in Sec. 3)

(d) Bandwidth of carrier filter: use standard sizes—2.5, 5, 7.5, 10, 15, 17.5, 20, 25, and 36 MHz.
(e) Frequency separation between carrier filters, or % guard band, allowed for each carrier (10% is typical).
(f) Spectrum parameter (σ for gaussian approximation). If the carrier is FDM/FM, give the number of channels; use standard sizes: 12, 72, 132, 192, 252, 312, . . . , (60 K + 12), etc. (Program uses CCIR formulas[4] for spectrum calculation). If the carrier is TV/FM, give the (±) peak deviation. If the carrier is BPSK or QPSK, give the ½ bandwidth.
(g) Desired carrier-to-noise ratio: use CCIR formulas[4] for FDM/FM carriers; >12 dB for FM carriers; >8 dB for BPSK or QPSK carriers.
(h) Uplink parameters: saturation flux density (SFD) plus satellite G/T.
(i) Downlink parameters: satellite effective isotropic radiated power (EIRP) plus earth station G/T.
(j) Choice of optimization routine:
    1. Optimize using margin values
    2. Optimize using positive gradient
    3. Optimize using equal margin line
    4. Optimize using margin values plus linear search (see Sec. 4.5)

5. Examples

5.1 Six FDM/FM voice carriers in two transponders

We are given 6 FDM/FM carriers to be placed in 2 transponders and we seek to maximize the minimum margin in the worst case. Let the number of voice channels in each carrier be 432, 432, 132, 132, 72 and 72, i.e., there are 3 pairs of carriers. Table 1 gives additional information on the carriers.

$(C/N)_D$ values are based on the CCIR formulas[4] except in the last two cases where the values (in brackets) were below FM threshold and consequently were reset to 12.0 dB. Uplink and downlink parameters are

Table 1—Carrier Data

Number of Channels	Bandwidth (MHz)	C/N)D (dB)	Uplink parameter (dB) (SFD + G/T)	Downlink parameter (dB) (FIRP + G/T)
432	17.5	18.51	−86.0	66.7
132	10.0	12.0 (10.50)	−86.0	66.7
72	7.5	12.0 (7.61)	−86.0	66.7

the approximate values for the RCA Americom earth station at Vernon Valley, NJ; SFD = −82.0 dB, satellite G/T = −4.0 dB; EIRP = 34.3 dB and earth station G/T = 32.4 dB.

Two types of placements of the carriers are possible, each with several permutations.

Type 1:	Transponder 1:	432, 432	
	Transponder 2:	132, 132, 72, 72 with 4 permutations	
Type 2:	Transponder 1:	432, 132, 72	each with 3 permutations
	Transponder 2:	432, 132, 72	

Thus, a total of eight arrangements must be optimized to determine the maximum margin. Using the OPTX program, the results given in Table 2 were obtained. Note that two transponders each with 3 carriers (432, 132, and 72 channels) produce the highest margin (1.160 dB).

Table 2—OPTX Results for 6 FDM/FM Carriers in Two Transponders

Transponder Carriers (Number of Channels)	Total Input Backoff (dB)	Margin (dB)
432, 432	−1.6	.388
132, 132, 72, 72	−7.7	1.664
132, 72, 132, 72	−7.8	1.526
72, 132, 132, 72	−7.8	1.496
132, 72, 72, 132	−7.7	1.598
432, 132, 72	−3.7	1.160
432, 72, 132	−3.8	1.037
132, 432, 72	−6.0	−.924

5.2 Capacity of n Equal FDM/FM Carriers in One Transponder

We are given n identical FDM/FM carriers to be placed in one transponder; we want to calculate how many voice channels can be carried by the n carriers. For the purpose of this calculation, let us suspend two rules of operation (see Sec. 4.6). The first rule is that the number of channels carried by an FDM/FM voice carrier is restricted to $60K + 12$ channels where K is an integer. The second rule to be suspended is the limitation on filter bandwidths, i.e., other than standard sizes are allowed. Under these conditions, the results given in Table 3 are obtained with OPTX. Note that as the number of FDM/FM carriers increases, the total voice channel capacity of a transponder decreases.

Table 3—OPTX Results for n Equal FDM/FM Carriers in One Transponder

No. of Carriers (n)	BW (MHz)	Channels per Carrier	Total No. of Channels	% of Maximum No. of Channels	Total Input (Backoff) (dB)	Margin (dB)
1	36.0	1115	1115	100.00	0.0	.000
2	17.5	443	886	79.46	−1.6	.002
3	12.0	225	675	60.54	−7.0	.012
4	9.0	148	592	53.36	−7.8	.054

5.3 Margin for n Equal Digital Carriers in One Transponder

We are given several T2 digital carriers (6.312 megabits/sec) to be placed in one transponder with 35 MHz of useable bandwidth (the bandwidth at the edge of the transponder is not useable because it contains regions with large variation in group delay); we want to calculate the maximum margin available when uniform frequency spacing is used.

The required bandwidth for a 6.312 mbs QPSK carrier is (0.6) (6.312) = 3.7872 MHz. The smallest standard size filter that fits this carrier is 5 MHz. Consequently, the maximum number of T2 carriers that one can fit in a transponder is 35/5 or 7. Table 4 shows the results of 3 OPTX calculations for fitting 5, 6 and 7 T2 carriers in one transponder.

If we now allow the carriers to be shifted about with the aid of the frequency sliding routine, a higher maximum margin can be achieved. In effect, the routine tries to push as much intermodulation power as it can into the spaces between the carriers and into the exterior regions. The results are shown in Table 5 after using several runs of the frequency sliding routine to set the frequency separations.

The 5-carrier case shows a margin improvement of 1.083 dB while the 6-carrier case shows a margin improvement of 0.313 dB. In the 7-carrier case, there is no extra frequency space available; hence the margin improvement is 0.0 dB.

Another way to select the frequency spacings is to use the Babcock Sequences[5,6] which are designed to keep all 3rd order IM lines from falling on carrier lines. The Babcock sequences for $n = 5$ and $n = 6$ are

Table 4—OPTX Results for Fitting 5, 6, and 7 T2 Carriers in one Transponder (10% Guard Band)

No. of Carriers (n)	Frequency Separation (MHz)	BW (MHz)	$(C/N)_D$ (dB)	Total Input (Backoff) (dB)	Margin (dB)
5	2.50	5.0	8.0	−7.8	6.163
6	1.0	5.0	8.0	−7.5	5.466
7	0.0	5.0	8.0	−7.6	5.174

Table 5—OPTX Results Using Frequency Sliding Routine to Set Frequency Separations

No. of Carriers	Calculated Frequency Separations (MHz)	Total Input (Backoff) (dB)	Margin (dB)
5	.286, .799, 6.497, 2.417	−6.1	7.246
6	.547, .100, 3.443, .317, .590	−6.8	5.779
7	Not possible; full transponder	—	—

1, 2, 5, 10, 12 and 1, 2, 5, 11, 13, 18, respectively, so that the frequency spacings would be proportional to 1, 3, 5, 2 and 1, 3, 6, 2, 5. The results are shown in Table 6.

Note that the margin results show that Babcock frequency spacing is better than uniform spacing but poorer than the frequency spacing picked by the frequency sliding routine. This is to be expected, since the Babcock sequences are only optimum for the case of narrow bandwidth carriers.

Table 6—OTPX Results Using Babcock Sequences

No. of Carriers (n)	Babcock Frequency Separations (MHz)	Total Input (Backoff) (dB)	Margin (dB)
5	.909, 2.727, 4.545, 1.818	−6.6	6.842
6	.277, .833, 1.666, .555, 1.388	−7.3	5.524
7	Not possible; full transponder		

5.5 3 FDM/FM Carriers Plus 1 SCPC Group in One Transponder

We are given three FDM/FM carriers and one group of SCPC carriers to be placed in one transponder; we want to calculate the maximum margin available. Table 7 shows the results of a calculation of the optimum margin using the SCPCX program.

By using the permute routine, one finds that a better sequence for the

Table 7—SCPCX Results

Carrier Number	Type	No. of Channels	BW (MHz)	DCTN (dB)	Total Input (Backoff) (dB)	Margin (dB)
1	FDM/FM	252	15.	12.71	−6.4	0.728
2	FDM/FM	192	10.	14.98		
3	FDM/FM	72	5.	13.33		
4	SCPC	167*	5.	12.00		

* This number is the number of 30 kHz channels that will fit in a 5 MHz bandwidth.

4 carriers is 2, 1, 4, 3. With the aid of the optimize routine, the new margin is 1.086 dB at a total input backoff of −6.5 dB.

6. Anomalous Effects Not Predicted by OPTX

As indicated earlier, the system simulation produced by OPTX is incomplete; certain effects that show up in actual system operation do not appear in OPTX. For example, if we place two TV/FM carriers in one transponder, the color carrier in one TV signal contains crosstalk from the color carrier in the other TV signal. As a result, the picture color slowly varies at a frequency rate equal to the slight difference between the two baseband color carrier center frequencies (each carrier is at approximately 3.587 MHz) in its own baseband. The effect can be reduced by backing off both carriers well below the point that provides satisfactory C/N for both carriers. However, the lower C/N at the new backoff point may produce TV pictures that are not of broadcast quality. (A special technique for reducing this effect without lowering the backoff point has been developed and patented.[7])

At first, it was thought that this effect was produced by the TWT 3rd order IM voltages:

$$v_{112} \exp[j(2\theta_1 - \theta_2)] \text{ and } v_{221} \exp[j(2\theta_2 - \theta_1)].$$

However, this theory was quickly discarded when it was observed that the effect was not a function of the difference in center frequency between the two TV/FM carriers. (When we calculate the frequencies of the spectral lines produced by two carriers, each FM modulated by a color carrier at 3.587 MHz, and by the two 3rd order IM terms produced by these carriers, we find that the exact locations of the lines depends entirely on the frequency separation between the two carriers.)

The present explanation for this effect is that it is caused by the RF filters for the TV/FM signals, which eliminate some of the high frequency energy in the TV/FM carrier spectrums. The result is that the TV/FM carriers have amplitude modulation on them that contains phase information. By placing the two TV/FM signals in a TWT that has AM-to-PM conversion, the amplitude modulation of the 1st carrier is added to the phase modulation of the 2nd carrier (and vice-versa). Then, when the 2nd carrier is demodulated, both phase modulations are present. The weaker color carrier (#1) added to the stronger color carrier (#2) forms a total color carrier with slowly varying phase and amplitude that produces the observed effect—slowly varying color in the TV picture.

Crosstalk effects such as this one can also occur between a data carrier and a TV carrier and between several data carriers. Intelligible crosstalk between two large FDM/FM voice carriers is also possible,[8] especially

if they are overdeviated. In addition, there are probably some cases in which the intermodulation distortion terms cannot be regarded as random gaussian noise since they are correlated with the original signals. However, no examples are presently known.

7. Conclusions

The OPTX and SCPCX computer programs can be used as a guide in optimizing satellite transponder utilization, but they do not guarantee satisfactory operation simply because margin requirements are met. Many transponder arrangements can be tested out quickly and conveniently and at low cost.

References:

[1] J. Fuenzalida, O. Shimbo, and W. Cook, "Time Domain Analysis of Intermodulation Effects Caused by Nonlinear Amplifiers," *COMSAT Tech. Rev.*, **3**, No. 1, Spring 1973, p. 89–143.

[2] R. Lyons, "A Stochastic Analysis of Signal Sharing in a Bandpass Nonlinearity," *IEEE Trans.*, **COM-22**, Nov. 1974, p. 1778–1788.

[3] L. Cooper and D. Steinberg, *Introduction to Methods of Optimization*, Saunders Co., Phila., PA (1970), p. 136–147.

[4] P. Bargellini, "The Intelsat IV Communication System," *COMSAT Tech. Rev.*, **2**, No. 2, Fall 1972, p. 460.

[5] W. Babcock, "Intermodulation Interference in Radio Systems," *Bell Syst. Tech. J.*, **32**, Jan. 1953, p. 63–73.

[6] R. Fang and W. Sandrin, "Carrier Frequency Assignment for Nonlinear Repeaters," *COMSAT Tech. Rev.*, **7**, No. 1, Spring 1977, p. 227–245.

[7] L. Abbott, G. Beakley, and R. Flory, "System for Passing Two Color TV Signals Thru Non-linear Path," U.S. Patent No. 4,120,001, Oct. 10, 1978.

[8] C. Cotner and A. Barnes, "Intelligible Crosstalk Between Large FDM/FM Carriers Amplified by Klystrons," *COMSAT Tech. Rev.*, **9**, No. 2B, Fall 1979, p. 705–716.

Maximum Transponder Capacity for Transmission of FDM/FM Channels

M. R. Freeling and W. H. Braun

RCA Americom, Princeton, NJ 08540

Abstract—This paper discusses six techniques employed in the RCA Satcom system to maximize the number of FDM/FM channels that can be transmitted through a single transponder: companding, overdeviation, reduction of multichannel load factor, group delay equalization, reduction of peak factor, and use of nonstandard pre- and de-emphasis networks. Transponder channel capacity tests of RCA Americom's F1 Satellite are described. These tests verify that 2892 companded FDM/FM channels can be successfully transmitted through one Satcom transponder with a nominal bandwidth of 36 MHz. The tests further demonstrate the validity of the analytical model. Excellent agreement is shown between theoretical predictions and experimental results.

1. Introduction

Extensive theoretical studies and analyses have been performed of mechanisms to increase the number of FDM/FM channels that can be transmitted through one satellite transponder. Among the techniques examined have been companding, overdeviation, reduction of multichannel load factor, and group delay equalization.[1,2] The RCA Satcom system has made use of these techniques, as well as reduction of peak factor and use of nonstandard pre- and de-emphasis characteristics, to maximize transponder capacity.

The first part of this paper considers the effect of each of these mechanisms on the capacity of an FDM/FM link through a satellite transponder. Predictions are made for the increase in transponder channel capacity accomplished by the adoption of each approach. A

maximum transponder capacity of 2892 channels for the RCA Americom system is envisioned at present.

In the second part of the paper, transponder channel capacity tests performed at Americom's Vernon Valley and Atlanta Earth Stations to test the theoretical predictions are presented. Two series of tests verified that 2892 companded FDM/FM channels can be successfully transmitted through a single transponder of the Satcom satellite.

2. Capacity Expansion Techniques

2.1 Companding

One method of increasing channel capacity is the use of a compandor in each baseband channel, i.e., compressing the baseband signals at the transmission end of the system and expanding them at the receiving end. Fig. 1 illustrates the use of compandors in an FDM/FM communications link through a satellite. The advantage of companding voice frequency signals is that the dynamic range of the signals is reduced, i.e., peak signal power is decreased and minimum signal power is increased. The amount of dynamic range reduction achieved is determined by the compression ratio. Further, the increase in minimum signal power improves the minimum signal-to-noise ratio of small-amplitude signals. At the receive locations, the expandor returns the signal to its original dynamic range.

In a frequency division multiplex (FDM) system, this reduction of peak power level of the composite baseband signal reduces the peak carrier deviation. Therefore, through the use of companding, a greater number of channels can be transmitted through a single satellite transponder than would be possible without companding.

A listener comparing a companded voice channel with an uncompanded voice channel will subjectively perceive them to be equivalent in quality, even if the objective signal-to-noise ratio of the companded channel is less than that of the uncompanded channel. The difference in dB between the signal-to-noise ratio of an uncompanded channel and its subjectively equivalent companded channel is the gross companding advantage. For the companding characteristics employed in RCA Americom's FDM/FM communications systems, the gross companding advantage is 16 dB. That is, a listener will judge a companded voice channel with a 35-dB signal-to-noise ratio to be equivalent in quality to an uncompanded voice channel with a 51 dB signal-to-noise ratio.

The compressor output, C_{out} in dBm0, is related to the compressor input, C_{in}, by the equation

$$C_{out} = \frac{C_{in} + U}{K}.$$

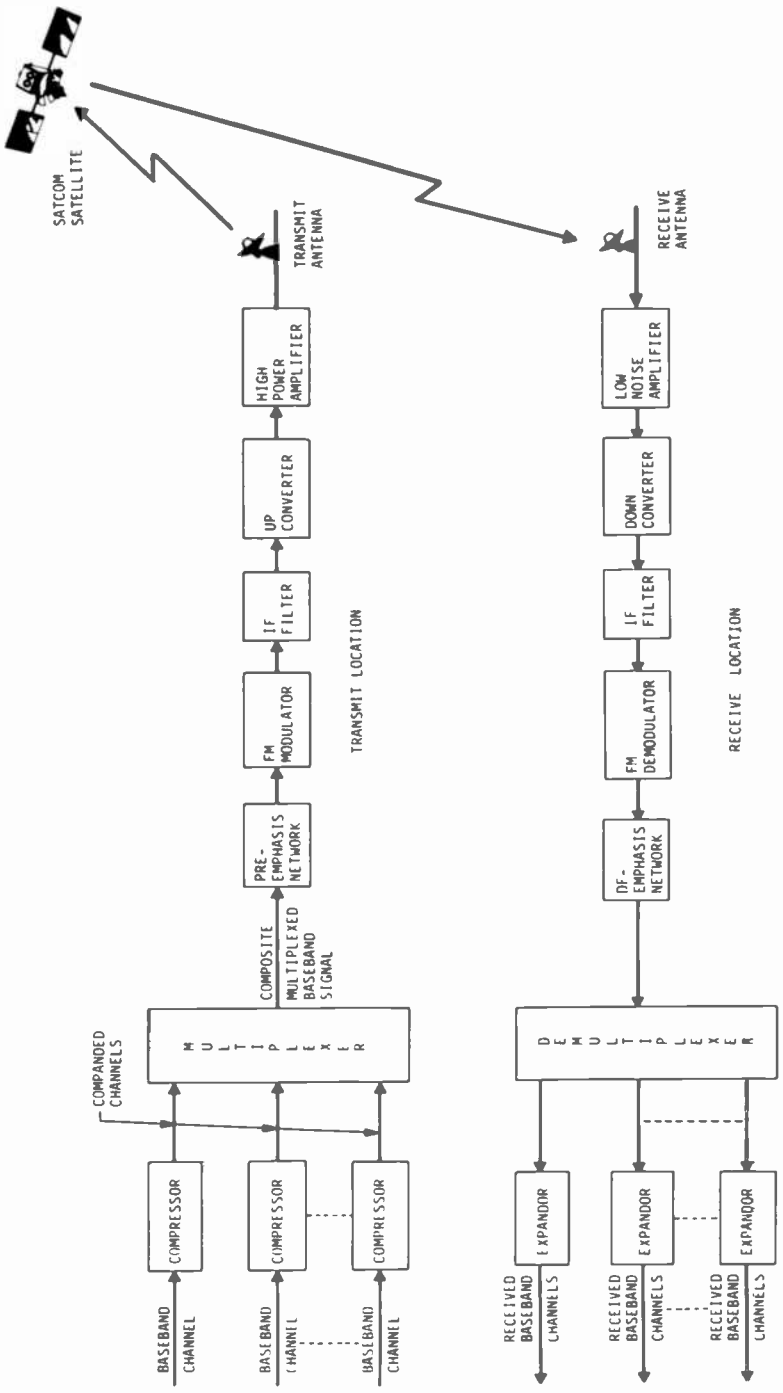

Fig. 1—Use of compandors in an FDM/FM link through a satellite.

Here, U is the unaffected signal level in dBm0, i.e., a signal of level U impressed at the input of a compressor in series with an expandor reaches the output of the expandor unchanged. K is the compression ratio, or the amount by which the dynamic range of the input signal is decreased. For the compressors employed in the RCA FDM/FM system, $U = -32$ dBm0 and $K = 2$. Throughout the remainder of this paper the compandors discussed will be assumed to have these characteristics.

Fig. 2 traces the transmission of signals of several amplitudes through a compressor in series with an expandor, and shows the power levels of the signals at several points in the transmission path. An initial dynamic range of 65 dB is compressed to 32.5 dB by a compression ratio of 2. Fig. 2 also shows the unaffected signal level, $U = -32$ dBm0. As shown, the compressor output for a -15 dBm0 sinusoidal tone input is -23.5 dBm0. For an input to the compressor of a signal carrying speech (rather than a tone), -15 dBm0 represents the CCITT prescribed value of average talker power.[3] Studies conducted of the statistical properties of speech and verified by the experimental measurements have determined that the compressor output for a typical -15 dBm0 speech input is -27 dBm0.* Therefore (for -32 dBm0 unaffected level), companding reduces the loading of a voice channel by 12 dB. This is the net compandor advantage, the amount in dB by which the system carrier-to-noise ratio of a companded channel is below the system carrier-to-noise ratio of an uncompanded channel to which it is subjectively equivalent.

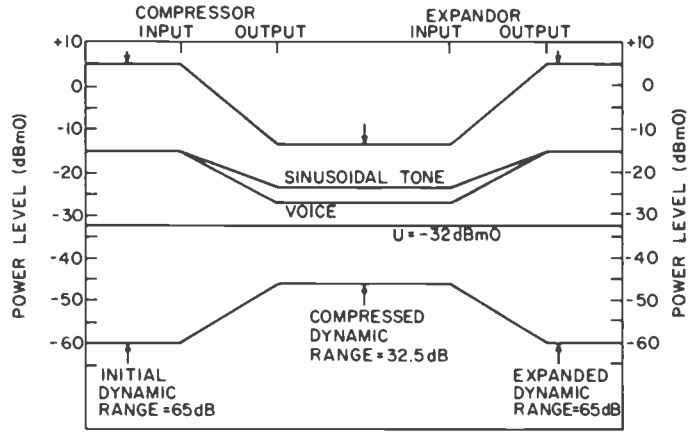

Fig. 2—Transmission of signals through compressor and expandor in series ($U = -32$ dBm0, $K = 2$).

* Reduction of speech power by 12 dB may be seen by considering that a compandor with an unaffected level of -32 dBm0 is equivalent to a compandor with 0 dBm0 unaffected level followed by a 16-dB attenuator. The average speech power out of a compressor with 0 dBm0 unaffected level has been found empirically to be typically 4 dB higher than the average speech power into it. At the output of the attenuator then the speech power is 12 dB less than at the input to the compressor.

For uncompanded FDM/FM traffic through a satellite link, the signal-to-noise ratio in dB is given by[4]

$$S/N = C/N + 10\log(B_a/b) + 20\log(\Delta f_{rms}/F_{mt}) + P + W, \quad [1]$$

where,

S/N = weighted signal-to-noise ratio for a 0 dBm0 test tone
C/N = system carrier-to-noise ratio in a Carson's Rule bandwidth of B_a
B_a = allocated bandwidth (36 MHz for a Satcom transponder)
b = channel bandwidth (3.1 kHz)
Δf_{rms} = RMS deviation for 0 dBm0 test tone
F_{mt} = top baseband frequency
W = psophometric weighting factor (2.5 dB)
P = pre-emphasis weighting factor (4 dB for standard CCIR recommendation)

From Carson's Rule,

$$B_a = 2(\Delta F_{pk} + F_{mt})$$

where ΔF_{pk} is the multichannel peak deviation.

The peak factor in dB is defined by

$$\text{P.F.} = 20\log(\Delta F_{pk}/\Delta F_{rms})$$

where ΔF_{rms} is the multichannel RMS deviation. ΔF_{rms} and Δf_{rms} are related by

$$20\log(\Delta F_{rms}/\Delta f_{rms}) = \text{L},$$

where L is the multichannel load factor:[5]

$$L = -15 + 10\log n \text{ for } n \geq 240 \text{ channels}$$

$$= -1 + 4\log n \text{ for } n < 240 \text{ channels}$$

The standard RCA Americom specification requires a minimum signal to noise ratio of 51 dB in the top baseband channel for the entire link from the transmit earth station through the satellite transponder to the receive earth station. Fig. 3 shows a computer printout of a link calculation of a saturating carrier transmitted from the Vernon Valley Earth Station in Transponder 16 of the F1 Satellite and retransmitted from the satellite back to the Vernon Valley Earth Station. It can be seen from the computer printout that the maximum value of system C/N that can be achieved in this loopback link is 19.4 dB. For S/N = 51.0 dB and C/N = 19.4 dB, Eq. [1] yields a maximum channel capacity (uncompanded operation) for the Satcom transponder of 1092 channels with the following parameters:

$$F_{mt} = 4396 \text{ kHz}$$

LINK BUDGET PARAMETERS
****

NPTST

SYSTEM PARAMETERS

IF FILTER BANDWIDTH:	36.000	MHZ
TRANSPONDER INPUT BACKOFF:	0.0	DB
TRANSPONDER OUTPUT BACKOFF:	0.0	DB
CARRIER TO INTERFERENCE RATIO:	23.3	DB
TRANSPONDER USABLE BANDWIDTH:	36.0	MHZ
FADED SYSTEM MARGIN:	0.0	DB

UPLINK PARAMETERS

TRANSMIT SITE:	VERNON VALLEY	
TRANSPONDER CENTER FREQUENCY:	6245.0	MHZ
TRANSMIT EIRP:	77.9	DBW
FREE SPACE LOSS:	200.5	DB
UPLINK MARGIN:	1.5	DB
SATURATED SATELLITE FLUX DENSITY:	-86.7	DBW/M
SATELLITE G/T:	+0.2	DB/K

DOWNLINK PARAMETERS

RECEIVE SITE	SATURATED SATELLITE EIRP (DBW)	FREE SPACE LOSS (DB)	DOWNLINK MARGIN (DB)	EARTH STATION G/T (DB/K)	REQ'D. C/N (DB)
VERNON VALLEY	34.0	196.6	1.0	32.0	19.4

COMPUTED RESULTS

RECEIVE SITE	C/N UP (DB)	SATELLITE EIRP (DBW)	C/N DOWN (DB)	C/N NOMINAL (DB)	C/N REQ'D. (DB)	TOTAL MARGIN (DB)
VERNON VALLEY	29.1	34.0	22.5	19.4	19.4	-0.0

OCCUPIED BANDWIDTH:	36.000	MHZ
TRANSPONDER BANDWIDTH USED:	100.00	%
TRANSPONDER POWER USED:	100.00	%

Fig. 3—Computer printout of uplink and downlink calculations for a saturating carrier between Vernon Valley and satellite.

$$\Delta f_{rms} = 732 \text{ kHz}$$

$$\Delta F_{rms} = 4302 \text{ kHz}$$

If each of the 1092 channels is companded, then the multichannel load factor is reduced by 12 dB from 15.4 to 3.4 dBm0. It can then be seen from Eq. [1] that for a subjectively perceived S/N of 51 dB, the required system C/N is 7.4 dB. The difference between this and the 19.4 figure given above for uncompanded operation is 12 dB, the net companding advantage. In actual operation, of course, the system carrier-to-noise ratio could not be as low as 7.4 dB, since this value is below the threshold of the FM demodulator, which is typically 9 to 10 dB.

Compandors have, in the past, been used to improve the perceived performance of marginal or poor circuits, i.e. those with inadequate signal-to-noise ratio. The approach used here, however, is to use compandors on circuits that are already of high quality. The objective is to realize higher channel capacities while maintaining a subjectively

equivalent signal-to-noise ratio. Table 1 shows solutions of Eq. [1] for several different values of companded channel loadings. This table shows transmission parameters and the system carrier-to-noise ratio required for a signal-to-noise ratio of 51 dB for the several loadings of companded FDM/FM channels.

It can be seen from Table 1 that for a Vernon Valley loopback through Transponder 16 of the F1 Satellite, the maximum capacity would be approximately 1992 channels (Case #2). Therefore, the ratio of transponder channel capacity with companding to channel capacity without companding would be approximately 1992/1092 = 1.82, an 82% increase in capacity.

2.2 Overdeviation

To avoid introducing interference into adjacent co-polarized transponders, a signal transmitted to the Satcom satellite may not be more than 40 MHz wide, and an uplink i-f filter is employed to ensure this limitation (Fig. 1). Filters located in the satellite transponder further limit the bandwidth to 36 MHz (Fig. 4). The 82% increase in transponder capacity effected by companding computed in Sec. 2.1 is for an allocated bandwidth, B_a, of 36 MHz. However, the bandwidth, B_o actually occupied by the uplink FDM/FM traffic after modulation and prior to filtering need not be limited by these bandwidth constraints. As can be seen from Eq. [1], increasing Δf_{rms} increases the signal-to-noise ratio S/N for a given channel loading. Alternatively, increasing Δf_{rms} increases the number of channels that can be transmitted through a transponder for a given S/N. As n (the number of channels), Δf_{rms}, ΔF_{rms}, and B_o all increase, distortion will increase due to bandpass nonlinearities of the filters in the satellite and earth station.

For our study on maximizing channel capacity, a value of 48 MHz was empirically chosen as the initial value for B_o. It had previously been determined that a bandwidth capability of 48 MHz could be achieved through relatively minor modifications of existing earth station equipment. Later analysis, confirmed by experimental measurements at the Atlanta Earth Station, indicated that a larger value of B_o, 57.6 MHz, could be employed to achieve greater channel capacity.

The ratio of signal-to-total noise $(S/N)_T$ for the case of overdeviation is given by

$$(S/N)_T = (S/N) \oplus (S/N)_D \qquad [2]$$

where

$(S/N)_T$ = weighted ratio, for a 0 dBm0 test tone, of signal-to-total noise,

Table 1—Transmission Parameters for FDM/FM Channels for Companded Operation

Case No.	Number of Channels n	Top Baseband Frequency Fmt (kHz)	RMS Deviation for 0 dBm0 Test Tone Δf_{rms} (kHz)	Multichannel RMS Deviation ΔF_{rms} (kHz)	Required C/N in B_a for 8000 pWp (S/N = 51 dB) C/N (dB)
1	1932	8428	1549.0	3026.9	18.56
2	1992	8676	1486.0	2948.5	19.18
3	2052	8924	1425.2	2870.1	19.78

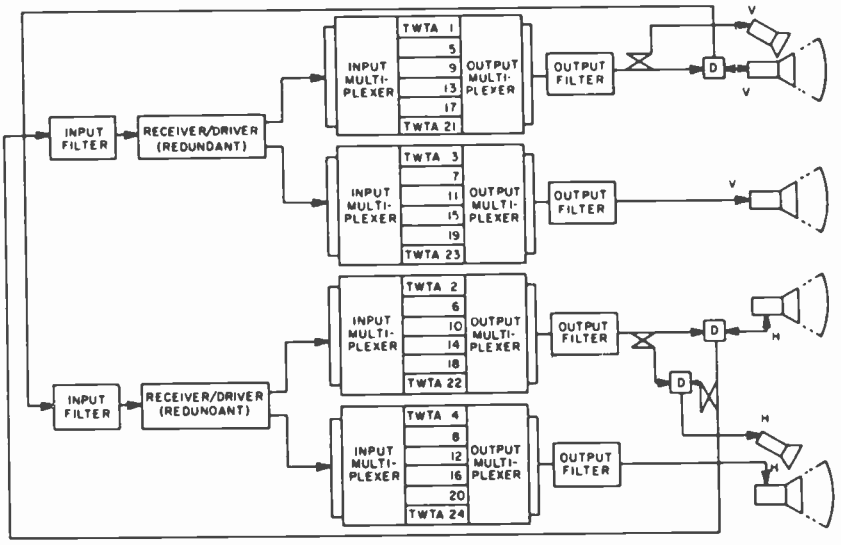

Fig. 4—Block diagram of transponder.

(S/N) = weighted signal-to-noise ratio for a 0 dBm0 test tone, as determined in Eq. 1,

$(S/N)_D$ = weighted ratio, for a 0 dBm0 test tone, of signal to distortion noise caused by overdeviation,

$\oplus$ = power summation.

It can be seen from Eq. [2] that distortion noise due to exceeding a bandwidth of 36 MHz reduces the signal-to-noise ratio that was originally achieved without overdeviation.

The criterion for determining the maximum channel capacity was arbitrarily established as follows. Channel capacity was defined to be the maximum number of channels for which a signal-to-noise ratio of 52.0 dB could be achieved. For that number of channels, a degradation due to distortion of as much as 1.0 dB in S/N could be tolerated and the objective of 51.0 dB would still be achieved.

The transmission parameters and required system C/N for several loadings of FDM/FM channels for the case of companding and overdeviation to an occupied bandwidth, B_o, of 48 MHz are shown in Table 2. The computer printout (Fig. 3) shows that for a Vernon Valley to Vernon Valley loopback in Transponder 16 of F1, a maximum value of system C/N of 19.4 dB can be achieved. From Table 2, it can be seen that for a loading of 2412 channels, Case #2, the signal-to-noise ratio achieved in the absence of degradations due to distortion is approximately 52 dB,

Table 2—Transmission Parameters for FDM/FM Channels for Companding and Overdeviation (B_o = 48 MHz, B_a = 36 MHz)

Case No.	Number of Channels n	Top Baseband Frequency F_{mt} (kHz)	RMS Deviation for 0 dBM0 Test Tone Δf_{rms} (kHz)	Multichannel RMS Deviation ΔF_{rms} (kHz)	Required C/N in B_a for 8000 pWp (S/N = 51 dB) C/N (dB)
1	2352	10164	2029.3	4375.3	17.84
2	2412	10412	1968.0	4296.9	18.32
3	2472	10660	1908.5	4218.5	18.79
4	2532	10908	1850.7	4140.1	19.26
5	2592	11156	1794.5	4061.6	19.72

which meets the established criterion. This channel capacity is an increase of 21% over the capacity achieved through the use of companding alone (1992 channels) and a 121% increase over the basic 1092 channel capacity.

2.3 Multichannel Load Factor

The derivations in Secs. 2.1 and 2.2 of transponder channel capacity for the cases of transmission with no companding, with companding, and with companding plus overdeviation assumed the multichannel loading factor to be given by $L = -15 + 10 \log n$ ($n \geq 240$ channels) without companding and $L = -27 + 10 \log n$ ($n \geq 240$ channels) for a system employing RCA's companding parameters. These values of L, in turn, assumed an average talker power per channel of -15 dBm0, as recommended by the CCITT.

Studies have been conducted and reported on in the literature[6] which indicate that the actual average talker power per channel may be as low as -22.3 dBm0. Bell System measurements of signal power in multiplexed telephone channels in a wide range of locations in the United States have indicated an average talker power per channel of -19.6 dBm0.[7] For a system employing RCA Americom's companding parameters, average talker power and the multichannel loading factor are related as follows:

Average Talker Power (dBm0)	Multichannel Load Factor (dBm0)
-15	$-27.0 + 10 \log n$
-17	$-28.0 + 10 \log n$
-19	$-29.0 + 10 \log n$
-21	$-30.0 + 10 \log n$
-22	$-30.5 + 10 \log n$

Table 3 shows the parameters and the system carrier-to-noise ratio required for the transmission of FDM/FM channels by a satellite communication system employing the techniques of companding, overdeviation to an occupied bandwidth of 48 MHz, and reduction of the assumed talker power to -21 dBm0. The table shows that, again subject to the constraint that a minimum margin of 1 dB in S/N ratio be allowed for degradation due to distortion caused by overdeviation, the maximum channel capacity is 2772 channels, Case #2. That is, through the use of companding, overdeviation, and reduction of multichannel load factor, a transponder channel capacity can be achieved that is 2.5 times (2772/1092) that for the case in which none of these capacity expansion techniques is employed.

Table 3—Transmission Parameters for FDM/FM Channels for Companding, Overdeviation, and Reduction of Average Talker Power (B_o = 48 MHz, B_a = 36 MHz, P_{AV} = −21 dBm0)

Case No.	Number of Channels n	Top Baseband Frequency F_{mt} (kHz)	RMS Deviation for 0 dBm0 Test Tone Δf_{rms} (kHz)	Multichannel RMS Deviation ΔF_{rms} (kHz)	Required C/N in B_a for 8000 pWp (S/N = 51 dB) C/N (dB)
1	2712	11652	2370.8	3904.8	17.68
2	2772	11900	2298.1	3826.4	18.14
3	2832	12148	2226.9	3747.9	18.59
4	2892	12388	2158.8	3672.0	19.03
5	2952	12710	2078.2	3570.5	19.68

2.4 Group Delay

It was shown in Eq. [2] that the ratio of signal-to-total-noise $(S/N)_T$ could be expressed as the power summation of two constituent signal-to-noise ratios. $(S/N)_D$, the ratio of signal to distortion noise caused by overdeviation (for a 0 dBm0 test tone), may in turn be expressed as the power sum of several signal-to-noise ratios:

$$(S/N)_D = (S/N)_{\substack{\text{linear}\\ \text{slope, G.D.}}} \oplus (S/N)_{\substack{\text{parabolic}\\ \text{G.D.}}} \qquad [3]$$

where,

$(S/N)_{\substack{\text{linear}\\ \text{slope G.D.}}}$ = weighted ratio, for a 0 dBm0 test tone of signal-to-noise due to linear or slope group delay

$(S/N)_{\substack{\text{parabolic}\\ \text{G.D.}}}$ = weighted ratio, for a 0 dBm0 test tone, of signal-to-noise due to parabolic group delay

These two signal-to-noise ratios have been found to be the main contributions of group delay noise. For the case of no companding, they are given by[8]

$$(S/N)_{\substack{\text{linear}\\ \text{slope G.D.}}} 10 \log_{10} \frac{10^6}{\pi^2 S^2 (\Delta F_{rms})^2 F_{ml}{}^2} + 19.0 \text{ dB}, \qquad [4]$$

$$(S/N)_{\substack{\text{parabolic}\\ \text{G.D.}}} = 10 \log_{10} \frac{7.5 \times 10^5}{\pi^2 P_T{}^2 (\Delta F_{rms})^4 F_{ml}{}^2} + 19.0 \text{ dB}, \qquad [5]$$

where S is the linear coefficient of group delay (ns/MHz) and P_T is the parabolic coefficient of group delay (ns/(MHz)^2).

Noise caused by group delay can be reduced by compensatory equalization, i.e., through the introduction into the link of a network with group delay characteristics equal and opposite to the group delay characteristic of the rest of the link. Prior to the inception of the transponder channel capacity expansion program, RCA had determined empirically that the use of uplink i-f or "mop up" equalizers would result in an improvement of about 1.0 dB in the signal-to-noise ratio of the top baseband channel in an FDM/FM system. For the case in which the average talker power per channel is the conventional −15 dBm0, it can be seen from Table 2 that a 1.0 dB improvement in S/N would result in an increase in channel capacity from 2412 channels to 2532 channels, a 5% increase. Table 3 shows that, for an average talker power per channel of −21 dBm0, use of uplink group delay equalization should result in an increase in capacity from 2772 channels to 2892 channels, a 4.3% increase.

In brief, through the use of companding, overdeviation, and group delay equalization, a transponder channel capacity of 2532 can be

achieved. If, in addition, the average talker power per channel is reduced from −15 to −21 dBm0, the channel capacity is 2892.

2.5 Peak Factor

As was indicated in Sec. 2.2, the RCA Satcom system design for expanded transponder channel capacity employed an occupied bandwidth, B_o, that exceeds the allocated bandwidth, B_a, for the case of overdeviation. Carson's Rule for the occupied bandwidth is

$$B_o = 2(F_{mt} + \Delta F_{pk}).$$

The multichannel peak deviation, ΔF_{pk}, is related to the multichannel RMS deviation, ΔF_{rms}, by the peak factor:

$$\text{P.F.} = 20 \log_{10}(\Delta F_{pk}/\Delta F_{rms}).$$

The peak factor is a measure of the margin allocated to allow for amplitude excursions greater than those that produce the RMS or average deviation. Conventional FDM/FM design employs a peak factor of 10 dB, and this value was used in the calculations of transmission parameters in the previous sections.

An investigation was undertaken to determine what increase in channel capacity could be obtained through the design of an FDM/FM system with a peak factor lower than the standard 10 dB. As part of this investigation, we also examined the possible degradation of system performance, other than channel capacity, caused by the use of peak factors less than 10 dB. Tradeoffs were considered between some aspects of system performance and the achievement of greater channel capacity. Fig. 5 shows the probability of exceeding ΔF_{pk} (i.e., of overdeviating beyond B_o) as a function of the peak factor.[9] For the standard peak factor of 10 dB, the probability of exceeding the design value of ΔF_{pk} is 1.83×10^{-3}. From Fig. 5, the expectation of overdeviation as a function of peak factor is

Peak Factor (dB)	Probability of Exceeding ΔF_{pk}
10.0	1.83×10^{-3}
9.0	5.00×10^{-3}
8.0	1.27×10^{-2}
7.0	2.78×10^{-2}

For the initial design and series of tests, it was decided that an increase in probability of overdeviation from 1.83×10^{-3} to 5.00×10^{-3} would have minimal impact on system performance and a peak factor of 9 dB was chosen. Table 4 shows parameters for transmission of FDM/FM

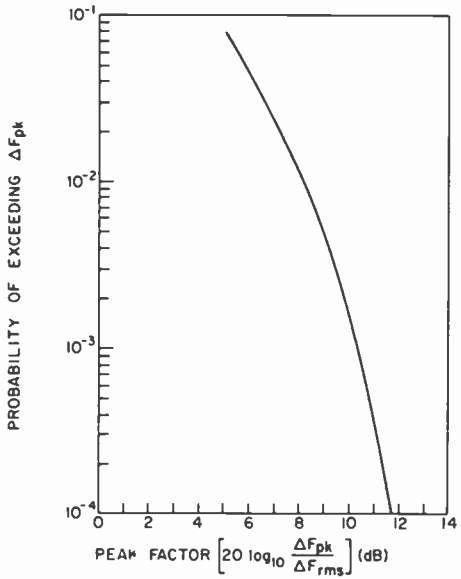

Fig. 5—Probability of exceeding multichannel peak deviation (ΔF_{pk}) as a function of peak factor.

channels by satellite, for an average talker power of −15 dBm0, when the following expansion techniques are employed: companding, overdeviation (B_o = 48 MHz), group delay equalization, and 9-dB peak factor.

Table 5 shows transmission parameters and required system C/N for employment of these four capacity expansion techniques plus reduction of the average talker power per channel to −21 dBm0. As can be seen, a channel capacity of 3012 channels (Case #5) results.

2.6 Nonstandard Pre- and De-emphasis

The standard pre-emphasis characteristic recommended by CCIR is shown in Fig. 6. This characteristic in an FDM/FM system will result in an pre- and de-emphasis improvement (PDI) in signal-to-noise ratio in the top baseband channel of 4 dB. In an effort to increase signal-to-noise ratio and therefore channel capacity, pre- and de-emphasis networks were designed to provide advantages greater than the conventional 4 dB. Tests at the Vernon Valley Earth Station (see Sec. 3.2) showed that the use of these networks resulted in an additional improvement of signal-to-noise ratio in the top baseband channel of approximately 0.5 dB above the conventional 4 dB. Since the networks employed did not have the optimum characteristics to maximize channel capacity, pre-

Table 4—Transmission Parameters for FDM/FM Channels for Companding, Overdeviation, Group Delay Equalization, and Reduction of Peak Factor (B_o = 48 MHz, B_a = MHz, P.F. = 9 dB)

Case No.	Number of Channels n	Top Baseband Frequency F_{mt} (kHz)	RMS Deviation for 0 dBm0 Test Tone Δf_{rms} (kHz)	Multichannel RMS Deviation ΔF_{rms} (kHz)	Required C/N in B_a for 8000 pWp (S/N = 51 dB) C/N (dB)
1	2592	11156	2004.8	4557.1	18.76
2	2652	11404	1943.1	4469.2	19.22
3	2712	11652	1883.6	4381.2	19.68
4	2892	12388	1715.1	4120.0	21.03
5	3012	13080	1580.4	3874.6	22.21
6	3072	13328	1529.7	3787.1	22.65

Table 5—Transmission Parameters for FDM/FM Channels for Companding, Overdeviation, Group Delay Equalization, Reduction of Peak Factor, and Reduction of Average Talker Power (B_o = 48 MHz, B_a = 36 MHz, P.F. = 9 dB, P_{AV} = −21 dBm0).

Case No.	Number of Channels n	Top Baseband Frequency F_{mt} (kHz)	RMS Deviation for 0 dBm0 Test Tone Δf_{rms} (kHz)	Multichannel RMS Deviation ΔF_{rms} (kHz)	Required C/N in B_a for 8000 pWp (S/N = 51 dB) C/N (dB)
1	2592	11156	2830.5	4557.1	15.76
2	2652	11404	2743.5	4469.2	16.23
3	2712	11652	2660.1	4381.1	16.68
4	2892	12388	2422.7	4120.0	18.03
5	3012	13080	2231.9	3874.6	19.21
6	3072	13328	2160.7	3787.1	19.65

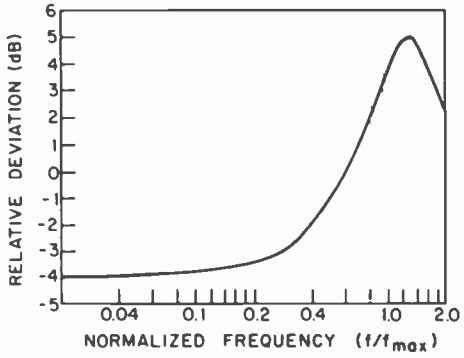

Fig. 6—Standard pre-emphasis characteristic curve.

dictions have not been included of the expected increase in channel capacity due to their use.

2.7 Summary of Predicted Increases in Channel Capacity

Table 6 is a summary of predictions of channel capacities that will be achieved through the use of the various combinations of the expansion techniques described above.

3. In-Orbit Tests

The objective of the in-orbit tests, which were conducted at RCA Americom's Vernon Valley Earth Station, was to establish experimentally the maximum number of FDM/FM channels that could be transmitted via a satellite transponder when the capacity expansion mechanisms described in the previous section are used.

Table 6—Summary of Predicted Channel Capacities as Various Expansion Techniques are Added to the System

Expansion Techniques Added to System*	Predicted Transponder Channel Capacity	Ratio of Transponder to Baseline Capacity	Percent Increase over Baseline Capacity
None (Baseline)	1092	1.00	—
(1) added	1992	1.82	82
(1) and (2) added	2412	2.21	121
(1), (2), and (3) added	2532	2.32	132
(1), (2), (3), and (4) added	2652	2.43	143
(1), (2), and (5) added	2772	2.54	154
(1), (2), (3), and (5) added	2892	2.65	165
(1)–(5) added	3012	2.76	176

* (1) Companding; (2) Overdeviation (B_o = 48 MHz); (3) Group Delay Equalization; (4) 9-dB Peak Factor; and (5) Reduction of Multichannel Load Factor.

The criterion ordinarily used to determine the maximum transponder capacity for conventional, uncompanded FDM/FM traffic is the CCIR recommendation for channel noise. The CCIR recommends that the weighted signal-to-noise ratio of the entire link in the worst (top) baseband channel be 50 dB or greater, corresponding to 10,000 pWp of noise power. RCA Americom link budgets allocate to the space segment 8,000 pWp or less, corresponding to a weighted signal-to-noise ratio of 51 dB or greater between earth stations. Extensive experimental efforts had determined that a companded channel with an objective weighted signal-to-noise ratio of 35 dB is subjectively perceived to be equivalent in quality to an uncompanded channel with a weighted signal-to-noise ratio of 51 dB.

3.1 Description of Tests

3.1.1 Noise Power Ratio (NPR)

To determine the weighted signal-to-noise ratio in the top baseband channel as a function of the number of channels, noise power ratio (NPR) tests were used. NPR is the ratio in dB of the total noise level in a desired channel with the entire baseband fully loaded to the noise level in the desired channel with all of the baseband fully loaded except the desired channel. In the NPR test, multichannel FDM/FM traffic is simulated by a continuous, uniform (white noise) frequency spectrum produced by a white noise generator. High-pass and low-pass filters are used to shape the spectrum to simulate a specific number of baseband channels. The noise power density at the output of the noise generator is adjusted to a level corresponding to the multichannel loading. The full baseband noise spectrum is then applied to the satellite carrier.

The NPR test has two steps. First, the narrow-band noise receiver is tuned to a 3-kHz baseband test slot in the frequency band produced by the noise generator. This procedure determines the frequency location in the baseband at which the NPR will be determined. The output from the unit under test is received by the noise receiver of the white noise test set, and the received signal level is adjusted by a reference set control to indicate a relative level of 0 dB on the meter on the front of the noise receiver. This procedure establishes the zero NPR level and calibrates the receiver to read NPR directly in dB.

In the second step, selected baseband channels are "turned off" by means of a band-stop filter. The center frequency of this band-stop filter is the same as the frequency of the test slot to which the noise receiver was first tuned. The received signal level is then adjusted by a variable attenuator to give the same meter reading as in the first step above. The

NPR of the unit under test is the difference in dB between the attenuator readings in the first and second steps.

The configuration of equipment for this test is shown in the block diagram of Fig. 7. Two channel loadings were tested: 2352 channels and 2892 channels. NPR tests were made of these channel capacities for several different sets of transmission parameters, which are shown in Table 7. The test frequency slots used in the 2352 channel loading test were: 16 kHz, 3886 kHz, 5340 kHz, 7600 kHz, and 9624 kHz. The test frequency slots used in the 2892-channel-loading test were the same as for the 2352-channel test, plus, with a view towards determining noise throughout the baseband, a slot at 11700 kHz.

For uncompanded operation the objective signal-to-noise ratio is related to NPR by[10]

$$S/N = \text{NPR} + 10 \log \frac{(\text{BW})_B}{3.1} - L + W,$$

where

S/N = weighted signal-to-noise ratio for a 0 dBm0 test tone
$(\text{BW})_B$ = bandwidth of composite baseband signal in kHz
L = multichannel load factor:
= $-15 + 10 \log n$ for $n \geq 240$
= $-1 + 4 \log n$ for $n < 240$
W = weighting factor in dB
= 2.5 dB for psophometric weighting

For loadings of 2352 uncompanded channels and 2892 uncompanded channels,

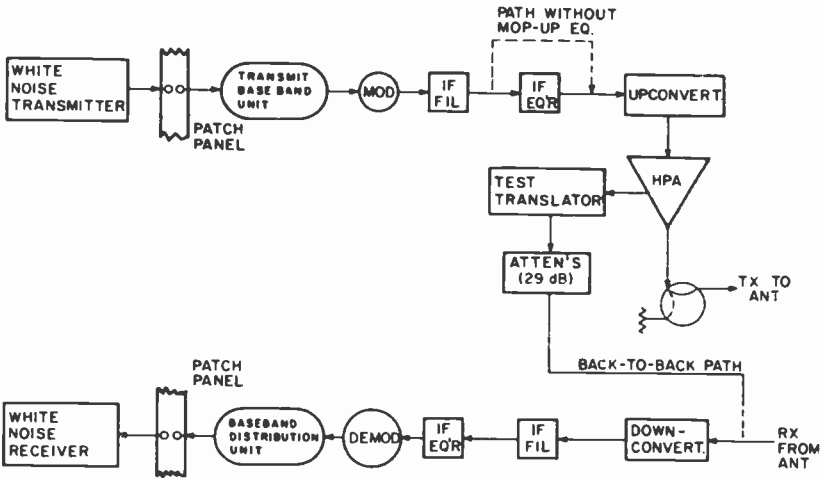

Fig. 7—Block diagram of NPR and BINR tests.

Table 7—Transmission Parameters for White-Noise Load Test of Companded Channels at Vernon Valley Earth Station

Case No.	Number of Channels	Top Baseband Frequency F_{mt} (kHz)	RMS Deviation for 0 dBm0 Test Tone Δf_{rms} (kHz)	Multichannel RMS Deviation ΔF_{rms} (kHz)	Multichannel Peak Deviation ΔF_{pk} (kHz)	Occupied Bandwidth B_o (MHz)	Allocated Bandwidth B_a (MHz)	Required C/N in B_a for 8000 pWp C/N (dB)	Test Tone Frequency = 0.608 F_{mt} (kHz)	Bessel-Null Test Tone Level (dBm0)	Average Talker Power P_{AV} (dBm0)	White Noise Loading Level L_N (dBm0)	Peak Factor (dB)
1	2352	10164	2029.325	4375.324	13836	48.0	36.0	17.84	6180.0	14.28	−15.0	6.71	10.0
2	2352	10164	2265.536	3475.332	10989	42.3	36.0	16.89	6180.0	13.33	−21.0	3.71	10.0
3	2892	12388	1535.920	3672.037	11612	48.0	36.0	21.98	7531.9	18.42	−15.0	7.61	10.0
4	2892	12388	2422.714	4120.068	11612	48.0	36.0	18.02	7531.9	14.46	−21.0	4.61	9.0

$$S/N = \text{NPR} + 19.0 \text{ dB}.$$

In baseband companding is employed in each channel, the objective signal-to-noise ratio is given by[11]

$$S/N = \text{NPR} + 15.0 \text{ dB}.$$

Addition of the 16-dB gross companding advantage gives the subjectively perceived weighted signal-to-noise ratio for 0 dBm0:

$$S/N = \text{NPR} + 31.0 \text{ dB for } P_{AV} = -15 \text{ dBm0}.$$

If the average talker power is reduced to −21 dBm0, the subjective signal-to-noise ratio improves by an additional 3 dB and

$$S/N = \text{NPR} + 34.0 \text{ dB for } P_{AV} = -21 \text{ dBm0}.$$

3.1.2 Baseband Intrinsic Noise Ratio (BINR)

The baseband intrinsic noise ratio is the ratio in dB of the noise in a test channel with the baseband fully loaded to the noise in that test channel with all noise loading removed. BINR is a measure of the thermal noise in the channel. The difference between NPR and BINR is a measure of the noise due to intermodulation distortion and crosstalk.

The equipment used in the BINR test and its configuration are the same as in the NPR test described above. The BINR test is performed in two steps. The noise spectrum of the noise generator is adjusted to simulate the bandwidth and power of a selected multichannel FDM/FM loading and is applied to the FM modulator. The received signal level is adjusted by the reference set control to indicate a relative level of 0 dB on the meter.

In the second step, the noise output of the noise generator is turned off, and the received signal level is adjusted by the variable attenuator to give the same meter reading as in the first step. The baseband intrinsic noise ratio of the unit under test is the difference in dB between the attenuator readings in the first and second steps. The configuration of the equipment for this test is also shown in the block diagram of Fig. 7.

At each test point, both BINR and NPR measurements were made.

3.2 Test Results

Results of the NPR and BINR tests are shown in Figs. 8 through 13. The NPR and BINR of Transponder 16 for 2352 channel loading are plotted versus baseband frequency in Fig. 8. As can be seen, the minimum NPR for 2352 channel loading, which occurs at the top baseband test slot frequency, is 21.0 dB. Fig. 9 shows plots of NPR and BINR versus ba-

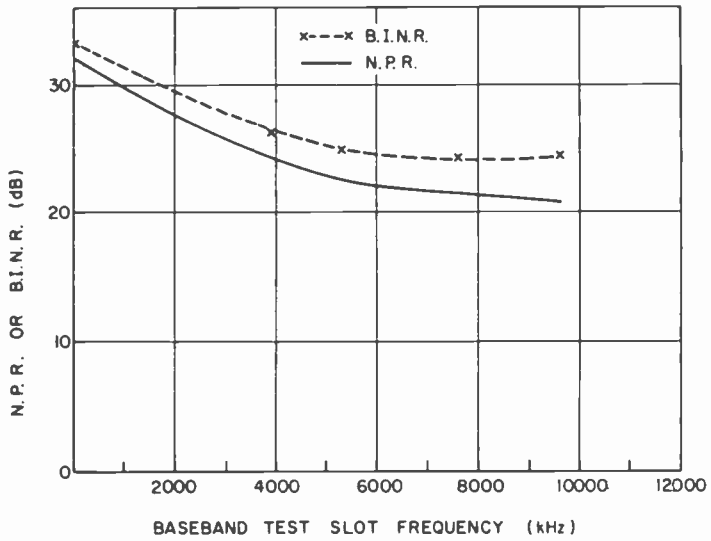

Fig. 8—Comparison of NPR and BINR of transponder 16: 2352-channel loading, measured with group delay equalization, Vernon Valley to Vernon Valley loopback link.

seband frequency for the case in which the average power per channel has been assumed to be −21 dBm0 instead of −15 dBm0 as in Fig. 8. As shown, use of transmission parameters derived under the assumption of lower average power per channel results in an improvement of signal-to-noise ratio as predicted. Fig. 9 shows that the minimum NPR for 2352 channel loading, which occurs at the top baseband test slot frequency, is 21.5 dB.

The NPR and BINR of Transponder 16 for 2892 channel loading are plotted versus baseband frequency in Fig. 10. The minimum NPR for 2892 companded channel loading, measured at a baseband test slot frequency of 11700 kHz, is 18 dB, corresponding to an objective weighted signal-to-noise ratio of 33.0 dB. For the parameters employed in RCA Americom's companded transmission systems, this objective signal-to-noise ratio would be perceived as equivalent to an uncompanded system with a signal-to-noise ratio of 49.0 dB.

Fig. 11 shows the effect of uplink i-f group delay equalization on NPR for a loading of 2892 companded channels. Use of the i-f group-delay equalizer results in a minimum improvement of 0.5 dB at the lowest test frequency and an improvement of 1.75 dB at the top frequency slot. The equalizer employed consisted of five sections, each section having a parabolic group delay coefficient of 0.02 ns/(MHz)^2, for a total of 0.10 ns/(MHz)^2, or a delay of 32.2 ns across the nominal transponder bandwidth of 36 MHz. This equalizer was used to compensate for spacecraft filter nonlinearities.

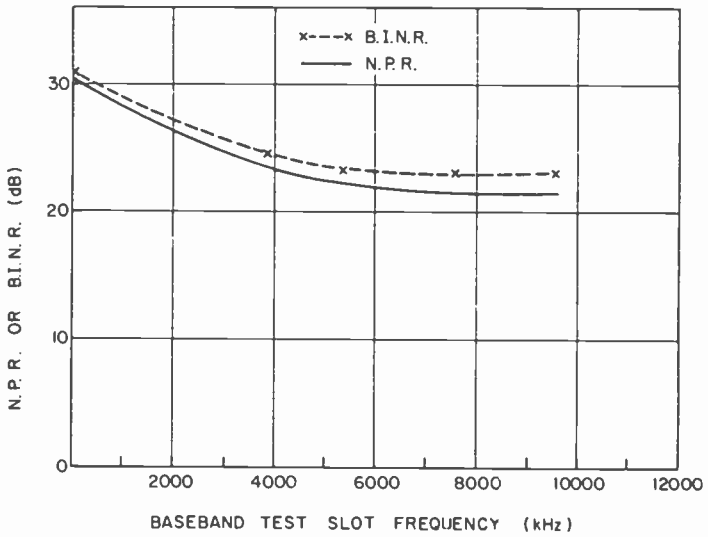

Fig. 9—Comparison of NPR and BINR of transponder 16: 2352-channel loading, measured with group delay equalization and reduced channel power, Vernon Valley to Vernon Valley loopback link.

In an effort to maximize NPR and, therefore, transponder capacity, 2892-channel pre- and de-emphasis networks were designed with advantages different from the conventional 4 dB recommended by the CCIR. Fig. 12 compares NPR's for 2892-channel loading measured with a 4-dB pre-emphasis network and a network with a nominal 6-dB pre-emphasis advantage. Use of 6-dB pre-emphasis advantage improves the NPR in the critical top frequency slot by 0.5 dB. The NPR in the lowest baseband slot is reduced by 5 dB through the use of this 6-dB pre-emphasis advantage. However, as may be seen from Fig. 12, NPR performance in the top test frequency slot remains the limiting case. Fig. 13 compares NPR performance for 2892-channel loading for 5-dB pre-emphasis advantage and 6-dB pre-emphasis advantage. Figs. 12 and 13 show that the greatest improvement of NPR performance thus far obtained is 0.5 dB, for a nominal 6-dB pre-emphasis advantage. Analysis of pre-emphasis advantages greater than 4 dB is being continued in an effort to increase NPR and thus increase transponder capacity.

Table 8 presents the system noise power ratio at the top baseband test slot frequency for Transponder 16 for loadings of 2352 and 2892 companded channels. In the table, each NPR is converted to an objective signal-to-noise ratio, the equivalent subjective signal-to-noise ratio, and the value of pWp corresponding to this equivalent ratio. From Table 8 it can be concluded that a transponder capacity of 2892 channels can be

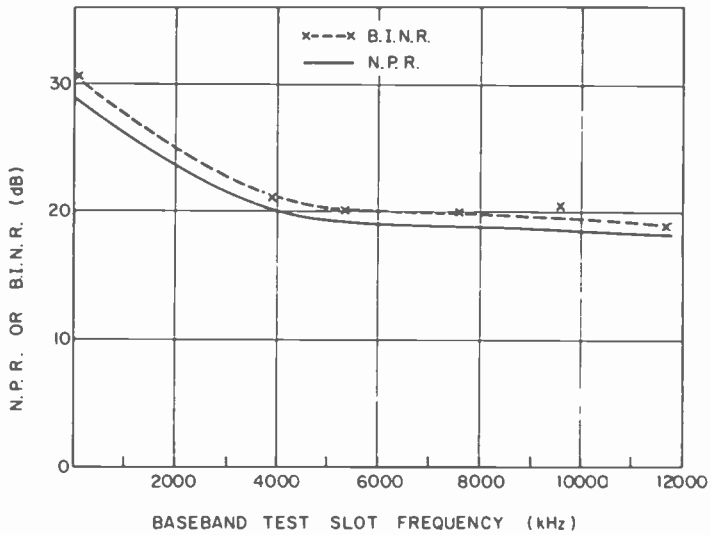

Fig. 10—Comparison of NPR and BINR of transponder 16: 2892-channel loading, measured with group delay equalization, Vernon Valley to Vernon Valley loopback link.

achieved with a margin of 1.0 dB above the specification requirement of 51.0 dB subjective signal-to-noise ratio. This capacity was achieved through the use of the capacity expansion techniques of companding,

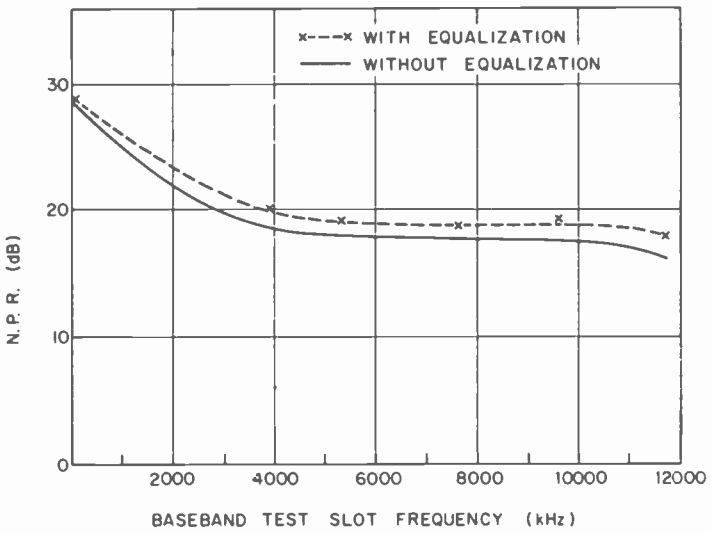

Fig. 11—NPR without and with equalization of transponder 16: 2892-channel loading, Vernon Valley to Vernon Valley loopback link.

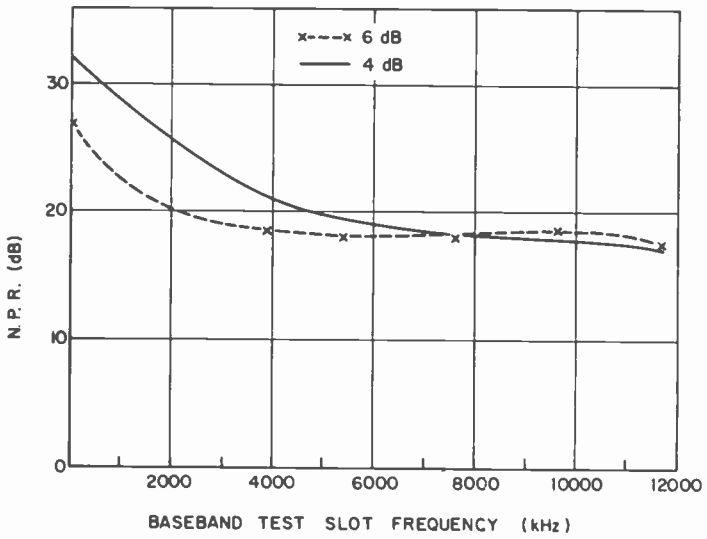

Fig. 12—NPR of transponder 16 with 4-dB and with 6-dB pre-emphasis advantage: 2892-channel loading, Vernon Valley to Vernon Valley loopback link.

Table 8—System Noise Power Ratio at Top Baseband Test Slot Frequency for Transponder 16 of Satcom F1 Satellite (Companding, Overdeviation, and Group Delay Equalization Employed)

Operational Mode	NPR (dB)	Objective S/N (dB)	Subjective S/N (dB)	pWp
2352 Companded Channels 4-dB PDI P_{AV} = −15 dBm0	21.0	36.0	52.0	6310
2352 Companded Channels 4-dB PDI P_{AV} = −21 dBm0	21.5	39.5	55.5	2818
2892 Companded Channels 6-dB PDI P_{AV} = −15 dBm0 P.F. = 10 dB	18.0	33.0	49.0	12589
2892 Companded Channels 6-dB PDI P_{AV} = −21 dBm0 P.F. = 9 dB	18.0	36.0	52.0	6310

overdeviation, group delay equalization, non-standard pre- and de-emphasis characteristics, reduction of peaking factor, and the use of an average talker power per channel of −21 dBm0. As indicated in Sec. 2.3, experimental measurements have indicated an actual average talker power per channel in the range between −22.3 dBm0 and −19.6 dBm0.

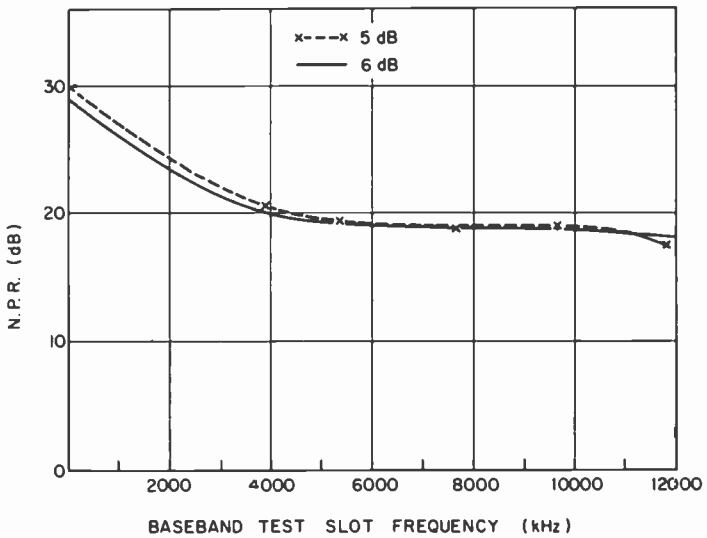

Fig. 13—NPR of transponder 16 with 5-dB and with 6-dB pre-emphasis advantage: 2892-channel loading, group delay equalization, Vernon Valley to Vernon Valley loopback link.

3.3 Atlanta Earth Station Tests

Upon conclusion of the loopback tests at the Vernon Valley Earth Station, the test results were analyzed. It was concluded that the experimental results obtained were in very close agreement with results predicted by the theoretical model and that transponder channel capacity could be further expanded through the use of more nearly optimum transmission parameters. These recommended new parameters are shown in Table 9 as Cases 3 and 4 for $P_{AV} = -15$ dBm0 and -21 dBm0, respectively.

A second series of transponder capacity tests were performed, at RCA Americom's Atlanta Earth Station. Uplink signals were transmitted by the 10-meter antenna in Transponder 23 of the Satcom F1 satellite. Downlink signals from the satellite were received by the same antenna. The companded FDM/FM transmission parameters employed during the tests are listed in Table 9.

Table 10 presents the system noise power ratio measured at the top baseband test slot frequency for Transponder 23 for a loading of 2892 companded channels. In the table, each NPR is converted to an objective signal-to-noise ratio, the equivalent subjective signal-to-noise ratio, and the value of pWp corresponding to this equivalent ratio. From Table 10 it can be concluded that a capacity of 2892 companded FDM/FM

Table 9—Transmission Parameters for White-Noise Load Test of Companded Channels at Atlanta Earth Station

Case No.	RMS Deviation for 0dBm0 Δf_{rms} (kHz)	Multichannel RMS Deviation ΔF_{rms} (kHz)	Multichannel Peak Deviation ΔF_{pk} (kHz)	Occupied Bandwidth B_o (MHz)	Allocated Bandwidth B_a (MHz)	Required C/N in B_a for 8000 pWp C/N (dB)	Test Tone Frequency = 0.608 F_{mt} (kHz)	Bessel-Null Test Tone Level (dBm0)	Average Talker Power P_{AV} (dBm0)	White Noise Loading Level (dBm0)	Peak Factor (dB)
1	1535.920	3672.037	11612	48.0	36.0	21.98	7531.9	18.42	−15.0	7.61	10.0
2	2422.714	4120.068	11612	48.0	36.0	18.02	7531.9	14.46	−21.0	4.61	9.0
3	2274.082	5186.880	16402	57.6	36.0	18.57	7531.9	15.01	−15.0	7.61	10.0
4	3299.996	5611.945	17745	60.3	36.0	15.34	7531.9	11.78	−21.0	4.61	10.0

Table 10—System Noise Power Ratio at Top Baseband Test Slot Frequency for Transponder 23 of Satcom F1 Satellite: 2892-Channel Loading (Companding, Overdeviation, and Group Delay Equalization Employed)

Operational Mode	NPR (dB)	Objective S/N (dB)	Subjective S/N (dB)	pWp
Case 1, Table 9 4-dB PDI $P_{AV} = -15$ dBm0	17.5	32.5	48.5	14125
Case 2, Table 9 4-dB PDI $P_{AV} = -21$ dBm0 P.F. = 9 dB	18.0	36.0	52.0	6310
Case 3, Table 9 4-dB PDI $P_{AV} = -15$ dBm0	18.4	33.4	49.4	11482
Case 4, Table 9 4-dB PDI $P_{AV} = -21$ dBm0	18.1	36.1	52.1	8166

channels can be achieved with a subjective signal-to-noise ratio of 49.4 dB for operation with the conventional talker power of −15 dBm0. For a more realistic value of average talker power of −21 dBm0, a capacity of 2892 companded FDM/FM channels can be achieved with a margin of 1.1 dB above the objective of 51.0 dB.

Fig. 14 shows the NPR and BINR of Transponder 23 for 2892 channel loading as a function of baseband frequency. Transmission parameters employed are those shown in Table 9, Case 3. As can be seen, the minimum NPR for 2892 channel loading, which occurs at the top baseband

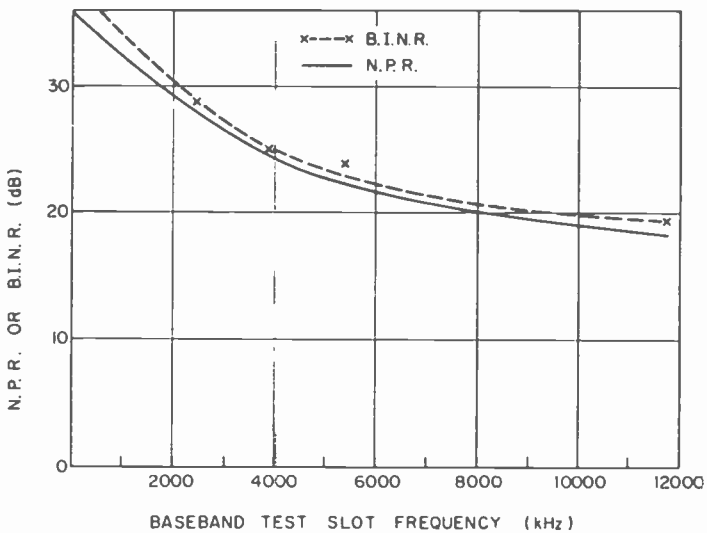

Fig. 14—NPR and BINR of transponder 23: 2892-channel loading, group delay equalization, Atlanta to Atlanta loopback link.

test slot frequency, is 18.4 dB. This value of NPR corresponds to an objective signal-to-noise ratio of 33.4 dB and a subjective S/N of 49.4 dB.

Fig. 15 shows the effect of the uplink i-f group delay equalization on NPR for a loading of 2892 companded channels. Use of the i-f equalizer results in an improvement of 2.4 dB at the top frequency slot. The i-f group delay equalizer employed a linear coefficient of −0.25 ns/MHz and a parabolic coeffcient of 0.03125 ns/(MHz)^2, resulting in total delays across the nominal transponder bandwidth of 36 MHz of 9.0 ns and 10.125 ns, respectively.

4. Comparison of Predicted Values and Test Results

During the transponder channel capacity tests at the Atlanta Earth Station, a system carrier-to-noise ratio of 19.6 dB was measured in an i-f bandwidth of 36 MHz at the input to the demodulator. Table 11 compares, for a C/N of 19.6 dB, the predicted and measured values of signal-to-noise ratio in a transponder loaded with 2892 companded channels. Predictions are shown for several values of multichannel RMS deviation, ΔF_{rms}. The predicted values of S/N were derived from a mathematical model developed at RCA's Princeton Laboratories.

It can be seen from Table 11 that there is excellent agreement between predicted and experimental values, the difference being less than 0.2 dB

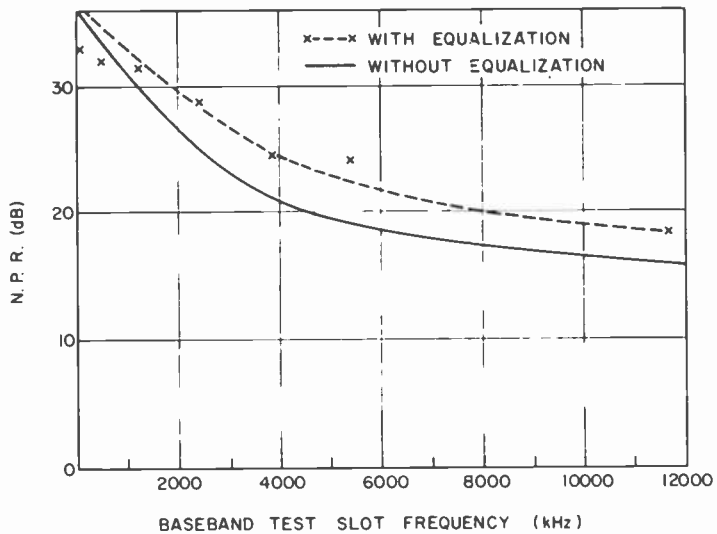

Fig. 15—NPR of transponder 23 without and with equalization: 2892-channel loading, Atlanta to Atlanta loopback link.

Table 11—Comparison of Predicted and Measured Values of S/N: Channel Capacity Tests at Atlanta Earth Station, Transponder Loading = 2892 Channels, C/N = 19.6 dB

Table 9 Case No.	ΔF_{rms} (kHz)	Signal-to-Noise Ratio	
		Predicted (dB)	Measured (dB)
1	3672.037	48.34	48.50
2	4120.068	52.11	52.00
4	5611.945	53.41	52.10

except for Case 4, for which the difference is 1.3 dB. The transmission parameters for Cases 1 and 2 were developed subject to the constraint that the ratio of signal to distortion noise caused by overdeviation, $(S/N)_D$, be 6 dB greater than (S/N). This constraint was not used in the derivation of parameters for Case 4, and the prediction for this case, therefore, is inherently less precise than for the others. The analytic model employed tends to break down and lose predictive accuracy for signal-to-distortion noise ratios less than 6 dB greater than (S/N).

5. Conclusion

Tests performed at the Vernon Valley and Atlanta Earth Stations have demonstrated that, by use of several capacity expansion techniques, 2892 FDM/FM channels can be successfully transmitted through a single transponder of RCA's Satcom satellite. During the tests, the subjectively perceived signal-to-noise ratio in the top baseband channel satisfied RCA Americom's standard criterion of 51.0 dB. The techniques employed were companding, overdeviation, reduction of multichannel load factor, group delay equalization, reduction of peak factor, and use of nonstandard pre- and de-emphasis. A transponder capacity of 2892 channels is 2.7 times the capacity in the baseline situation (1092 channels) in which no expansion techniques are employed. Further, there is evidence that by extension and refinement of the capacity expansion techniques described, still greater capacities, possibly as great as 3012 channels, can be achieved.

The tests also established the validity and predictive accuracy of the analytical model of FDM/FM channel capacity.

Acknowledgments

The authors wish to thank L. Schiff of RCA Laboratories for many helpful discussions and suggestions. The authors also wish to thank K. Jonnalagadda of RCA Laboratories for his cooperation and for invaluable contributions in the analysis of experimental results and in selection of

transmission parameters. We wish also to express our appreciation to the technical staff of RCA Americom's Vernon Valley and Atlanta Earth Stations for their assistance in this program.

References:

[1] K. Jonnalagadda, "Syllabic Companding and Voice Capacity of a Transponder," *RCA Review*, **41**, p. 275, Sept. 1980 (this issue).

[2] K. Jonnalagadda, private communication.

[3] *CCITT Orange Book*, Vol. III-1 (1977), Recommendation G-223, p. 133.

[4] CCIR, Vol. IV (1974), Report 211-3, pp. 113–136.

[5] See Ref. [3], Recommendation G-223, Para. 2.1, p. 135.

[6] W. C. Ahern, F. P. Duffy, and J. A. Maher, "Speech Signal Power in the Switched Message Network," *Bell, System Tech. J.*, **57**, p. 2695, Sept. 1978.

[7] Petition for Rulemaking Before the Federal Communications Commission, page 5, Submitted the American Telephone and Telegraph Co., March 12, 1980.

[8] G. J. Garrison, "Intermodulation Distortion in Frequency-Division-Multiplex FM Systems—A Tutorial Summary," *IEEE Trans. Communications Tech.*, **COM-16**, No. 2, p. 292, April 1968.

[9] D. H. Hamsher, Editor, *Communication System Engineering Handbook*, p. 16-15, McGraw-Hill Book Co., N.Y. (1967).

[10] M. J. Tant, *The White Noise Book*, p. 55, White Crescent Press, Ltd., Luton, England (1974).

[11] K. Jonalagadda and L. Schiff, private communication.

Capacity of Fixed-Assigned Versus Demand-Assigned SCPC Systems with Power-Limited Transponders

L. Schiff

RCA Laboratories, Princeton, NJ 08540

Abstract—Single channel per carrier satellite systems for thin route service can be operated in the demand-assigned (DA) mode or the fixed-assigned (FA) central station mode. This paper compares the traffic carrying capabilities of these systems when operated on a power limited transponder. It is shown that while the relative efficiency (as measured by the capacity of the FA system divided by the capacity of the DA system) is always less than one, the efficiency increases monotonically as a function of thin route station traffic. At the point where station traffic per trunk becomes larger than the ratio of power-limited capacity to bandwidth-limited capacity, the relative efficiency is essentially as large as it can be. This maximum efficiency depends on the percentage of double-hop calls in the FA system and is close to one when the percentage of such calls is close to zero.

1. Introduction

Single channel per carrier (SCPC) operation is well suited for thin route satellite telephony service. Each transmit voice channel modulates its own carrier, and two such carriers are used to make up a full duplex conversation. If the transponder is bandwidth limited the maximum number of carriers that can be used (including the effects of voice activated switching of the carrier, VOX) is simply the transponder bandwidth divided by the nominal carrier bandwidth (including guard bands). The number of full duplex channels, C, is half that amount. If the transponder is power limited, only $C^* \leq C$ full duplex channel can be

used. In reality, it is not the transponder that is power limited but rather the system. If earth stations with lower G/T's are used, more power is needed per carrier and fewer carriers can be accommodated per transponder. Hence a power limited operation is simply a way of trading lower earth station cost for higher space segment cost.

There are two basic methods of operating an SCPC system—demand assigned (DA) and fixed assigned (FA). The DA method of operation is typified by the SPADE system.[1] Each earth station has one or more modulator and demodulator that can be retuned on command and can use any channel not already in use. Hence the channels in a transponder form a common pool of "trunks" that any pair of earth stations can use to set up a call in an on-demand basis. In the FA method of operation, a subset of the channels are permanently assigned between a pair of earth stations. Modulators and demodulators are not tunable and that set of channels can only be used for calls between those stations. Fixed assigned plans are usually coupled with a "central station" concept and we shall restrict our attention to such a system. In this kind of plan one of the earth stations is the central station. The other stations are provided only with a trunk group or call path to the central station. The central station also has switching apparatus associated with it that can provide the switching function of a toll office for the outlying earth station. Hence, calls between the outlying stations are double hop and proceed over one trunk group into the central station and are routed out over the trunk group to the other outlying station via the switching equipment associated with the central station. Such a system can be effective when the outlying stations serve sparsely populated regions and the central station is located at an existing traffic hub or commercial center. Outlying stations can then be tied into the pre-existing telecommunication net of the area. It is often true that in such situations very little of the calling is from outlying station to outlying station. Most of the calling from an outlying station is to the central station or points that can be reached terrestrially from the central station. The bush telephone system in the state of Alaska is an example of such a system, with an Anchorage-serving earth station being the central station.

From the point of view of space-segment efficiency, the advantages of DA over FA have long been appreciated for a bandwidth-limited transponder. In the first place all calls between outlying stations tie up two full duplex channels in the FA case, but only one in the DA case. This synthetic increase in traffic in the FA case is fundamental but is only a small disadvantage if most calling is single hop.* The second difficulty is more fundamental, however. In the FA mode the available number

* There is a loss in quality for a double hop call as well, but we shall neglect this effect here.

of circuits, C, is subdivided into a large number of small trunk groups. The sum of all the trunks adds up to C but, as is well-known, this type of arrangement carries much lower traffic for a fixed blocking probability or grade of service.

It might seem that in the power-limited case things would be much the same. And, indeed, the first drawback mentioned above for FA is not changed. However, the second difficulty is not as strong a drawback in the power-limited situation as it is in the bandwidth-limited situation. In the DA case there are C^* channels, and the traffic (in erlangs) that this common pool trunk group handles, at reasonable blocking probabilities, is close to C^* if C^* is large. In the FA case, however, when all C^* circuits are assigned to many small trunk groups, the traffic is low compared to C^*. For that very reason, one can assign more than the C^* trunks and still have the average number of circuits in use less than C^*. In fact, one should keep assigning more trunks until either the total equals C or the probability of more than C^* being in use simultaneously exceeds some small number (whichever occurs first). As will be shown, using this technique on a power limited transponder can provide almost as efficient a service for FA as for DA mode as long as calling between outlying stations is small.

2. Model and Analysis

For simplicity, we assume that all outlying earth stations are identical. Each has a traffic, a', in erlangs and the fraction of its traffic to all other outlying stations (i.e., not to the central station) is ξ. The transponder is power limited to $C^* \leq C$ channels where C is the bandwidth-limited number of channels. We will compare the traffic capacity of a DA and FA system by computing the number, N_1, of such stations that can be allowed on the transponder in the DA mode and the number, N_2, of such stations that can be allowed in the FA mode. The comparison will be made with the constraint that calls in both systems have the same blocking probability P_b. As will be seen, there is some difficulty with this in that the peculiarities of each type of system do not lead to exact equality, but the comparison will be a fair one.

2.1 DA Case

Calls in a DA system actually have three distinct sources of blocking:

(a) failure to secure a channel unit at the initiating end†
(b) failure to secure a channel unit at the terminating end†
(c) failure to secure a circuit in the transponder.

† Each modem or channel unit is directly connected to a trunk coming from the switching equipment which the earth station serves. Hence failure to secure a trunk is identical with failure to secure the channel unit.

While (a) and (b) can be viewed as part of normal trunk group traffic engineering, the desired result is that the composite blocking be P_b. Hence blocking due to source (c) should be less than P_b. We make the assumption that is most *optimistic* for a DA system (i.e., results in N_1 being largest), namely, that sources (a) and (b) can be neglected and blocking due to satellite blocking is P_b.

By definition, a' is the traffic that would be carried by the trunk group connecting each outlying earth station with its local central office in the absence of blocking. And this is the traffic that would be used to calculate the proper size of that trunk group. However, a' is not the contribution of traffic to the pool of satellite circuits made by each outlying station unless $\xi = 0$. Calls between outlying stations are part of the traffic a' at each station, but only appear as a demand for one circuit to the satellite pool of circuits. Hence the contribution to total offered traffic to the satellite pool made by each outlying station is a, where

$$a = a'\left(1 - \frac{\xi}{2}\right). \tag{1}$$

Therefore, the total traffic offered to the DA pool by N_1 outlying stations is A, where

$$A = N_1 a. \tag{2}$$

The largest value that N_1 can assume is the value that produces an A such that

$$B(C^*,A) = P_b, \tag{3}$$

where $B(x,y)$ is the erlang B loss function[2]

$$B(x,y) = \frac{y^x/x!}{\sum_{i=0}^{x} (y^i/i!)}. \tag{4}$$

In other words, the largest value for A is calculated from Eq. [3] and N_1 is determined from Eq. [2].

2.2 FA Case

In the FA case each trunk at an outlying station terminates in an SCPC channel unit that corresponds to an SCPC satellite channel which has a matching channel unit and trunk at the central station. Hence determining the number of satellite circuits per outlying earth station is synonymous with trunk engineering at the outlying central office. The

traffic carried by this trunk group is a'. The number of channels units c is given by

$$B(c,a') = P_b. \quad [5]$$

Because the arguments of the erlang B function are much smaller than in Eq. [3], the discrete nature of c becomes important. Eq. [5] should be interpreted as finding the smallest integer c that reduces the RHS to below the value P_b. It must be recognized that while calls between outlying and central station have the same blocking probability as in the DA case, calls between outlying stations have blocking probability approximately $2P_b$ (assuming independence† and that P_b is small) because of the double hop. This is one of the ways in which grade of service is not quite identical in the DA case.

A naive way of determining N_2, the maximum number of stations in the FA, would be to set $N_2 = C^*/c$ (i.e., only assign C^* total circuits). This would result in an average number of circuits active far less than C^* and not effectively use the transponder. The number of circuits active in any trunk group of c circuits is a random variable with mean E (the average traffic carried = $a'(1 - P_b)$) and variance V. Since the total number of active circuits (a random variable) is the sum of N_2 identically distributed, essentially independent, random variables, the distribution of the number of active circuits is approximately normal with mean N_2E and variance N_2V. Hence the maximum value of N_2 is set by the constraint

$$N_2E + r\sqrt{N_2V} \leq C^*, \quad [6]$$

This assumes that the mean plus r standard deviation of the total traffic random variable is less than C^* and, hence, that the total number of circuits in use exceeds C^* with probability less than $Q(r)$, where

$$Q(r) = (2\pi)^{-1/2} \int_r^\infty e^{-t^2/2} dt.$$

In calculating numerical values, we will use $r = 2.33$, which makes the above probability 0.01. It is important to realize that nothing catastrophic happens when C^* is exceeded. The SNR of received signals will degrade for all channels, but as long as the probability is sufficiently low, we assume the result to be tolerable. Again this is a case where the service provided by the FA system is different than in the DA case, but if 0.01 is deemed too high, lower values of probability (higher r) can be used. The qualitative conclusions reached will still be the same.

Eq. [6] is one constraint N_2 must obey. The other is, of course,

$$N_2c \leq C. \quad [7]$$

† Since only a very small fraction of the traffic of any outlying station trunk group is due to the traffic of any other outlying station trunk group, virtual independence is assured.

3. Comparison of Capacity

The calculations above demonstrate the respective capacities of a DA and FA system operated through the same power limited transponder. A direct comparison is simply the quotient N_2/N_1. Using Eqs. [2] and [6] for N_1 and N_2 and substituting Eq. [1] gives

$$\frac{N_2}{N_1} \leq \frac{a'}{c}\left(1 - \frac{\xi}{2}\right)\frac{C}{C^*}\frac{C^*}{A}. \qquad [8]$$

On the other hand if Eq. [6] is rewritten

$$r\sqrt{N_2 V} \leq C^* - N_2 E \qquad [9]$$

and if both sides are squared and the solution of the quadratic is found and only the negative-root solution is retained,‡ the result is

$$N_2 \leq \frac{C^*}{E} + \frac{r^2 V}{2E^2} - \sqrt{\frac{r^4 V^2}{4E^4} + \frac{r^2 V C^*}{E^3}}. \qquad [10]$$

Dividing N_2 by N_1 and using Eqs. [1] and [2], we have

$$\frac{N_2}{N_1} \leq \frac{C^*}{A}\frac{a'(1-\xi/2)}{E} + \frac{a'(1-\xi/2)r^2 V}{2AE^2}\left\{1 - \sqrt{1 + \frac{4EC^*}{r^2 V}}\right\}. \qquad [11]$$

Both inequalities [8] and [11] must be obeyed. As a' varies, we compute the c needed to produce P_b (or equivalently let c vary and find the a' that produces P_b) and use inequality [8] to compute one bound on N_2/N_1. From a' and c one can determine E and V and use inequality [11] to give another band. The quantity E is well known[3] to be $a'(1 - P_b)$ but V is more difficult and can only be calculated by integrating over the state probabilities of the erlang distribution. Because we are interested in values of P_b around 0.01, we will use an approximation that simplifies our calculation,

$$a' \approx E \approx V \qquad [12]$$

This expression says that the statistics of carried traffic and offered traffic are the same, or at least the first two moments are. Substituting Eq. [12] into [11] yields

$$\frac{N_2}{N_1} \leq (1 - \xi/2)\frac{C^* - r\sqrt{C^*}}{A}. \qquad [13]$$

Eqs. [8] and [13] establish the carrying capacity of the FA system relative to a DA system, since the equalities sign can be realized. One may think of C, C^*, and ξ as fixed parameters of the system. For large values

‡ The negative root corresponds to values of N_2 for which the RHS of Eq. [9] is large and negative.

of C^* (in the hundreds of channels), as would be encountered in practice, A is fairly close to C^*. Therefore, for small ξ, Eq. [13] puts a ceiling on N_2/N_1 fairly close to unity. Eq. (8) can be viewed as a monotonically increasing function of station size (neglecting the integer nature of c). Either a' or c can be viewed as the independent variable with the ratio a'/c monotonically increasing as either variable is increased using a fixed P_b. Fig. 1 plots N_2/N_1 as a function of c for $P_b = 0.01$, $\xi = 0$, $C = 600$, and $C^* = 600$, 450, 300, and 200. The results that come out of [13] are different horizontal line segments for the different values of C^*, but all appear to blend together as one line segment in Fig. 1. As can be seen from Eqs. [9] and [13], the curves for $\xi \neq 0$ would look the same except that the numerical value of N_2/N_1 would be reduced by a factor of $1 - (\xi/2)$. Note that for $C^* = C$ (the bandwidth limited case), even very large size stations (requiring tens of trunks to achieve a blocking probability of 0.01) will achieve efficiencies substantially less than unity even for $\xi = 0$. On the other hand for $C^* < C$, say $C^* = 200$, relatively modest stations requiring as little as 5 or 6 trunks, achieve over 90% of the DA capacity with a FA method of operation if ξ is close to zero. For higher values of ξ the capacity relative to a DA system must be scaled down by the factor $1 - (\xi/2)$. For the very smallest sized station, of course, the FA method of operation is very inefficient compared to DA.

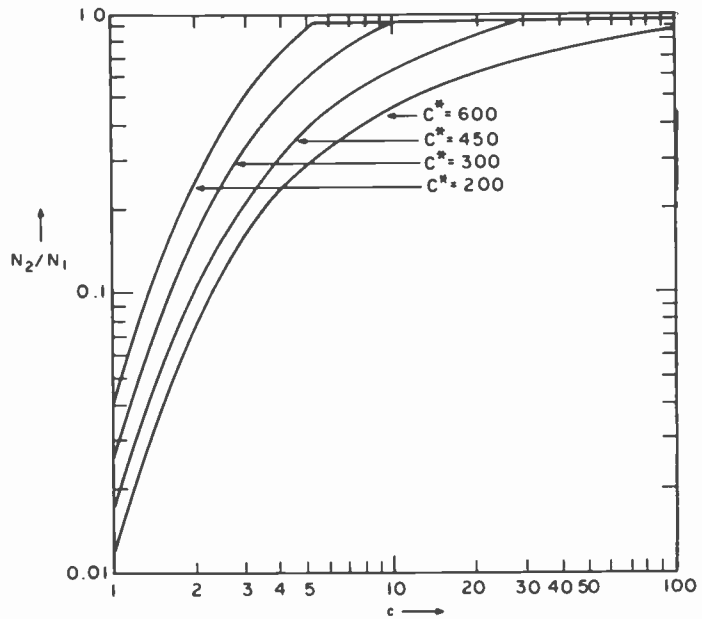

Fig. 1—Ratio of N_2/N_1 for $C = 600$, $\xi = 0$, and $P_b = 0.01$ as a function of c.

4. Summary and Conclusion

We have considered FA and DA systems and compared their carrying capacities. We have concluded that for C^* significantly less than C and small calling between outlying stations, an FA system can have almost the capacity of a DA system for earth stations of relatively modest traffic. The service offered in the two systems is not precisely the same in that

(a) the FA system has double hops when needed
(b) the blocking probabilities are not identical on all types of calls
(c) the FA system occasionally (with probability 0.01 in the busy hour) has more than C^* circuits off hook.

However, we believe that the comparison is a fair one and that subscribers would basically not perceive very much difference between the qualities of the two possible offerings.

We can summarize the results by setting the RHS of Eqs. [8] and [13] equal and making the additional approximation that $r\sqrt{C^*}$ is small compared to C^*. This gives a "rule of thumb" that if stations are large enough so that the average trunk loading a'/c is greater than C^*/C, an FA system is operating as efficiently as it can. Again roughly, that efficiency is $1 - (\xi/2)$ compared to a DA system operating with the same C^*.

There are two demurrers, however. The first is that in most practical situations the stations to be served all have different traffic intensities and each requires a different number of trunks to make the required grade of service. If one retraces the arguments made in the previous section, one finds that the critical ratio $a'/c(a')$ (explicitly writing c as a function of a') in Eq. [8] must be replaced by $\langle a' \rangle / \langle c(a') \rangle$. On the other hand if we compared this case with what we considered in the previous section, with each station having identical traffic equal to $\langle a' \rangle$, the RHS of Eq. [8] would depend on $\langle a' \rangle / c(\langle a' \rangle)$. Because of the convex upward behavior of $c(a')$, $c(\langle a' \rangle) \leq \langle c(a') \rangle$. Hence the value of N_2/N_1, for the case of each station having a different traffic with the average being $\langle a' \rangle$, is lower than for the case where the traffics at each station are the same and equal to $\langle a' \rangle$. Therefore, when there is significant spread on the sizes of the various stations, the results of the previous section can be somewhat optimistic in predicting FA system carrying capacity.

The second factor that must be mentioned involves intermodulation performance in a transponder using $C^* < C$ channels. McClure[4] has shown that in the bandwidth-limited case, one can achieve reduction in intermodulation by carefully choosing the frequencies as compared to taking the same number of carriers and choosing their frequencies at

random. In our FA case, where the curves of Fig. 1 are rising, all channels are assigned, while in the flat topped portion of the curve only a subset are assigned. In all cases, however, more channels are assigned than would be the case in the DA version. Hence in the DA system, one can choose the channels to minimize intermod, while for the FA system less gain can be obtained for such an optimization in the case of stations with large traffic and none at all for small stations (one is then in the rising portion of the curve) where frequency use is random. Because intermod plays a major role in determining C^*, the practical upshot of this is that the effective C^* for a DA system can be slightly larger than the C^* value for a FA system, and the smaller the traffic per earth station, the larger the discrepancy.

In conclusion, we wish to point out how the considerations we have made in this paper enter into the choice one makes in picking a FA or DA system for a thin route service. The considerations are based on total system cost, but the arguments we shall make are qualitative.

In Fig. 2 we plot cost as a function of C^*. The cost is broken into space segment cost and earth segment cost for both the FA and DA systems. For both FA and DA systems, we indicate that station cost is a rising function of C^*. This is a kind of backward way of looking at things in that the G/T of the station (which is a large determinant of station cost) fixes C^*, but we can interpret the effect as if we were choosing C^* lower, which allows for lower G/T and hence lower station cost. The cost of all stations for the DA case is shown as always higher than for the FA case. The argument goes that except for the extra logic and modem frequency retuneability in the DA station, it is the same as the FA station, and the

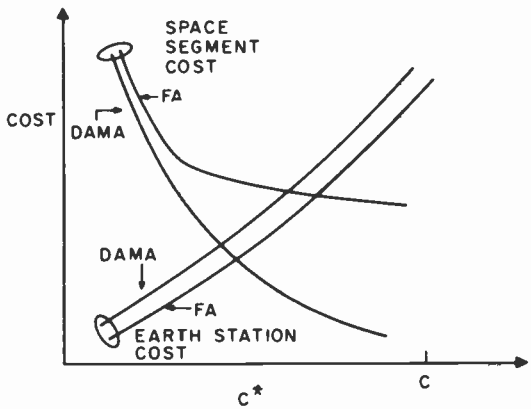

Fig. 2—Cost versus C^*. Both space segment and earth station costs are shown.

extra gear will cost something.† With respect to space segment costs, we take the point of view that as C^* increases, the carrying capacity per transponder increases. Hence the fixed capacity needed to be carried will either require a smaller fraction of a transponder or fewer transponders. In any case this translates to smaller space segment costs for the system under consideration. For small values of C^*, the space segment curve for the FA case is higher and parallel to the DA curve. For any given load, a', if C^* is low enough, the quantity N_2/N_1 is in the flat portion, and since the FA system carries a fixed fraction of the DA system, the FA curve tracks the DA curve. For high enough C^*, however, the value of N_2/N_1 will start to decrease rapidly as C^* increases (as can be seen in Fig. 1). While the space segment cost for FA operation continues to drop as C^* increases, it will not decrease as fast as the corresponding curve for DA operation.

The total cost of each type of system is the sum of space segment cost and earth station cost. Depending on the actual numbers, this total cost (for either system) may reach its minimum value for $C^* < C$ or $C^* = C$, and either system may have the lowest minimum.

References:

[1] J. G. Puente and A. M. Werth, "Demand-Assigned Service for the Intelsat Global Network," *IEEE Spectrum*, Jan. '71.

[2] T. Frankel, *Tables for Traffic Management and Design, Book 1—Trunking*, Lee's *ABC of the Telephone*, Geneva, Ill. (1976).

[3] R. I. Wilkinson, "Theories for Toll Traffic Engineering in the USA;" *Bell Syst. Tech. J.*, **35**, p. 421, March '56.

[4] R. B. McClure, "Analysis of Intermodulation Distortion in a FDMA Satellite Communications System with a Bandwidth Constraint," *Conference Record of ICC*, 1970, pp. 8–29.

† We have, however, neglected the costs of the switching equipment that would be needed in the FA case for calls between outlying stations. Also, in cases where the switch and the central earth station are not co-located, a backhaul transmission system is needed to connect them. This, too, is neglected.

Cancellation of Visible Color Crosstalk Between Two TV Signals By Use of Alternate Line Delay

Liston Abbott

RCA Laboratories, Princeton, NJ 08540

Abstract—One of the major problems encountered in transmitting two TV modulated carriers in a single satellite transponder is the resultant crosstalk between the two TV channels, caused by the transponder and bandpass filter nonlinearities. The visibility of this crosstalk has been eliminated by the development and implementation of a video processing scheme called Alternate Line Delay. The use of this equipment has enabled the implementation of two-TV-channel-per-transponder service between the "lower 48" and the State of Alaska, with a higher level of performance than had been achieved before.

1. Introduction

Starting in early 1976, RCA started a program of field experiments to determine the feasibility and practicality of transmitting two television channels in a single satellite transponder. Previous analysis[1] had shown that the expected picture quality could still be quite acceptable even to expert viewers, albeit not as good as conventional single-TV-per-transponder service. The initial field experiments confirmed most of the assumptions made in the analysis, but a significantly high level of crosstalk between the two TV channels was found. Subsequent field experiments were carried out to determine the nature of the mechanisms causing the crosstalk and to make parametric tradeoff studies to optimize the 2-for-1 TV service.[2]

It became evident that some special techniques or equipment had to be developed to eliminate the visible crosstalk in the TV pictures in order to make the two TV-channel-per-transponder service viable.

This paper discusses the nature of the mechanisms that cause the crosstalk, the nature and perceptibility of the crosstalk, laboratory simulation of the crosstalk, various approaches to eliminate it, and the development and performance of the Alternate Line Delay equipment used to eliminate the visible crosstalk in both television channels of the 2-for-1 transponder service implemented by RCA.

2. Mechanisms Causing Crosstalk

Crosstalk between two television channels is the result of the amplitude variations of one TV signal being impressed on to the signal in the other channel. This may be due to several causes, such as coupling or radiation between adjacent signal-carrying conductors, coupling across the source impedance of a common power supply, intermodulation due to passage through a nonlinear device, or amplitude modulation to phase modulation (AM/PM) conversion in some amplifying devices, e.g., the travelling-wave-tube amplifiers (TWTA) used in satellite and earth station equipment.

The major sources of crosstalk in a two-TV-channel-per-transponder service are the TWTA nonlinearities in the output versus input power relationship and the AM/PM conversion characteristics. Figs. 1 and 2 show these characteristics for a typical satellite transponder. Conventional single TV channel service using one constant-amplitude frequency-modulated carrier centered in the transponder channel is not adversely affected by these nonlinearities. However, when two independently modulated carriers, each offset from the center frequency of the transponder, are combined for the two-TV-channel-per-transponder service, the resulting signal through the transponder has considerable

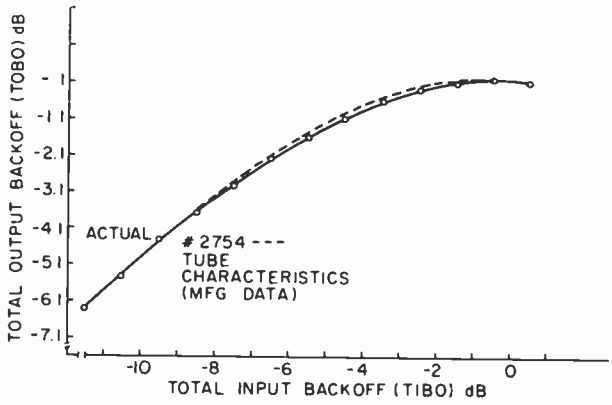

Fig. 1—Power out versus power in relationship for a typical satellite transponder.

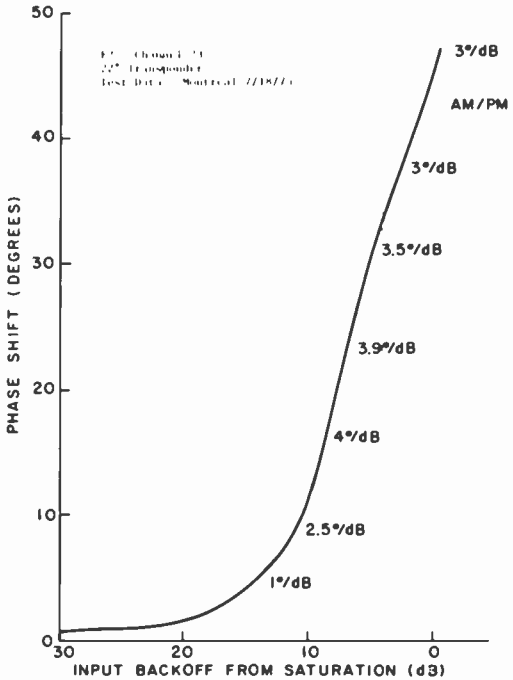

Fig. 2—Amplitude versus phase characteristics for a typical satellite transponder (F2—Channel 23, 22° Transponder, Test data—Montreal 7/18/75).

amplitude variations. The transponder nonlinearities then create inband intermodulation products, particularly the odd-order products such as 3rd and 5th order, and AM/PM conversion, that transfer some of the modulation from one TV channel to the other.

In addition, the frequency deviations of the rf carriers on to the slopes at the band edges of the bandpass and input mux filters cause amplitude variations of the signal through the transponder, and group delay distortion causes phase modulation of the composite rf signal. The effects of the parametric variations of carrier frequency offset and group delay equalization on the resulting amount of crosstalk are covered in another paper in this issue of *RCA Review*.[2]

3. Simulation of Crosstalk

Crosstalk identical to that encountered in a 2-for-1 satellite transmission system has been simulated in the laboratory, using a relatively simple linear device. Fig. 3 shows a block diagram of the crosstalk simulator. Each of the input video signals is pre-emphasized as for conventional

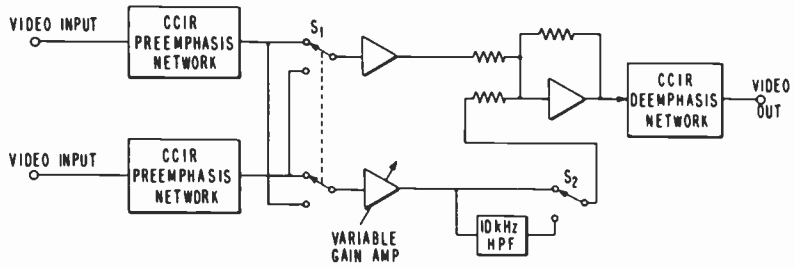

Fig. 3—Crosstalk simulator for two-TV-channel-per-transponder service.

FM carrier systems. Switch S_1 is used to select one of the inputs as the desired channel and the other input as the interfering channel. A variable gain amplifier is used to set the level of interference into the desired channel. The two signals are then passed through a summing amplifier and then a matching de-emphasis network. Switch S_2 is used to select full bandwidth interference or interference through a 10-kHz high-pass filter (HPF). The simulator provides unity overall gain to the desired signal and from 0 to 14% gain of the interfering channel. With the 10-kHz HPF switched out, the simulator has flat frequency response and linear phase characteristics. The high-pass filter is used in some tests to reduce the effects of low frequency interference when observations are made at levels of interference significantly higher than those encountered in the actual satellite transmission system. The simulator output signal as displayed on a waveform monitor and vectorscope as well as on a TV monitor exactly duplicated the results found in tests made on the actual satellite link.[2]

4. Display and Perception of Crosstalk

Both laboratory experiments and field tests of the two-TV-channels-per-transponder system using dual rf carriers showed that the resulting visible crosstalk was predominantly due to transfer of chrominance information from one TV channel to another. There was no perceptible crosstalk between black and white pictures. Reduction of the chrominance subcarrier level in the interfering TV channel produced a reduction in the amount of crosstalk after demodulation and before amplification at the receiver.[2] Amplification of the chrominance back to its correct level at the receiver also brought the color crosstalk in the TV picture back to its original level.

Color crosstalk may be analyzed as the summation of two vectors as shown in Fig. 4. Vector A is the desired color signal representing a given hue and saturation. Vector B_1 is the interfering color signal from the

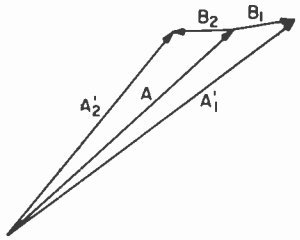

Fig. 4—Vector diagram of color signal with interference.

other TV channel. The relative amplitude of B_1 is exaggerated for this discussion. Vector A_1' is the summation of A and B_1 and represents the perceived hue and saturation in the TV picture. Since the color subcarrier frequency of an NTSC video signal must meet FCC specifications of 3579545 ± 10 Hz, the two subcarrier frequencies may differ by as much as 20 Hz. Vector B_2 of Fig. 4 represents the same interfering signal as B_1, but at another instant in time. Vector A_2', therefore, represents the perceived hue and saturation of the desired color signal at the second instant in time.

Vector B over a period of time appears to rotate about the tip of Vector A at a rate equal to the frequency difference between the two color subcarriers, thus causing both hue and saturation errors on a time varying basis. The perception of the color crosstalk in the TV picture is that of a "breathing" effect in the displayed colors. Its perception depends on both the amplitude and frequency difference of the interference. For a given typical level of interference, (3 to 5%), the highest perceptibility occurs at a frequency difference of 5 to 8 Hz. At less than 1 Hz, the perceptibility is low and it takes about 10 seconds or more, depending on the picture content, to detect crosstalk. As the frequency difference increases above about 8 Hz, the perception of the crosstalk decreases and crosstalk is generally imperceptible at 20 Hz.

Fig. 5 shows a set of vectorscope displays of the signal output of the laboratory crosstalk simulator described earlier. The two video input signals were a magenta field (80 IRE color subcarrier on a 50 IRE pedestal), and an EIA 75% saturated color bars test signal. The magenta field signal is referred to as the CW signal, and the color bars signal is referred to as the C.B. signal. Fig. 5(A) shows the vector display when the CW signal is selected as the desired signal and the interference is turned off. Fig. 5(B) shows the vector display when the C.B. signal is selected and the interference is turned off. Fig. 5(C) shows the CW signal with 10% interference from the C.B. signal. The CW signal is genlocked (locked in frequency and fixed phase) to the C.B. In this figure, instead of a single point at the tip of the magenta vector, there is a cluster of 8 points, each

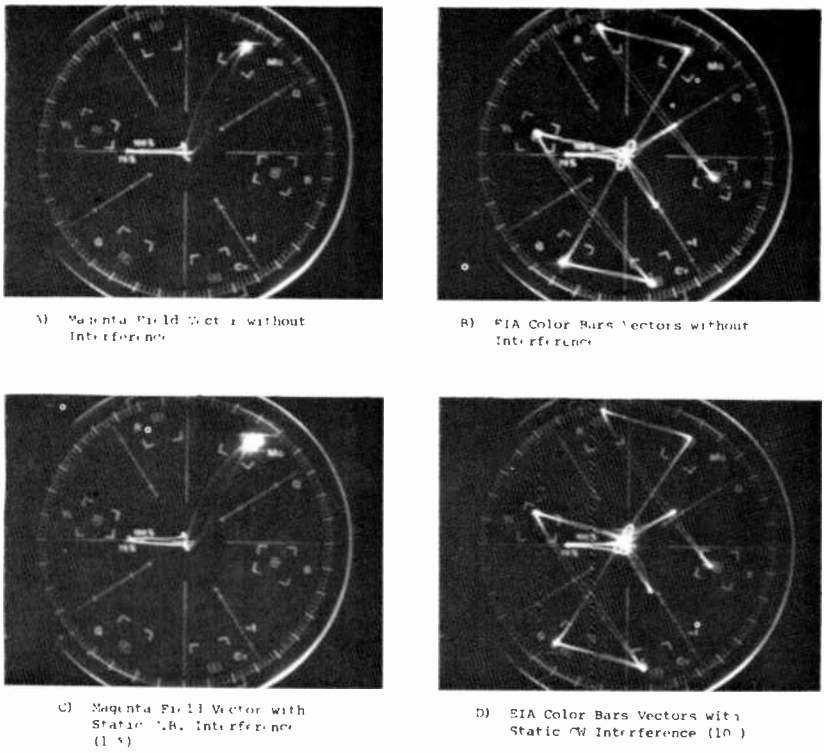

Fig. 5—Vectorscope displays for zero and 10% static interference.

one representing a different vector resulting from interference from the 6 color bars and the $-I$ and Q components in the C.B. signal. In Fig. 5(D), the C.B. signal is desired and the genlocked CW is the interference. Each color bar and the $-I$ and Q vectors is singularly displaced due to the CW interference. The static hue and saturation errors in this C.B. signal can be detected by only the most acute expert viewers who know a priori exactly how the correct C.B. test pattern display should look on a TV monitor.

Fig. 6 shows the waveform monitor display of the magenta field signal without and with 10% static interference. The amplitude variations in the CW signal can be seen in Fig. 6(B), and these show up in the TV picture display as faint color bars in the background of the magenta field.

Fig. 7 shows the vectorscope displays for the CW and C.B. desired signals with the interfering signals "free-running" with respect to the desired signals. These photographs were taken with exposure times of 2 seconds. The distinct differences in the appearance of the signals at

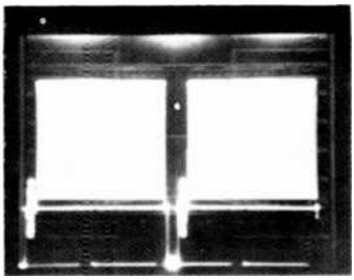

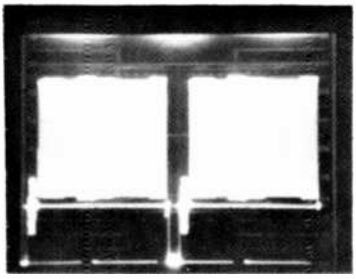

Fig. 6—Waveform monitor display of magenta field signal.

different times can be clearly seen. Similarly, the perception of the crosstalk in the displayed TV pictures varies with time. The crosstalk is more easily perceived at the time the vectorscope displays look like Figs. 7(C) and 7(D), as compared to Figs. 7A and 7B. The reason for the greater perceptibility of the crosstalk in the second set of TV pictures is that the color bursts used as a reference are affected by the interfering signals, whereas, they are not affected by the interference for Figs. 7(A) and 7(B) (the color burst of Fig. 7(B) was affected just before the end of the exposure time). There is no color crosstalk into the color bursts of the desired signal when the interfering signal is going through either a synchronizing pulse interval or low-level chrominance period in time coincidence with the color bursts of the desired signal. This condition may persist for several seconds if the frequency difference of the two color subcarriers is small.

5. Color Crosstalk Concellation Techniques

Several techniques to cancel or eliminate the visible color crosstalk have been proposed. Some of the techniques considered, with an evaluation of their feasibility, are as follows:

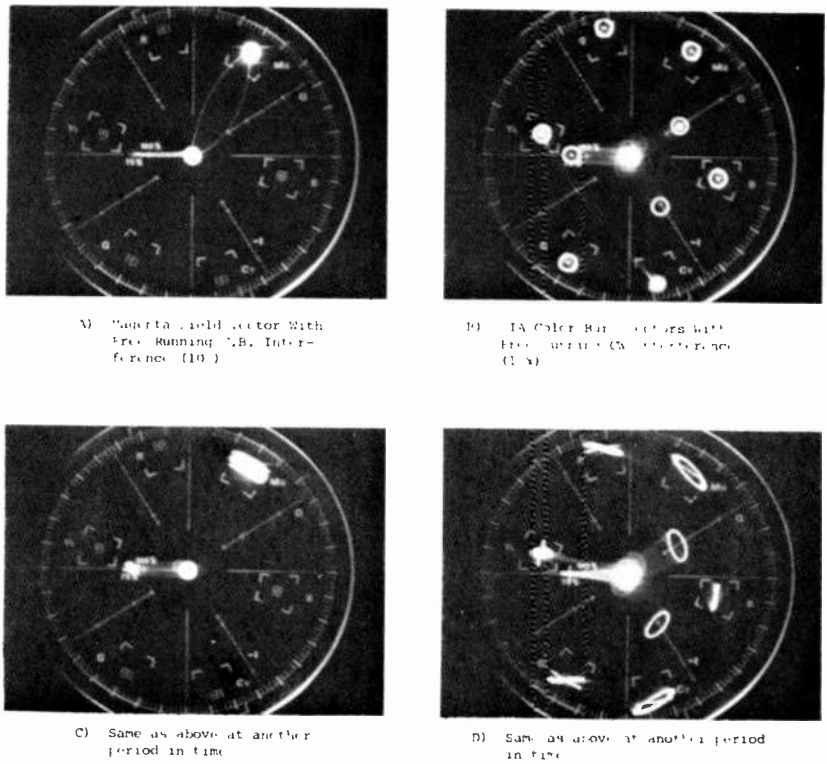

Fig. 7—Vectorscope displays of CW and C.B. signals with interference.

Use a PAL system for the satellite link segment of the transmission system: The PAL system, with its phase alternation on a line-to-line basis might provide effective cancellation of the color errors due to crosstalk. Implementation of such a scheme in a U.S. domestic system entails the use of costly standards converters, or other complicated signal processing.

Genlock the two color signals: This scheme results in static hue and saturation errors in both pictures, even though they are not perceptible or disturbing unless the viewer knows a priori what the correct picture should look like. It also requires that both TV signals be available at a common uplink earth station, unless costly and complicated techniques are used to allow synchronization of the signals at separate uplink earth stations.

Increase the frequency difference between the color subcarriers on the satellite link to more than 20 Hz: This may be accomplished by sepa-

rating the chrominance and luminance components of one of the TV signals, translating the color information to a different subcarrier frequency by a heterodyne process, and recombining the components before modulation and transmission to the satellite. The reverse process would then be done at the receiver to recreate the original NTSC signal.

Invert the polarity of one of the TV signals on alternate scan lines: This causes the relative phase of the interfering color subcarrier to switch by 180 degrees on a line-to-line basis as shown in Fig. 8. The interfering vector **B** is represented in sequence by **B**1, −**B**2, **B**3, −**B**4, **B**5, etc., and appears to rotate at a rate of one-half the TV line rate, or about 7,867 Hz, which makes the color crosstalk imperceptible in the TV picture. An appropriate voltage offset must be added to the inverted signal to limit the overall peak-to-peak swing of the resulting signal to avoid excessive deviation of the FM carrier, and the received signal must be inverted in a complementary fashion with precisely the same voltage offset applied. In addition, since the spectral distribution of the rf carrier is different for the alternately inverted video signal, there is likely to be a difference in the resulting performance between the two TV channels, or different parameter tradeoffs may be needed to achieve equal performance between the two channels. This technique was tried in the laboratory and found to be effective in eliminating the crosstalk between the channels.

Separate the chrominance and luminance components of one TV signal, invert the chrominance on an alternate line basis, and recombine the video signal before modulation: The same vector relationships as shown in Fig. 8 should occur, and the color crosstalk should be rendered imperceptible.

Delay alternate lines of one video signal by one-half period of the color

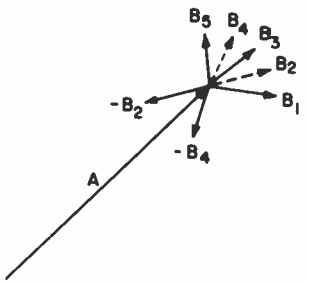

Fig. 8—Vector diagram of desired signal (A) and interfering signals (B) with alternate line phase reversals.

subcarrier: This technique also switches the relative phase of the interfering color signal by 180 degrees on a line-by-line basis, effectively eliminating the visible color crosstalk. This technique was pursued most extensively, because of its relative simplicity and ease of implementation.

6. Alternate Line Delay Implementation

Fig. 9 is a block diagram of the Alternate-Line-Delay (ALD) unit. Both the incoming video signal and an approximately 140 nanosecond delayed version of it are fed to a multiplexer. The multiplexer selects and passes either one of its two input signals depending on the logic level of a gating signal from the alternate-line-gate generator. In the transmit mode, the gating signal is fed directly to the multiplexer, whereas in the receive mode, the inverted gating signal is fed to the multiplexer. The gating signal is made unsymmetrical to insure that the synchronizing pulses are always selected from the same input to the multiplexer, i.e., only the color burst reference and active video portion of the TV scan line is alternately delayed and undelayed at the output of the unit.

The vertical sync pulse is used in the timing and gate generators to establish an unambiguous switching sequence so that those video lines that are undelayed at the transmitter are delayed at the receiver. Thus, all video lines, including the sync pulses, are delayed equally from end-to-end, resulting in a normal NTSC signal format and TV picture display.

Figs. 10(A) and 10(B) show the vector displays of the desired TV signals when the second TV signal is genlocked and processed by the ALD before interfering with the desired signal. A dual set of vectors is created in each case, because of the 180 degree change in the interfering vectors on a line-to-line basis. The viewer can take a mental average of the vector

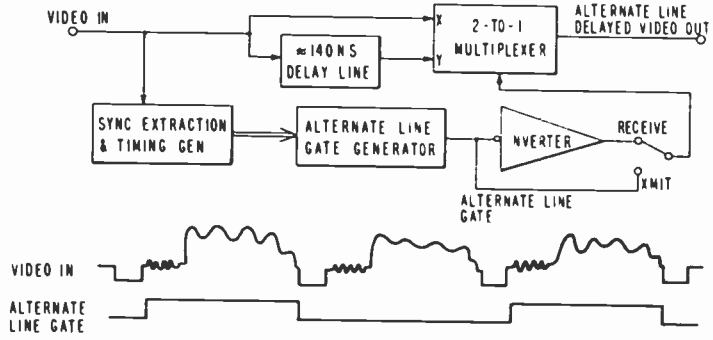

Fig. 9—Block and timing diagrams for the alternate line delay unit.

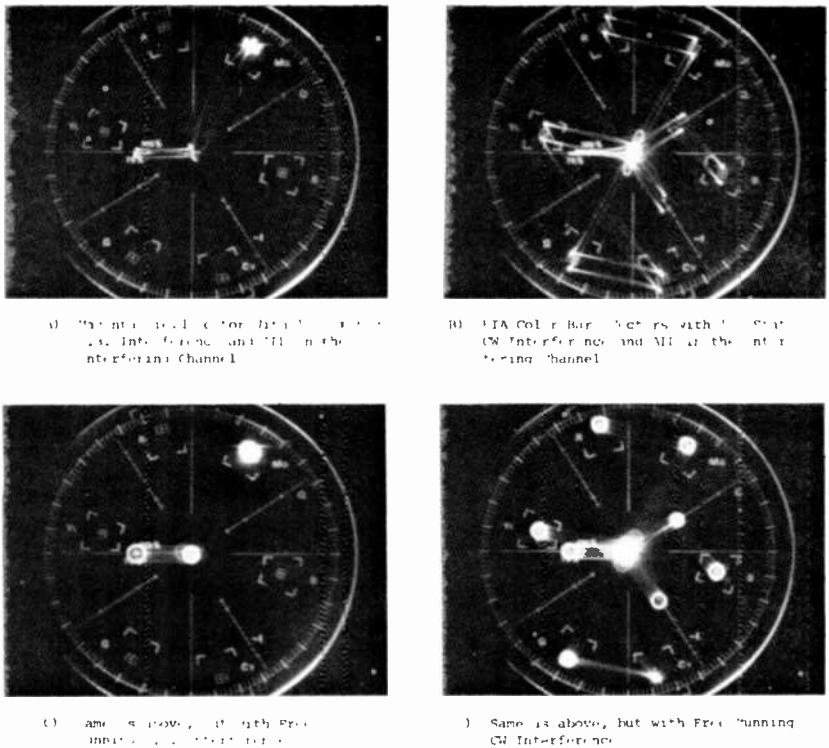

Fig. 10—Vectorscope displays of desired signals with the ALD in the intefering channel.

display and realize that the result would be a single set of vectors with the correct amplitude and phase, as shown in Figs. 5(A) and 5(B). When the signals represented by Figs. 10(A) and 10(B) are fed to the TV monitor or receiver, an averaging process occurs because of the response characteristics of the TV set and because of the viewer's perceptual process. This results in the cancellation of the visible color crosstalk.

Figs. 10(C) and 10(D) show the vector displays when the interfering signal is allowed to free-run. The photographs appear similar to those of Figs. 7(A) and 7(B). However, in actuality, the rate of rotation of the vector tips around the average value has been changed from less than 20 Hz to about 7867 Hz, and the perception of the crosstalk is eliminated.

Fig. 11 shows vector displays of the desired signals when they are processed by the ALD at the transmitter and subsequently interfered with by the non-ALD-processed channel. The dual sets of main vectors with the 180-degree relationships are now produced by the ALD process, while the locus of points at the vector tips is caused by the interfering

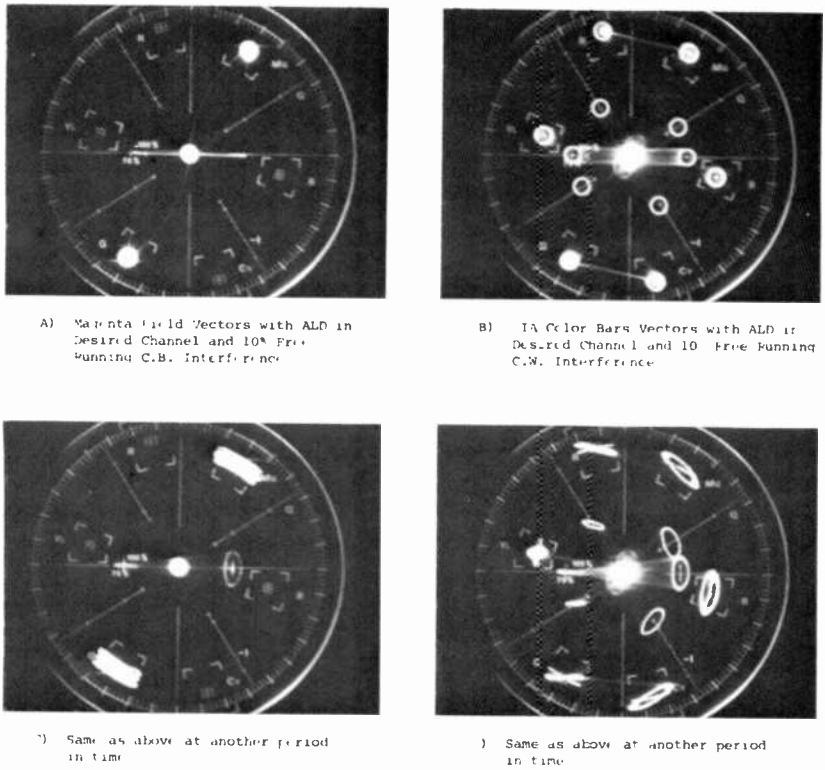

A) Magenta Field Vectors with ALD in Desired Channel and 10% Free Running C.B. Interference

B) IA Color Bars Vectors with ALD in Desired Channel and 10% Free Running C.W. Interference

C) Same as above at another period in time

D) Same as above at another period in time

Fig. 11 —Vectorscope displays of the desired signals with the ALD in the desired channel.

color signals. If these signals are fed directly to a TV monitor or receiver, the displays appear as black and white pictures with line-to-line displacement of all the vertical and diagonal details. However, when the signals are processed by an ALD at the receiver, the vectorscope displays appear as in Figs. 10(C) and 10(D) and the TV pictures are restored to normal with no visible color crosstalk.

When the ALD is implemented in its simplest form as described before, the visible crosstalk from the ALD-processed channel into the non-ALD-processed channel is always eliminated. However, some crosstalk is still perceptible in pictures produced from the ALD-processed channel if the model of TV receiver used has an extended burst gate that starts at the leading edge of the horizontal sync pulse and ends after the color burst. In this case, the color interference occurring during the sync pulse interval of the received signal comes from a non-ALD-processed signal and is coherent on a line-to-line basis, causing interference with the color subcarrier regeneration process in the receiver.

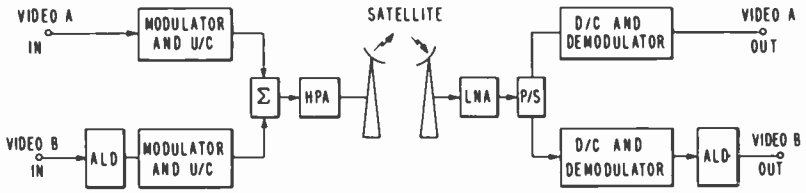

Fig. 12—Block diagram of two-TV-channels-per-transponder system.

The problem does not occur when the burst gate is open solely during the color burst interval. This problem may be avoided by using the appropriate models of TV receivers or regenerating the color burst with a video processing amplifier. The best solution, however, has been the incorporation of a circuit to differentially cancel the color interference during the sync interval within the receive ALD itself.

Fig. 12 shows a block diagram of the two-TV-channel-per-transponder system that is currently in operation[2] providing service between Los Angeles, California, and Alaska.

7. Chroma Averaging

Laboratory experiments have shown that the use of chrominance averaging devices following the receive ALD enhances the overall operation by reducing the crosstalk effects in the waveform monitor and vectorscope displays under normal operation. This makes it easier to make measurements and signal analysis. In addition, at extremely high levels of crosstalk produced in the laboratory, the chroma averager also reduced some residual luminance crosstalk effects in the picture. Chrominance averagers using delay-line comb filters, as shown in Fig. 13, also yield approximately 3-dB of signal-to-random-noise improvement in the chrominance band of the composite video signal. If this is combined with a luminance noise reduction process, such as "coring" (removing low-level high-frequency noise), an overall 3-dB SNR improvement may be achieved.

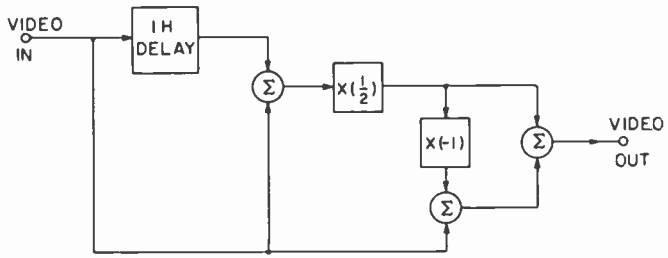

Fig. 13—Block diagram of chroma averager.

8. Conclusions

Crosstalk between two TV channels transmitted by dual rf carriers via a single satellite transponder is caused by the nonlinearities of the TWT amplifiers and channel bandpass filters. The crosstalk is predominantly related to the color subcarriers in the composite baseband video signal. Its level and perception depends on various factors, such as chrominance levels, chrominance frequency difference, channel equalization, and TWT power levels. A color crosstalk simulator has been developed to duplicate the crosstalk effects of satellite transmission and is a useful tool in laboratory experimentation. Several techniques proposed for crosstalk cancellation have been discussed, including genlocking the two TV signals, PAL signal processing, subcarrier frequency translation, alternate line inversion of the composite signal, alternate line inversion of the color subcarrier, and alternate line delay of the composite video signal.

An alternate line delay (ALD) device has been developed to eliminate the visible color crosstalk and is currently used by RCA in a two-TV-channel-per-transponder service between Los Angeles, California and Alaska. The ALD permits operation of the system at higher carrier power levels than could otherwise be used and, thus, yields about 4.5-dB SNR improvements in both TV channels. Even higher levels of improvement are possible using the ALD in conjunction with chroma averaging.

Acknowledgments

The author acknowledges the very significant contributions by Guy W. Beakley and Robert F. Flory, in discussions, consultations, and encouragement.

References:

[1] Guy W. Beakley, Private Communication.

[2] Liston Abbott, Guy W. Beakley, William T. Rowse, "Parameter Tradeoffs for Transmitting Two Television Channels Per Transponder," *RCA Review*, **41**, p. 363, Sept. 1980 (this issue).

Parameter Tradeoffs for Transmitting Two Television Channels Per Transponder

L. Abbott*, G. W. Beakley†, W. T. Rowse‡

Abstract—A two-television-channel-per-transponder service has been implemented by RCA Americom and the former RCA Alascom (now Alascom, Inc.) for the State of Alaska. This service was officially started in January 1977, after extensive tests to determine the optimum operating parameters, and the development of a crosstalk cancellation device. The system uses a dual rf carrier technique, dual i-f filtering and channel equalization, and color crosstalk cancellation. The program audio has been carried by pre-existing SCPC equipment using a separate transponder, but tests show that it may be carried in the same transponder along with the video with relatively little degradation. The video performance is excellent by TASO standards.

1. Introduction

A satellite television service providing two TV channels per transponder has been implemented for the State of Alaska by RCA Americom and RCA Alascom (now Alascom, Inc.). This service is used to transmit real-time television from the "lower 48" to earth stations in the large communities in Alaska. The TV programs are then relayed to local TV stations for immediate or time-delayed broadcast. The programs are also rebroadcast by satellite in a different single-channel-per-transponder format to small, inexpensive earth stations in the rural "bush" communities. The selection of the TV programs to be transmitted via the satellite system is made by the Alaskan user community.

The parameters for transmitting two color television channels per transponder to the large earth stations in Alaska have been analyzed elsewhere.[1] This paper reports on a number of experiments that were made over the RCA Satcom satellites to determine the optimum parameters to use for the Alaskan two-channel-per-transponder service. The television signals were received at various times by earth stations with antenna diameters of 10 meters, 13 meters, and 30 meters. The following parameters were varied:

* RCA Laboratories, Princeton, NJ 08540.
† Now with Scientific-Atlanta, Inc., Atlanta, Georgia.
‡ RCA Americom, Princeton, NJ 08540.

(1) Power backoff: saturation to −15 dB
(2) Peak Video Deviation: 5 to 8 MHz
(3) IF Bandwidth: 15 MHz, 16 MHz, and 17.5 MHz
(4) Carrier Position: ±8 to ± 10 MHz from channel center
(5) Location of audio subcarrier: 5.8 MHz, 6.2 MHz, 6.8 MHz
(6) Peak Deviation of the main carrier by the Audio Subcarrier: 1—2 MHz.

Data was taken for tests over the satellite and in various back-to-back modes. Data on carrier-to-noise ratio (CNR), CCIR weighted signal-to-noise ratio (SNR), video impulse noise, video crosstalk, short-time waveform distortion, chrominance-luminance delay, differential gain, differential phase, audio-to-video crosstalk, audio clicks, audio SNR, and total harmonic distortion were taken for many variations of transmission parameters. This paper will concentrate on the experiments, conducted in September 1976, to and from a 10-meter transportable earth terminal located at the RCA Americom Earth Station at South Mountain, outside of Los Angeles, CA, as well as subsequent performance tests made in the main Earth Station when the system was implemented in January 1977.

At operating power levels near the saturation point of the satellite transponder, considerable color crosstalk between the two channels occurs when there is a highly saturated color on either of the two channels. This crosstalk is caused by the nonlinearities of the satellite transponder. The combination of two fm carriers results in a signal with both amplitude and phase modulation in the transponder. The amplitude modulation, which contains contributions from both signals, is converted into additional phase modulation (AM/PM conversion) by the TWT in the satellite. The primary phase modulation, which also contains contributions from both signals, is affected by the group delay inequalities in the transponder. Both effects result in crosstalk between the two television signals.

The three main methods used to reduce the video crosstalk were (1) input backoff, (2) group delay equalization on the transmit side, and (3) a video processing technique called Alternate Line Delay (ALD).[2] The inclusion of group delay equalization reduces the video crosstalk in actual transmission by almost one half and improves the video distortion parameters significantly. The ALD processing allows increased transmitted power, resulting in a higher CNR margin above threshold and a higher SNR for the received picture. It also makes any otherwise visible color crosstalk imperceptible on television sets.

The parameters selected for the Alaskan two channel per transponder transmission were:

(1) Total Input Backoff ≈ 6 dB
(2) Peak Video Deviation = 6.7 MHz

(3) Peak-Peak Energy Dispersal = 0.5 MHz
(4) Carrier Separation = 19 MHz
(5) IF Bandwidth = 17.5 MHz each channel
(6) Transmit Group delay equalization in both channels
+2.5 ns/MHz, plus 0.25 ns/MHz^2 on the low-frequency side
−3 ns/MHz, plus 0.12 ns/MHz^2 on the high-frequency side
(7) ALD in one channel
(8) Audio transmitted by SCPC in another transponder.

The resulting video parameters measured at the 13 meter RCA Americom Earth Station (G/T = 32.7 dB/K) outside Los Angeles, CA, were

(1) SNR = 48.5 dB
(2) CNR = 18.3 dB
(3) Differential gain = 6%
(4) Differential phase = 2 degrees
(5) Average crosstalk^2 = 3.6% (not visible in the picture due to the ALD)

The SNR and CNR compare to a theoretical CNR of 17.9 dB and SNR of 48.8 dB. The power transmitted can be reduced 7 dB before impulse noise appears in the picture. This means, for example, that the CNR margin is at least 7 dB. Table 1 shows the additional carrier-to-noise that can be lost in the up and down links. For example, if 5 dB is lost in the uplink another 2.9 dB can be lost in the downlink before just noticeable impulse distortion (JND) appears in an EIA color bars test pattern.

The theoretical signal-to-noise that could be received by other earth stations is shown in Table 2 for an EIRP = 34 dBw and an antenna look angle of about 30 degrees. It should be noted that the CNR margin for the 10m, 190K earth station is becoming marginal for the two channel per transponder case.

The two-channel-per-transponder service is not "broadcast quality" (SNR = 56 dB). However, a picture that has an SNR of 48 dB, for example, is better than any point on the TASO scale.[3] One can make a linear projection of the TASO data that indicates that 80% of the people

Table 1—Carrier-To-Noise Margin in the Up and Down Links

Up	Down
7 dB	0 dB
6	1.6
5	2.9
4	4.2
3	5.2
2	6.1
1	6.8
0	7.4

Table 2—Theoretical SNR for Receiving Earth Station

Antenna Diameter (m)	LNA Noise Temp (K)	G/T (dB/K)	CNR (dB)	SNR (dB)
30	55	40	20.8	51.7
13	55	32.7	17.9	48.8
10	55	30.0	16.3	47.2
10	190	26.5	13.8	44.7

would rate the picture as excellent.[4] Cavenaugh and Lessman[5] indicate that about 2 of 10 expert viewers would rate the noise as just perceptible or better, i.e., most expert viewers can readily see the noise. A 48-dB picture has noise that can be seen at close range by experts, but the noise is so insignificant that the picture is judged as excellent by most people.

It was noted that the SNR can be increased by reducing the backoff. The crosstalk, however, increases. Even though the increased crosstalk is not visible in the picture because of the use of an ALD, it does appear on the waveform monitor and vectorscope.

The SNR can also be increased by noise reduction techniques. About 3 dB of noise reduction can be accomplished by video line-to-line techniques (chroma averaging and luminance coring) and 6 dB or more can be obtained by frame-to-frame digital techniques with essentially no resulting artifacts.

The two TV channel per transponder service using the parameters outlined in this paper began serving the state of Alaska on a regular basis on January 15, 1977. The received video SNR is 53 dB at the Anchorage earth station and 49 dB at the Juneau earth station. The service has also been used successfully for teleconferencing with uplinks from multiple locations simultaneously. It is therefore concluded that the two-channel-per-transponder service offers promise for many television applications.

2. SYSTEM ANALYSIS

2. TWTA Input Versus Output Characteristics

One of the major concerns in a multiple-video-per-transponder system using multiple rf carriers is the input versus output characteristics of the traveling wave tube amplifier in the satellite. In the standard single-channel operation, the TWT is operated at its most efficient point, just at saturation where its output power is at a maximum. The power input versus power output characteristics is highly nonlinear for operation at or near saturation, as shown in Fig. 1. This diagram shows the relationship between the total output carrier power backoff (TOBO)

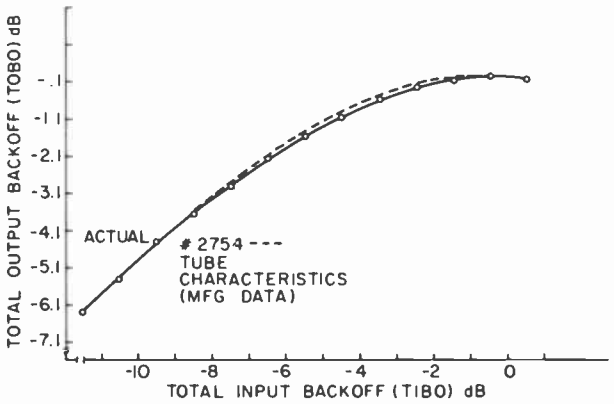

Fig. 1—Single carrier backoff characteristics.

from saturation as the total input carrier power backoff (TIBO) is varied. Both the manufacturer's data and the data from actual tests with unmodulated carriers are plotted.

The nonlinear input versus output relationship of the TWT can be tolerated in the standard single-channel-per-transponder operation because the rf carrier is frequency modulated and has a constant amplitude. Therefore, no deleterious intermodulation products or AM to PM conversion is created. The earth station video receiver uses a limiter-discriminator or other amplitude insensitive demodulator, and generally excellent TV pictures can be recovered.

In two-channel-per-transponder operation, two separately modulated rf carriers are passed through the same TWTA in the satellite. There are three main effects resulting from this mode of operation. First, the output power of each carrier (as well as the total output power) is lower for any given input carrier power level. Fig. 2 shows the output-carrier power backoff versus the input-carrier power backoff characteristics for the two-carrier case.

Second, when two carriers are passed through the TWT, the nonlinearities cause intermodulation products, some of which are at frequencies within the desired channel bandwidths. These beats, with their modulated sidebands, cause perceptible interference in the TV pictures produced from each channel.

Third, the combination of the two rf carriers also results in a varying amplitude signal passing through the TWTA. The amplitude variations of the TWT input signal cause phase variations in the output signal. This AM/PM conversion results in a crossmodulation between the two channels and perceptible crosstalk in both TV pictures. Fig. 3 shows a typical AM/PM characteristic of a satellite transponder.

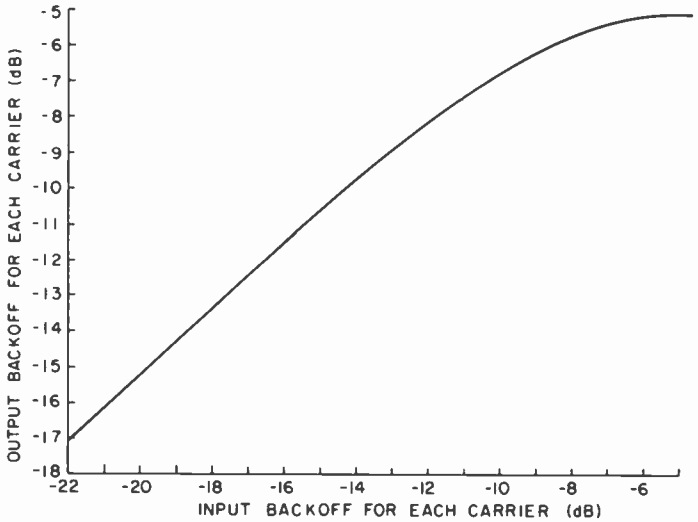

Fig. 2—Two-carrier input versus output backoff relative to single-carrier saturation. Carriers at ±9.5 MHz from transponder center (composite from 8/25/76 and 9/1/76, includes HPA)

2.2 Link Calculations

The satellite used for these experiments is RCA spacecraft F2, which is located at 119 degrees west longitude and has 6 transponders with a

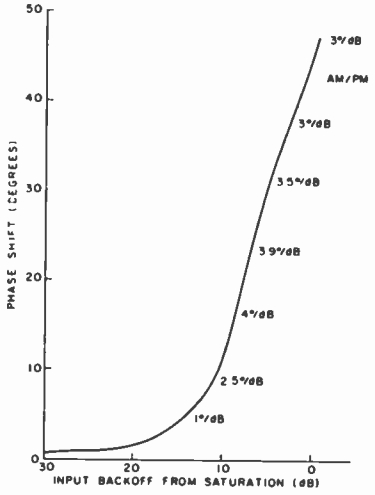

Fig. 3—AM to PM (conversion: F2-channel 23, 22° transponder, test data-Montreal 7/18/75).

3 degree tilt toward Alaska. The EIRP (effective isotropically radiated power) used in this paper were computer generated based on values measured on the test range and verified at earth stations throughout the U.S. The EIRP assumed for the South Mountain, CA, location is 34 dBW. The saturated flux density (SFD) is -82.5 dBW/m^2 and the $(G/T)_s$ of the satellite is about -3 dB/K. The transmit frequency was 6385 MHz and the receive frequency was 4160 MHz. The carrier-to-noise density on the uplink is

$$\left(\frac{C}{kT}\right)_u = \text{SFD} - \text{IBOE} + 10 \log \frac{\lambda^2(\text{uplink})}{4\pi} - k + \left(\frac{G}{T}\right)_s - L_0,$$

where IBOE is the input backoff of each carrier. Assuming an average loss above free space loss of 1 dB, the following (C/kT) is obtained

$$\left(\frac{C}{kT}\right)_u = 104.4 - \text{IBOE}.$$

The carrier-to-noise density on the downlink is given by

$$\left(\frac{C}{kT}\right)_D = \text{EIRP} - \text{OBOE} - (L_{FS} + L_0) + \left(\frac{G}{T}\right)_{ES} - k.$$

Assuming a 0.4 dB average loss above free space loss and $(G/T)_{ES} = 32.7$ dB/K, the carrier-to-noise density is

$$\left(\frac{C}{kT}\right)_D = 98.7 - \text{OBOE}.$$

The received noise results from a combination of the uplink and downlink noise and intermodulation products. Using a computer program developed by A. Guida of RCA Laboratories, in which Gaussian spectral shapes for each television signal is assumed, calculations of intermodulation products were made for various operating conditions. The various link noise powers versus transponder power backoff are shown in Table 3. TIBO is the total backoff. The SNR was calculated by[4]

$$\text{SNR} = \text{CNR} + 10 \log (\Delta F^2 B) + 2 \text{ dB},$$

where ΔF is the peak deviation in MHz and B is the i-f bandwidth in MHz.

3. Satellite Transponder and Earth Station Equipment

Fig. 4 is a simplified block diagram of the satellite repeater system. In fact, there are multiple antennas on the spacecraft, as well as multiple filter banks and TWTA's. There is also equipment redundancy and appropriate switching matrices. The uplink frequency range is 5925 to

Table 3—Link Attributes Versus Transponder Backoff

TIBO	IBOE	$(C/kT)_u$	OBOE	$(C/kT)_D$	$(C/kT)_{u+D}$	$(C/\mathrm{IM})_{17.5}$	$CNR_{17.5}$	$SNR_{\Delta F=6.68}$
−2	1	103.4	4.9	93.8	93.3			
−1	2	102.4	4.6	94.1	93.5			
0	3	101.4	4.5	94.2	93.4			
1	4	100.4	4.4	94.3	93.3	20.3	17.6	48.5
2	5	99.4	4.5	94.2	93.1	21.6	18.1	49.0
3	6	98.4	4.7	94.0	92.7	22.9	18.4	49.3
4	7	97.4	4.9	93.8	92.2	24.2	18.5	49.4
5	8	96.4	5.2	93.5	91.7	25.3	18.3	49.2
6	9	95.4	5.7	93.0	91.0	26.3	17.9	48.8
7	10	94.4	6.2	92.5	90.3	27.3	17.4	48.3
8	11	93.4	6.8	91.9	89.6	28.2	16.9	47.8
9	12	92.4	7.5	91.2	88.7	29.1	16.1	47.0
10	13	91.4	8.3	90.4	87.9	30.2	15.4	46.3
11	14	90.4	9.2	89.5	86.9	31.7	14.4	45.3
12	15	89.4	10.1	88.6	86.0	33.4	13.5	44.4
13	16	88.4	11.1	87.6	85.0	35.3	12.5	43.4

6425 MHz and the downlink frequency range is 3700 to 4200 MHz. The 24 transponders on the RCA Satcom satellites have center frequencies 20 MHz apart on alternate horizontal and vertical polarizations. The useful bandwidth of each transponder is about 36 MHz. Each transponder has its own TWTA.

Fig. 5 is a block diagram of the earth station equipment configuration used in the testing and optimization of the two channel per transponder operation. The variable attenuators in the uplink setup were used to set carrier deviations and power levels. The frequency synthesizers were used to set the carrier frequencies on the up and down links. The i-f filter bandwidth was varied by changing the plug-in i-f filter modules. Group delay equilization at i-f was included in the transmit link; it is varied by selection of plug-in cards on the equalizer units. An ALD unit was placed

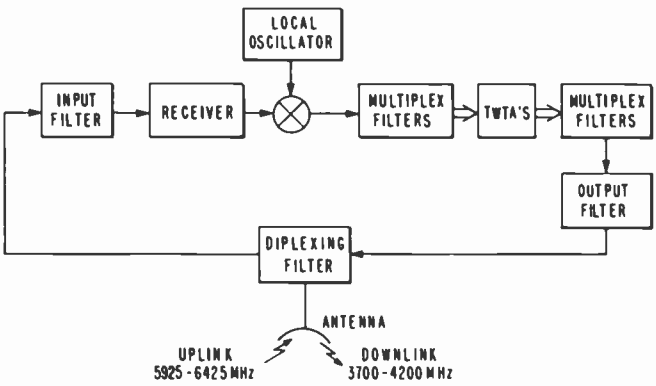

Fig. 4—Simplified block diagram of satellite repeater.

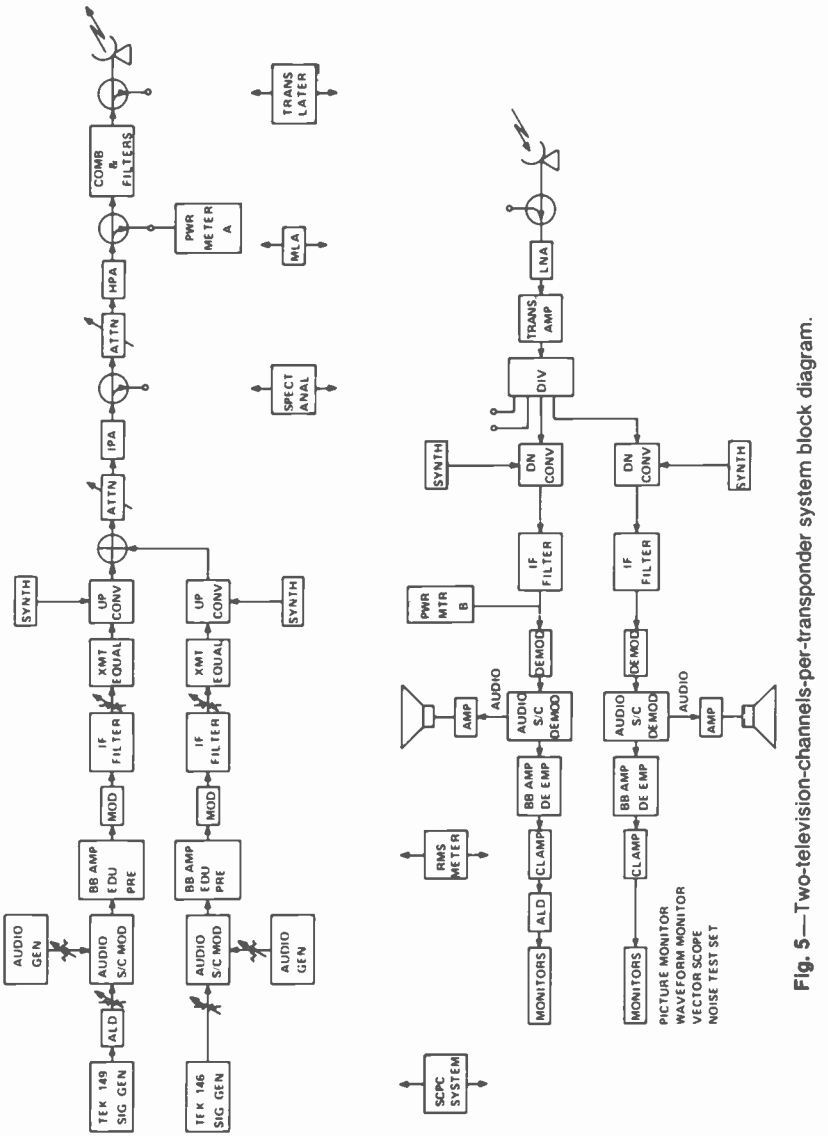

Fig. 5—Two-television-channels-per-transponder system block diagram.

in one up and down-link channel only. The ALD unit has provisions for switching its crosstalk cancellation processing in or out to permit measurements in both modes. The various test points used for monitoring and measuring the system performance are also shown. Some of the key pieces of test equipment are also indicated in Fig. 5.

4. System characterization

Input backoff versus output backoff curves were run for each test day. A typical single carrier IBO versus OBO curve is shown in Fig. 1. The dashed lines show one manufacturer's published TWT data. It should

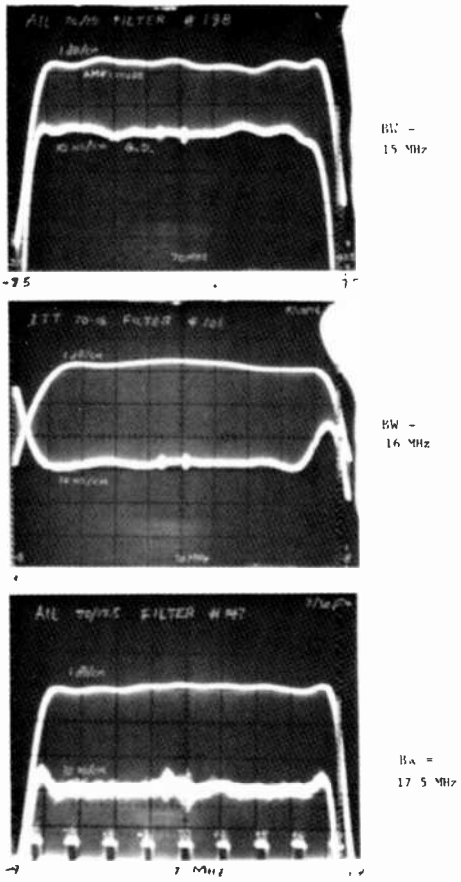

Fig. 6—Typical i-f filter characteristics (scales: amplitude—1 dB/div, group delay—10 ns/div).

be noted that the saturation point varied by about 1 dB from day to day, probably due to equipment drift and/or atmospheric changes.

A typical two carrier IBO versus OBO curve is shown in Fig. 2. The carrier levels were balanced on the uplink, and the down-link carriers were averaged for this curve. The downlink carriers were typically unbalanced from about 0.2 dB to 0.5 dB. Notice, however, that the characteristics shown are very close to those previously used in the calculations. For example, at an IBOE of 6 dB, the theoretical OBOE was 5.7 dB and the experimental OBOE was about 5.2 dB. For an IBOE of 13 dB, the theoretical OBOE was 8.3 dB and the experimental OBOE was 8.5 dB.

Typical IF filter characteristics are shown in Fig. 6. The amplitude

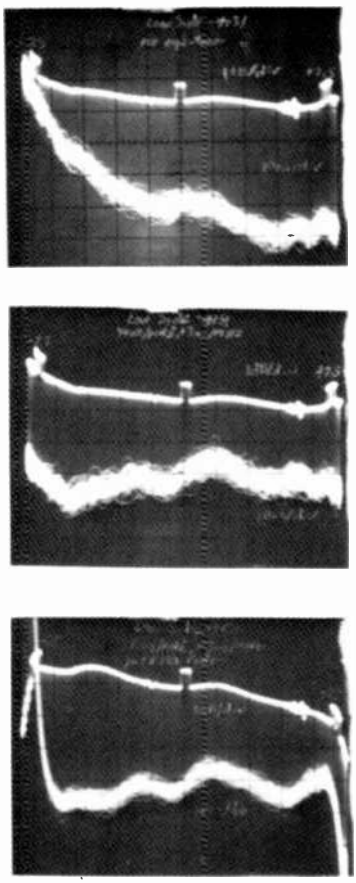

Fig. 7—Low-frequency group delay ecualization (scales: amplitude-1 dB/div, group delay—10 ns/div, frequency markers at 70 ± 7.5 MHz).

characteristics (top curve in each photo) are shown at one dB per division and the group delay characteristics at 10 ns per division. Notice that the frequency scales are different from the filters. The 15 MHz filter is down 5 dB at about 7.5 MHz from channel center and the 17.5 MHz filter is down 5 dB at about 8.5 MHz.

The group delay characteristics of the rf channel, without the i-f filters, are shown in Fig. 7 for the low-frequency side of the transponder channel (below 70 MHz) and in Fig. 8 for the high-frequency side (above 70 MHz). The top picture shows amplitude and phase characteristics of the satellite channel without equalization. The middle picture shows the best equalization that could be obtained using only linear and parabolic equalizers. The bottom picture shows this equalization when including

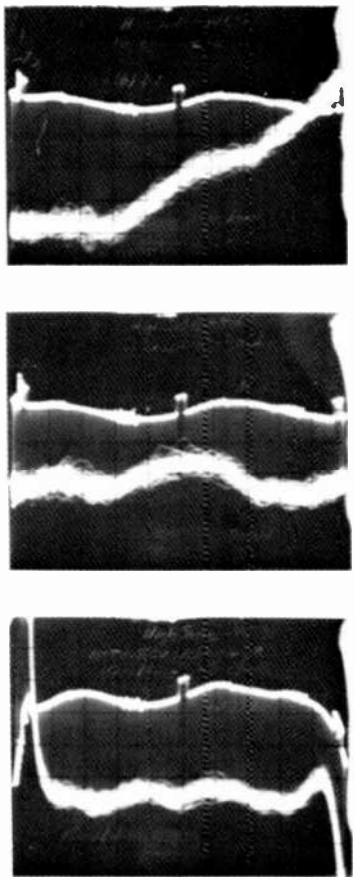

Fig. 8—High-frequency group delay equalization (scales: amplitude—1 dB/div, group delay—10 ns/div, frequency markers at 70 ± 7.5 MHz).

transmit and receive i-f filters. The amplitude curve was flat within 1.5 dB on the low-frequency channel and 1 dB on the high-frequency channel, and both group-delay curves were within 10 ns in the pass band. Group delay equalizers were included in all test setups that follow unless otherwise noted.

5. Parameter Variations and Tradeoffs

Earlier field tests conducted at the RCA Americom Earth Station at Vernon Valley, NJ, in the first quarter of 1976, showed that the major impediment to good system performance was the video to video crosstalk between the two TV channels. However, it was considered necessary to observe and measure other performance factors such as video distortion, audio distortion, audio into video and video into audio crosstalk, impulse noise, multipath effects, and interference into and from the adjacent co-polarized and cross-polarized transponders.

5.1 Perception And Measurement Of Color Crosstalk

At a transmitted power that causes the satellite transponder to operate near saturation, considerable color crosstalk (cross modulation) occurs when there is a high saturated color on either of the two channels. The variation of the interference is proportional to the frequency difference of the two color subcarriers. If the color subcarrier frequency in one channel is 3579545 Hz and the subcarrier frequency in the other channel is 3579550 Hz, the resulting crosstalk is observed as a variation or "breathing" in the colors at a rate of 5 times a second.

The degree of perception of the color crosstalk is related to the color-subcarrier frequency difference. The crosstalk is not visible if the two TV signals are genlocked since the interference pattern is static. However, there are fixed color errors that can be measured on the vectorscope. A less than 0.5-Hz difference can be seen only by looking for a very slowly changing hue. For the same level of crosstalk, the interference becomes more objectionable as the frequency of the interference increases. It appears to be most objectionable when the frequency difference is 5–10 Hz and the picture seems to flash at the viewer. The perceptibility of the interference decreases as the frequency difference increases and finally vanishes as the frequency difference becomes greater than 20 Hz.

The preferred method for measuring color crosstalk is to measure both phase and amplitude errors for two arbitrary signals. However, the measurement of phase errors was difficult due to the noise on the re-

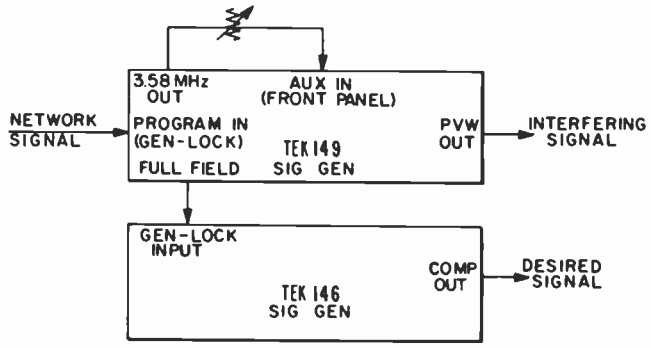

NOTES:

146 FREE RUNNING (INT. STD) EXCEPT TO MAKE MEASUREMENTS

149 PREVIEW OUTPUT IS 50 IRE FLAT FIELD WITH 79 IRE CW SUBCARRIER SUPERIMPOSED.

Fig. 9—Color crosstalk test signal generator setup.

ceived signals. Therefore, only measurements of amplitude error were made.

Two different signals were used for measuring the crosstalk. One was a 79 IRE p-p full field cw signal with APL = 50 IRE. This signal was derived from a Tektronix 149 signal generator. The 79 IRE signal was chosen because it is approximately equal to the p-p chrominance expected with 75% saturation color bars. The other signal was the standard 75% EIA split field color bars test signal which was derived from a Tektronix 146 signal generator. These signals were generated as shown in Fig. 9.

The Tektronix 146 signal generator was set for free-running (internal reference) to make visual interference checks in the TV pictures. To make the crosstalk measurements, the color bars were genlocked to the 79 IRE cw signal. Then the variation in the downlink demodulated signal was observed as the subcarrier phase control on the 146 was rotated. The difference in the p-p levels of the maximum and minimum chrominance levels of the desired signal was recorded at the crosstalk. It was then defined in percentage terms as the p-p difference relative to 100 IRE.

The change in the desired color vector due to the interference was, in general, elliptical in form, as shown in Fig. 10. For example, suppose the desired color is represented by vector A. If interfering vector B_1 is superimposed upon this vector the resulting vector is A_1. (The interference vectors are greatly exaggerated in this figure over those actually found in the experiments in order to illustrate the effect). If interfering vector B_2 is superimposed upon A, the resulting vector is A_2. The min and max A vectors were measured and the difference recorded as the p-p interference.

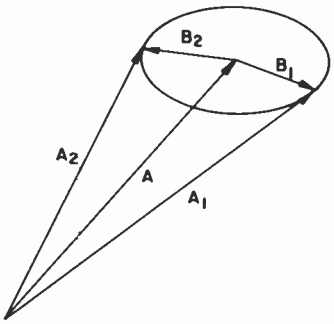

Fig. 10—Vector diagram of color crosstalk components.

The crosstalk levels varied with the luminance level of the desired signal as well as the chrominance level of both the desired and interfering signal. The luminance and chrominance level of the interfering signal was 50 IRE and 79 IRE p-p, respectively. The crosstalk in the desired signal was measured in the yellow color bar, which has high luminance and low chrominance, and in the red bar, which has low luminance and high chrominance. For every parameter variation, crosstalk was measured in both the red and yellow bars in both high-frequency and low-frequency channels. These four numbers were then averaged to obtain a color crosstalk number for each particular parameter variation.

5.2 Color Crosstalk Versus Input Backoff

Curves of color crosstalk versus total input backoff are shown in Fig. 11. These curves were made with group delay equalization in the i-f section at the transmit location. Notice that the crosstalk decreased as the backoff increased (as the transmitted power was reduced). It is seen that for any backoff, the level of the crosstalk changes as other parameters change. For example, there are two curves shown for carrier center spacings of ±9.5 MHz from transponder center and peak video deviations of 5.63 MHz. It is seen that there is less crosstalk with the 15-MHz filter than with the 16-MHz filter. This indeed seems to be the case as is discussed in the next section. There were power-level and noise-floor problems for the tests with the $f_c = \pm 9$ MHz, $B = 17.5$ MHz, and $\Delta F = 7.5$ MHz case, so these results have some uncertainty and are possibly on the high crosstalk side.

The color crosstalk could be seen in the picture when its average p-p level was 1.5 IRE or greater. In general the crosstalk was not visible in the picture and not readily measurable on the waveform monitor at a TIBO of 13 dB (16 dB per carrier). It is estimated that the crosstalk is down about 55 dB below the peak luminance level at a TIBO of 13 dB.

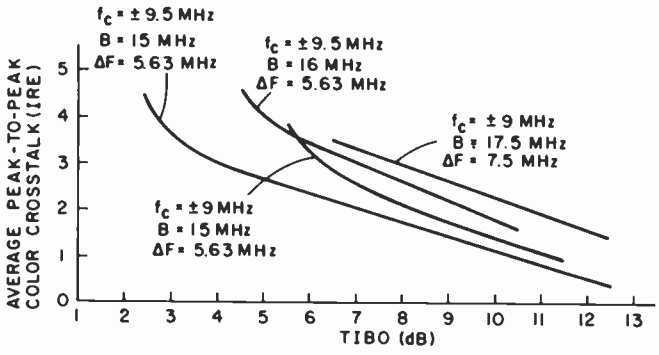

Fig. 11—Color crosstalk versus total input backoff.

The increased noise tends to mask the crosstalk at this backoff. The SNR into the 13 m earth station is only about 43.5 dB at this point. Also, the CNR is close to fm threshold for the 13 m earth station and it would be below threshold for a 10 m, 55 K earth station. The alternate line delay was used to make the crosstalk disappear from the picture and allow a decreased TIBO to 6 dB. This allowed the SNR to increase to about 48.5 dB. It should be noted that the crosstalk measurable on the waveform monitor (though not visible in the TV picture) increased from about 0.4 IRE to 3.6 IRE.

5.3 Crosstalk Versus Filter Bandwidth

As reported in the previous section, there was less crosstalk with the 15-MHz filter than with the other i-f filters. The crosstalk in the 17.5-MHz filters and the 16-MHz filters were found to be roughly the same. The crosstalk averaged over about 20 experiments was about 25% less for the 15-MHz filters than for the 16- or 17.5-MHz filters. This phenomenon was not fully understood at the time and it was decided that it should be investigated further at some future time in the laboratory with other i-f filters, using a test translator or satellite transponder simulator. The 25% reduction in crosstalk may be due to the extra 5-dB attenuation due to rolloff of the 15-MHz i-f filter at the band edges or the gain-slope and group delay characteristics of the filters. This is a question yet to be resolved.

17.5-MHz filters were eventually chosen for the Alaskan 2-for-1 transmission and a 2 dB increase in SNR was achieved by increasing the deviation. It is speculated that for other services one might wish to use 15-MHz filters, put SCPC audio carriers in the same transponder and take the 2-dB reduction in video SNR to gain the 25% reduction in crosstalk.

5.4 Color Crosstalk Versus Video Deviation

The peak video deviation was varied from 6.68 to 7.5 MHz in a 17.5-MHz filter at TIBO = 5 dB and from 5.01 to 6.68 MHz in a 15-MHz filter at TIBO = 5 and 9 dB. There were no significant changes in crosstalk versus deviation.

5.5 Color Crosstalk Versus Equalization

Various experiments were conducted with and without transmit group delay equalizers. For B = 17.5 MHz, f_c = ±9.5 MHz, TIBO = 8 dB, and ΔF = 5.31 MHz, the average p-p crosstalk went from 5.1 IRE without equalization to 2.8 IRE with equalization. In addition, the differential phase went from 6 degrees in one channel and 8 degrees in the other channel to less than ½ degree in both channels with proper equalization. The differential gain did not change substantially with equalization.

Another experiment was conducted with B = 15 MHz, f_c = ±9.5 MHz, TIBO = 6.5 dB, and ΔF = 5.62 MHz. The crosstalk was measured with the low-frequency equalizer in the low-frequency channel and the high-frequency equalizer in the high-frequency channel. Then the equalizers were put in the opposite channels (low frequency equalizer in the high channel and high frequency equalizer in the low channel). The color crosstalk jumped by a factor of 2.5 to 3.

Another experiment concerned the use of group-delay equalization at the receive location rather than the transmit location. When the group-delay equalizers were used at the receive location, the differential phase was reduced from that obtained when no equalization was used. However, the crosstalk remained the same with and without equalization at the receive location.

5.6 Color Crosstalk Versus Inclusion Of Audio Subcarriers

No change in color crosstalk was observed with and without the use of audio subcarriers.

5.7 Color Crosstalk Vs. Chroma Levels

Measurements of crosstalk were made of interfering signals with chrominance levels from 90 IRE peak-to-peak to no chrominance for B = 15 MHz, TIBO = 6.5 dB, f_c = ±9.5 MHz, and ΔF = 5.62 MHz. The results are shown in Fig. 12. The color crosstalk increased monotonically with increased color saturation of the interfering signal. There was no crosstalk from a black-and-white picture as long as there was no color

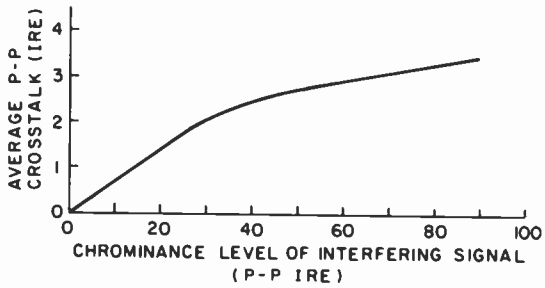

Fig. 12—Color crosstalk versus chroma level of interfering signal.

burst for the black-and-white picture. There is, of course, no color crosstalk between two black-and-white pictures.

Experiments were then made to test the use of chroma de-emphasis. The chroma level of the desired signal was reduced before transmission and then expanded after the receiver. The interfering signal chrominance level was kept constant. The crosstalk remained constant in the transmitted signal as shown by the dashed lines of Fig. 13. This means that the crosstalk after emphasis was actually increased. It is hypothesized that the crosstalk would remain about the same after emphasis if de-emphasis were used in both channels. However, the knee of the curve of Fig. 12 might have some impact.

5.8 Color Crosstalk Versus Carrier Center Frequency

The carrier center frequency was varied in 0.5 MHz steps from ±8.5 MHz to ±10 MHz from the transponder center. The average p-p crosstalk

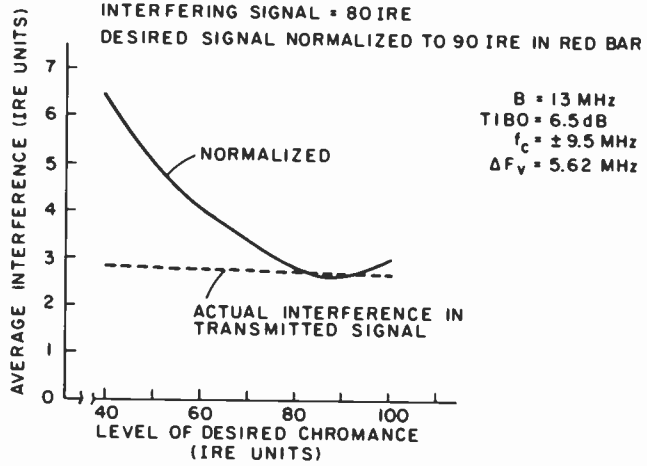

Fig. 13—Effect of chroma de-emphasis.

Low Frequency Channel

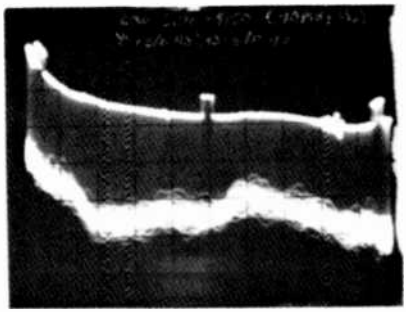

High Frequency Channel

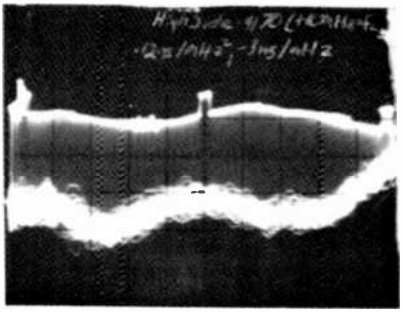

Fig. 14—Amplitude and group delay response with carrier center frequencies ±10 MHz from the transponder center (amplitude—1 dB/div, group delay—10 ns/div).

versus carrier frequency is shown in Table 4 for the following parameters: B = 15 MHz, ΔF = 5.62 MHz, and TIBO = 7 dB.

One-quarter-MHz spacings about ±9.5-MHz-carrier spacings were later tried with parameters B = 15 MHz, ΔF = 6.31 MHz, TIBO = 9 dB. The results were a crosstalk of 1.9 IRE for carriers ±9.25 MHz from the transponder center and 1.8 IRE for carriers at ±9.5 MHz and ±9.75 MHz. Carrier frequencies of ±9.5 MHz were chosen to avoid the excess group delay at the transponder edges (see Fig. 14) and to minimize

Table 4—Crosstalk Versus Carrier Frequency (B = 15 MHz, ΔF = 5.62 MHz, and TIBO = 7 dB)

Carrier Center Frequency	Average p-p Crosstalk
±8.5 MHz	2.5 IRE
±9 MHz	2.8 IRE
±9.5 MHz	1.9 IRE
±10 MHz	2.3 IRE

possible crosspolarization problems with adjacent crosspolarized 2-channel-per-transponder services.[1]

5.9 Color Crosstalk Versus Carrier Imbalance

The two carriers were transmitted at unequal power levels in order to duplicate a condition that might occur when the rf carriers originate at different earth stations. This was done for B = 15 MHz, TIBO = 6.5 dB, f_c = ±9.5 MHz, and ΔF = 5.62 MHz. When the carriers were balanced on the down link, the uplink lower-frequency carrier was found to be 0.6 dB smaller than the uplink higher-frequency carrier. Likewise, when the carriers were balanced on the uplink, the downlink lower-frequency carrier was 0.6 dB larger than the downlink higher-frequency carrier. The color crosstalk did not change appreciably with carrier imbalance of ±1 dB, as shown in Fig. 15. It would be best to set the relative carrier levels on the uplink to obtain the same amount of crosstalk in the

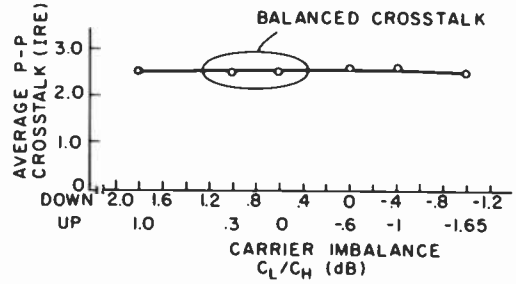

Fig. 15—Color crosstalk versus carrier imbalance.

two television pictures. Balanced crosstalk was found for C_L/C_H (Up) = 0 dB and +.3 dB. Balancing the carriers on the uplink is, of course, more difficult if the carriers are originating at different locations.

5.10 Effect of Different Parameters on Video Impulse Noise

The occurrence of impulse noise in the TV pictures was dependent on the combination of several factors, i.e., TIBO, i-f bandwidth, carrier deviation, and the presence or absence of audio subcarriers.

In general, with all other conditions fixed, the onset of just noticeable impulse distortion (JND) occurred at 1 dB higher CNR (lower backoff) when audio subcarriers were included than when they were not.

JND also occurred at higher CNR as the i-f bandwidth was reduced. For example, with a peak carrier deviation of 5.62 MHz, TIBO = 8.5 dB,

and $f_c = \pm 9.5$ MHz, the impulses were rated as JND with 16-MHz i-f filters, but worse with 15-MHz and better with 17.5-MHz filters.

For other conditions fixed, JND occurred at a higher CNR as the carrier deviation was increased.

5.11 Cancellation of Visible Color Crosstalk

The experimental results of the September 1976 field tests, as well as previous tests, indicated that the visible crosstalk in the TV pictures from both channels in the same transponder could be eliminated by backing off the uplink carrier power at least 13 dB (16 dB per carrier). This amount of backoff, however, is intolerable in most applications because of the sacrifice in the SNR of the received picture. After investigating various means of eliminating the crosstalk in the picture, the development of the alternate line delay unit evolved.[2] This device is installed at both transmit and receive ends of the link in one channel only as shown in Fig. 5. The ALD units were found to be effective in cancelling the otherwise visible crosstalk in both TV pictures in all cases, even with no backoff on either uplink carrier.

Although the ALD processing makes the crosstalk imperceptible in the TV pictures, it does not remove it from the video waveform displays. At TIBO of less than 6 dB (9 dB per carrier), the actual crosstalk still evident in the video waveform displays made it difficult to measure the video performance of the system. It was also difficult to convince many onlookers that the observed TV pictures with no visible video distortions, artifacts, crosstalk, or instabilities were produced by the wildly gyrating signals displayed on the waveform monitor and vectorscope. Since the capability for making routine video performance measurements on the waveform displays was desired, a 6-dB TIBO was selected for the two-for-one system implementation. The resultant crosstalk as measured on the waveform monitor and vectorscope was 3.6 IRE, but it is absolutely imperceptible in either TV picture.

6. Final Parameter Selections and Performance Test Results

Based on the results of the various parameter variations and tradeoffs described previously, the following operating parameters were selected for the RCA two-television-channels-per-transponder service:

Total Input Backoff = 6 dB (9 dB/carrier)
Carrier Deviation for Video = 6.7 MHz (peak)
Carrier Deviation for Energy Dispersal = 0.5 MHz (peak-peak)
Carrier Separation = 19 MHz

IF Bandwidth = 17.5 MHz
Transmit Group Delay Equalization
Alternate Line Delay Unit in one Channel
Audio transmitted by SCPC in another transponder

The key performance measurement results at the 13 m RCA Americom Earth Station at South Mountain, CA (G/T = 32.7 dB/K) were:

SNR = 48.5 dB (CCIR weighted)
CNR = 18.3 dB
Differential Gain = 6%
Differential Phase = 2 Degrees
Average Crosstalk = 3.6 Degrees (Not visible in either picture due to ALD)

The margin in CNR above the impulse noise threshold was 7 dB. The possible allocations of the CNR margin is shown in Table I. The SNR that can be expected by other earth stations is also given in Sec. I.

Table 5—Comparison of Two-Channel-Per-Transponder Services

	Telesat	Intelsat IV-A	RCA-Alaska
BW (MHz)	16	17.5	17.5
TIBO(TOBO)(dB)	4(2)	~(3.5) Comsat 7(3.2)IV Labs 9 (4.5) IVA	6(2.7)
$f_c L/H$(MHz)	±8.75	±9.75	±9.5
F_V(MHz)	6.5	7.5	6.68
$f_{sc} L/H$(MHz)	5.4/5.5	NA	NA
ΔF_A(kHz)	40	NA	NA
ΔF_{sc}(MHz)	1.0	NA	NA
ΔF_{ED}(MHz)	0.2	1–2	.25
CNR(dB)	15	17.2	18.3
EIRP(dBW)	35	26–29	34
G/T(dB/K)	26	41	32.7
SNR_v(dB)	45	>49	48.5
SNR_A(dB)	47	NA	NA
DG	<10%	<10%	6%
DP	<4 degrees	<4 degrees	2 degrees
$EIRP_{up}$		88 dBW	76 dBW
Crosstalk	Yes	Yes	~4 IRE not visible due to ALD

A 6 dB TIBO resulted in a video SNR that is about 8.7 dB worse than could have been obtained with no input backoff. By reducing the backoff of either one or both carriers, the individual SNR's may be increased with no discernible deterioration in either TV picture. Thus, other 2-for-1 systems may be implemented with input backoffs of less than 9 dB per

carrier. The potential advantages of this would be to obtain better TV picture quality and/or allow the use of less expensive receiving earth stations. The disadvantage would be the difficulty, caused by crosstalk, in making standard objective video performance measurements while the system is operating in a full 2-for-1 mode.

It should be noted that the two-TV-channel-per-transponder service was implemented with the program audio transmitted by existing SCPC circuits via another channel. The parameter tradeoff tests described earlier in this paper, as well as further laboratory tests, indicate that the audio may be transmitted on subcarriers in the same transponder as the two TV channels using the same rf carrier levels with no more than 1-dB degration in video SNR.

Interference tests were also made to determine if the two-TV-channel-per-transponder service caused interference into or received interference from the adjacent cross-polarized or co-polarized transponders. The test results showed that no interference could be detected. Similarly, tests for multipath effects via the satellite showed no adverse effects.

Subsequent field tests of transmissions from two separate earth stations have been carried out in Alaska. These tests were quite successful and such services have been implemented on special occasions.

7. Conclusions

We will conclude with a comparison of the Alaskan two-channel service with the two-channel services being offered by other satellite carriers. Table 5 shows comparative parameters for the Telesat service, the Intelsat IV-A service, and the RCA-Alaska service. One can note a number of differences. These differences generally arise from the type of receive earth station and the EIRP, TWTA characteristics, and multiplex filter characteristics of the satellite. The parameter values found in the table may not be current. For example, the Intelsat system could at any time include an audio subcarrier. There is no reason why the RCA system should not include audio as separate carriers, subcarriers, or sound-in-sync with appropriate changes in other parameters. The parameters should change depending on the desired service. This paper should be helpful in making some of these parameter tradeoffs.

Acknowledgments

The authors would like to thank the many people of RCA Americom, RCA Alascom, RCA Laboratories, and the State of Alaska who participated in this program. Particular gratitude is expressed to R. P. Borchardt, R. P. Dowling, G. Elliot, D. Fremont, D. Greenspan, and R. Wilson.

References:

[1] G. W. Beakley, Private communication.

[2] L. Abbott, "Cancellation of Visible Color Crosstalk Between Two TV Signals by Use of Alternate Line Delay," *RCA Review*, **41**, p. 349, Sept 1980 (this issue).

[3] TASO (Television Allocations Study Organization), "Engineering Aspects of Television Allocations," Report of TASO to the FCC, March 1959.

[4] G. W. Beakley, and P. M. Nadkarni, Private Communication.

[5] J. R. Cavenaugh and A. M. Lessman, "The Subjective Effect of Random Noise Spectra on 525 Line NTSC Color Television," *J. SMPTE*, **83**, No. 11, Oct. 1974.

Two-For-One Video Over Microwave Terrestrial Links

Richard J. Klensch and Kevin Kelly

RCA Laboratories, Princeton, NJ 08540

Abstract—Terrestrial microwave radios are used to carry traffic to earth stations for distribution via satellite. RCA Americom is therefore interested in transmission efficiencies in the terrestrial link as well as over the satellite path. Results are given here of a laboratory research program to determine the optimum operating parameters for a two-carrier analog technique to be used in a terrestrial microwave link to double the video capacity. Several alternate approaches that were considered are also described. The effects of system nonlinearities and their control are discussed as is resulting performance as a function of availability. After the laboratory experiments were completed, the modified microwave radio system was installed in an operating link by RCA Americom, where it continues to function at twice normal video capacity.

Introduction

The general goal of the effort described in this paper was to increase the capacity of an existing terrestrial microwave communications link. The approach, while directed toward expanding the video capacity of a particular path, uses techniques that could be applicable to any terrestrial communication path. The specific path is the link that RCA Americom uses to carry video programming from New York City to its main earth station in Vernon Valley, N.J.

Video transmission via terrestrial microwave is typically accomplished by using assigned 20- to 40-MHz wide channels within FCC allocated frequency bands. The specific bands, in this case, are at 6 and 11 GHz. A frequency modulated transmitter having output power capability of

one to ten watts is common for many applications. Fig. 1 shows a simplified block diagram of a microwave radio.

The frequency deviation commonly used in microwave systems carrying video signals is 4 MHz peak. To determine the required bandwidth for transmission, the Carson equation, $BW = 2(\Delta f + f_m)$, is generally used, where Δf is the peak deviation (4 MHz) and f_m is the upper baseband frequency (4.2 MHz for NTSC video). The Carson bandwidth is quite generous and provides for passage of all sidebands that are greater than 10% of the unmodulated carrier level. Furthermore, a microwave channel bandwidth for video transmission in the 6-GHz band, as assigned, is 30 MHz, which is about twice the Carson bandwidth.

Approaches

A number of established techniques are currently in use that allow multiple signals to be carried in a single communication channel. They may be divided into single-carrier/multicarrier and frequency-division/time-division groups.

A carrier can be modulated by one or many independent signal sources by frequency division multiplexing (FDM) where each of the independent signals are given a different frequency slot within the baseband. The composite FDM signal can then modulate the carrier. When frequency modulation is used, the system is referred to as FDM-FM.

Time Division Multiplex (TDM) systems require that the input channels be sampled at the Nyquist rate or higher. These samples are then sequentially combined, and the carrier is modulated by the resultant composite waveform.

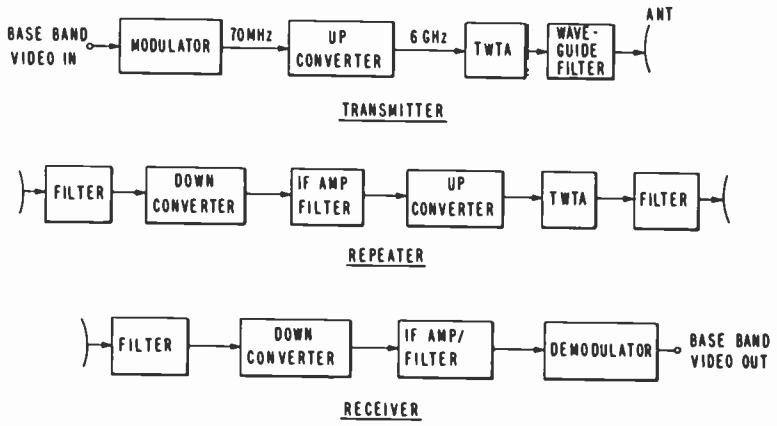

Fig. 1—Simplified block diagram of microwave radios.

Multicarrier systems are also used within a given bandwidth. A single input waveform may modulate each carrier, which is called SCPC (single channel per carrier), or a number of input signals can be combined (FDM or TDM) to modulate any of the carriers.

A further consideration is whether the transmission is analog or digital. Usually digital transmission is incorporated when TDM is used. The output binary data stream phase modulates the carrier using a specially developed modulator-demodulator (modem).*

Obviously, then, a number of methods exist that could provide a doubling of video capacity. In evaluating the various techniques available, we considered, in addition to technical parameters, the cost of implementation. Moreover, it was decided that the candidates for our investigation were to employ equipment that was already in existence and could be conveniently modified for experimentation. Work done by others[1] in the same general area but directed primarily toward satellite communications were considered, as well as commercially available equipment that could be used in either terrestrial or satellite communications.

Baseband Diplexing

One of the first methods to be explored employed commercially available equipment† designed to carry one TV channel and approximately 900 voice channels. The system used FDM with the voice channels occupying the baseband portion, 0 to 5.5 MHz, while the TV signal (after translation) occupies the 6.8 to 12.0 MHz portion of the baseband. The video signal was translated by vestigial sideband amplitude modulation of a 6.8 MHz carrier.

Fig. 2 shows a block diagram of the video-over-voice baseband diplexing system as modified for use in the video-over-video configuration. By replacing the intended 900 voice channel allocation by a baseband video signal, it was possible to carry two TV signals in a baseband of 12 MHz. This composite signal was then used to FM modulate the single carrier in an assigned operating band. No other modification of existing equipment is required when this system is used.

At the transmitter end of the system, the two channels were adjusted so as to produce the same output S/N at the receiver. The lower channel video was pre-emphasized in the usual manner and the upper channel was operated without pre-emphasis. The upper channel deviation was adjusted to provide a Δf of 4 MHz (the standard value). Because of the triangular noise voltage spectrum at the output of an FM demodulator,

* The term modem is used to describe any modulator and demodulator pair.
† Made available through the efforts of D. Fremont of RCA Americom.

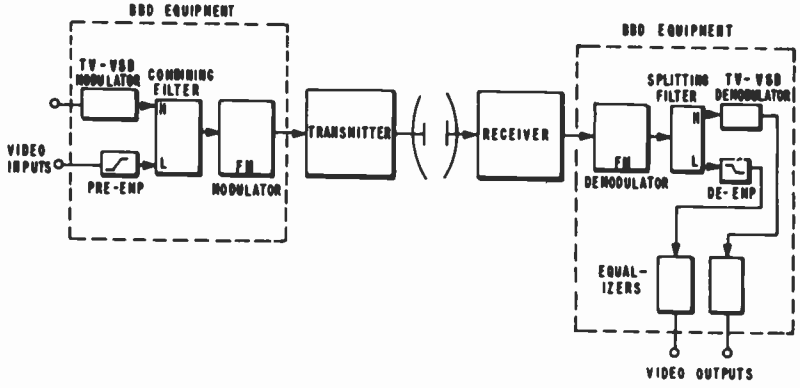

Fig. 2—Baseband diplex system block diagram.

the noise in this upper channel was 16 dB greater than in the lower channel. In other words, the S/N of the upper channel is 16 dB lower than standard. Thus, the two equal S/N signals were 16 dB below the S/N of a standard single channel operating at a Δf of 4 MHz.

At the receiving end, the demodulated signal is applied to a filter that separates the low and high channel video signals. The high channel signal is translated back to baseband and the low channel is de-emphasized and amplified. Both signals are passed through a video equalizer which is used to compensate for the group delay distortion introduced by the combining and separating filters.

The baseband diplexing system was tested over a 3-hop simulated microwave link in the laboratory. The peak deviation was set at 4 MHz for the high channel. To avoid luminance crosstalk from the high channel to the low channel, the modems have to be very linear and must accept the 12 MHz baseband signal. This luminance crosstalk is due only to the nonlinearity of the modems and is not affected by the number of hops in the microwave link. The use of typical microwave modems, which are not designed to handle a 12 MHz baseband, resulted in a signal-to-crosstalk ratio of 17 dB in the low channel. The use of a laboratory modem, which was wideband (15 MHz) and very linear, resulted in a signal-to-crosstalk ratio of about 40 dB when equalized for rf group delay and adjusted for minimum distortion.

Some experiments were carried out to determine how the audio portion of the signal could be carried. Appropriately placed subcarriers were added (4.9 MHz in the low channel and 5.5 MHz in the upper channel) at locations and amplitudes to minimize crosstalk. We measured 63 dB peak S/N with no fading. A technique that placed the audio in the horizontal sync (two 10-bit samples per sync pulse) resulted in a S/N of 71 dB with carrier fades up to 35 dB.

The linearity constraint on the modulators and demodulators for acceptable crosstalk, the 16 dB reduction in FM processing gain, and the high cost of the equipment were the reasons this system was shelved.

Digital TDM

Digital techniques are advancing rapidly and considerable effort has been expended in the area of TV transmission. For example, a system that can handle a number of video signals simultaneously and primarily directed toward satellite applications has been demonstrated. The maximum output bit rate was 64 Mbps and was achieved when two or three video signals were multiplexed together. A single channel could operate up to 32 Mbps and at that rate the picture quality was very good, even in action shots. When 22 Mbps or slower bit rates were used, stop-action was sometimes noticed. This was a result of the buffer overflow.

The system incorporates an 8-bit/sample, 10.7-MHz sampling rate, differential-pulse-code-modulation (DPCM) technique using a frame of storage and sending only difference information via a buffer. Pictures with many changes frame-to-frame require more data to be transmitted and may eventually fill the buffer. At that point the picture is re-transmitted and the stop-action momentarily occurs.

The 64 Mbps data rate requires about 38 MHz of bandwidth when using a QPSK (quadraphase-shift-keying) modem. For satellite applications this is probably acceptable. A microwave channel, however, typically has 30 MHz of bandwidth available and would require a 50 Mbps data rate to properly confine the rf spectrum. Thus, for two-video bit streams, 25 Mbps would be required for each. Pictures sent at this data rate exhibit more of the artifacts in high action shots and could be objectionable.

The system did have a feature that could help in this regard. An adaptive data rate (dependent on the demand) was possible to allow a higher data rate on the "action" picture and a reduced data rate on the slower changing "still" picture. This feature, except when both sources require high data rates simultaneously, would reduce the frequency of occurrence of the stop-action artifacts.

When equipment costs are reduced and further improvements in adaptiveness are incorporated, digital systems for TV transmission will become more common. At this time, however, a low cost analog technique seems most appropriate.

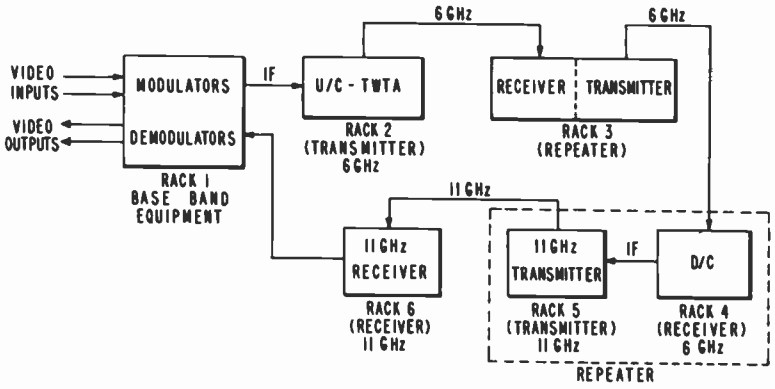

Fig. 3—Experimental three-hop microwave radio system.

Two-Carrier Analog System

As mentioned in a previous paper in this issue of *RCA Review*,[1] a two carrier approach has been used for satellite TV transmission. The constraints for microwave radio use of this system are somewhat different, however, and an experimental program was initiated to determine the optimum configuration and operating parameters for this application. To simulate the actual field conditions, RCA Americom provided a complete three-hop microwave radio system (operating at 6 and 11 GHz) as shown in Fig. 3. Path loss was simulated by fixed attenuators in series with the interconnecting waveguides (variable attenuators were used to simulate fades).

Fig. 4 illustrates the basic premise of the two-carrier approach. Rather than a single carrier centered in the operating bandwidth two carriers are used, each offset from the center. The dashed lines represent the standard carrier location and its modulation spectrum, and the solid lines indicate the locations and associated spectra when two carriers are em-

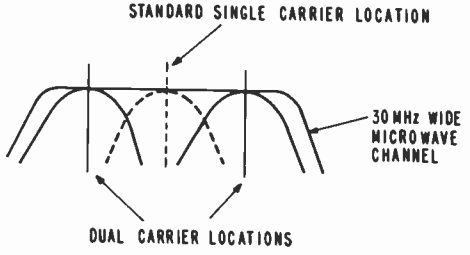

Fig. 4—Carrier locations for single-carrier and dual-carrier approaches.

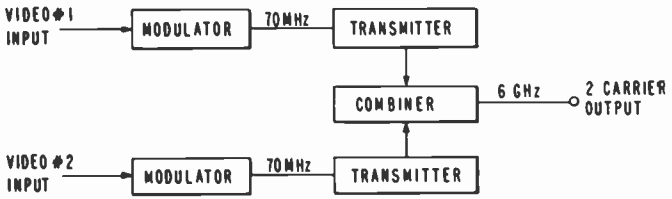

Fig. 5—Implementation of two-carrier system at transmitter site.

ployed. Fig. 5 is a block diagram of the transmitter of the three-hop experimental set-up of Fig. 3. Each of the transmitters consist of an up-converter and the power output TWTA. The up-converter, which is crystal controlled, converts the 70 MHz input i-f signal to the assigned output frequency (in this case the 6 GHz band). The up-converter has sufficient output to drive the TWTA to its saturated output power rating of 10 watts. By simply changing the crystal frequency in each up-converter, the desired offset for the two carriers is obtained. Once that is accomplished, the outputs of the two up-converters could be summed and used to drive a single TWTA. This is not done here, however, for several reasons.

A TWTA, when operated at its maximum output power, is nonlinear and therefore produces unwanted intermodulation products when more than one carrier is present at its input. Also, the TWTA exhibits AM to

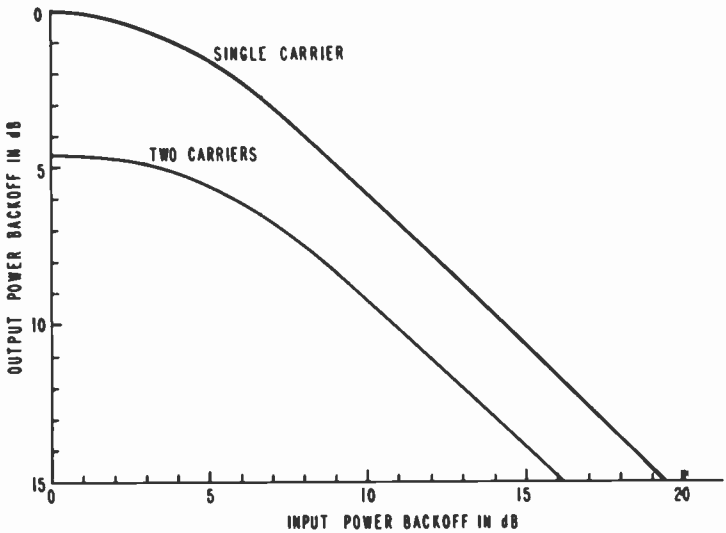

Fig. 6—TWTA output power versus input power characteristics.

PM conversion when operated near saturation and can cause visible crosstalk. The curves in Figs. 6 and 7, which are based on measurements made on a TWTA, indicate the input–output power relationship as well as the output phase versus input power characteristic. To reduce the effects caused by these characteristics, the input signals to the TWTA are attenuated, moving the operating point into the more linear region of the tube. The obvious disadvantage of this solution is the resulting reduction of output carrier power. While a power reduction may be acceptable in some cases, it was not for the simulated path of the experiment (the path simulated was New York City to Green Pond, N.J., a distance of 32 miles).

For this case the preferred implementation was to use two TWTA's, one for each carrier and each operating at full saturated power. Their outputs are then summed in a waveguide hybrid. The summing operation

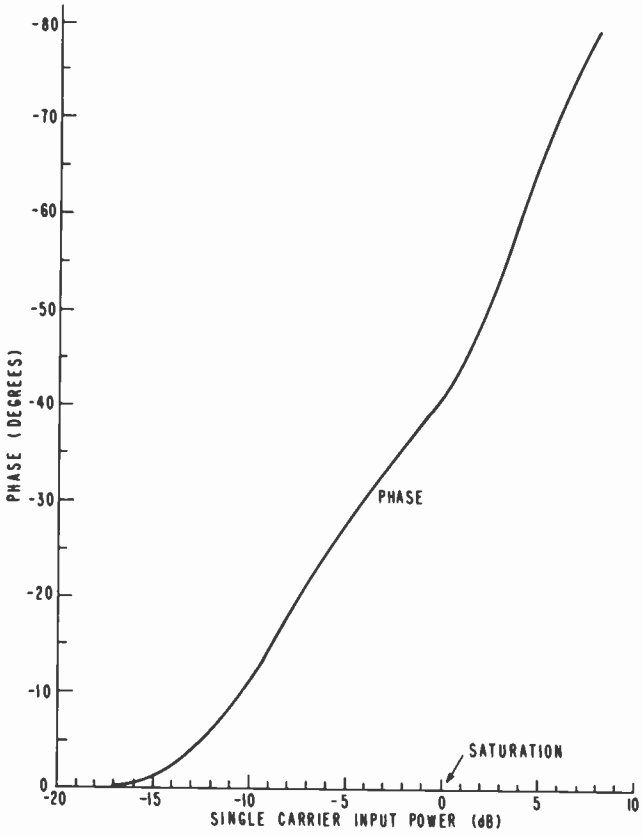

Fig. 7—TWTA output phase versus input power characteristic.

introduces a 3-dB loss per carrier. However, when a single backed-off tube is used, the loss is at least 4.5 dB and can be as much as 11 dB for some conditions. Shorter hops, which require the TWTA drive to be reduced to prevent receiver overload, would not need the second TWTA.

The repeater sites can take on somewhat different configurations depending on the power output requirements. Fig. 8 is block diagram of a dual-channel implementation providing maximum output power but requiring substantial added equipment. Note that the two carriers are separated by filtering and treated independently through the repeater. The two TWTA amplifiers are operated at saturation and their outputs summed at rf, as explained previously.

For cases where some output power reduction is tolerable, consistent with the desired S/N versus availability, there is a simpler preferred mode. Fig. 9 is the block diagram of a single-channel configuration that was actually used in the field implementation of this system. The differences between this arrangement and the original unmodified equipment are minor.

Regardless of how the transmitter at the origination point (New York) and the repeaters are configured, the receiver at the termination point is implemented as shown in Fig. 10. Two down-converters, one offset to the high side and the other to the low side of band center are used, in conjunction with standard 70 MHz i-f filters of appropriate bandwidth, to separate the two FM video carriers. Each of the respective signals is then amplified and demodulated using standard 70 MHz microwave radio FM demodulators.

In its simplest version then, the two-for-one system requires one extra modulator and up-converter at the transmitter and one extra demodulator, filter, and down-converter at the receiver. For the version used in our specific application, an extra TWTA and rf summing network was required at the transmitter end of the link.

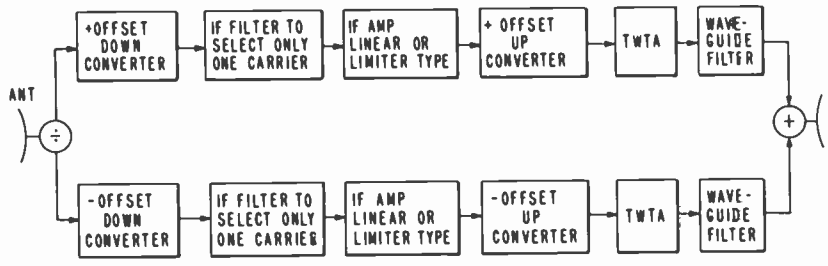

Fig. 8—Dual-channel two-carrier repeater configuration.

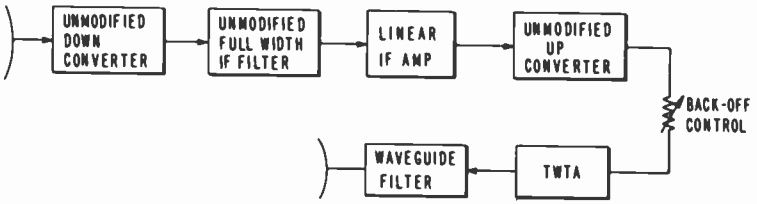

Fig. 9—Single-channel two-carrier repeater configuration.

System Optimization

Three important operating parameters must be determined to optimize system performance:

(1) carrier spacing,
(2) frequency deviation,
(3) magnitude of power backoffs.

Since output signal-to-noise ratio is proportional to received power and to the square of frequency deviation, items 2 and 3 should be maximized and minimized, respectively. The optimum carrier spacing is determined by items 2 and 3 as well as signal distortion considerations. The three parameters are mutually dependent but can be optimized experimentally.

In addition to video distortion and S/N considerations within the operating band, there are other constraints that place limits on these parameters. One, mentioned earlier, has to do with the assigned bandwidth and the required bandwidth of an FM signal. There are FCC rules regarding out-of-band radiation levels. One such rule states, "99% of the signal spectrum power should be confined to the assigned bandwidth." There are other specifications regarding spurious signal levels caused by image frequencies or intermodulation products. The latter specifi-

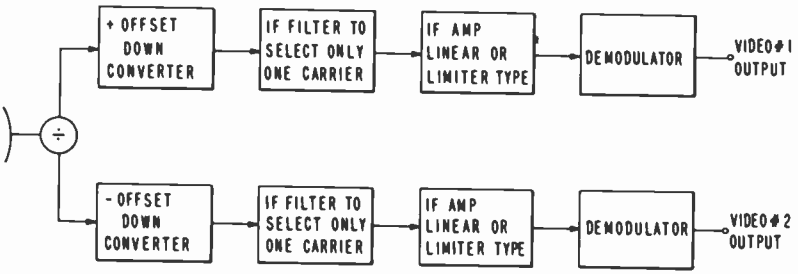

Fig. 10—Implementation of two-carrier system at receiver site.

cation is given as a "mask," an example of which is shown in Fig. 11. Armed with this information as well as the knowledge of allowable video distortion limits,[2] and given the actual equipment available together with band-pass filters, we can begin the process of optimization.

The frequencies of the two up-converters in the transmitter were made variable by the addition of external signal generators. This was also done for the receiver's down-converters. Level setting attenuators were added at the repeaters to allow adjustment of power back-off. If filters of various bandwidths were on hand to correspond to different deviations (these filters are used at the receive end of the system, as shown in Fig. 10). The use of available i-f filters in the transmitter to reduce the radiated spectrum proved to be ineffective when using the maximum possible Δf because they added amplitude and nonlinear phase characteristics that act on the higher deviation components of the input signal. When the signal is passed through a TWTA having AM to PM conversion, the result is spectrum spreading to a degree that produces essentially the same radiated bandwidth as in the unfiltered case. The magnitude of this known effect was determined experimentally. When filters are cascaded, the resultant total amplitude and phase characteristic require a reduction of Δf to maintain the quality of the video distortion parameters; unfortunately this leads to reduced S/N (or availability). It is therefore desirable to use a minimum of filters. The system described uses only one i-f filter per video channel.

The first experiment was done on the repeaters to determine the backoff necessary to keep out-of-band intermodulation (IM) products within the FCC specifications. Some microwave radio repeaters use limiting (clipping) stages in their i-f amplifiers, but such amplifiers

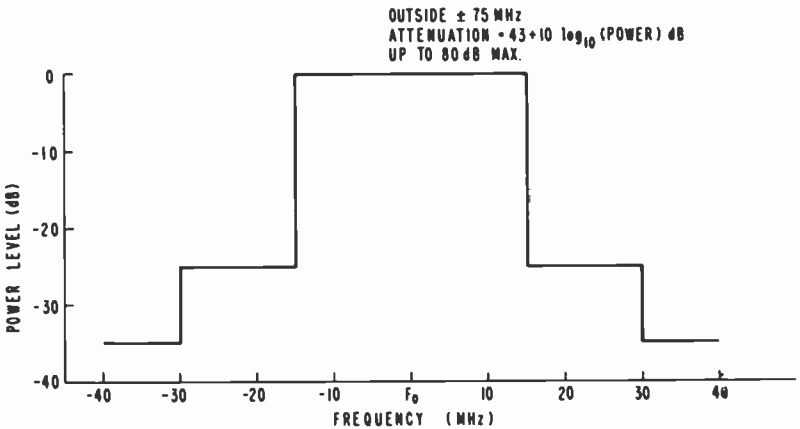

Fig. 11—FCC mask for spurious response in the 6-GHz band.

generate IM products and often have poor AM to PM conversion which is a source of cross modulation. IF amplifiers using linear automatic gain control (AGC) have essentially none of these problems.

Since, in this system, the two carriers are common to all stages of the repeater (down-converter, i-f amplifier, up-converter, and TWTA), all stages should be operated in a linear mode. Those microwave radio repeaters using limiters must have them replaced by linear AGC amplifiers. When the "dual" repeater is used for reasons of higher output power, as shown in Fig. 8, limiting stages may be used, because the individual carriers are separated by i-f filters prior to the nonlinearity and therefore can not produce the unwanted products. As explained previously, the use of additional i-f filters requires reduced deviation and, therefore, tends to eliminate any advantage derived from higher output power. The reduction in drive to the TWTA necessary to keep the IM products within specification depends on the channel filters following the TWTA as well as the tube itself. Fig. 12 is a spectral distribution of IM products generated at the broadly tuned output of a saturated TWTA with two equal-amplitude input signals.

Due to the nonlinearity of the TWTA at saturation, the magnitude of the two desired output carriers are each about 4.6 dB (not 3 dB) below the single-carrier saturated output. The characteristics of output filters vary from manufacturer-to-manufacturer as do TWTAs and, as a result, the required output backoffs must be tailored to the particular equipment being used. Typical total output backoff requirements found in the laboratory were 5.6 to 11 dB per carrier relative to single saturated carrier; that is to say, there is a 1.0 to 6.4 dB loss, depending on the tube, in addition to the 4.6 dB loss per carrier for saturated operation.

The spacing of the two carriers is initially set by locating each carrier half way from the center to the band edge (see Fig. 4). For a 30 MHz wide channel the placement of the carriers is, therefore, ± 7.5 MHz from band center. The intermod products are then located ± 22.5 MHz from band center (the 3rd-order IM), ± 37.5 MHz (5th order), etc. (The spacing of the IM products is equal to the spacing of the two carriers.) The 3rd-order products, when compared to higher order products, are the most critical in that they are the largest and are the least affected by the output channel filter. In this sense, increased carrier spacing reduces 3rd-order IM due to the resulting increased attenuation of the output filter. Other factors, however, have a stronger influence on carrier spacing.

As stated before, the frequency deviation (Δf) of an FM system affects the resultant signal-to-noise ratio as Δf^2. There are limits on how large Δf can become. If we assume that the bandwidth of each of the two carriers (plus sidebands) is 15 MHz (half the original 30 MHz bandwidth) and that the Carson rule applies (BW = $2[\Delta f + f_m]$), then for f_m = 4.2

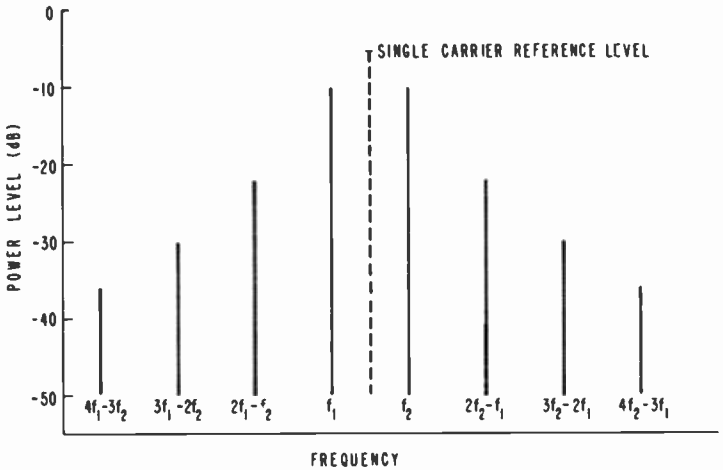

Fig. 12—Two-tone intermodulation spectrum of TWTA operating at saturation.

MHz (maximum modulation frequency for the NTSC system) the peak value for Δf is 3.3 MHz.

Deviation experiments were performed using 10, 12, and 16 MHz i-f filters. First, the maximum allowable deviation through each filter was determined using the set-up shown in Fig. 13. By increasing the deviation until accepted standards of video distortion are just exceeded in the ideal test set-up, an absolute maximum deviation is obtained for each filter. Typical values are Δf = 2.0, 3.0, and 4.0 MHz for the 10, 12, and 16 MHz filters, respectively. A list of video distortion parameters and their broadcast quality limits is given in Table 1. Some video distribution services have less stringent requirements and result in greater maximum allowable deviations. The trade-off for increased S/N is increased video distortion.

A series of measurements were made for each of the three filters to observe the effects of carrier spacing. For minimum crosstalk, the optimum spacing (for two different manufacturer's microwave radio equipments) was ± 8 MHz from band center regardless of the i-f filter used. The optimum was reasonably broad, as shown in Fig. 14. For smaller carrier spacings, the crosstalk was primarily due to spectral components of one signal falling in the pass-band of the other's filter. Increasing the spacing much beyond the optimum value results in increased crosstalk due to AM to PM conversion in the TWTA.

Fig. 13—Test setup for filter experiments.

Table 1—Video Distortion Parameters, Specified and Measured Values for Δf = 4 MHz and IF BW = 16 MHz.

Distortion Parameters	NTC 7 Specifications	Measured Values
Chrom-Lum Delay (nsec)	≤75	6
Chrom-Lum Gain (%)	±6	−6
Field Time Distortion (%)	≤4	<1
Line Time Distortion (%)	≤4	<1
Short Time Distortion (%)	±6	−1
Luminance Nonlinearity (%)	≤10	<1
Gain/Frequency Distortion (%)	+6/−10	−10
Differential Gain (%)	≤15	<0.5
Differential Phase	≤5°	2.6°
Chrominance Nonlinearity (%)	±10	−1.3
Chrominance Phase Nonlinearity	≤5°	<1°
Chrom-Lum Intermod (%)	≤3	≪1

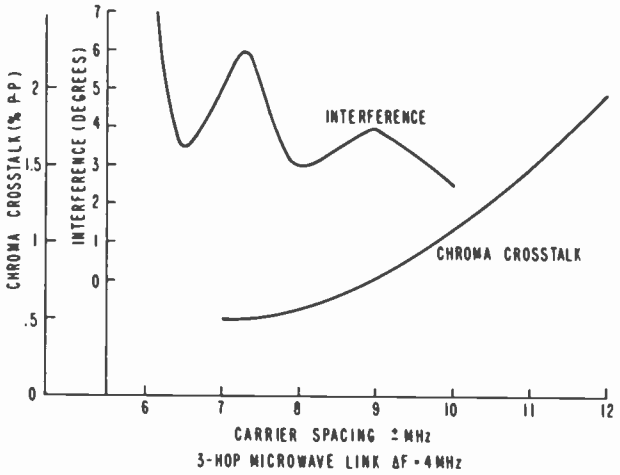

Fig. 14—Crosstalk versus carrier spacing.

The source of the amplitude variation results from the effects of the filter "skirts" operating on the FM spectrum, as illustrated in Fig. 15. Nonlinear phase as well as non-flat amplitude response contribute to the FM to AM conversion. The component of the spectrum most prevalent at band edge, where the problem is most severe, is the 3.58 MHz color sub-carrier and this therefore is the major contributor to the amplitude variation. Thus, the cross modulation produced in the other channel is observed most particularly in the chroma (3.58 MHz) portion of the picture. This chroma crosstalk is easily observed when the interfering signal contains high chrominance and the other channel has color bars as its input modulation. With the sub-carriers not locked to one another, the effect is seen as an amplitude modulation on the color bars

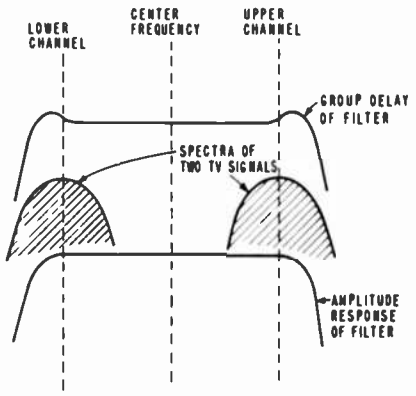

Fig. 15—FM to AM conversion mechanism for carriers with excessive spacing.

having a modulation rate equal to the difference between the two subcarrier frequencies. A waveform monitor is used for this observation. When viewed on a picture monitor, the visual effect is described as "breathing." The vectorscope presentation also gives an indication of the phase modulation of the vector due to the summation of the interfering 3.58 MHz signal.

For a point of reference, just perceptible crosstalk occurs (for a skilled observer viewing a picture monitor) when the amplitude variation as seen on the waveform monitor is 1.5% p-p of maximum luminance signal (100 IRE units on the waveform monitor represents maximum luminance signal). This 1.5% figure is true for the worst case of subcarrier difference frequency, namely, in the few cycles per second region. If the subcarriers are locked or differ at a rate too fast for the eye to track, the subjective result indicates that the figure is increased considerably from 1.5%.[1]

As shown in Fig. 14, the chroma crosstalk can be as low as 0.5% when the path is well equalized. The units of interference in Fig. 14, given in degrees, indicate when the carriers are too close. These units are values obtained from using the vectorscope as the measurement means (for reasons of accuracy and repeatability). The just-perceptible value of crosstalk interference in these units was 3 degrees (a p-p value of phase variation).

If the TWTA backoff requirements were eased (for example, because the output filters eliminated the out-of-band IM products), there could still be a limitation on output power due to AM-to-PM crosstalk. In that case, a combination of TWTA backoff to reduce AM-to-PM conversion and/or a reduction in deviation (Δf) to reduce the FM-to-AM conversion would be necessary.

The occupied bandwidth of the two-carrier system was measured

under conditions of abnormally high, but allowable, input video programming. Both channels were driven with 75% color bars at a Δf of 4 MHz. This signal is rich in 3.58 MHz content and produces a spectrum that is typically twice as wide as program video. The FCC specification that 99% of the total radiated spectral power be confined to the assigned channel bandwidth (30 MHz) was just met when both carriers were modulated by the 75% color bars. This answers the question regarding increasing the filter bandwidths and deviation beyond 16 MHz and 4 MHz, respectively, to further increase S/N. There appears to be insufficient bandwidth to handle larger deviations without violating FCC regulations when very large chroma signals are applied.

Additional Comments and Summary of Dual Carrier 2-For-1 System

The two-for-one video system described has been optimized for microwave radio systems based on experiments made on two different manufacturers' equipments. This technique is attractive in that only minor modifications must be made to existing microwave links for its incorporation. Although there were differences (in one case requiring a change from a limiter i-f to a linear AGC i-f), the results were quite similar. A Δf of 4 MHz, with 16-MHz i-f filters at the receiver, and a carrier spacing of $\pm$ 8 MHz from band center were found optimum in each case. One radio had narrower output rf filters and therefore required less TWTA output backoff. Adequate performance was achieved with a 4.5 to 11.0 dB output-power back-off relative to the original saturated single carrier, depending on specific equipment. This is not considering that some TWTA's produce more output power at saturation than others and may result in more optimistic results regarding backoff requirements.

A feature not mentioned yet is the technique for carrying the audio portion of the video program in this particular implementation. One convenient way of handling the audio is to send it over another microwave radio that is carrying other voice and program channels. Some limited experiments indicate that a frequency-modulated subcarrier in the 5.5 to 7.0 MHz region can be added to each video baseband signal, but the magnitude of the subcarriers and any possible deviation reduction required due to their presence has not yet been determined.

An experiment using the previously mentioned sound-in-sync equipment required a reduction of Δf from 4 to 2 MHz in order to keep crosstalk at just perceptible levels. The subcarrier approach should provide a more promising solution.

Link Analysis and Availability

To determine how well a given microwave path performs when carrying video programming requires a knowledge of the received carrier strength, expected fades, and other factors. Assuming no interference or fades, the received $S/N = (C/N) + 10 \log (\Delta f^2 B) + 2$ dB* (including the FM pre-emphasis gain and noise weighting factor) where

C/N is the received carrier-to-noise in the receiver i-f bandwidth B in MHz,
Δf is the peak deviation in MHz (4 for this case),
B is assumed to be the Carson bandwidth $= 2(\Delta f + f_m)$,
f_m is the highest modulation frequency (4.2 MHz for NTSC TV).

For the above conditions, $S/N = C/N + 26.1$ dB. A requirement for C/N is that it be above threshold for the demodulator being used.

Threshold is the C/N at which the onset of impulse noise occurs. There is a rapid deterioration of the picture as C/N is reduced below that value. Threshold is dependent on the particular receiver used. The use of various "threshold extension" techniques result in quoted thresholds as low as 6 dB. More commonly 8 to 10 dB thresholds are available on receivers so equipped. A conservative figure for a receiver without extension is 13 dB.

The equation for received power is

$$P_r = \frac{P_t G_t}{4\pi R^2} A_r,$$

where

P_t = transmitted output power
G_t = Gain of transmitter antenna
A_r = effective area of receiver antenna
R = range.

This equation neglects losses that are usually present between the transmitter output and its antenna, as well as between the receiver input and its antenna. These losses plus a 3-dB splitting loss at the receiver (where 2 receivers are coupled to the antenna for redundancy) can reach a total of 10 dB.

The received power is calculated for the following conditions:

* This equation stems from the more fundamental $S/N = 3(C/N)\beta^2$, where C/N is measured in a bandwidth of $2f_m$ and $\beta = \Delta f / f_m$.

P_T = 10 watts (40 dBm)
G_T = 45 dB (12-foot dish at 6 GHz)
R = 30 miles
A_R = 74 ft^2 (12-foot dish, 65% effective area)
Total losses = 9 dB (waveguide + splitter).

Substituting, we obtain $P_R \approx 10\ \mu$W or −20 dBm.

The noise power at the receiver is kTB times the noise figure, which gives 6.4×10^{-13} watts ($\approx$ −92 dBm) for a noise figure of 10 dB. The C/N is, therefore, −20 dBm − (−92) dBm = 72 dB. From before, $S/N = C/N + 26.1 \approx 98$ dB. This value of S/N is well beyond the capabilities of modems and most other equipment.

However, this apparent overkill may be required if very high signal-to-noise is to be maintained in high fade conditions. Considerable work has been done in the area of terrestrial microwave radio fading[4] and the following equation is a result of that work:

$$P = \frac{6 \times 10^{-7} D^3 C f}{L}$$

where P is the probability that a fade of factor L will occur over a path length of D kilometers at frequency f (GHz) and path condition C (typically 1/2 or 1). Substituting D = 48 (30 miles $\approx$ 48 Km), $C = 1, f = 6$, and $L = 10^5$ (for a 50 dB fade) into the equation, the probability $P = 3.98 \times 10^{-6}$ results. Stated differently, an availability of 99.999602% is possible for fades not exceeding 50 dB. The total time per year that fades of 50 dB or more will exist is 126 seconds for this example. A 60 dB or more fade will exist 12.6 seconds per year, etc.

In the S/N calculation, a result of 98 dB (unfaded) was obtained. From the information concerning fades, it is clear that for 126 seconds per year the received S/N will be 98 − 50 = 48 dB, or less, and for 12.6 seconds per year the S/N will be 38 dB or less. (A 60 dB fade reduces the C/N to 12, dB which is approximately the threshold condition for the receiver; it is therefore likely that for about 10 seconds per year the signal would be below threshold and essentially unuseable.)

Of further interest, along these lines, is the average time of a fade. From a paper on this subject[4] the average fade time in seconds is given by $400/\sqrt{L}$ where L is again the fade level in power units as a factor (as before, $L = 10^5$ for a 50 dB fade). Using a 50 dB fade as an example, the average length of fade is, therefore, 1.26 seconds. Since (as calculated above) the total yearly fade time is 126 seconds, there are roughly 100 fades per year of 1.26 seconds, each having a magnitude of 50 dB.

A listing of S/N versus availability is useful and is given in Table 2 for the single-hop path used in the example. Also listed in the table are the minimum magnitudes of fades that occur for the given availabilities, as

Table 2—S/N Versus Availability

	Availability			
	99.9%	99.99%	99.999%	99.9999%
S/N	72 dB	62 dB	52 dB	42 dB
Fade Levels	26 dB	36 dB	46 dB	56 dB
Time per year that S/N is lower than above value	32,000 sec	3,200 sec	320 sec	32 sec

well as the time per year that the received S/N is less than the value given in the respective columns.

TDM Approach for Further Increasing Video Capacity

A further increase in video capacity is possible by use of a manufactured equipment called Strap.[3] This equipment time division multiplexes two video signals and transmits alternate fields of each one. Using a Strap system on each carrier would allow the transmission of four video signals over a single channel. Certain artifacts are produced when using this technique. Motion or high action pictures tend to flicker around black/white transitions. A line-to-line interpolation performed on the stored field (the stored field provides signal for the field "lost" at the transmitter during multiplexing) helps in the reduction of the artifact visibility. Ref. [3] describes the results when using Strap via a satellite channel. This system was not considered for use in the experimental implementation because the artifacts were unacceptable for that application.

Conclusion

These laboratory experiments made on terrestrial microwave radio equipment currently in use indicate that, with minor changes, their video handling capacity can be doubled. The resulting picture quality meets video transmission specifications and the output power loss per carrier, due to summing and/or back-offs, affects only the availability.

A 10 dB loss in carrier level for the example in the previous section would result in an unfaded S/N of 88 dB which is still beyond the capability of standard equipment and therefore would go unnoticed. The likelihood of the S/N dropping to 42 dB, however, would rise from 32 to 320 sec per year. Because of the large fade margins used in terrestrial links, the trade-off of doubling channel capacity for (in the worse case) 11 dB of fade margin is an effective one.

Program audio can be transmitted via other microwave channels already carrying voice and program material or may be added by means

of subcarrier to the video baseband. The trade-offs for optimization of the latter approach have not yet been experimentally determined.

Acknowledgments

The authors express their thanks to G. Beakley, W. Houghton, D. Walters, and Paul Schnitzler, who at various times helpfully managed this project and to Dave Zarodnansky for assisting in data gathering. Many invaluable technical discussions were had with L. Abbott, A. Schroeder, Dave Fremont, Gary Abernathy, Gerry Kaplan, and particularly, H. Staras, regarding propagation, TV standards, and microwave radio equipment in general.

References:

[1] L. Abbott, G. Beakley, and W. T. Rowse, "Parameter Tradeoffs for Transmitting Two TV Channels per Transponder," *RCA Review*, **41**, p. 363, Sept. 1980 (this issue).

[2] NTC Report No. 7, *Video Facility Testing—Technical Performance Objectives*, Network Transmission Committee of the Video Transmission Engineering Advisory Committee. Published by The Public Broadcasting Service, June 1975, revised 1976.

[3] L. Abbott "Transmission of Four Simultaneous Television Programs via Single Satellite Channel," *SMPTE*, **88**, p. 106, Feb. 1979.

[4] A. Vigants, "Space Diversity Engineering," *Bell Syst. Tech. J.*, **54**, No. 1, 000, Jan. 1975.

A New Technique for Transmitting Two High Quality Video Signals Over a Single Terrestrial Microwave Channel

G. S. Kaplan

RCA American Communications, Princeton, NJ 08540

Abstract—The growth in the use of communication satellites for distribution of TV signals has generated an incentive to more efficiently utilize the frequency spectrum available for communications. In many cases, video transmissions originate from TV studios located in metropolitan centers and must be conveyed (via a terrestrial microwave link) to earth stations for transmission to the satellite. In large urban areas, frequency allocations for the terrestrial radio link are extremely difficult to obtain. A new video transmission system has recently been installed on RCA Americom's terrestrial microwave link between New York City and its major video satellite transmission facility at Vernon Valley, NJ. In this system, two video channels are conveyed within the frequency allocation assigned to a single microwave channel. This effectively doubles the capacity of the video transmission facilities without a concomitant increase in frequency allocations. The new system has undergone both subjective and objective testing and also has been operated in tandem with the satellite link. Its performance is fully comparable to that achieved with prior transmission techniques, yielding high quality television pictures which should meet the stringent requirements of both broadcasters and the cable TV industry. This paper describes this system, discusses some of the considerations relevant to design, presents the performance measured, and relates this performance to overall end-to-end performance, including the satellite link in tandem with the terrestrial link.

1. Introduction

The growth in the utilization of communication satellites for the distribution of television signals (primarily for the cable television industry, but also for network broadcasters) has created a corresponding increase in the demand on the frequency spectrum. This resource, which is becoming increasingly scarce, is administered or allocated by the Federal Communications Commission (FCC). The frequency allocation (which amounts to permission to use a certain portion of the spectrum) is reserved for use by a communications common carrier, such as RCA Americom. The FCC grants the frequency allocation only after the applicant has coordinated the proposed usage with all other users in the area.

Since video transmissions originate from TV studios located in metropolitan centers, while transmission to the satellite originates at earth stations that are usually located far from the center of the city, a terrestrial microwave radio link is needed to convey the signals to the earth station. Additional frequency allocations for these microwave links are extremely difficult to obtain due to the congestion of the airwaves. The problem is particularly acute in the New York City area. RCA Americom has recently installed a new video transmission system on its terrestrial microwave link between New York and its major video satellite transmission facility at Vernon Valley, New Jersey, in which two video channels are carried within the frequency allocation assigned to a single microwave channel. This doubles the video transmission capacity of the facilities without a concomitant increase in required frequency allocations.

The performance of the new system is fully comparable to that achieved with prior transmission techniques, yielding high quality television pictures that should meet the stringent requirements of both broadcasters and the cable TV industry.

This paper describes the system installed, discusses some of the considerations relevant to system design, presents performance measured over the terrestrial link for both the new and prior transmission techniques, and relates this performance to overall end-to-end performance, including the satellite link in tandem with the terrestrial link. A companion paper by Klensch and Kelly in this issue of *RCA Review* describes the experimental tests that confirmed the operational parameters of the system described here.

2. System Description

To better understand the considerations that led to the new transmission system, which achieves a doubling of video capacity, a brief description of the prior conventional one-channel system will prove helpful. Video signals originating from New York City are transmitted to RCA Americom's satellites for further distribution. The communications satellites are accessed via Americom's earth station located at Vernon Valley, NJ. The video signals are conveyed from New York City to Vernon Valley via a terrestrial link (see Fig. 1) consisting of three "hops". The first hop out of New York City (between 60 Broad Street and the first repeater at Greenpond) is the longest (32 miles) and is at a frequency in the 6-GHz band. The other hops are much shorter (11 miles and 2 miles) and utilize frequencies in the 11-GHz band. The transmission technique used previously employed a single carrier located in the center of a band of frequencies allocated to the path. In addition to the video signal, one or more audio channels are carried by frequency modulating separate subcarriers and combining these subcarriers with the video signal to produce an extended baseband, which is then used to frequency modulate the single rf carrier. The bandwidth required to carry this information without imparting any noticeable distortion to the TV signal is a function of the frequency deviation of the rf carrier, maximum baseband frequency, and number and spectral location of the audio subcarriers.

The typical terrestrial system uses a peak deviation of 4 MHz due to video alone, and since the video signal falls off considerably in spectral content above 4.2 MHz, the amount of bandwidth required to convey

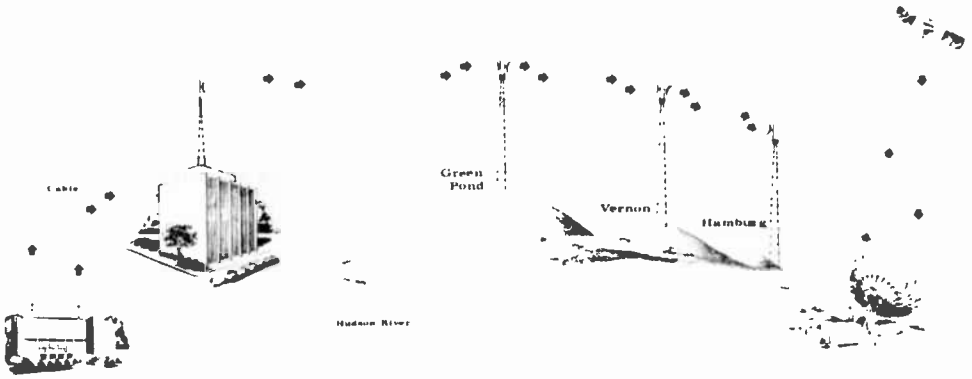

Fig. 1—New York to Hamburg (Vernon Valley), New Jersey, terrestrial microwave link.

the video information alone is approximately 14 to 16 MHz for an excellent (broadcast) quality signal. The bandwidth allocated for video transmission at 6 GHz is 30 MHz wide which is much more than is required, as shown in Fig. 2. When audio is conveyed over the same microwave channel as the video, the bandwidth required will increase unless the deviation due to the video is reduced. The increased bandwidth required for video and audio is still well within the allocated bandwidth of 30 MHz for 6 GHz carriers and 40 MHz for 11 GHz carriers. This conventional system provides a full broadcast quality signal and has been the standard transmission technique.

When RCA began investigating approaches that would increase the capacity of its microwave link for video transmission, it was decided to concentrate on a system that provided signal quality virtually indistinguishable from the conventionally transmitted signal. It was also decided to utilize a system that would use the same power limits, be within the same allocated bandwidth, and meet the same out-of-band emissions limits as are currently specified for the conventional video system in order to facilitate obtaining FCC authorization.

The approach chosen, which meets all of the above criteria, is as follows. Instead of a single carrier located in the center of the allocated bandwidth, two separate carriers are utilized, each offset in frequency from the center of the band as shown in Fig. 2(b). Each carrier is frequency modulated by video program material. Methods for carrying the audio channels that are associated with the video will be presented later. The video signals are completely independent and no synchronization between them is required. The operational parameters such as frequency

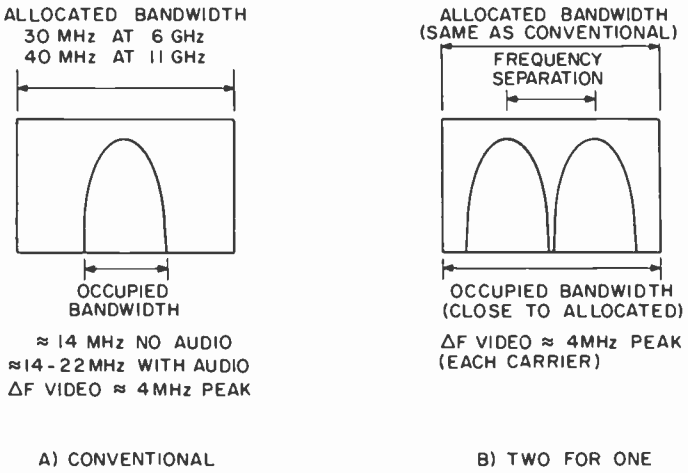

Fig. 2—Bandwidth considerations.

separation between carriers, frequency deviation due to the video signal, and strength of each carrier were chosen to optimize the performance characterized by signal to noise ratio, various video distortion parameters, intermodulation and crosstalk, and FCC regulatory constraints. The dual carrier approach may be implemented in many different ways, with the specific implementation having profound effects on performance. The approach chosen was oriented towards optimizing the performance over the New York to Vernon Valley terrestrial link. As we examine the implementation for this particular link, the system considerations involved will become clear and the applicability to other terrestrial paths highlighted. A block diagram of the basic system is shown in Fig. 3. All components such as modulators, transmitters, receivers, circulators, and bandpass filters are off-the-shelf items which have been designed for conventional video transmission.

System operation is described by starting in New York at the transmit site where there are two separate video modulators and two separate transmitters. The transmitters operate on adjacent frequencies separated from each other by approximately 16 MHz. Each transmitter is operated at the same (maximum) power as it would operate at for conventional operation. Although the traveling wave tubes (TWT), which provide the final power amplification, are operated in a saturated mode which is inherently highly nonlinear, this does not cause any difficulty at the origination site in New York because each transmitter is only handling a single carrier. The output of the two transmitters is combined in a summer which is a purely passive device (a magic tee in this case). The magic tee combiner provides isolation between the transmitters and also introduces a 3 dB loss in each carrier so that the total power radiated is the same as for a single transmitter before the combiner. The output of the combiner consists of two frequency modulated carriers which are

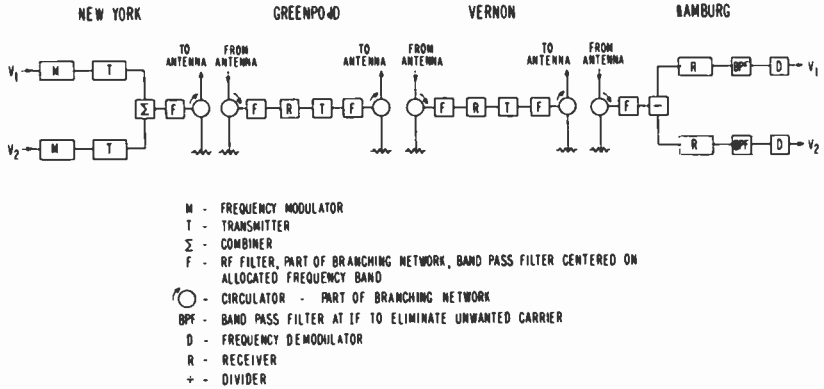

Fig. 3—Two video signals in a single terrestrial channel (basic system).

offset in frequency and therefore do not overlap or interfere with each other. Both carriers are sent through the same bandpass filter and circulator (which is part of the conventional branching network), combined with the other transmissions from the New York site and radiated from the transmitting antenna to the first repeater site, at Greenpond, 32 miles away.

At the Greenpond repeater, after reception at the antenna, the two carriers are passed through the microwave bandpass filter which is tuned to reject all received signals except the two carriers in the desired frequency band. Again, this is still conventional. Both carriers are now *simultaneously* fed to the single receiver which is tuned to the center of the frequency band. In other words, at the repeater, the receiver's local oscillator is at the same frequency for two-for-one transmission as for conventional transmission. The output of the receiver (in the 70-MHz range) is fed to the single transmitter whose output is then (after passing through the conventional branching network) radiated to the next repeater located at Vernon Valley (about 11 miles away). The local oscillator for the transmitter (at the repeater) is tuned to the center of the frequency band and is therefore at the same frequency for single video or two-for-one video transmission.

We have been using conventional components, tuned to the standard frequencies (except for the offset carriers transmitted from New York). However, the fact that this technique has both carriers simultaneously in the same receiver and transmitter (at the repeater sites) has several implications on operation that differ from the single video operation.

The reason that two-for-one video requires a change in operation arises from the nature of the signals that are carried by the repeaters. A frequency modulated carrier has essentially no amplitude fluctuations. However, two frequency modulated carriers (one for each video channel) have significant amplitude fluctuations. Therefore, any nonlinear effects in the TWT would cause distortions through the intermodulation products whereas these same nonlinearities could be ignored previously.

Fortunately, the nonlinearities involved may be dealt with in a simple manner which allows a practical system to be attained. One major nonlinearity is due to the output TWT of the transmitter. To overcome this nonlinearity, one can operate the TWT in a linear mode by backing off (or attenuating) the input signal a sufficient amount. This of course reduces the output power from the TWT. However, on this particular path between New York and the earth station at Vernon Valley, the hop out of New York dominates the link performance. But here two TWT's are used, each at saturation; therefore, there is no significant loss in performance. The reduction in power from the transmitters at Greenpond

and Vernon are not large enough to cause these hops to introduce any significant effects on performance. The system calculations and measured performance, presented later, will verify this.

The backoff must also be sufficient to ensure that the constraints on out-of-band emissions and cross-talk are satisfied. The required backoff is a function of the TWT and upconverter nonlinearities as well as the nominal output level from the IF amplifier feeding the transmitter upconverter. With the parameters obtained for the microwave equipment installed on the New York to Vernon Valley path, an output backoff at Greenpond of about 12 dB for each single carrier (or 9 dB total) is sufficient to provide excellent performance.

There was one additional potential source of nonlinearity that is present in terrestrial microwave systems that was necessary to investigate before a viable system could be configured.

Due to the nature of terrestrial propagation at microwave frequencies, it is expected that at times a significant amount of signal fluctuation may occur. Fluctuations of 20 to 40 dB may occur and the system must be designed to accommodate them. At each receiver an i-f amplifier is used which maintains the signal fed to the transmitter upconverter at a constant level (i.e., independent of fluctuations). There are a number of ways of accomplishing this, and the various manufacturers of radio equipment take different approaches.

One approach is to operate the i-f amplifier in a saturated mode with limiters used to maintain signal level. A different approach is to sense any variations in the output level and actually adjust the gain of the amplifier to accommodate the fading. Since the fading is a relatively slow phenomena, the automatic gain control (AGC) circuits are set to respond to these slow variations. These two approaches, while both adequate for single video operation, affect the two-for-one video operation in very different ways.

The first approach (using hard limiting) does not work with amplitude varying signals as it tends to eliminate all amplitude fluctuations. This leads to excessive intermodulation and crosstalk and is not acceptable.

The second approach (true AGC sensing) utilizes circuitry which responds to the slow (fading) variations and keeps the i-f output level insensitive to those variations. On the other hand, the AGC circuits will not respond to the much faster fluctuations due to dual carrier operation. This has the effect of introducing a nonlinear gain for slow fading and a linear gain for the fast fluctuations. It turns out that the linearity of the i-f amplifier is sufficient to permit dual carrier operation with excellent performance, as verified by testing in an operational link.

At the last receiving site (Vernon Valley) the two carriers are separated

from each other and the two video signals demodulated. The separation is accomplished by having each receiver tuned to the frequency of one of the carriers and employing a narrow band (about 16-MHz wide) bandpass filter to accept the desired carrier and reject the undesired carrier.

The system which has been described above has been implemented on the New York to Vernon Valley terrestrial path. The fully operational system is a protected service (hot standby) as shown in Fig. 4. The performance, as measured on the actual path, is presented in the next section.

3. Performance

Due to the complex nature of the video signal, performance is generally characterized by a plethora of parameters which measure various imperfections that may be imparted by the communications channel. These parameters portray an objective measure of performance and indicate in a quantitative manner the deleterious effects of the non-ideal (real world) transmission system.

The imperfections usually considered result from the addition of noise and interference, or crosstalk, to the desired signal as well as a multiplicity of distortions, which may be linear or nonlinear.

The performance of the two-for-one video terrestrial system has been characterized by a series of measurements of the video parameters. While measurements were performed on one of the two-for-one terrestrial radio channels, a color bar test signal was simultaneously carried over the other channel. The color bar test signal is considered to have strong interference potential.

Since the terrestrial system is used to convey video signals to the earth station for transmission via satellite, the performance of the terrestrial channel in tandem with the satellite system was also measured. For these

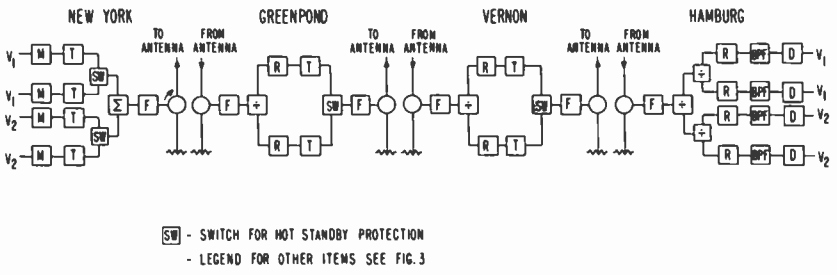

Fig. 4—Two video signals in a single terrestrial channel (operational system, fully protected).

tests, two different transponders (20 and 24 on RCA Americom's F1 Satellite located at 135°W) were accessed using up and downlinks at the earth station at Vernon Valley. The results of the measurements are presented in Table 1. The performance objectives recommended by the Network Transmission Committee of the Video Transmission Engineering Advisory Committee are also shown in this table, along with a somewhat more stringent objective which, if met, will provide an even higher quality signal. For these tests, the peak frequency deviation due to the video signal was 4 MHz, the frequency separation between video carriers was 16 MHz, and the i-f filters in the receivers at Hamburg each had a bandwidth of 16 MHz.

It is clear from Table 1 that the performance objectives have been met and that excellent quality video signals have been provided.

After the objective tests were completed, some time was spent in subjective tests. Observations of the programs transmitted over a two-for-one video channel and (for comparison) a conventional video channel over the terrestrial link were made. The pictures were of excellent quality with no marked viewer preference for one over the other. The video distortion measurements showed that performance of the two-for-one terrestrial link by itself and in tandem with the satellite link should be acceptable.

As part of the subjective evaluation, two unlocked color bar test signals were used as sources for the two-for-one video terrestrial microwave links. No discernible crosstalk effects were noted. Actually, by viewing the monitor, it was not possible to ascertain whether the adjacent channel was carrying modulation.

4. Signal-To-Noise Considerations

The previous section presented data that showed that excellent performance had been obtained for the two-for-one video terrestrial system. Some consideration is now given to the effects of noise and specifically how the nature of terrestrial propagation affects system performance. Specific results for the New York City to Vernon Valley terrestrial microwave link (see Fig. 1) will be shown.

The major problem on terrestrial microwave links is fading. Fading over these links has two basic origins. The first is multipath propagation which causes a reduction in signal strength due to interference between signals arriving at the receiver from different paths. The second major cause of fading is attenuation due to rain. For links using 6-GHz frequencies, the fading is dominated by multipath considerations. For 11-GHz links, the deep fades (occurring rarely) are caused by rain attenuation while the less severe, but more frequent, fades occur because of multipath.

Table 1—Measured Video Performance for Two-for-One Terrestrial Link and Two-for-One Terrestrial Link in Tandem with Satellite Link and Performance Objectives

Parameter	Signal	Terrestrial Channel A	Terrestrial Channel B	Channel A+ Trans. 20	Channel B+ Trans. 24	End-End Objectives	NTC-7 End-End Objectives
Insertion Gain Sync Amplitude Burst Amplitude	Bar Sync Burst	100 IRE 40 IRE 39 IRE	100 40 40	100 40 40	100 40 39	100 ± 3 IRE	100 ± 3 IRE
Line Time Waveform Distortion	Bar	1 IRE	1	1	2	4 IRE pk-pk	4 IRE pk-pk
Short Time Waveform Distortion	2T	98 IRE	102	98	102	100 ± 4 IRE	100 ± 6 IRE
	Bar Edge	4 IRE	2	5	5	7 pk-pk	10 pk-pk
Chroma-Lum. Gain Inequality	Chroma Pulse	95 IRE	97	97	97	100 ± 3 IRE	100 ± 3 IRE
Chroma-Lum. Delay Inequality	Chroma Pulse	0 nsec.	20	0	0	40 nsec.	75 nsec.
Differential Gain	Staircase	2 IRE	3	3	5	8 IRE	15 IRE
Differential Phase	Staircase	1°	1.2°	1°	.5°	3°	5°
Gain-Frequency Distortion	Multi-Burst					50 ± 3 IRE	45 IRE to 53 IRE
	0.5 MHz	48 IRE	50	48	50		
	1.0 MHz	48 IRE	50	47	49		
	2.0 MHz	48 IRE	51	48	50		
	3.0 MHz	49 IRE	52	51	49		
	3.58 MHz	48 IRE	50	51	50		
	4.2 MHz	49 IRE	50	52	51		

Table 1 (continued)

Parameter	Signal	Terrestrial Channel A	Terrestrial Channel B	Channel A+ Trans. 20	Channel B+ Trans. 24	End-End Objectives	NTC-7 End-End Objectives
Chroma Non-Linear Gain Distortion	3 Level Chroma	20 IRE 40 IRE 78 IRE	21 40 77	20 40 77	21 40 75	20 ± 2 IRE 40 IRE 80 ± 5 IRE	20 ± 2 IRE 40 IRE 80 ± 8 IRE
Chroma Non-Linear Phase Distortion	3 Level Chroma	0.5°	1.3°	1.5°	1.5°	3°	5°
Chroma-Luminance Intermodulation	3 Level Chroma	0 IRE	0	0	0	3 IRE	3 IRE
Field Time Waveform Distortion	Square Wave	0 IRE	0	1	0	4 IRE	4 IRE
Signal-to-Noise Ratio (weighted)	*	over 60 dB	over 60 dB	55 dB	57 dB	55 dB	53 dB

* Note: The signal-to-noise ratio over the terrestrial link was measured at over 60 dB. It was also found that there was little difference in signal-to-noise between the two for one terrestrial channel and a standard (one for one) microwave channel.

The calculations presented here make use of the propagation results presented by Vigants[1] and Lin[2] of Bell Laboratories as well as storm models and rainfall statistics.[3,4] The results of the prior work have been applied to RCA Americom's New York to Vernon Valley terrestrial microwave link. The relative performance between a two-for-one and a conventional channel may be readily ascertained, although the absolute accuracy of the fading distribution is of course dependent on the quality of the propagation statistics utilized. A summary of the results is shown in Table 2.

The performance for three different systems is presented in Table 2. The first system is the two-for-one system as implemented while the second system is the same equipment configured as for a conventional implementation (no combiner in New York, no backoff at the repeaters, and one divider deleted at Hamburg). Since the previous transmitting antenna at New York City had a lower gain than the transmitting antenna currently being used, the performance calculations were repeated to show what the performance of a conventional system would have been.

Availability refers to the fraction of the the time that the signal-to-noise ratio is expected to exceed the value shown in Table 2. Note that an availability of .9999 implies that only for less than one hour per year will the signal-to-noise ratio be poorer than the value indicated in Table 2.

The results indicate that during the bulk of the time the terrestrial link will provide greater than 60 dB signal-to-noise ratio and that only for a small fraction of time (totaling less than one hour per year) will the signal-to-noise fall below that value. The difference in performance over the terrestrial link between the two-for-one and one-for-one systems is about 7 dB at .9999 availability. However, had the one-for-one system been implemented with the previous transmitting antenna, there would

Table 2—Performance of Video Over Microwave Channel (New York to Vernon Valley)

System	Availability		
	.99	.999	.9999
Two-for-One Video Hot Standby Present Antenna	>60 dB	>60 dB	49.5 dB
Single Video Hot Standby Present Antenna	>60 dB	>60 dB	57.0 dB
Single Video Hot Standby Previous Antenna	>60 dB	>60 dB	54.0 dB

Note: (1) Frequency deviation due to video is 4 MHz in all cases. (2) Present antenna in New York City has gain of 44.7 dB. The previous antenna had a gain of 41.3 dB.

be only a 4-dB difference in performance at the .9999 availability. It should be noted that at this high degree of availability, the deep fades are of extremely short duration (typically around 4 seconds) and the subjective effect on a video signal would be extremely difficult to discern.

Since the signals are conveyed over the microwave link for the purpose of re-transmission via satellite, the end user sees the effects of the satellite link in tandem with the terrestrial link. In most cases, this performance will be completely dominated by the satellite link and not the terrestrial link. This was verified by calculating the signal-to-noise ratio expected for the space segment with the uplink at Vernon Valley and the downlink at various sites across the country. The earth stations at most of these sites were assumed to be typical of those installed for the cable television industry (with a G/T of approximately 21 dB/k).

As shown in Table 3, the space segment generally provides lower signal-to-noise ratios than the terrestrial link and performance is indeed dominated by the space link. If a two-for-one terrestrial channel were substituted for a single video (conventional) channel, the end user viewing the combined space and terrestrial effects would not see any difference.

This was also verified in subjective tests carried out at Vernon Vailey which has a much better space segment performance than the CATV earth stations.

Table 3—Video Signal-to-Noise

Terrestrial Only	Availability .99	.999	.9999
Two-for-One, present antenna	>60 dB	>60 dB	49.5 dB
Single Video, present antenna	>60 dB	>60 dB	57 0 dB
Single Video, previous antenna	>60 dB	>60 dB	54.0 dB

Space Segment Only*		Availability .99	.999	.9999
Receive Site	G/T			
Starke, FL	21	46.9 dB	46.8 dB	46.0 dB
Starke, FL	28	53.0 dB	52.9 dB	51.6 dB
Spruce, NC	21	49.0 dB	48.9 dB	48.3 dB
Vernon Valley, NJ	21	49.2 dB	49.1 dB	48.5 dB
Vernon Valley, NJ	32	58.1 dB	58.0 dB	55.6 dB
Houston, TX	21	48.1 dB	48.0 dB	47.5 dB
San Jose, CA	21	46.8 dB	46.7 dB	46.2 dB

* Uplink at Vernon Valley, Transponder 24, F1.

5. Audio Transmission

The initial emphasis in establishing the viability of the two-for-one video transmission system has been on conveying the video information. Associated with every video program of course is an audio channel and it is equally important to convey this audio information in a manner which preserves excellent performance in a reliable manner. A number of techniques for the transmission of audio have been considered. Although the final decision as to which technique will be utilized has not been made, all of the four techniques presented here will provide excellent performance in an operational environment.

The first technique considered is to simply add the audio via a standard program channel frequency modulated subcarrier located just above the video baseband. This is, of course, the same way that the audio is carried on the single video channels. The advantage of this method is that since video and audio are carried over the same radio, it is simple from an operational standpoint. The disadvantage of this approach is that in order to keep the two channels constrained to the same bandwidth as previously required, it will be necessary to reduce the deviation due to the video to compensate for the increased baseband necessitated by the audio subcarrier. This will decrease the video signal-to-noise performance. It is estimated that a reduction of between 1.5 to 2.5 dB in video signal-to-noise may result. This will still provide excellent performance.

Other techniques considered convey the audio over a different microwave radio. There are several variations.

The current terrestrial microwave system between New York and Vernon Valley has basically two types of microwave radio traffic. One is video and the second is message. The standard video (one-for-one) is capable of carrying up to four audio channels using the frequency modulated subcarrier approach. Therefore, if the microwave system contains a mixture of two-for-one and one-for-one video channels, some or all of the audio channels may be carried on the one-for-one video radios.

If the audio capacity of the one-for-one video channels proves inadequate, then the capacity could be increased by utilizing a recently developed digital technique called Digital Audio for Television (DATE).[5] This technique which conveys four high quality audio channels on a single subcarrier, when used in conjunction with an additional frequency modulated subcarrier, could extend the capacity of the single video channels to five audio channels.

Even if the video requirements dictate that all video channels be converted to two-for-one operation, thereby precluding the above one-

for-one techniques from being implemented, it is still possible to provide excellent audio performance. This may be accomplished by using the message radio. A single group (of twelve telephone type channels occupying 48-kHz bandwidth) may be replaced by one or two 15-kHz program audio channels using currently available (off the shelf) equipment.

The advantage of carrying the audio in a separate microwave radio is that the two-for-one video channels will not experience any loss in signal-to-noise ratio due to the audio. The disadvantage of the techniques which utilize a separate radio is that some customers are uneasy about this approach. There might be operational problems that could lead to the loss of audio while video is still present or vice versa. Since any operational installation will be fully redundant, the likelihood of outages due to equipment failure will be low.

To summarize, the audio associated with the video may be conveyed either in the same microwave radio or a separate radio. Each approach has its own consideration but it is clear that excellent audio performance may be obtained. In our tests with the two-for-one video system, the audio was carried in a separate radio over one of the one-for-one video channels.

6. Conclusions

A system for transmitting two video programs within the frequency allocation assigned to a single video channel has been installed and tested over the New York City to Vernon Valley terrestrial microwave link. The system is such that the transmissions use the same total power as the single video channel. The performance has been excellent as confirmed by extensive objective and subjective observations for both signal-to-noise and video distortion effects. In the system tests, the audio has been conveyed via a frequency modulated subcarrier over another terrestrial video channel.

Acknowledgments

Many people from both RCA Americom and RCA Laboratories have cooperated or assisted in bringing the system to its current state. Many of the initial discussions with Liston Abbott, Harold Staras, Richard Klensch, and Dan Walters were helpful in formulating some of the system considerations. The availability calculations were carried out using information and techniques suggested by Harold Staras. Many of the video modulation parameters were confirmed or determined experimentally by Richard Klensch, assisted by Kevin Kelley and David

Zarodnansky. The installation and checkout of the microwave radios was carried out with the cooperation of Frank DeMille and the testing of the system over the microwave link and also the satellite received the significant assistance and cooperation from Frank DeMille, Bob Berntzen, Bob Kalb, Jim Easton, and Jack Brodersen.

References:

[1] A. Vigants, "Space-Diversity Engineering," *Bell Syst. Tech. J.*, **54**, No. 1, p. 103, Jan. 1975.

[2] S. H. Lin, "A Method for Calculating Rain Attenuation Distributions on Microwave Paths," *Bell Syst. Tech. J.*, **54**, No. 6, p. 1051, July–Aug. 1972.

[3] H. E. Bussey, "Microwave Attenuation Statistics Estimated from Rainfall and Water Vapor Statistics," *Proc. IRE*, **38**, p. 781, July 1950.

[4] A. E. Freeny and J. D. Gabbe, "A Statistical Description of Intense Rainfall," *Bell Syst. Tech. J.*, **43**, p. 1789, July–Aug. 1969.

[5] S. Salamoff, "Program Audio Distribution Via Existing Video Transmission Facilities," presented at 120th SMPTE Tech. Conf., Oct. 31, 1978.

Security of a Popular Scrambling Scheme for TV Pictures

V. Mangulis

RCA Laboratories, Princeton, NJ 08540

Abstract—Signal voltage inversion on random lines has been proposed as a means of securing satellite transmissions of TV signals against unauthorized reception. We have simulated a possible configuration of equipment needed by an unauthorized earth station to steal a signal; the computer simulation shows that relatively simple line-to-line correlation can be used to unscramble the picture with some degree of success.

1. Introduction

At the present time, TV signals for the networks and for cable TV are transmitted via satellites without any safeguards against reception by unauthorized earth stations. To provide protection against this type of theft, a pseudo-random scrambling scheme for the TV picture may be utilized. The scheme should be such that (a) the scrambled picture is not satisfactory for viewing, (b) the cost of building a good unscrambler without the knowledge of the pseudo-random scrambling sequence is high, and (c) the cost of building an unscrambler for authorized earth stations which know the scrambling sequence is low.

A frequently proposed simple scrambling method would invert the signal voltage of pseudo-random lines in a TV frame (only for the picture part of the line, the synchronization part would remain uninverted); the inversion would be done around the voltage corresponding to medium gray. Consequently, the inverted line corresponds to the photographic negative for a black-and-white TV picture. For color video, most

scrambled pictures appear black-and-white because (1) the scrambling destroys the normal 180-degree phase shift between chrominance signals on adjacent lines and (2) the same line in the next frame will have the chrominance 180 degrees out of phase if it is inverted. Fig. 2 shows a scrambled version of Fig. 1; because only a single frame is shown, some color does appear in Fig. 2.

We have studied the security of this scrambling scheme, and have simulated on a computer a particular configuration of a potential thief's equipment that unscrambles the picture by simple line-to-line correlation. The simulated equipment has been applied to the ten pictures shown, Fig. 1 and Figs. 3–11. The computer simulation shows that this relatively simple unscrambling method succeeds even if there is a horizontal movement of the scene from frame to frame. Consequently, the use of voltage inversion for scrambling may not provide sufficient security.

2. Configuration of Unauthorized Receiver

We assume that the unauthorized receiver produces both an inverted and an uninverted version of a received line and that it correlates both with the previous line in the field. The best fitting of the two is then chosen as the true signal. The top line is saved from field to field to give a starting line for correlation. Such a top line will be wrong when a new scene begins; therefore, a human operator may have to intervene to invert the whole picture if the wrong decision is made at the top.

If the wrong decision is made in the middle of the picture, the picture will be inverted in the bottom half only; consequently, the operator should be able to override the automatic equipment and to invert selected parts of the picture manually.

If there is a sharp horizontal edge separating areas of black and white (or dark gray and light gray or, for example, dark cyan and light red), the equipment will make the wrong decision. However, not all such wrong decisions are bad; for example, Fig. 12a would become 12b, which could be acceptable.

We assumed that the received signal voltage for 2/3 of the line is divided into N line segments (we used only 2/3 of the line so that we could simulate horizontal movement of a scene by shifting lines horizontally, as explained below). Thus a large N means short segments and a small N means long segments. Correlation was performed between segments. The thief's equipment would use only one particular N; we tried several to determine the optimum. To obtain a decision criterion based on luminance, we integrated the signal voltage over each of the N line segments (the integration process eliminates most of the high frequency

Fig. 1—First scene.

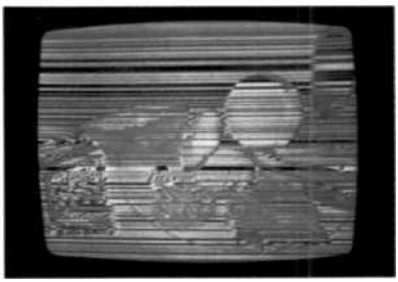

Fig. 2—First scene scrambled by voltage inversion.

Fig. 3—Second scene.

Fig. 4—Third scene

Fig. 5—Fourth scene.

Fig. 6—Fifth scene.

Fig. 7—Sixth scene.

Fig. 8—Seventh scene.

Fig. 9—Eighth scene.

Fig. 10—Ninth scene.

Fig. 11—Tenth scene.

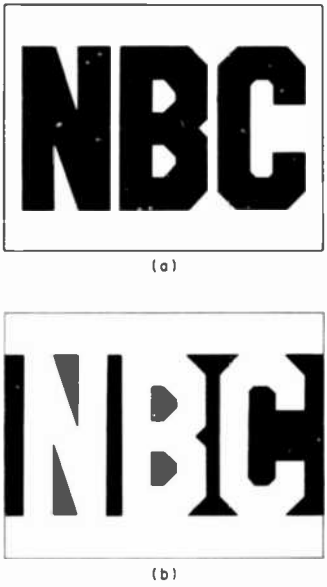

Fig. 12—Effects of sharp artificial boundaries: (a) original picture and (b) mistakenly correlated picture.

chrominance) and then calculated the sum of N squares of the difference between the integrated voltages of the previous line and of the present line, the latter both uninverted and inverted. The correct line should have the smaller sum of squares if the luminance distribution of the two lines is correlated.

To obtain a decision criterion based on chrominance, we demodulated the received signal by multiplying it by a sine wave at the color subcarrier frequency, both in phase and in quadrature. The demodulated signal was then processed the same way as for luminance, except that this time the correct line should have the larger sum of squares because chrominance is 180 degrees out of phase on adjacent lines.

We assumed that the two decision criteria will be combined. The relative strength of each criterion in the combined criterion could be adjusted by the human operator to reflect the color qualities of the presently received picture; for example, the chrominance criterion would be eliminated for black-and-white pictures.

3. Simulation Results

3.1 Mistakes Within a Frame

The thief's equipment was simulated on a computer. One field from each of the 10 pictures (Figs. 1 and 3–11) was digitized and processed on the

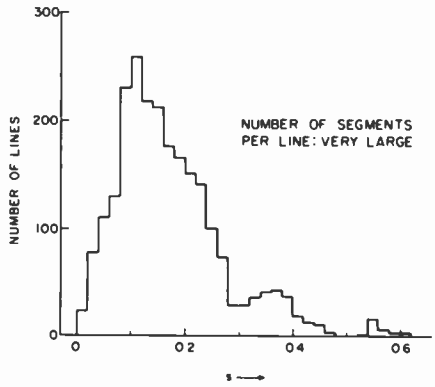

Fig. 13—Decision criterion histogram, luminance only, very large number of segments.

computer to yield an estimate of how often a mistake will be made in natural scenes (without artificially sharp boundaries).

We would expect that a large N (short line segments) would give a good correlation of fine luminance details from line-to-line within the same frame, and that the number of mistakes made would be increased if the number of segments N is decreased. This is confirmed by Figs. 13–15. These figures show histograms of the number of lines that have a particular luminance decision criterion value s, where s is the difference between the sums of squares for the inverted and uninverted line, nor-

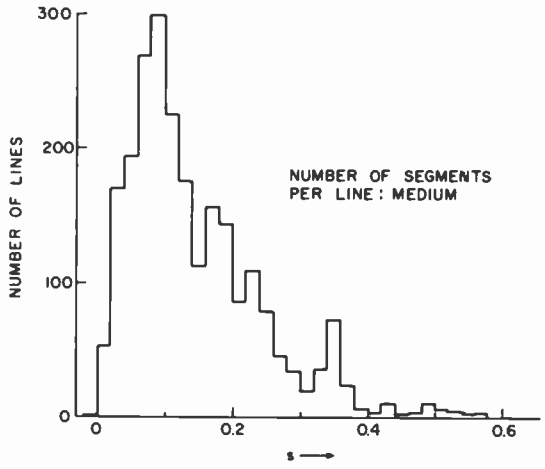

Fig. 14—Decision criterion histogram, luminance only, medium number of segments.

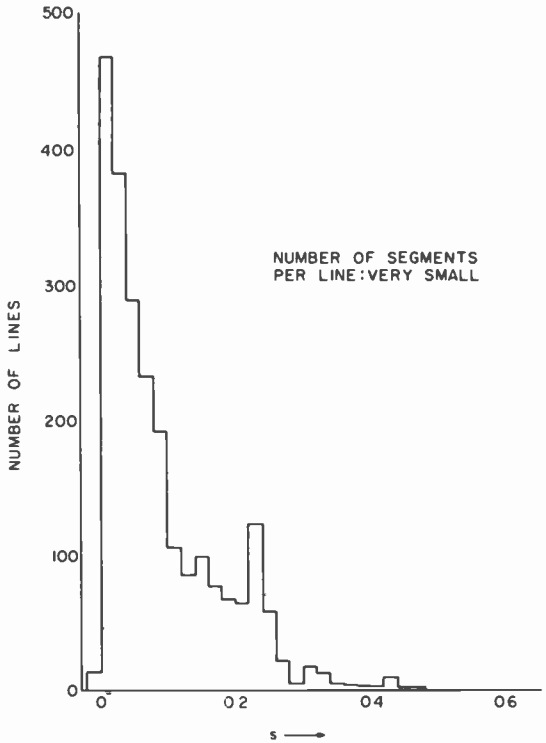

Fig. 15—Decision criterion histogram, luminance only, very small number of segments.

malized so as to lie between −1 and +1. A mistake is made when s is negative. As can be seen by comparing the figures, the number of mistakes increases and the distribution shifts towards negative values as N decreases.

On the other hand, we would expect that a very large N may give a poor chrominance value, because the demodulation process is not very

Table 1—Percent of Frames With at Least One Error

Number of Segments Per Line	Decision Criterion Based On		
	Luminance Alone	Balanced Chrominance and Luminance	Domination by Chrominance
Extremely large	0	0	50
Very large	0	0	10
Large	0	0	0
Medium	10	0	0
Small	30	0	0
Very small	70	10	10
Extremely small	90	20	20

Table 2—Percent of Frame-To-Frame Errors for Horizontal Movement and a Decision Criterion Based on Luminance Above

Number of Segments Per Line	Horizontal Shift from Frame-To-Frame (%)				
	0	2.1	4.2	8.4	16.8
Very large	0	0.08	0.08	5.2	25.3
Large	0	0.04	0.08	5.2	25.0
Medium	0	0	0.30	3.6	25.0
Small	0.13	0.13	0.21	1.4	20.5
Very Small	0.72	0.93	1.6	5.4	15.6

effective for a short signal segment. A high frequency luminance component, such as the vertical lines visible at the top of the PanAm building in Fig. 8, may masquerade as chrominance in the sum of squares for the inverted line because it would be 180 degrees out of phase (as required) in the inverted line. Yet a very small N may not be very successful either, because the color may change rapidly along the line. Consequently, we would expect an intermediate value of N to do best. This is confirmed by the last column in Table 1. Table 1 shows the percent of pictures (from our sample of 10) with at least one mistake versus the number of segments N for a decision criterion (a) based on luminance alone, (b) balanced between luminance and chrominance, and (c) dominated by chrominance.

For extremely large N and decision criterion dominated by chrominance, the five pictures with at least one error are Figs. 7–11. They have at least some areas with little color and some periodic variations of luminance which, for the inverted line, are mistakenly interpreted as chrominance, the example of the vertical lines at the top of the PanAm building in Fig. 8 has already been mentioned; in Fig. 7 the mistakes are made in the curved black-and-white sign where the lettering provides a periodic variation of luminance.

3.2 Mistakes from Frame to Frame

To obtain an estimate of the probability of making a mistake at the beginning of a frame when the first line is correlated with the first line saved

Table 3—Percent of Frame-To-Frame Errors for Horizontal Movement and a Decision Criterion Based on Balanced Chrominance and Luminance

Number of Segments Per Line	Horizontal Shift from Frame-To-Frame (%)				
	0	2.1	4.2	8.4	16.8
Very large	0	0	0	1.4	10.9
Large	0	0	0	1.5	10.6
Medium	0	0	0	0.80	9.9
Small	0	0	0	0.04	6.6
Very small	0.25	0.25	0.30	1.3	6.7

Table 4—Percent of Frame-To-Frame Errors for Horizontal Movement and a Decision Criterion Based on Domination By Chrominance

Number of Segments Per Line	Horizontal Shift from Frame-To-Frame (%)				
	0	2.1	4.2	8.4	16.8
Very Large	0.08	0	0.04	0.68	6.3
Large	0	0	0	0.72	6.1
Medium	0	0	0	0.47	5.1
Small	0	0	0	0	4.2
Very Small	0.17	0.30	0.17	0.51	3.2

from the previous frame, we processed each and every one of the lines in the 10 unscrambled pictures as if it were the first line in a new frame. We simulated horizontal motion (camera movement or a moving scene such as a train passing a stationary camera) by shifting the two lines to be correlated relative to each other. A shift of 8.4% corresponds to a speed of 45 mph at right angles to the camera line-of-sight at a distance of 100 feet when the field of view is 15 degrees (135-mm lens).

Tables 2 through 4 show the percent of mistakes made as a function of the horizontal movement and of the number of segments N. Note that when N is small and the decision criterion is dominated by chrominance, the equipment did not make any mistakes even for as large a shift as 8.4%. This is in accordance with what one would expect. Larger segments (smaller N) should do better when there is motion because fine details are shifted and thus do not correlate, but the average properties over larger segments do correlate.

Note that in Table 4 for N very large, there are more mistakes for no horizontal movement than for a slight shift of 2.1%. The mistakes for 0% shift are due to periodic luminance mistaken for chrominance; at the 2.1% shift, the correlation between the periodic luminance has been destroyed, and thus there are no mistakes.

We simulated vertical motion by skipping several lines between the two lines to be correlated. A skip of 26 lines in the field corresponds to the 8.4% horizontal movement described above. Tables 5 and 6 show the percent of mistakes made as a function of the vertical motion and of the number of segments N. The number of mistakes is much greater than

Table 5—Percent of Frame-To-Frame Errors for Vertical Movement and a Decision Criterion Based on Balanced Chrominance and Luminance

Number of Segments Per Line	Number of Lines Skipped in the Field				
	0	6	12	26	54
Very Large	0	0.38	0.99	3.8	8.4
Large	0	0.33	1.1	3.6	8.0
Medium	0	0.27	0.82	3.1	8.0
Small	0	0.27	0.82	3.5	7.5
Very Small	0.25	0.71	1.8	4.0	9.4

Table 6—Percent of Frame-To-Frame Errors for Vertical Movement and a Decision Criterion Based on Dominance by Chrominance

Number of Segments Per Line	Number of Lines Skipped in the Field				
	0	6	12	26	54
Very Large	0.08	0.60	1.6	4.6	8.6
Large	0	0.55	1.6	4.3	8.6
Medium	0	0.44	1.3	4.0	8.7
Small	0	0.44	1.4	4.3	8.2
Very Small	0.17	0.88	1.5	4.1	8.6

for horizontal motion. One would not expect the two motions to yield the same results, because for horizontal motion the correlation is performed along a line in the same direction as the motion, while for vertical motion the correlation is performed at right angles (i.e., the two situations are not symmetrical).

An error percentage of, say, 0.27% would yield an error rate of 5 errors per minute which may not be tolerable. However, rapid vertical motion is probably less likely than rapid horizontal motion. The errors were confined to a few pictures. For example, errors were made only in Figs. 7 and 11 when the number of lines skipped was 26, the number of segments per line was small, and the decision criterion was based on domination by chrominance. In those two pictures, the skipping of the lines eliminates gradual blurred transition from light to dark; a jump from a light area to a dark area generates a mistake.

Similar problems can be expected when zooming is employed.

4. Conclusions

Edges in natural scenes (such as the edge of the table in Fig. 5) are sufficiently blurred and may not be perfectly horizontal so that the lines are correlated correctly. Sharp artificial horizontal edges may be correlated incorrectly but such mistakes sometimes can be tolerated. Vertical motion may produce errors from frame to frame if the top of the picture moves from light into dark or vice versa. However, rapid vertical motion probably does not occur very often.

A small number of segments per line (a large length of each segment) and a decision criterion emphasizing chrominance yields very few mistakes for stationary scenes and for motion horizontally. Consequently, it should be relatively easy to unscramble the picture most of the time, and the use of voltage inversion for scrambling may not provide sufficient security.

Acknowledgment

The scrambled picture shown in Fig. 2, was obtained by the use of equipment provided by Liston Abbott of RCA Laboratories.

Time Division Multiple Access of Satellite Transponders by Analog Video Signals (On a Field or Frame Interleaved Basis)

A. Acampora and G. Saulnier

RCA Laboratories, Princeton, NJ 08540

Abstract—Multiple access of a single transponder channel carrier from two spatially separated video uplink sites is feasible. In order to time share the channel on a field (or frame) basis, certain requirements must be met. This paper describes the implementation of an analog video TDMA system with respect to acquiring the appropriate time slot and generating the transmitter baseband signals. Concepts of signal recovery are also presented.

1. Introduction

Techniques for carrying two or more video signals in one satellite transponder exist. Full-duplex operation is afforded by dual carrier techniques; for simplex half (or full) transponder operation, commercially available, field interleaved techniques can be used. The unexplored area is point-to-point or point-to-multipoint partial transponder operation by time-division sharing of a single video FM carrier. Such a system, using multiple access to some portion of a transponder's bandwidth to effectively interleave video signals in the space segment, can be readily used in a full duplex mode (e.g., teleconferencing) or as two independent simplex circuits. In either case, the video signals occupy the same segment of the transponder bandwidth. A project was thus undertaken to investigate and develop time division multiple access (TDMA) techniques for carrying two (or more) analog video signals originating from two (or more) locations, in partial satellite transponder bandwidths.

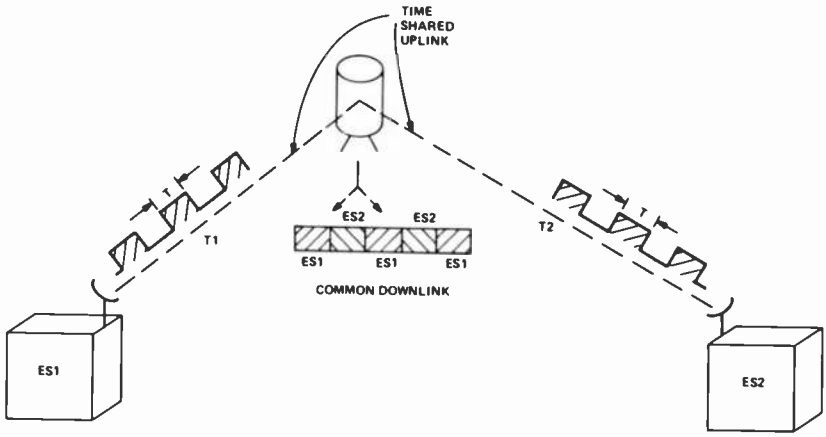

Fig. 1—Configuration for two earth station.

Fig. 1 is a pictorial representation of the multiplexing function. In this case, two earth stations are sending out bursts of information (by modulator keying) with equal on and off intervals of T units of time. Consider the signals from the respective earth stations to be phased on an absolute time scale such that the two signals interleave in the satellite transponder without destructive interference (i.e., no overlap). Under this condition, combined (or aggregate) signals can occupy a common downlink as shown, thus providing full duplex point-to-point operation in one transponder (or half-transponder channel).

Taking advantage of the line, field, and frame periodicity of video signals, two television stations could uplink independent bursts of video information using the same transponder (or partial transponder) bandwidth in a TDMA mode. Three different stages are involved in such a system:

(1) *Aquisition:* the burst intervals at any one station must be determined in real time such that proper interleaving can take place in the satellite.
(2) *Synchronous Signal Generation:* the signals to be transmitted by each station must be arranged in such a way that the "aggregate" downlink behaves properly.
(3) *Signal Recovery:* the downlink aggregate signal must be decoded to permit retrieval of the "other" signal.

This paper describes research into the requirements of aquisition and generation and presents experimental results obtained with some of the subsystems developed. Some interesting results in the area of signal recovery are also presented.

Aquisition

Suppose there is a continuum of signal bursts in the satellite as shown in Fig. 2. This signal has originated at some (master) earth station, ES1, and is being received by a second (remote) earth station, ES2. The information on and off intervals are each T time units long, as shown. If the transit delay from the satellite to ES2 is D units of time,* then the signal received at ES2 will be as shown in Fig. 2. The question is whether or not the second earth station can directly use these recovered time intervals to initiate its own information transmission intervals.

Assume, as a starting point, that the second earth station does use these received intervals to determine the transmission intervals. Then the information bursts transmitted by ES2 based on these intervals, will reach the satellite D time units later. Relative to satellite time, they will be received $2D$ units of lapsed time after the reference edge. As can be seen from Fig. 2, the signals reaching the satellite from the second earth station will not fall properly within the open time intervals unless $2D$ equals some integer multiple of T, i.e.,

$$2D = nT, \text{ where } n \text{ if an integer,}$$

which would pratically never be the case.

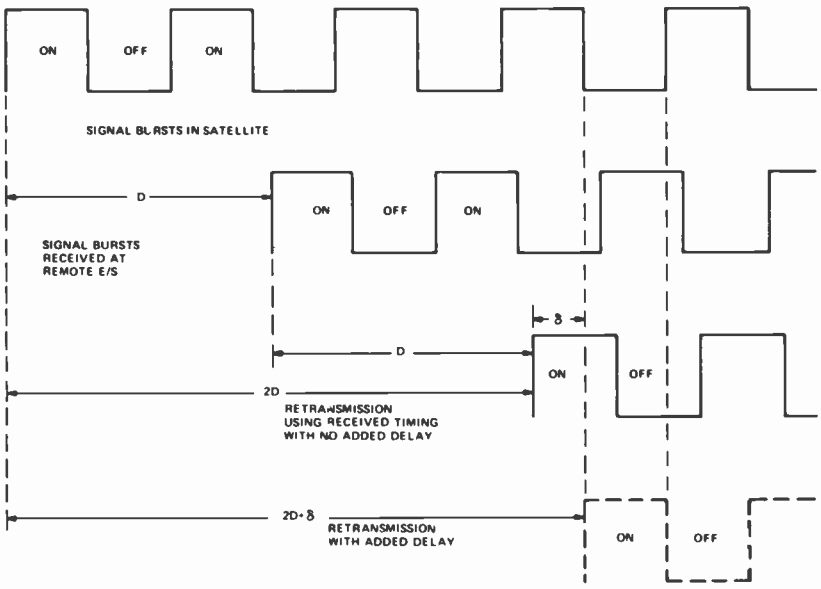

Fig. 2—Satellite and remote earth station timing.

* Usually, $D \gg T$, especially for video signals.

Obviously, some delay, δ, can be introduced prior to utilization of the received timing signal (as a transmit gate) by the second earth station to ensure the relationship

$$2D + \delta = nT,$$

where the added delay, δ, needed to arrive at the smallest possible n, is always less than T time units.

This establishes the algorithm that defines the transmission intervals at the second earth station, namely, observe the time intervals received from the originating earth station and retime (shift) these intervals by δ. In this context, the first earth station is the master station, issuing transmission bursts timed to its own video generation equipment. The second earth station must then derive its transmission intervals from, as well as synchronize its own video to, the received signal.

It is necessary, therefore, to determine the delay increment, δ, and to shift the edges of the observed information intervals from the master earth station by this amount. To accomplish this, consider the timing diagrams of Fig. 3. Suppose at the remote earth station there exists a reference generator whose periodicity and duty cycle match exactly the system information burst timing. Such a signal need only be frequency locked but not necessarily phased locked, to the system timing.

If this signal were uplinked from the second station, and observed on the downlink side (loop-back mode), then the trip to the satellite would take D time units, and the return would also take D units, as shown. The time duration between the edges of the return signal and the edges of the reference signal is δ, the delay factor sought. Measurement of this time interval therefore establishes δ.

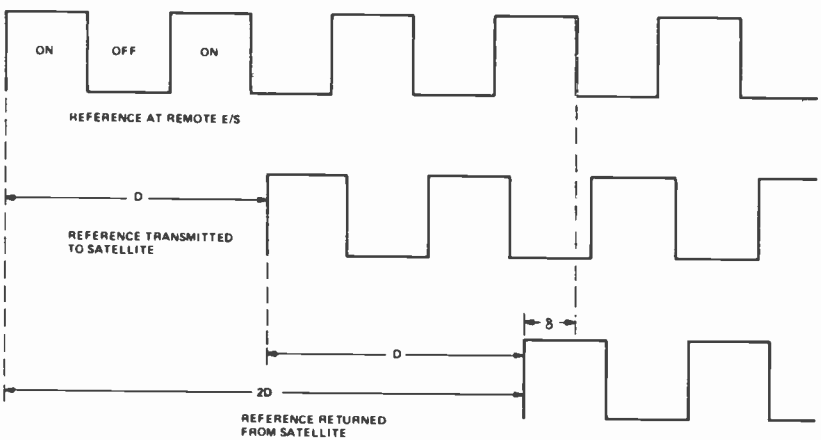

Fig. 3—Delta measurement technique.

In practice, frequency lock of the reference to the system information burst timing can be guaranteed by direct utilization of the received (system) timing to create the reference. Methods of accomplishing this are presented next.

2.1 Timing Subsystem

The block diagram of the timing unit is shown in Fig. 4. The operation of the unit presumes the existence of marker pulses, at the remote station, that denote the beginning and end of the transmission time slots from the master. The derivation of these pulses will be discussed at length in the sections dealing with signal generation. It suffices here to say that the marker pulses can be obtained by direct observation of the downlink rf bursts from the master, although they can be more rigorously derived from the video baseband itself, such as by vertical interval detection.

The marker pulses proceed to a timing pulse generator that forms a square-wave signal. This signal is high for the interval of signal presence and low for the interval of signal absence. The square-wave signal is the reference signal to be looped-back in the satellite for ranging measurements. It also is the timing signal for the remote station after it is shifted (i.e. retimed) by the δ increment.

To measure the δ increment, the returned reference signal starts an interval counter (counting on a stable, local, time-base clock). The end

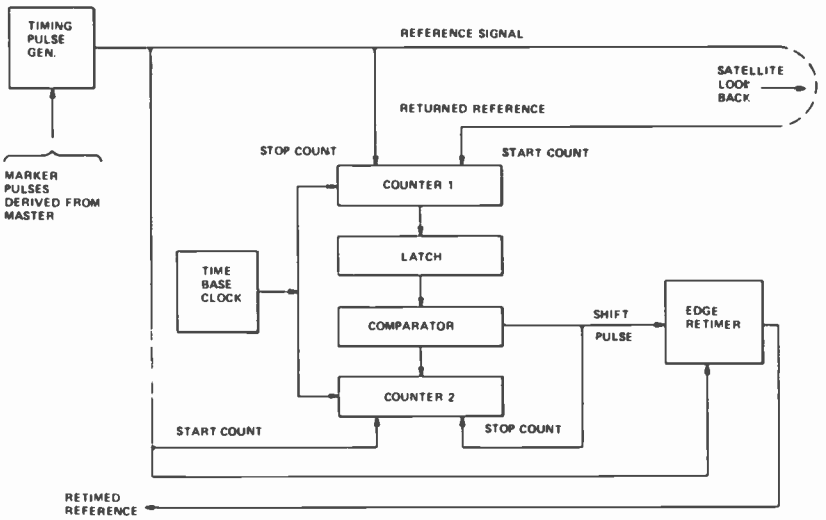

Fig. 4—Timing subsystem block diagram.

of the count interval is determined by the edge of the reference signal itself. The binary number of local clock pulses contained in the interval between the returned reference and the original reference is stored in a latch.

The reference signal edge also initiates a second interval counter, which also counts the local clock in a second counter. When the number of clock pulses that have entered the second counter matches the number previously stored in the latch, a comparator issues a shift pulse. This shift pulse retimes the reference square wave to the appropriate edges such that it can now be used as the transmission interval marker for the remote station.

2.2 Timing System Test Results

In the experimental system, the emphasis was placed upon information intervals that were one field time long. That is, the philosophy adopted was to issue only even fields from one site, and odd fields from the other site. This was not due to any conceptual restrictions, but because a commercial alternate field recovery system existed that could be used to measure overall system performance. Using field rates, the information intervals at each site were thus "on" for about 1/60 sec and "off" for the same duration. The timing reference at each station was then a square wave with an approximate frequency of 30 Hz.

As seen from the previous discussion, the timing reference derived at the remote station must be looped-back on a side channel in order to measure the retiming interval. Conceptually, several methods could be used, including

(1) frequency modulation of a standard audio program channel subcarrier by the reference signal
(2) encoding of the reference edges with unique digital words to be subsequently modulated on a Single Channel Per Carrier (SCPC) basis.

Method (1) was chosen as being the most expeditious, while still proving the feasibility of the timing system.

The timing system was given a field trial at the Vernon Valley, New Jersey, Earth Station using the test set-up shown in Fig. 5. Video (EIA color bars) was received (from South Mountain) on Transponder 24. A video processing system was used to extract the vertical intervals (drives) from the composite video. These pulses were used to generate a square wave (in the timing pulse generator) that was high for alternate fields of received video, and low for the intervening fields.

This square wave was used to modulate the 6.8 MHz aural subcarrier

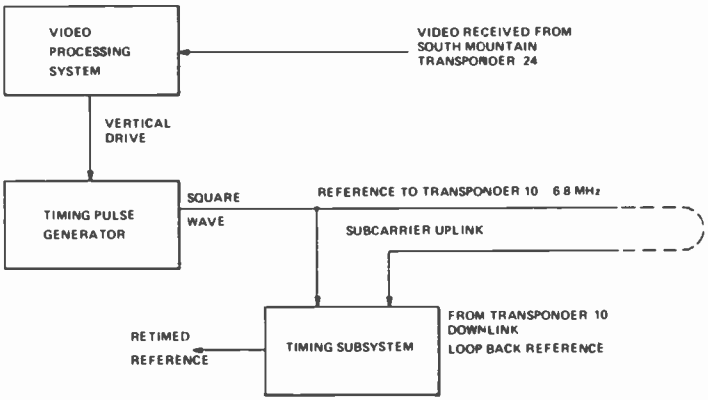

Fig. 5—Initial test configuration at Vernon Valley.

of Transponder 10. Subsequent local demodulation of the channel provided the looped-back reference signal.

The looped back and local reference signals were used to generate retiming of the local reference signal as shown. Since the modulating reference signal was a 30 Hz frequency square wave, which is at the baseband cut-off of the program channel (30-15,000 Hz) severe low frequency distortion of the recovered loop back signal resulted. Additionally, the rise time of the looped-back reference signal was of the order of 30 microseconds. The thresholds of the squaring circuitry within the time base correction system were not suitable to deal with such parameters. The edge jitter after squaring was approximately 5 microseconds, as shown in Fig. 6, despite the fact that the actual jitter of the loop back signal was several orders of magnitude lower.

To conclude the tests, the modified configuration shown in Fig. 7 was used. The video received on Transponder 24 was up-linked on the Transponder 10 video channel and looped back in the satellite. Extracting vertical drive signals from each of the demodulated video signals (Transponders 24 and 10) gave very stable indications of the local and looped-back references.

Introducing these vertical signals into the timing subsystem produced a returned reference that appeared to be favorably positioned in timing. In order to verify this, the retimed reference was uplinked on the Transponder aural subcarrier and observed on the down-link side. Comparison of this signal with the received local reference signal is shown in Fig. 8 where the edge alignment of the two signals indicates proper phase relationships existing in the satellite itself.

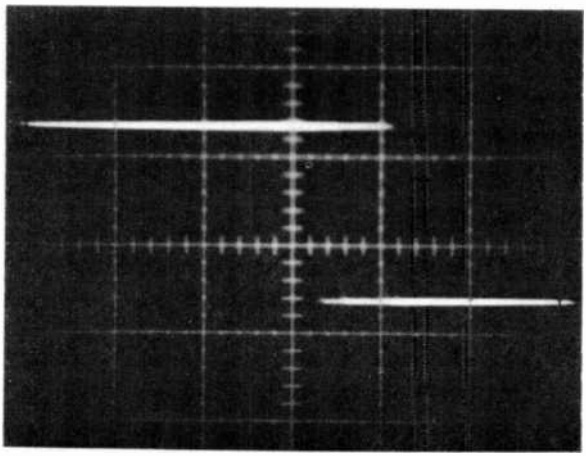

Fig. 6—Recovered loopback reference signal after squaring.

3. Synchronous Signal Generation

The video signal generation at both the master and remote stations must be so arranged that the "aggregate" downlink will behave as much like a continuous video channel as possible. This section describes, through block diagrams the implementation of the processes at both sites.

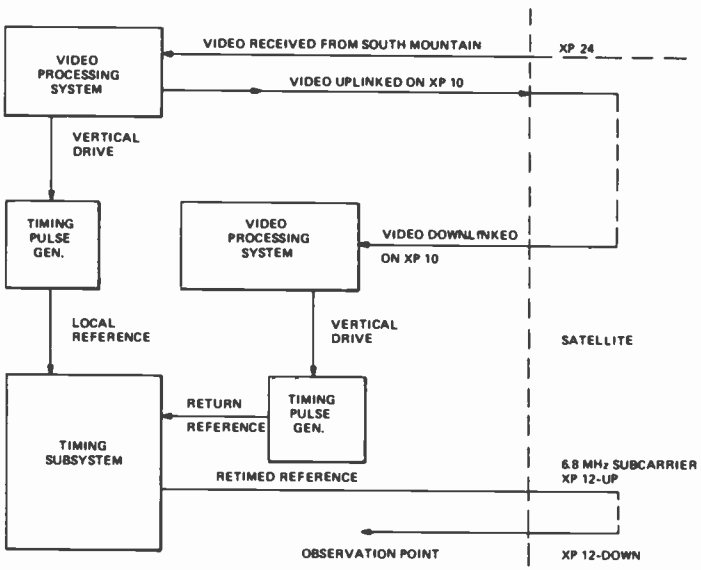

Fig. 7—Modified test configuration.

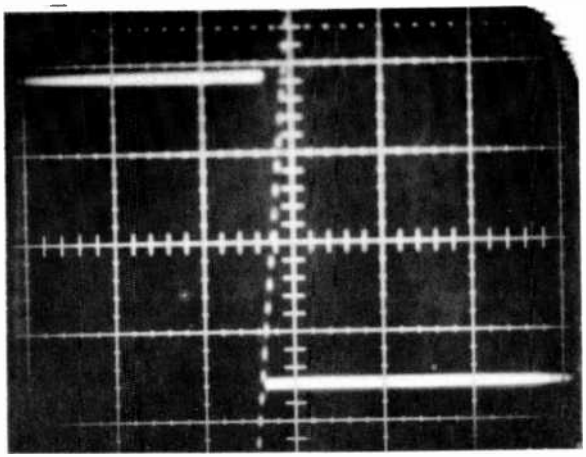

Fig. 8—Signal waveforms at local reference and observation points.

3.1 Master Station

The master earth station initiates the interleaving process by uplinking even video fields surrounded by both even and odd vertical intervals. As shown in the block diagram (Fig. 9), a sync generator produces composite sync, color subcarrier, vertical drive, and odd-field indicators. A video source is locked to the composite sync and color subcarrier, while a controller uses the vertical drive and odd field indicators to close the switch during even fields and vertical intervals. This switch is placed after the modulator to insure that both video and carrier are switched and to avoid unwanted transients associated with modulator startup and shutdown. These bursts of signal are then uplinked to the satellite.

3.2 Remote Station

The remote station must generate and uplink odd fields of video without vertical intervals with proper timing such that they fill the empty time

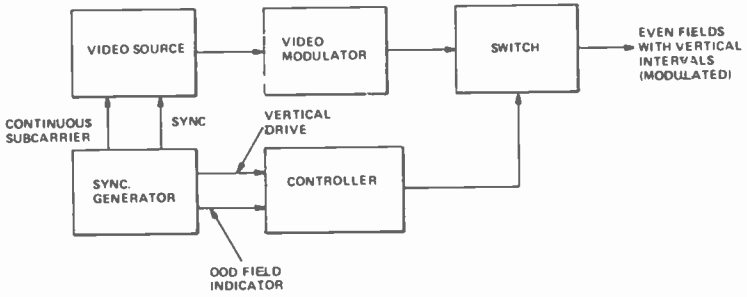

Fig. 9—Master station block diagram.

slots left by the master station. This process is complicated, because the remote station must attain gen-lock to the alternate-field video of the master station rather than to full-frame video. Fig. 10 is the block diagram of a system to produce the desired results. Shading indicates that units have not yet been completely designed; the remaining units have been designed and largely breadboarded and tested.

The video from the master station is demodulated and fed into the GATE. This device must isolate the even fields and vertical intervals, which comprise the master station's signal, from the odd field. The odd field interval may be an actual field of video from the remote station's uplink or, in the case of startup, a burst of noise. The nature of the algorithm to produce this separation in the case of noise has not been determined. The possibilities of using a phase-locked loop to find vertical intervals or employing a "handshake" procedure, where the master uplinks full video during start-up, have been considered.

The GATE provides even fields with vertical intervals, with the odd field replaced by a dc voltage to a SYNC SEPARATOR and COLOR LOCK MODULE. The latter is designed to derive color subcarrier from the input video by synchronizing both the phase and frequency of an internal-voltage-controlled crystal oscillator to the input subcarrier bursts. In operation, the unit functions normally during the field of video; during the missing field, it holds the frequency steady at its average value. The resulting output 3.58 MHz color subcarrier must be very stable, with less than 5 nanoseconds jitter.

The SYNC SEPARATOR is necessary for the COLOR LOCK

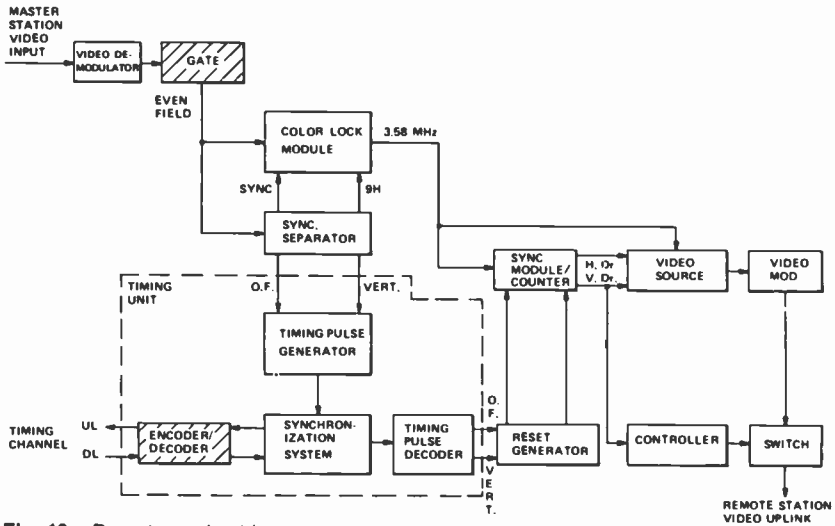

Fig. 10—Remote station block diagram.

MODULE operation. It provides gating information to the sensor circuits in order to sample the input video during the subcarrier bursts. The sync edges give line-by-line burst gate-timing indicators, while the 9H signal inhibits the gating during the burst-free vertical intervals. The 9H signal is on intervals in the vertical blanking period and encompasses the nine lines of equalizer and serrated pulses.

Sync lock is next achieved using a SYNC MODULE and a COUNTER. Rather than direct extraction of horizontal and vertical sync from the input video, the SYNC MODULE unit derives them from the locked 3.58 MHz color subcarrier. The sync is locked in frequency because it is derived from the locked color carrier, but is of arbitrary phase. A phase lock can be achieved be resetting the SYNC MODULE counter at the appropriate time.

Recall, that the phasing of the video at the remote station must be such that when alternate fields of this video are uplinked on the common channel, they will interleave with the existing master station video in the satellite. The determination of this phase relationship (i.e., the acquisition of the available information intervals) is accomplished by the TIMING UNIT SUBSYSTEM discussed in the previous section.

As shown on the diagram of Fig. 10, the TIMING UNIT consists of 4 distinct circuits. The TIMING PULSE GENERATOR takes vertical sync and odd-field indicators from the SYNC SEPARATOR and creates a square wave (high during odd fields and low during even ones). This signal enters the SYNCHRONIZATION SYSTEM which, in turn, sends it to the ENCODER/DECODER. This device interfaces the SYNCHRONIZATION SYSTEM with the timing channel. The nature of the timing method and the type of side channel used will determine the ENCODER/DECODER design. The ENCODER/DECODER returns a squarewave to the SYNCHRONIZATION system. The phase relationship between the received and returned ENCODER/DECODER signals represents the delay of a signal looped through the satellite. The SYNCHRONIZATION SYSTEM uses the two offset square waves to produce another square wave that provides the timing information for the signal to be uplinked. The TIMING PULSE DECODER translates this square wave into vertical sync and odd-field indicators for use in the RESET GENERATOR.

The RESET GENERATOR makes reset pulses for the COUNTER section of the SYNC MODULE. These resets force the output horizontal and vertical drive pulses into the appropriate phasing for the signal to be uplinked.

The remainder of the system functions exactly as the master station. A VIDEO SOURCE is gen-locked and modulated, while a CON-

TROLLER produces the gating pulses for the SWITCH to allow only odd fields without vertical intervals to be uplinked.

4. Preliminary Results

The phase-locked loop used for alternate-field color subcarrier extraction performed remarkably well. Figure 11(A) is a photograph taken with one-second exposure of the recovered subcarrier. The amount of jitter is negligible. If the hold-over capacitors are removed, the resulting deterioration is obvious [see Fig. 11(B)].

To further test the system concepts, a configuration using a field interleaved decoder system (see Fig. 12) was used. In this application the decoder accepts alternate field video, and separates the input into two

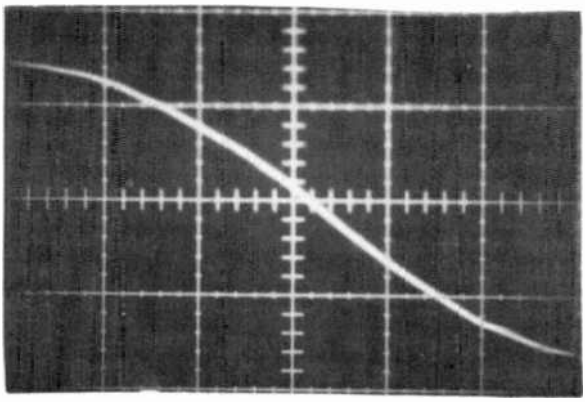

(A)

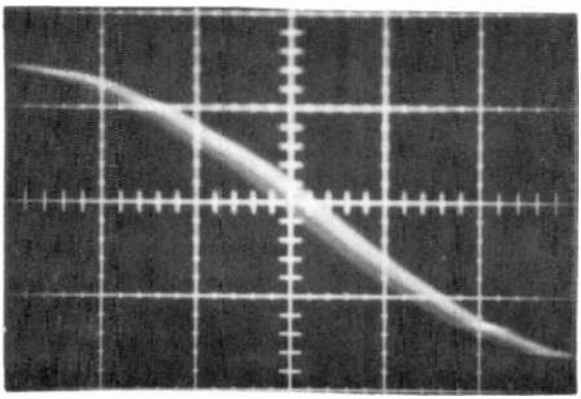

(B)

Fig. 11—Recovered locked color subcarrier (A) with field hold-over circuit operational and (B) with field hold-over circuit removed.

independent video signals. In both decoder outputs, the missing fields are created by an interpolation process.

In the test set-up, the master station video source was either color bars from a test generator or a video signal obtained from the RCA Americom satellite and received using a 4.5 meter antenna at RCA Laboratories. Sync timing was extracted from this source and used to control a master switch. The switching operated to pass just the even fields, thereby simulating a master station transmission.

The even fields from the master station were presented to the remote station, which created the color lock and drive signals, as shown in Fig. 10. These recovered signals were then used to gen-lock a remote-station video source (color-bar test generator). The remote source was switched to extract odd fields. The even fields from the master, and the odd fields from the remote were added to form a composite alternate field signal, which simulated the common downlink.

For the case where the master station video source was the locally generated alternate fields of color-bar signal, the output of the remote video source is shown on the vectorscope Fig. 13(A). Notice that the use of the derived subcarrier causes some phase and amplitude distortions in the color vectors.

The simulated downlink alternate field signal was presented to the decoder. The decoder was able to separate the fields, as shown in Fig. 13(B).

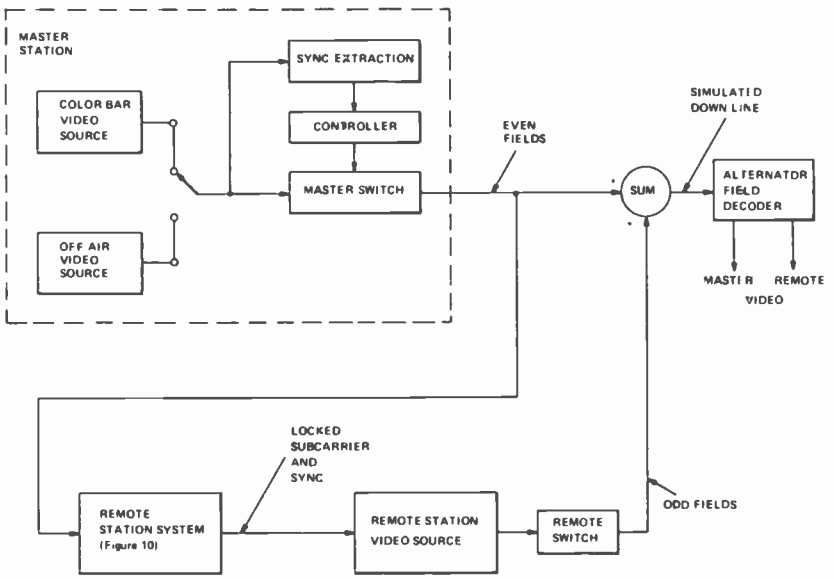

Fig. 12—Tests using interpolation recovery system.

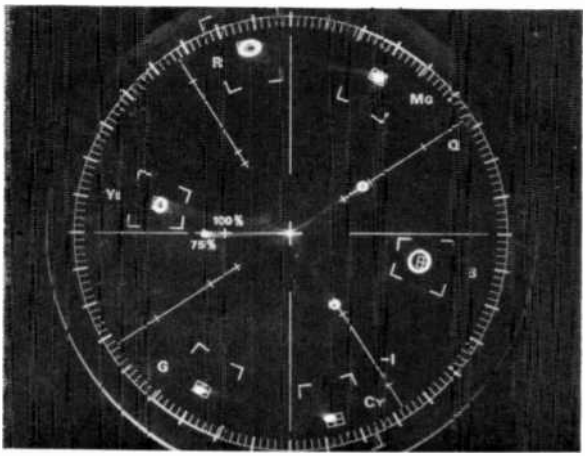

(A)

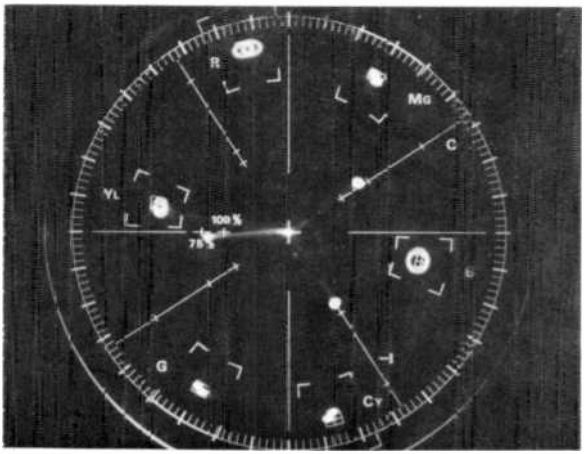

(B)

Fig. 13—Vectorsccpe waveforms with studio color bars as video source: (A) signal from remote source and (B) signal at decoder output.

A more representative test is to present the remote station with alternate fields of video from an actual satellite TV downlink. To accomplish this, a signal received from the RCA Laboratories' earth station was again gated by the controller, and fed to the remote station. The vectorscope recording of the remote station video [Fig. 14(A)] again shows the distortions. Fig. 14(B) is the recovered video after decoding.

The distortions introduced in Fig. 13(B) and 14(B) are fairly similar. This suggests that the perturbations are caused by the system, rather than by the inherently noisier off-air signal.

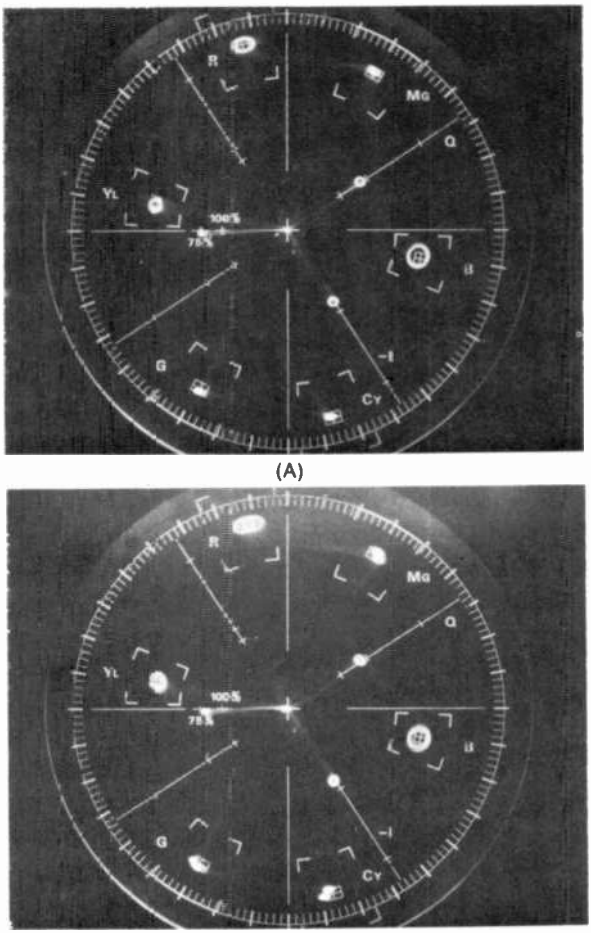

Fig. 14—Vectorscope waveforms with received satellite signal as video source: (A) signal from remote source and (B) signal at decoder output.

Comments on Signal Recovery

The composite downlink from the satellite will have a continuity of sync like that of standard video signal. The color subcarrier will have two distinct phases, however, one in the even fields and another in the odd fields. This is because the subcarrier is not subjected to a retiming process like the sync and, indeed, cannot be phased in this manner due to the extremely low allowable phase error and the impractically high clock frequency necessary for such resolution. Nevertheless, continuity of sync is sufficient to allow decoding of the composite signal if a field store-and-repeat philosophy is used. At the remote station, a GATE extracts

the master station's signal and provides a dc voltage in the empty field. If this combined signal is fed into a storage device that will repeat the even-field video into the odd-field vacancy, the new signal can be viewed on a monitor. Similarly, the master station can employ a GATE that extracts odd fields with vertical intervals and once again use a storage device and monitor.

The use of an interpolation recovery system presents some advantages over the system described above. In this system, the decoder takes the composite downlink and extracts both signals while interpolating the missing fields. This improves resolution, a desirable effect, but requires continuity of subcarrier phase. Fig. 15 is an expanded version of Fig. 10 that incorporates a method to phase subcarriers at the remote station. The GATE now separates both odd and even fields, allowing a second SYNC SEPARATOR system to achieve color lock to the bursts in the odd-field video uplinked from the remote station itself. A PHASE DETECTOR compares the subcarrier from the master (even field) to that from the remote. If the composite video has continuity of subcarrier, the PHASE DETECTOR will indicate so and no phase shift is necessary. If a phase difference is detected, the PHASE SHIFTER adjusts the phase of the subcarrier feeding both the VIDEO SOURCE and the SYNC MODULE COUNTER. The operation of this phase-locked loop must be very slow to account for the long delay due to transmission times and to prevent oscillatory behavior.

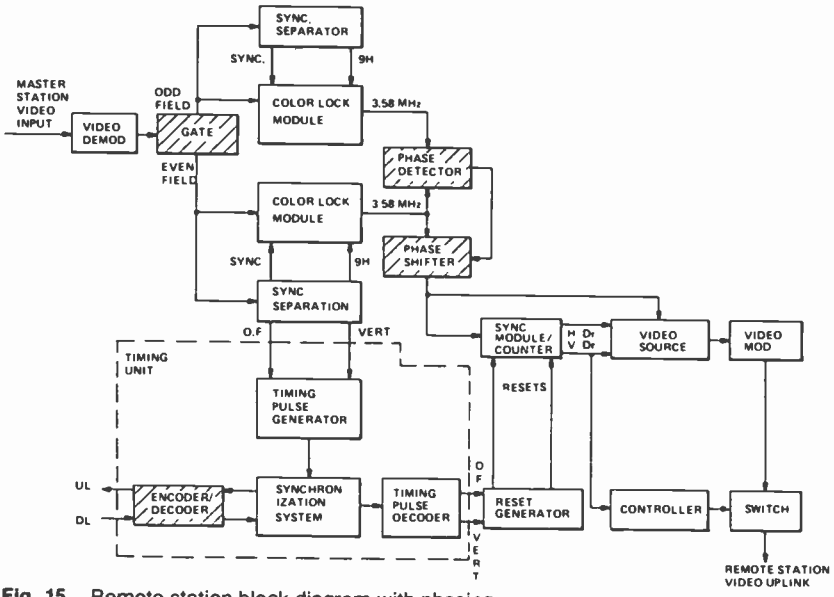

Fig. 15—Remote station block diagram with phasing.

Dynamics of the Generalized Dual-Spin Turn

Carl Hubert

RCA Astro Electronics, Princeton, NJ 08540

Abstract—The generalized dual-spin turn is an attitude acquisition technique for use on a spacecraft containing a rotor. Through this method, the spin axis of the rotor may be aligned parallel to the total angular momentum vector of the spacecraft, regardless of the initial rotational state of the system. The dual-spin turn is operationally simpler than alternative approaches and it is the standard attitude acquisition technique for all RCA-built communications satellites. Although the dynamics of such maneuvers are quite complex, it is shown that a simple geometrical representation can be an effective aid in the visualization and understanding of the motions.

1. Introduction

In designing a satellite or an interplanetary probe, engineers are often confronted with the requirement that the spacecraft maintain a constant orientation relative to inertial space. Dual-spin stabilization is a simple, commonly used technique for meeting this requirement. By definition, a "dual-spin spacecraft" consists of two distinct parts that rotate at different rates about a common axis. Usually, one portion of the spacecraft is either controlled to spin at a very low rate (e.g., orbital rate) or it does not spin at all. The other portion spins at a relatively high rate to provide gyroscopic stability. This method of stabilization is used by all currently operating commercial communications satellites.

In practice, dual-spin spacecraft tend to fall into two distinct classes. Spacecraft in the first class are known as "gyrostats." On a gyrostat, the rotor consists of the bulk of the vehicle, with the despun platform containing only those components (e.g., antennas and sensors) that have specific orientation requirements.

The second class of dual-spin spacecraft is usually described as "momentum-biased," and it is for this class that the current discussion holds the greatest relevance. In a momentum-biased spacecraft, the bulk of the vehicle is despun and the rotor consists of a relatively small, rapidly spinning, internal wheel. Although an attitude sensor is sometimes mounted on the wheel for scanning purposes, most momentum-biased spacecraft utilize the wheel exclusively as a momentum storage device.

Prior to achievement of their final orbits, satellites that are eventually to be momentum-biased are often operated in a state of simple spin with the wheel deactivated. The spin serves to minimize solar-induced thermal gradients, ensures that solar panels will be illuminated, and minimizes the effect of rocket motor thrust axis misalignments. Spin may be about either the major or minor axis, although major axis spin is preferred because it does not require the use of an active stabilization system. Due to launch vehicle geometric constraints, however, it is not always possible to design the spacecraft to spin about its maximum moment of inertia axis.

Once the final orbit has been achieved, the spacecraft must be reoriented to its operational attitude, the body of the spacecraft must be despun, and the wheel must be spun up. Because of a variety of design constraints, the rotor spin axis is often perpendicular to the initial spin axis of the satellite and this complicates the procedure for implementing these events. The conventional approach would be to use thrusters to despin and reorient the spacecraft and then to use a motor to spin up the wheel relative to the body of the spacecraft. As the wheel spins up, thrusters are used to keep the motor reaction torque from spinning up the body in the opposite direction.

The difficulty occurs during the interval between completion of the despin of the body and the start of wheel spin-up. At that time there is no angular momentum and a technique other than momentum stabilization must be used for attitude control. This usually requires additional sensors and other equipment and can add substantially to the cost of the spacecraft. In addition to the cost, the extra equipment adds weight and occupies space, both precious commodities on a spacecraft. In the mid-1970's, however, a way around this difficulty was achieved by a dynamical technique for simultaneously despinning the platform, reorienting the spacecraft, and spinning-up the wheel. The maneuver is called a "dual-spin turn."

The dual-spin turn is an open-loop procedure for acquiring a stable dual-spin configuration with the rotor axis aligned parallel to either the spacecraft's minimum or intermediate moment of inertia axis; it requires no special equipment other than the wheel and its motor. The spacecraft

is assumed to be initially in a state of simple spin about the axis of maximum moment of inertia. Reorientation is accomplished by torquing the rotor until it reaches a speed consistent with the stability requirements for the nominal operational orientation. Reaction torque applied to the spacecraft body during wheel spin-up produces most of the required attitude change. Perfect alignment of the wheel axis with the angular momentum vector, however, cannot be achieved by open-loop wheel torquing alone. A residual nutation will essentially always be present. Since the dual-spin configuration is stable, however, ultimate convergence can be assured by the incorporation of a passive energy dissipation mechanism on the platform of the spacecraft.* The first spacecraft to employ this attitude acquisition technique was RCA Satcom I in December, 1975.

In the mid-1970's, investigation of the dual-spin turn centered on the dynamic effects of rotor spin-up.[1–4] This work placed the maneuver on a firm analytical footing, but it also indicated that other maneuvers of this type may not be feasible. For some configurations, reaction torques during rotor spin-up cause the spacecraft to turn so that the rotor momentum vector is oriented opposite to the total angular momentum vector, rather than in the same direction, as is required. Furthermore, rather than despinning, the platform acquires an even higher momentum. Recent studies by the author,[5,6] however, have demonstrated that these maneuvers can be successfully completed despite initial divergence from the desired end condition.

The author's technique is essentially a generalization of the dual-spin turn. The maneuver is performed not by the dynamics of rotor spin-up, but by passive energy dissipation which occurs after the rotor is up to speed. Through this method, the rotor axis may be aligned with the total angular momentum vector regardless (1) of the orientation of the rotor within the spacecraft, (2) of the initial conditions, and (3) of the dynamics associated with rotor spin-up.

The maneuver is based on minimization of the "core" energy, which is defined as being equal to the total energy of the spacecraft minus that portion of the rotor energy that is due to the relative rotation between the rotor and the platform. It has been shown that if an energy dissipation device is mounted on the platform, the core energy of a dual-spin spacecraft will always approach a minimum.[7] Thus, if the rotor speed is such that the desired orientation represents a core energy minimum and if the minimum is unique, then convergence to that attitude is assured. A rotor speed can always be found to meet the uniqueness con-

* While the energy dissipation mechanisms inherent in the spacecraft are often sufficient to cause convergence, they are usually not well defined and cannot be depended on. Hence, mechanisms specifically designed to dissipate energy are generally used.

dition if the rotor axis is parallel to a principal axis of the spacecraft.[5,6]

In this paper, we describe the dynamics of these generalized dual-spin turns. A geometrical approach is used to aid visualization of the complex rotation motions. The discussion is illustrated by computer simulation results.

2. System Definition

The spacecraft under consideration is illustrated in Fig. 1. It consists of a rigid platform and a rigid symmetric momentum wheel (also called the "rotor"). A motor mounted on the platform is used to spin up the wheel and, when the desired speed is achieved, continues to drive the wheel so that it maintains a constant rate relative to the platform. In general, a non-zero motor torque is needed to maintain a constant relative rate during arbitrary spacecraft rotational motion. It is assumed that no external torques are applied to the spacecraft and, therefore, that the total angular momentum vector, **h**, is constant both in magnitude and inertial orientation. The magnitude of **h** is denoted H.

For most dual-spin spacecraft, the wheel axis is parallel to a principal moment-of-inertia axis of the spacecraft, and that is the case treated here. The three principal axes are denoted 1, 2, and 3, with the 3-axis being parallel to the rotor axis. These axes form a coordinate system that is fixed in the platform and that has its origin located at the spacecraft center of mass. The moments of inertia about the 1, 2, and 3 axes are denoted I_1, I_2, and I_3, respectively. These inertias are for the entire

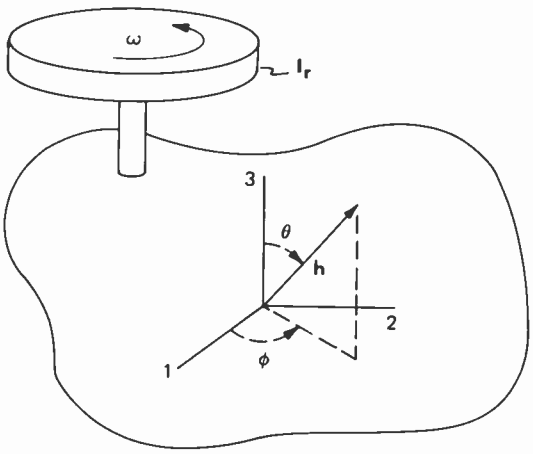

Fig. 1—Spacecraft configuration and coordinate system.

spacecraft treated as a single rigid body (i.e., with the wheel stationary relative to the platform).

The axial moment of inertia of the wheel is denoted I_r, and the angular rate of the wheel relative to the platform is denoted ω. For convenience, we define the normalized wheel momentum, ψ, by the relationship

$$\psi \equiv \omega I_r / H. \qquad [1]$$

The orientation of the total angular momentum vector relative to the body axes is described by two angles, the angle between the positive 3-axis and $\mathbf{h}$, θ, and the angle between the positive 1-axis and the projection of $\mathbf{h}$ on the 1–2 plane, ϕ. These angles are, in general, functions of time. The angle θ will be referred to as the "nutation angle." This definition is used in a very broad sense and is not meant to imply that the motion is always characterized by nutation as it is understood in classical rigid-body dynamics. The object of the generalized dual-spin turn is to cause θ to become equal to zero.

Although it is not shown in Fig. 1, the platform is assumed to contain an energy dissipation device. It is also assumed, however, that the mass, inertias, and motions of this device are sufficiently small that its energy is negligible relative to the spacecraft core energy. The dissipator, therefore, may be treated simply as an undefined "energy-sink."

3. The Core Energy

In analyzing any dynamical system, one of the most useful and satisfying results that can be obtained is a closed form solution of the equations of motion. Unfortunately, the equations of motion describing dual-spin spacecraft are nonlinear, and a closed form solution does not seem to exist. Although approximate solutions can be found, these are (by their nature) restricted to special cases and yield little information about motion in the large. Fortunately, there are alternatives to solving the equations of motion. For the dual-spin spacecraft, a kinetic energy analysis can yield a great deal of valuable qualitative and quantitative information.

As mentioned in the introduction, the presence of energy dissipation on the platform will cause the core energy of a dual-spin spacecraft to approach a minimum (provided the wheel maintains a constant rate of rotation relative to the platform). Because of this fact, the core energy is central to the current discussion. If the energy dissipation mechanism is treated as an unmodeled "energy-sink," then the core energy, C, of the system under consideration is given by

$$C(\theta,\phi) = \tfrac{1}{2}H^2[(I_1^{-1}\cos^2\phi + I_2^{-1}\sin^2\phi)\sin^2\theta + I_3^{-1}(\psi - \cos\theta)^2]. \qquad [2]$$

Note that C is completely independent of the wheel inertia, I_r. The wheel appears only through ψ, the normalized wheel momentum. The dynamics of the spacecraft is not a function of the physical size of the rotor. Only its momentum matters.

If the system parameters are chosen so that $C(\theta,\phi)$ has a minimum at $\theta = 0$, and the minimum is unique, passive energy dissipation will cause the wheel axis to become aligned with the angular momentum vector, regardless of the initial conditions. The requirement for uniqueness is important. If $C(\theta,\phi)$ does not have a unique minimum, it is possible for the spacecraft to converge to an unwanted orientation. Undesirable minima can be described as "energy traps."

Ref. [5] demonstrates that the core energy will have a unique minimum at $\theta = 0$ if

$$\psi > |1 - (I_3/I_m)|, \qquad [3]$$

where I_m is equal to I_1 or I_2, whichever is greater. Hence, the generalized dual-spin turn may be initiated simply by spinning-up the momentum wheel to a sufficiently high rate so that ψ satisfies Eq. [3]. Once the wheel is up to speed, that speed is maintained while passive energy dissipation completes the maneuver.

Although Eq. [3] presents the criterion necessary to assure successful completion of the dual-spin turn, it provides virtually no information concerning the dynamics associated with rotor spin-up and the nature of the motion after the rotor is up to speed.

In the presence of kinetic energy dissipation, the rotational motion of a dual-spin spacecraft can be quite complex. There is, however, a geometrical technique, involving curves of constant energy on the surface of a sphere, that can be a useful aid to visualization of this motion. The application of this geometrical method to simple rotating bodies is described by Lamy and Burns[8] and a somewhat less detailed discussion may be found in *Mechanics* by Landau and Lifshitz.[9] The author is aware of only one previous application of the geometrical method to dual-spin spacecraft, and that is by Barba and Aubrun.[4]

To apply this technique, it is necessary to define a geometrical construct called the "angular momentum sphere." This sphere is fixed in the platform of the spacecraft and has a radius equal to the length of the total spacecraft angular momentum vector, **h**. Since, by definition, there are no external torques, the length of the momentum vector and the radius of the sphere are constant. During spacecraft rotational motion, the tip of the angular momentum vector traces a path on the surface of the angular momentum sphere. By constructing this path, one can readily grasp the nature of the motion. One must recognize, of course, that the angular momentum vector is fixed in inertial space and it is the sphere that is actually moving.

With H, ψ, and the spacecraft inertias all constant, [2] defines the relationship between the core energy and the orientation of the total angular momentum vector relative to the platform. For a given constant value of C, this equation defines one or two loci of points (θ, ϕ) on the momentum sphere. Each locus is either a single point (representing steady rotation about the angular momentum vector), a simple closed curve (representing periodic motion), or a closed self-intersecting curve (representing a separatrix between different periodic modes). By choosing different values of C, one can generate a complete family of constant energy curves that may be plotted as shown in Fig. 2. In this diagram, two views of the same sphere are shown for easier visualization. One view shows the "top" of the sphere and the other shows the "bottom."

In Fig. 2, and in all subsequent plots of this type, a dotted reference grid with 30 degree spacing is incorporated to aid interpretation. The dotted lines of "latitude" represent constant values of θ, and the lines of "longitude" represent constant values of ϕ. The "top" of the sphere is the point where $\theta = 0°$ and the "bottom" is the point where $\theta = 180°$. Recall that $\theta = 0°$ is the point that is to be occupied by the unique core energy minimum when ψ is chosen to have the correct value. In this figure, however, $\psi = 0$ and the energy curves are, therefore, those of a simple rigid body.

Fig. 2 and the similar diagrams that follow were generated under the assumption that the momentum wheel rotates at a constant rate relative to the platform (the rate is zero for Fig. 2). Thus, the spacecraft is assumed to have three rotational degrees of freedom, and the angular rates are governed by a third-order system of differential equations.

By introducing conservation of angular momentum (in the form of the angular momentum sphere) and conservation of energy (in the form of closed curves on the surface of the sphere), we have introduced two

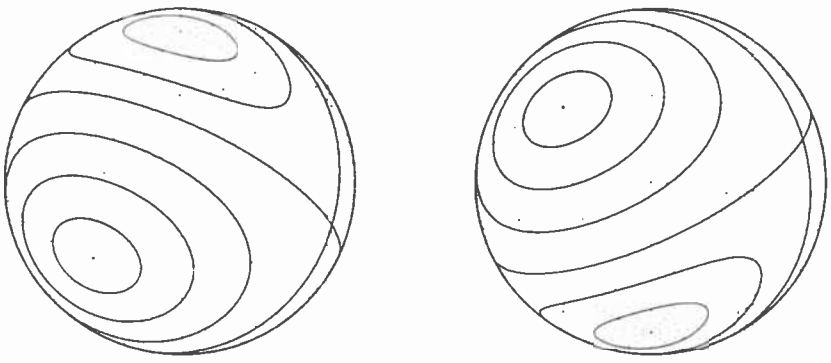

Fig. 2—Curves of constant energy for a simple spinning body.

integrals of the motion. Hence, the motion can be described by a single first-order differential equation. In essence, this equation represents the motion of the tip of the angular momentum vector along one of the closed curves on the angular momentum sphere. Thus, the three-dimensional diagrams presented in Fig. 2, and in subsequent figures, accurately depict the motion of the spacecraft when energy is conserved.

As stated earlier, the generalized dual-spin turn is based on the decay of the core energy. The introduction of an energy dissipation mechanism, however, adds at least one degree of freedom to the system (depending upon the nature of the mechanism). Since, in reality, the spacecraft now has at least four degrees of freedom, its motion cannot be represented by a three-dimensional diagram with perfect accuracy. Nevertheless, if the motion of the damper is small and the dissipation rate is relatively slow, a three-space representation can be a good approximation of the actual spacecraft motion.

In the presence of energy dissipation, the tip of the momentum vector does not follow a closed path on the surface of the angular momentum sphere. Rather, it can be considered as moving from closed path to closed path as the core energy decreases. Thus, although diagrams such as Fig. 2 do not represent the precise motion of a dissipative spacecraft, they can be useful aids in visualizing the true motion. This will be graphically illustrated later when we make comparisons between energy diagrams and computer simulation results.

In generating Fig. 2, the axis passing through the "top" and "bottom" of the angular momentum sphere was chosen to be the axis of maximum moment of inertia. Thus, $\theta = 0°$ and $\theta = 180°$ represent points of minimum rotational energy. Since the figure was produced with the assumption that energy is conserved, the closed curves encircling $\theta = 0°$ and $\theta = 180°$ represent paths of precessional motion about the major axis for the nondissipative case. These two regions of precession are divided by a separatrix from two regions of precession about the minor axis. Note that the separatrix intersects itself at two points. These points coincide with the axis of intermediate moment of inertia.

In the presence of energy dissipation, as mentioned above, the tip of the momentum vector no longer follows a closed path such as those illustrated in Fig. 2 and, thus, the motion is no longer characterized by simple precession. To visualize the nature of the true motion, consider the angular momentum vector to be initially in the vicinity of the minor axis. At time progresses, energy dissipation causes the momentum vector to spiral away from the minor axis until it crosses the separatrix. In this case, the separatrix is not a trajectory. Rather, it is a boundary which, when crossed, represents a transition into a motion that is qualitatively

different. In the situation under discussion, crossing the separatrix denotes a transition from a condition of spiraling outward from the minor axis to a condition of spiraling inward toward the major axis. Note, however, the ambiguity of the final state. The momentum vector will spiral inward toward either $\theta = 0°$ or $\theta = 180°$, depending upon where the separatrix was crossed. By spinning up the wheel and satisfying Eq. [3], however, this ambiguity can be eliminated.

Although the nature of the curves depicted in Fig. 2 will be altered by raising ψ above zero, the interpretation follows similar lines. This will be done shortly for several cases of interest.

Energy plots of this type will exhibit two, four, or six critical points, the exact number being dependent on the magnitude of the normalized wheel momentum, ψ. These critical points are the points at which

$$\frac{\partial C}{\partial \theta} = \frac{\partial C}{\partial \phi} = 0. \qquad [4]$$

Each critical point represents a state of dynamic equilibrium and corresponds to a condition in which the platform undergoes a steady rotation about the angular momentum vector. The equilibrium may be either stable or unstable. For a simple rigid body there are six critical points on the momentum sphere. These are the points where the three principal axes intersect the sphere.

Two critical points are fixed and exist for all values of ψ. The remaining four points, if they exist, have positions that are dependent on ψ. The two fixed points are

$$\theta = 0°, \phi = \text{undefined}, \qquad [5]$$

and

$$\theta = 180°, \phi = \text{undefined}. \qquad [6]$$

These points are the "top" and "bottom" of the sphere. Note that from the definition of θ and ϕ, the value of ϕ is undefined at $\theta = 0°$ and $\theta = 180°$. Hence, Eqs. [5] and [6] each represent a single point and not a family of points. The four remaining critical points, if they exist, are located at

$$\theta = \cos^{-1}\left[\frac{\psi}{1 - (I_3/I_1)}\right], \phi = 0° \text{ or } 180°, \qquad [7]$$

and

$$\theta = \cos^{-1}\left[\frac{\psi}{1 - (I_3/I_2)}\right], \phi = \pm 90°. \qquad [8]$$

Note that Eq. [7] has a solution if and only if

$$\psi \leq |1 - (I_3/I_1)|, \qquad [9]$$

and Eq. [8] has a solution if and only if

$$\psi \leq |1 - (I_3/I_2)|. \qquad [10]$$

Comparison of Eqs. [9] and [10] with the convergence criterion of Eq. [3], reveals that $\theta = 0°$ represents a unique core-energy minimum only when ψ is large enough to eliminate at least one pair of critical points.

4. The Dynamics of the Turn

With the preliminary concepts defined, we can now discuss the effect on the spacecraft dynamics of having the wheel aligned with each of the principal axes (minimum, maximum, and intermediate). The discussion will be illustrated by curves of constant core energy on the angular momentum sphere and by the results of computer simulations. Since the primary aim is to demonstrate the effect of wheel speed and wheel orientation within the spacecraft, the principal moments of inertia are identical for all plots and numerical examples. The minimum, intermediate, and maximum moments of inertia were selected to be 91, 100, and 105 kg m^2, respectively. While these inertias do not represent any particular spacecraft, they can be considered fairly typical for a satellite in the 400 to 500 kg class.

For the purpose of the simulations, it was necessary to add a platform-mounted energy dissipation device to the mathematical model. In the computer program that produced the results presented here, the dissipator is modeled as a small wheel that is attached to the platform and that has its axis of rotation parallel to the 1-axis. The torque about this axis is proportional to the relative rate of rotation between the damper wheel and the platform (i.e., the dissipation mechanism is viscous damping). This particular dissipation mechanism was chosen for its mathematical simplicity and because its action is analogous to that of the often used fluid-filled ring damper. It should be noted, however, that the energy dissipation rate was chosen to be somewhat higher than one would normally find on a spacecraft. This was done to compress the time required for the various maneuvers so that the results might be more vividly demonstrated.

4.1 Minor Axis Wheel Alignment

The first case to be discussed is that in which the wheel spin axis is aligned parallel to the spacecraft's axis of minimum moment of inertia. For attitude acquisitions of this type, the spacecraft is usually initially spinning about its maximum moment of inertia axis.

The inertias for this case were chosen to be $I_1 = 100$ kg m^2, $I_2 = 105$

kg m^2, and $I_3 = 91$ kg m^2. Examination of conditions [9] and [10] shows that one pair of critical points will vanish at $\psi = 0.09$, and a second pair will be eliminated when $\psi = 0.1333\ldots$ Eq. [3] shows that $\theta = 0°$ will be the unique core energy minimum once $\psi > 0.1333\ldots$.

Figs. 3 and 4 show sequences of energy curves plotted on the angular momentum sphere for eight different values of ψ. Fig. 3 shows these curves as they look to an observer stationed over the point $\theta = 60°$, $\phi = 30°$. This point is called the "plot pole." For Fig. 4, the plot pole is (120°, 30°). The same two plot poles are used for all momentum sphere diagrams presented in this paper.

When $\psi = 0$, the point $\theta = 0°$ is occupied by an energy maximum and is thus an unstable equilibrium point. As ψ is raised above zero, the region within the separatrix surrounding this point shrinks as the two energy minima and the entire separatrix are drawn up toward $\theta = 0°$. When ψ reaches 0.09, this region collapses entirely and the separatrix is reduced to a figure-eight shape. There is now only one energy maximum (at $\theta = 180°$) but there are still two distinct minima (located by Eq. [8]).

As ψ continues to increase, these minima and the separatrix continue to be drawn up toward $\theta = 0°$. When ψ reaches $0.1333\ldots$, the separatrix degenerates to a point and $\theta = 0°$ becomes a unique minimum. Increasing ψ beyond $0.1333\ldots$ alters the shape of the energy curves but does not alter the locations of the maximum and minimum. These remain at $\theta = 180°$ and $\theta = 0°$, respectively.

These plots neatly illustrate the dynamics associated with the wheel spin-up. Consider the spacecraft to be initially in a state of simple spin about the maximum moment of inertia axis. As the wheel is spun up, the disturbance causes the momentum vector (as viewed from the body frame) to begin to precess about the energy minimum (recall that it started at a minimum). As may be seen from Figs. 3 and 4, however, spin-up causes the minimum to be drawn toward the point $\theta = 0°$ and the momentum vector simply follows it. Hence, wheel spin-up not only causes the point $\theta = 0°$ to be stable but the dynamics of spin-up actually complete the first stage of convergence of the momentum vector with the point $\theta = 0°$. Once spin-up is complete, all that remains is for energy dissipation to finish the job. This sequence of events represents a standard dual-spin turn.

Fig. 5 shows the nutation angle history generated by a simulation of this wheel spin-up. At time 0, $\psi = 0$. The normalized wheel speed reaches 0.09 at 96 seconds and 0.1333 at 143 sec. Spin-up is continued, however, until ψ reaches 0.20 at 209 sec. The wheel speed is held constant thereafter.

In this simulation, and in the others illustrated in this paper, the momentum wheel is spun up by a constant motor torque. The history

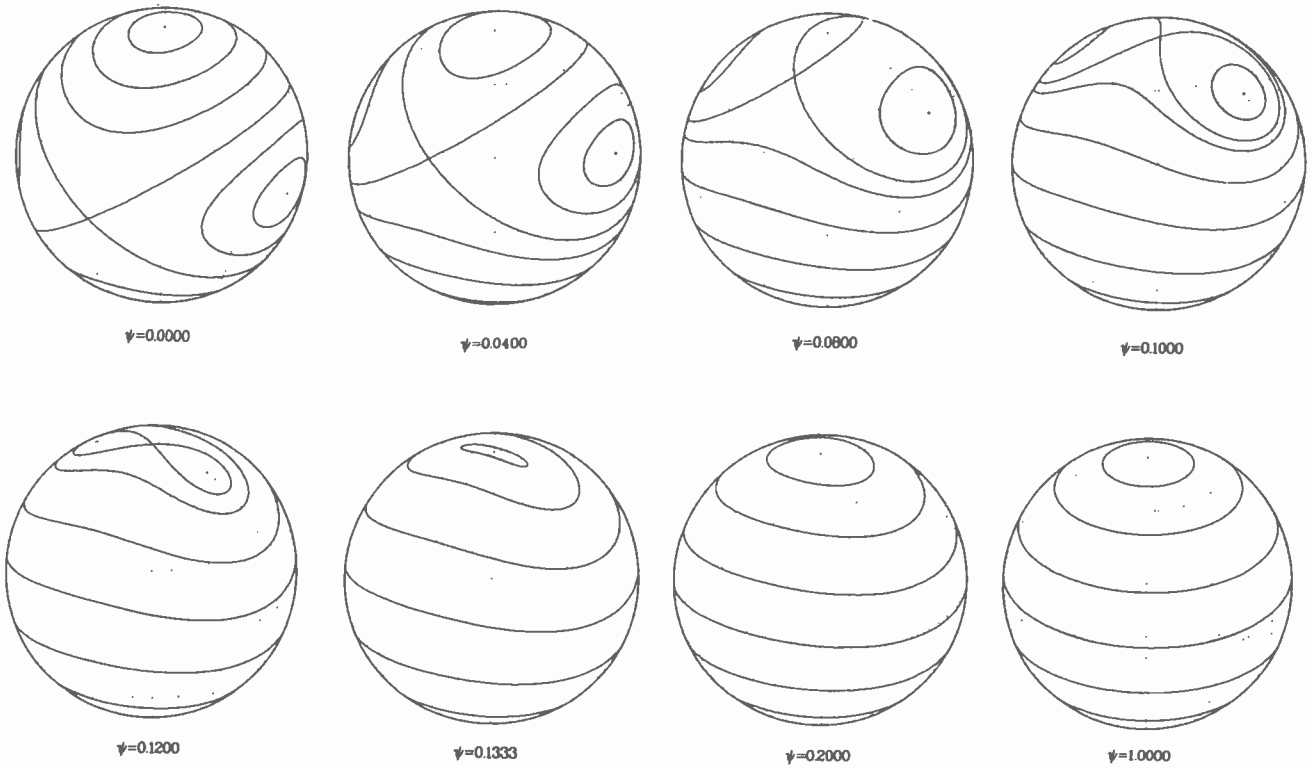

Fig. 3—Curves of constant energy for a spacecraft with a minor axis wheel, as seen from (60°, 30°).

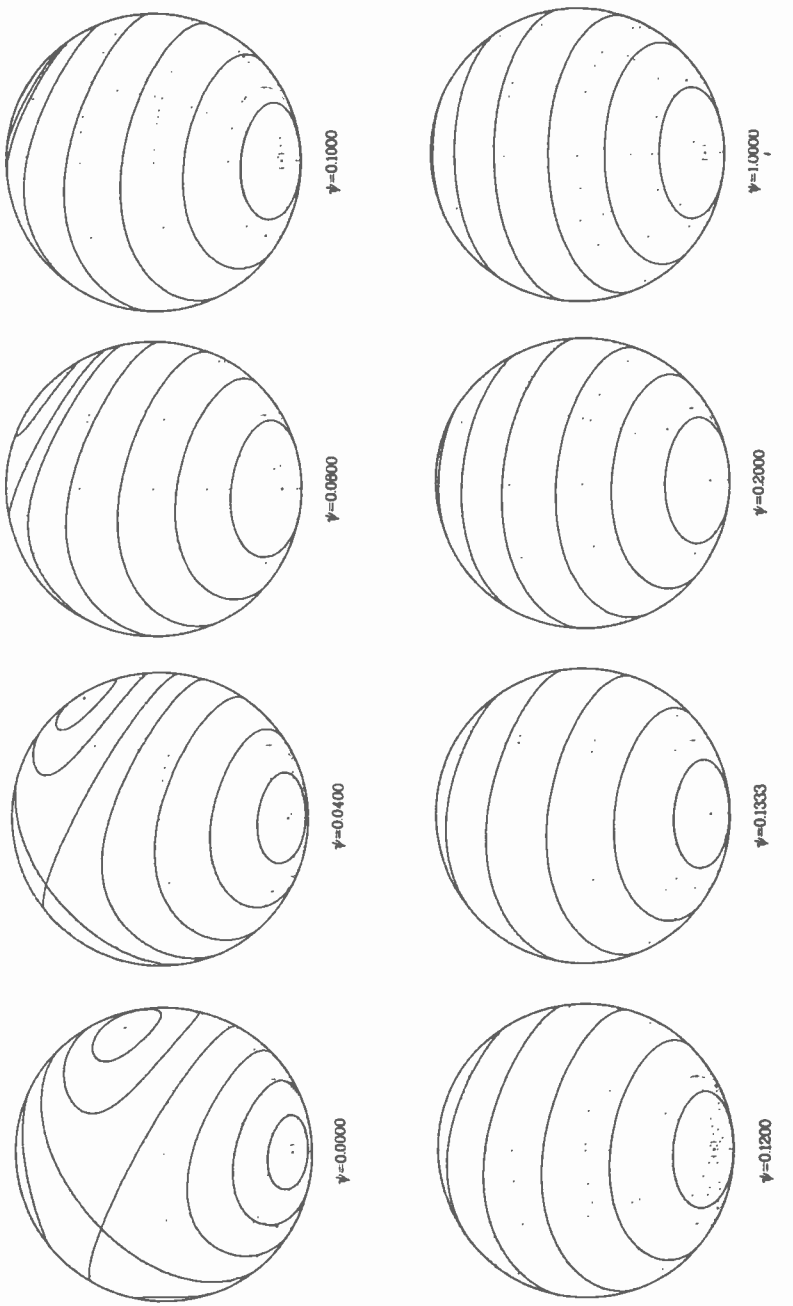

Fig. 4—Curves of constant energy for a spacecraft with a minor axis wheel, as seen from (120°, 30°).

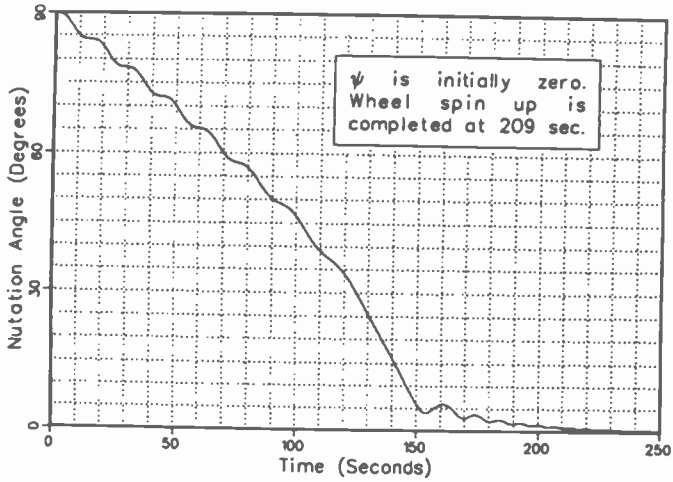

Fig. 5—Nutation angle versus time during a major to minor axis turn with $\psi = 0.20$.

of ψ illustrated in Fig. 6 is from the same simulation as Fig. 5. The history of ψ is not plotted for the remaining cases presented in this paper since the essential characteristics of Fig. 6 hold for all cases.

4.2 Major Axis Wheel Alignment

Here, the wheel spin axis is aligned parallel to the spacecraft's maximum moment of inertia axis. The inertias for the numerical examples were

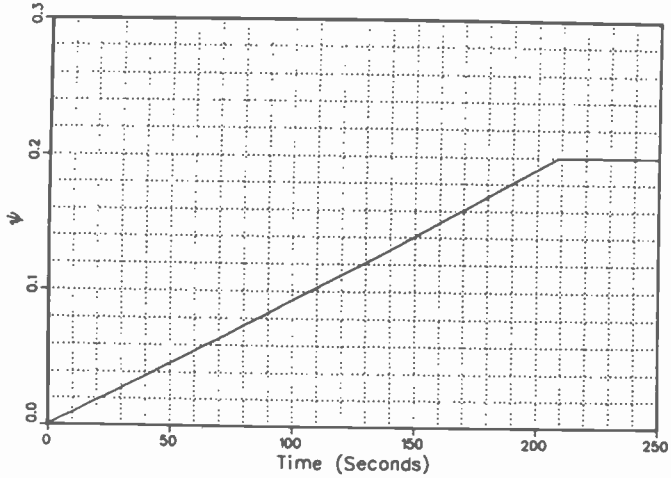

Fig. 6—ψ versus time during a major to minor axis turn.

chosen to be $I_1 = 91$ kg m^2, $I_2 = 100$ kg m^2, and $I_3 = 105$ kg m^2. Figs. 7 and 8 show sequences of energy plots for this case.

With the above inertias, the point $\theta = 0°$ is an energy minimum even when $\psi = 0$. Hence, it is a stable point even without the aid of the wheel. This minimum, however, is not unique. Another exists at $\theta = 180°$. Thus, as far as attitude acquisition is concerned, the primary purpose of the wheel is to eliminate the ambiguity. According to Eq. [3], this requires that ψ be greater than 0.05.

As ψ is raised above zero, the separatrix is drawn toward $\theta = 180°$ rather than toward $\theta = 0°$ as was the case for wheel alignment with the minimum moment of inertia axis. Hence, if the spacecraft is initially spinning about its minor axis, the dynamics of spin-up causes a divergence from the desired final orientation. This observation was made by Kaplan[1] as well as others and for this reason maneuvers of this type had been considered impossible. As a result of the analyses of Refs. [5] and [6], however, it is now known that the divergence is really only an inconvenience that poses no real problem. When ψ reaches 0.05, the undesirable energy minimum at $\theta = 180°$ vanishes and convergence to $\theta = 0°$ can be assured.

At $\psi = 0.05$, the separatrix assumes a figure-eight shape. Although there is now only one energy minimum, there are still two distinct maxima. By raising the normalized wheel momentum to 0.1538, the maxima can be merged with the saddle point to form a single energy maximum at $\theta = 180°$. This, however, is not required for successful completion of the attitude acquisition maneuver. As with the minor axis alignment case, increasing ψ beyond 0.1538 alters the shape of the energy curves but does not alter the locations of the maximum and minimum.

A series of simulations has been performed in order to illustrate the various aspects of this case. In the first simulation, the spacecraft is initially spinning about the minor axis ($\theta = 90°$) and the wheel is spun up until $\psi = 0.09$. Once that wheel speed is reached, the wheel is controlled at a constant rate relative to the body. The resulting nutation angle history is illustrated in Fig. 9.

The wheel spin-up is complete at about the 84-second mark. At this point, the spacecraft core energy lies within one of the lobes of the figure-eight and the nutation angle oscillates about $\theta = 125.8°$ (given by Eq. [7]). As energy is dissipated, the amplitude of the oscillation grows. At the 374-second mark, the separatrix is crossed and the nutation angle rapidly decays to zero.

For the second simulation, the wheel was spun up until $\psi = 0.1539$, sufficiently high to cause the separatrix to degenerate to a point. The results of this simulation are shown in Fig. 10. Note that the divergent

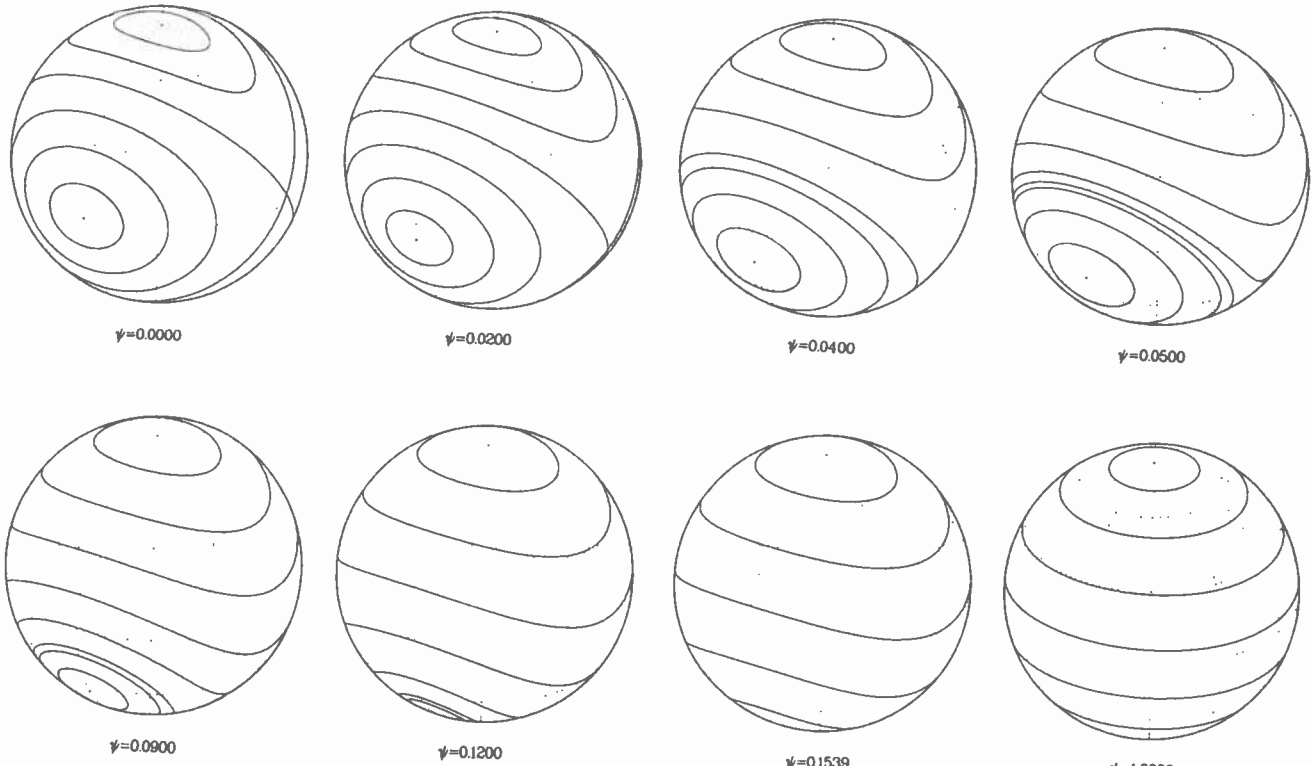

Fig. 7—Curves of constant energy for a spacecraft with a major axis wheel, as seen from (60°, 30°).

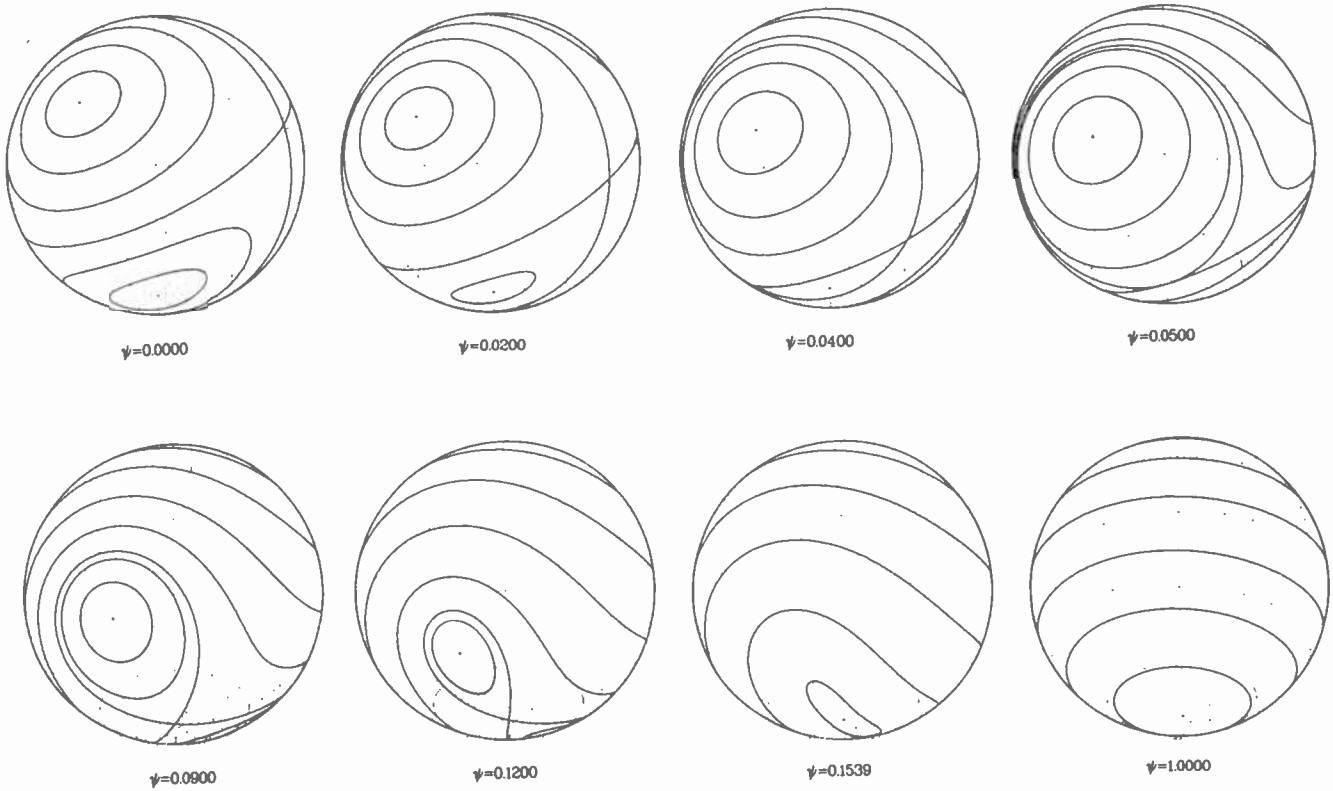

Fig. 8—Curves of constant energy for a spacecraft with a major axis wheel, as seen from (120°, 30°).

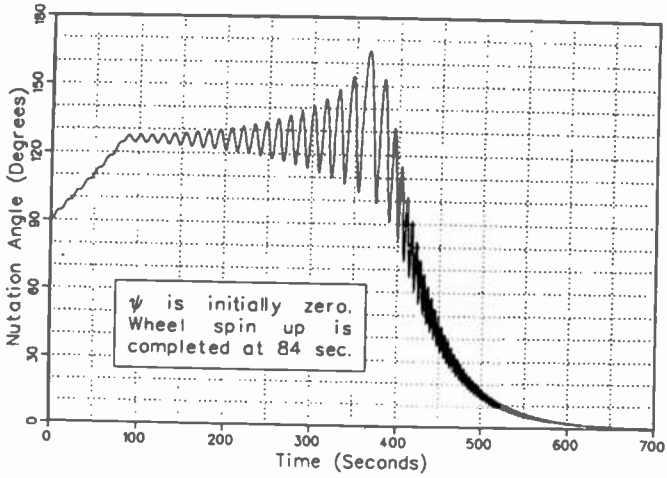

Fig. 9—Nutation angle versus time during a minor to major axis turn with $\psi = 0.09$.

oscillation which characterizes Fig. 9 is absent from Fig. 10. Once wheel spin-up is complete (at 143 sec.), the nutation angle simply decays to zero.

The third simulation is an example of how wheel spin-up can be used to creatively destabilize an initially stable motion. In this case, the spacecraft is initially spinning about the maximum moment of inertia axis and the object is to reverse the direction of the spin. The results are shown in Fig. 11. The procedure is to torque the wheel so that it acquires a spin opposite to that of the platform. When the wheel speed exceeds the rate required for $\psi = 0.05$, the initial orientation becomes unstable

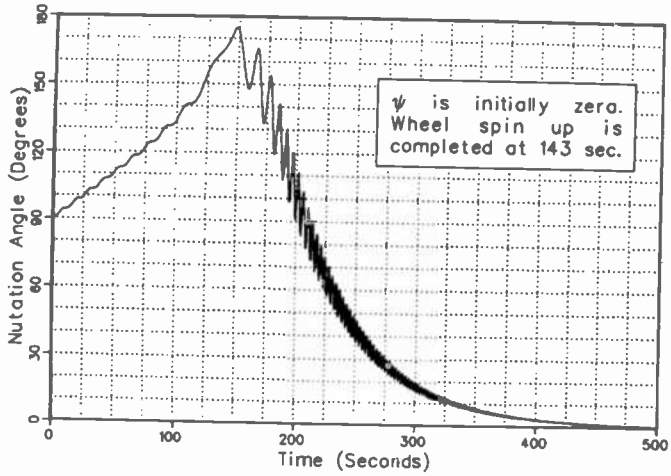

Fig. 10—Nutation angle versus time during a minor to major axis turn with $\psi = 0.1539$.

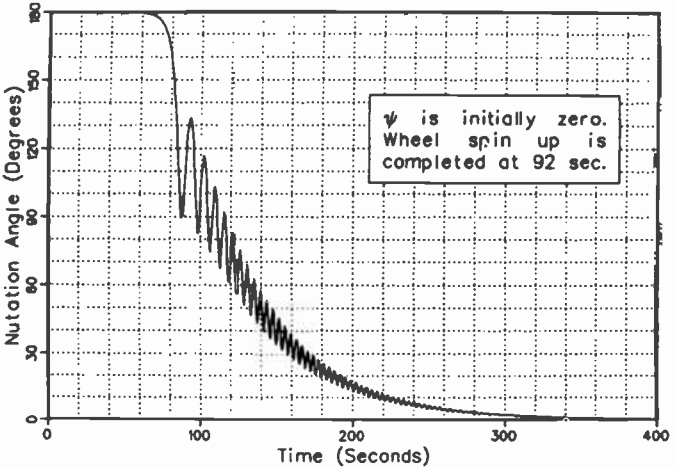

Fig. 11—Nutation angle versus time with $\psi = 0.09$ (reversal of spin about the major axis).

and an inversion occurs. For the results shown, the wheel was spun-up until $\psi = 0.09$. Destabilization ($\psi = 0.05$) occurs at the 50-second mark and spin-up is complete at 92 seconds.

Although it is not shown here, convergence to $\theta = 0°$ could be followed by despin of the wheel. This would leave the spacecraft, once again, in a state of simple spin about its maximum moment of inertia axis but with the direction of the spin reversed from the initial condition.

4.3 Intermediate Axis Wheel Alignment

The last case of principal axis wheel alignment is that in which the wheel axis is parallel to the spacecraft's intermediate moment of inertia axis. This case is particularly interesting because it can exhibit some rather bizarre dynamics that are not at all obvious from the equations of motion. This unusual behavior, however, can readily be predicted by examination of the curves of constant energy on the angular momentum sphere.

The inertias for the numerical examples were chosen to be $I_1 = 105$, $I_2 = 91$, and $I_3 = 100$ kg m^2. Figs. 12 and 13 show sequences of energy plots for this case. Here, $\theta = 0°$ and $\theta = 180°$ are saddle points when $\psi = 0$, and they are unstable whether or not energy dissipation mechanisms are present. Since $\theta = 0°$ is both a local energy maximum and a local energy minimum when $\psi = 0$, one might expect wheel spin-up for this case to exhibit characteristics of both major and minor axis wheel alignments. This is indeed what happens. The instant ψ is raised above zero, the separatrix splits into two, each fragment assuming a figure-eight shape. As ψ increases, the separatrix enclosing the energy minima is

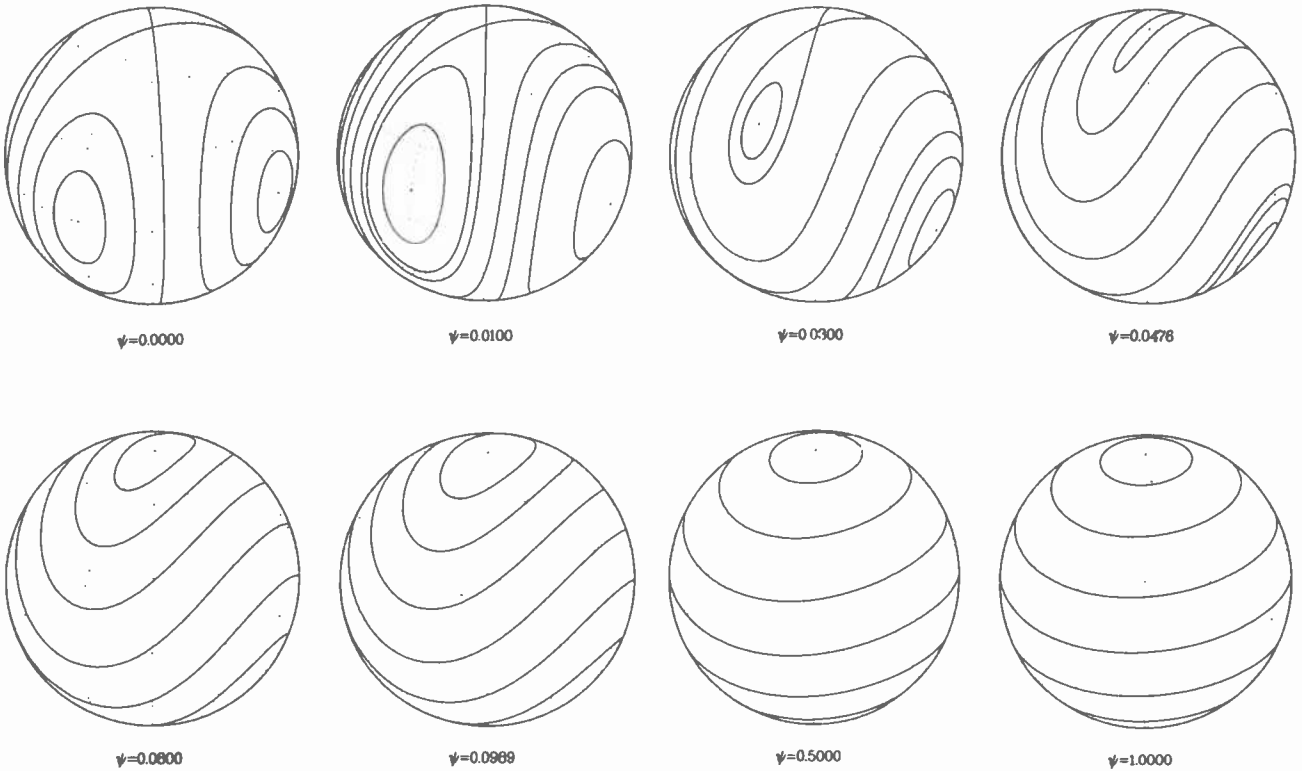

Fig. 12—Curves of constant energy for a spacecraft with an intermediate axis wheel, as seen from (60°, 30°).

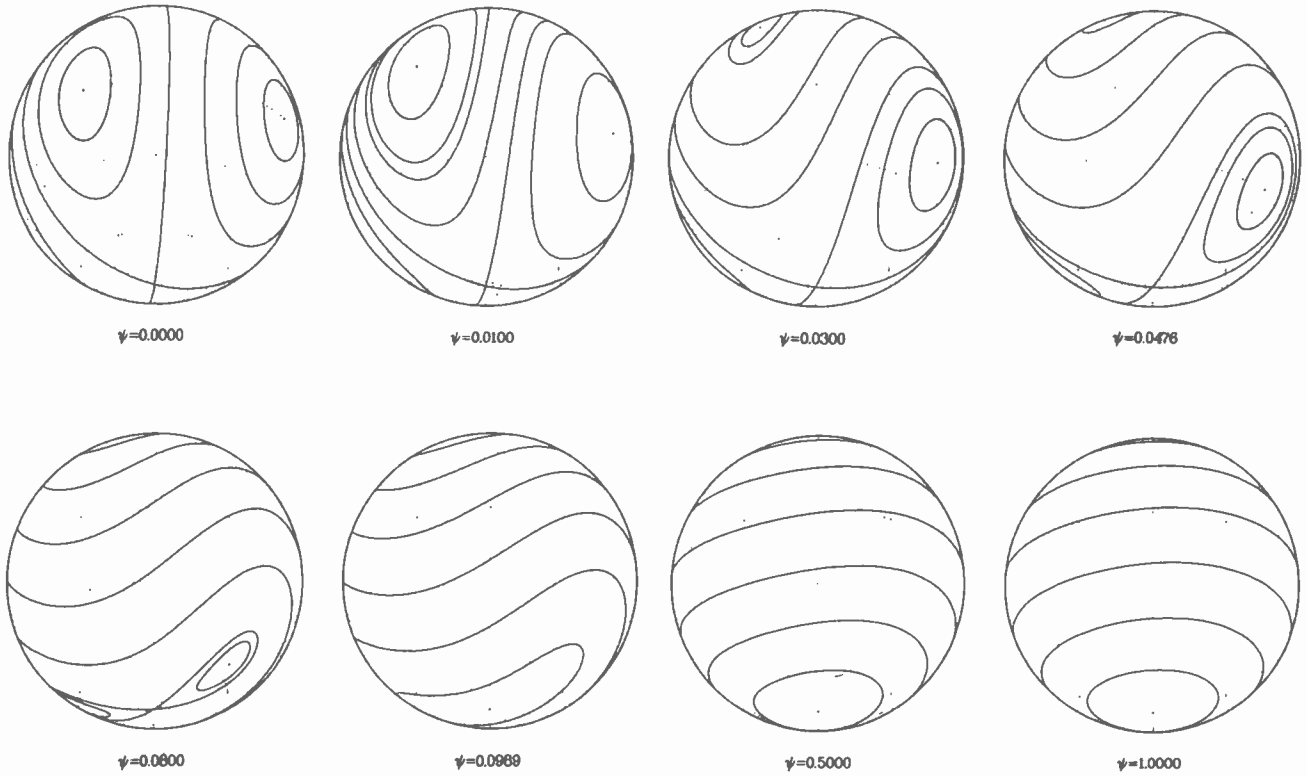

Fig. 13—Curves of constant energy for a spacecraft with an intermediate axis wheel, as seen from (120°, 30°).

drawn toward $\theta = 0°$ while the separatrix enclosing the maxima is drawn toward $\theta = 180°$.

Which of the separatrices degenerates to a point first is merely a matter of the inertia ratios I_3/I_1 and I_3/I_2. For this case, it is the separatrix enclosing the minima which vanishes first. This occurs when $\psi = 0.0476$. Once this value is exceeded, $\theta = 0°$ becomes a unique energy minimum and convergence to that point is assured. The second separatrix vanishes at $\psi = 0.0989$.

Two computer simulations have been performed to illustrate the dynamic behavior associated with this particular wheel orientation. The first simulation is illustrated in Fig. 14 and represents the case in which the spacecraft is initially spinning about its maximum moment of inertia axis. The wheel is spun-up until $\psi = 0.0989$, and this takes 108 seconds. At the 57-second mark, however, $\psi = 0.05$, and this is the value at which $\theta = 0°$ becomes a stable point. Note the similarity between this simulation and the one depicted in Fig. 5. This is also a "standard" dual-spin turn.

The second simulation is illustrated in Fig. 15. The spacecraft is initially spinning about its minimum moment of inertia axis. Once again, the wheel is spun up until $\psi = 0.0989$. In this case, however, rather than convergence to $\theta = 0°$, the spin-up initially causes a divergence toward $\theta = 180°$. This divergence, of course, is only a small setback and the nutation angle ultimately decays to zero. Here, the spin-up requires 88 seconds to complete, with $\psi = 0.05$ being passed at the 42-second mark. Note the similarity between this simulation and the one presented in Fig. 10.

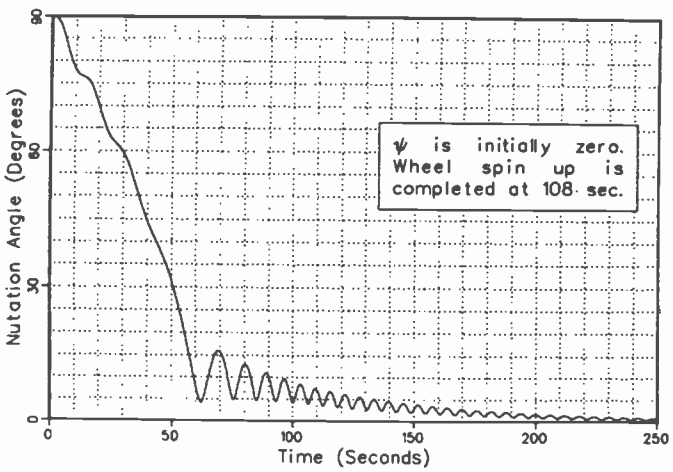

Fig. 14—Nutation angle versus time during a major to intermediate axis turn with $\psi = 0.0989$.

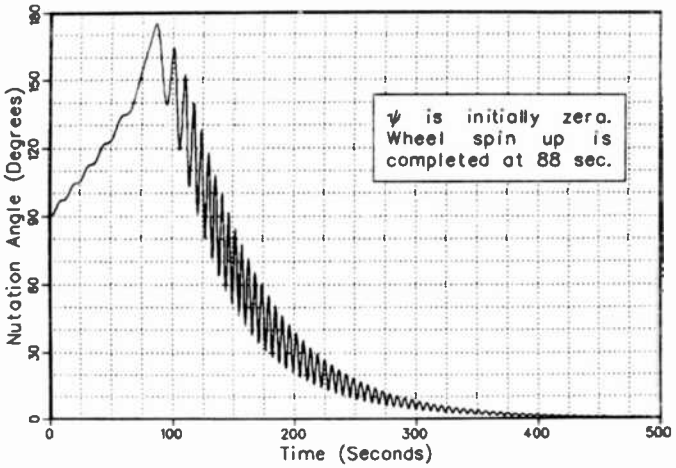

Fig. 15—Nutation angle versus time during a minor to intermediate axis turn with ψ = 0.0989.

5. Conclusion

The dynamics of dual-spin turns can be quite complex. It has been shown, however, that a simple geometrical technique can be an effective aid in the visualization and understanding of these useful maneuvers.

References:

[1] Kaplan, M. H., *Modern Spacecraft Dynamics and Control*, John Wiley & Sons, 1976, pp. 367–379.

[2] Kaplan, M. H. and T. C. Patterson, "Attitude Acquisition Maneuver for Bias Momentum Satellites," *COMSAT Technical Review*, Vol. 6, No. 1, Spring 1976, pp. 1–23.

[3] Gebman, J. R. and D. L. Mingori, "Perturbation Solution for the Flat Spin Recovery of a Dual-Spin Spacecraft," *AIAA Journal*, Vol. 14, No. 7, July 1976, pp. 859–867.

[4] Barba, P. M. and J. N. Aubrun, "Satellite Attitude Acquisition by Momentum Transfer," *AIAA Journal*, Vol. 14, No. 10, October 1976, pp. 1382–1386.

[5] Hubert, C., *Spacecraft Attitude Acquisition from an Arbitrary Spinning or Tumbling State*, AIAA paper No. 78-1387, presented at the AIAA/AAS Astrodynamics Conference, August 1978.

[6] Hubert, C., *An Attitude Acquisition Technique for Dual-Spin Spacecraft*, Ph.D. Dissertation, Cornell University, 1980.

[7] Hubert, C., *The Use of Energy Methods in the Study of Dual-Spin Spacecraft*, AIAA paper No. 80-1781, presented at the AIAA Guidance and Control Conference, August 1980.

[8] Lamy, P. L. and J. A. Burns, "Geometrical Approach to Torque Free Motion of a Rigid Body Having Internal Energy Dissipation," *American Journal of Physics*, Vol. 40, No. 3, March 1972, pp. 441–445.

[9] L. D. Landau and E. M. Lifshitz, *Mechanics*, Pergamon, 1976, 3rd ed.

A 4-GHz GaAs FET Power Amplifier: An Advanced Transmitter for Satellite Down-Link Communication Systems

B. Dornan, W. Slusark, Jr., Y. S. Wu, P. Pelka, R. Barton, H. Wolkstein, and H. Huang

RCA Laboratories, Princeton, NJ 08540

Abstract—The results of a program to develop a space-qualified solid-state power amplifier are presented. The amplifier design focuses not only on rf performance specifications but also producibility and reliability. The C-band amplifier was designed to replace the TWT's now used as the amplifier down-link transmitter for RCA's satellite communications (SATCOM) system. The 8.5-watt amplifier is designed to operate with an instantaneous bandwidth of 200 MHz in the 3.7–4.2 GHz band. The amplifier is designed to withstand the rigors of launch and to provide a useful life of 10 years in the space environment. It provides an operating gain of 55 dB with a dc-to-rf efficiency of 33%. It is fully compensated over the temperature range of −5 to +40°C.

1. Introduction

Domestic and international communications rely heavily on microwave satellite and ground-based communications radio links. Today, two-thirds of the world's international communications traffic (~15,000 two-way circuits) are accommodated by satellite communications systems. Domestic satellite traffic for network and cable TV accounts for approximately one-half of the overall long distance transmissions. Moreover, the growth rate for this service is estimated to be over 20% per year. Beginning with the first experimental active communication satellites, Bell Laboratories' Telstar and RCA's Relay, traveling-wave

tubes have been exclusively used as the major satellite component capable of meeting the stringent down-link performance specifications required for satellite communications systems. Although the traveling-wave tube has provided outstanding service in the past, overall system operation has been compromised by marginal TWTA performance in several important areas.

The first area is the need for large rf power back-off (well below saturation for TWTs) to reduce intermodulation distortion (IMD) in linear multitone service and phase distortion in FM-FDM service. This mode of operation—reduction of rf output power to reduce distortion in a satellite link as carrier density increases—leads to a correspondingly large reduction of TWT rf-to-dc efficiency. In addition, cathode wear-out in the TWT and other recognized failure modes associated with high voltage operation (TWT and electronic power conditioner) unduly restrict expected satellite service life and reliability.

This paper describes the development of an 8.5 W, C-band, solid-state power amplifier (SSPA) designed to replace the TWT now used as the amplifier down-link transmitter for RCA's satellite communications (SATCOM) system. The six-stage amplifier, which utilizes GaAs field-effect transistors (FETs), provides an operating gain of over 55 dB, a dc-to-rf efficiency of 33% and a bandwidth of 200 MHz over the 3.7 to 4.2 GHz range. The amplifier operates with relatively low dc voltages, requiring three fixed input potentials (+8.5 volts and +3.5 volts for drain operation and −3 volts for gate bias input). This is in contrast to the approximately 2500 volts required for TWT operation. Moreover, the SSPA provides for a 3rd order IMD product approximately 14 dB down from either of two (2) equal carriers at the operating output power level, which is typically about 6 dB better than a TWT under comparable operating conditions. The carrier-to-IMD separation improves significantly in comparison with the TWT as the carrier is backed off in amplitude.

The solid-state amplifier described is designed to withstand the rigors of launch and space environment and weighs 13 ounces (approximately one-half of the weight of the traveling wave tube it is intended to replace). This significant weight differential will be used to offset the lower rf-to-dc power efficiency of the SSPA compared to the efficiency of a two-collector TWT (33% vs. 37%) by adding the weight saved to the solar conversion panel of the satellite to generate the additional dc power required.

The extensive life test and reliability program that has been implemented and carried out for the high-power SSPA amplifier stages under high temperature accelerated life conditions will be reviewed. Statistical projections of this information indicate a better than 0.82 probability

of 24 channel availability for a 10-year mission, which is substantially higher than the 0.36 probability of success for a comparable TWT system.

This paper reviews the design, fabrication, performance, and reliability evaluation of the solid-state amplifier. Performance characteristics and reliability projections based on this evaluation of the solid-state amplifier and its components challenges the time honored traveling-wave tube as the preferred amplifier for commercial satellite systems.

2. Amplifier Design

The initial amplifier design focused not only on rf performance specifications, but also such aspects of design as producibility and reliability. These factors limited the choice of components available for the amplifier and also influenced its mechanical and thermal design. The preliminary design study resulted in an amplifier that would not only meet the rf program goals but would also be highly reliable and manufacturable in large numbers.

The proposed amplifier block diagram with its associated gain and power budget is shown in Fig. 1. The amplifier comprises six stages, which feature both high gain and linear amplification. The first two stages utilize low-noise FETs with high associated gain. A tempera-

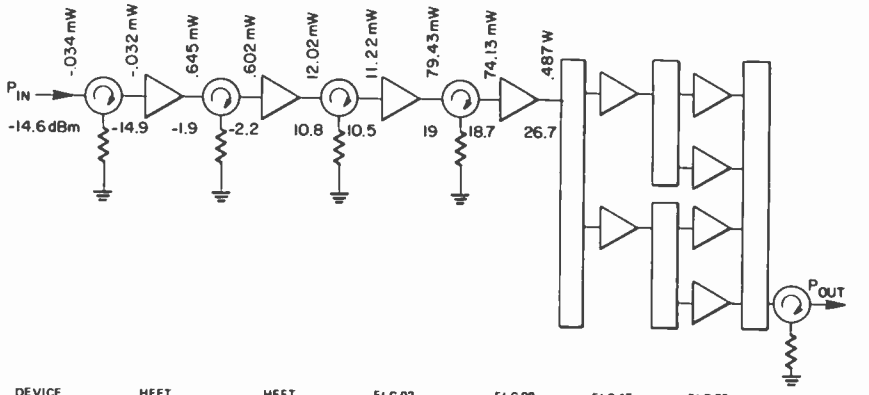

DEVICE		HFET 2201		HFET 2201		FLC-02		FLC-08		FLC-15		FLC-30		TOTAL	TOTAL
		12.7		25.4		33.6	41.3	41.3		48.1		54.5			
GAIN (dB)	-.3	13.0	-.3	13.0	-.3	8.5	-.3	8	-.2	7	-.2	6.6	.4	-.3	53.8
P_{DC} (WATTS)		.087		.087		.80		1.66		5.5		21.9			30
η_{PA} (%)		6.08		6.08		11.8		23.6		32.7		35.2			28.3
$P_{rf/device}$	-.032 mW	.645 mW	.602 mW	12.02 mW	11.22 mW	79.43 mW	74.13 mW	.487 W		1.13		2.47			8.5

Fig. 1—Power/gain/efficiency budget of 8.5-watt solid-state power amplifier.

ture-compensation network is incorporated in the gate bias circuit of these stages to achieve gain stability over the operating temperature range of −5 to +40°C. The third and fourth stages are linear amplifiers needed to drive the power stages. The last two stages are high-power FET amplifiers. The output stages consist of balanced amplifiers combined by 3-dB interdigitated couplers. An output power of 8.5 W is achieved by the parallel combination of four Fujitsu FLC-30 FETs. The ouput stage is driven by two Fujitsu FLC-15 FETs. There are input and output isolators used to ensure a VSWR of 1.25:1 at the input and a 1.15:1 at the output.

The amplifier is fabricated in modular form. This construction technique requires the use of isolators between the single-ended stages. No isolator is required between the balanced stages, because any mismatch present will be reflected into the terminated arm of the interdigitized coupler. The modular construction allows each stage to be fully tested prior to being integrated into the amplifier housing.

The design study also included the mechanical layout. The amplifier construction techniques selected allow for the lightest weight possible, while providing sufficient mechanical integrity to guarantee specified performance over the mission life of the amplifier.

HFET 2201 RUN @ 3.0,-1.02,25.0MA

S-PAR OF HFET 2201 3\7\79 M.C. B.D.

FREQ	S11		S21		S12		S22	
MHZ	MAG	ANG	MAG	ANG	MAG	ANG	MAG	ANG
3500.0	.870	-94.2	1.935	94.9	.029	21.8	.667	-53.8
3600.0	.877	-95.8	1.926	92.7	.030	19.3	.667	-55.2
3700.0	.876	-98.0	1.912	90.6	.030	16.5	.657	-56.3
3800.0	.873	-101.2	1.890	87.9	.030	14.1	.658	-58.4
3900.0	.879	-103.2	1.892	85.8	.030	13.2	.646	-59.2
4000.0	.874	-109.4	1.867	80.5	.030	8.2	.636	-64.4
4100.0	.876	-112.4	1.875	77.9	.030	6.6	.633	-66.1
4200.0	.879	-116.1	1.867	74.7	.032	4.5	.631	-68.7
4300.0	.882	-118.6	1.870	72.4	.033	2.6	.628	-70.0
4400.0	.886	-121.9	1.890	69.8	.033	1.0	.626	-71.7
4500.0	.889	-124.6	1.861	67.1	.034	-.8	.622	-73.7

REFL PLANES: 4.25 3.97 TRAN LIN: 8.22

S-PAR OF HFET 2201 3\7\79 M.C. B.D.

FREQ	MASON	MSG	MAG	MUG	GO	G1	G2	K	DELTA
3500.0	15.26	18.21	15.10	14.45	5.73	6.16	2.56	1.27	.59
3600.0	15.35	18.10	15.27	14.61	5.69	6.36	2.56	1.22	.59
3700.0	15.04	18.06	14.95	14.42	5.63	6.33	2.46	1.27	.59
3800.0	14.84	18.02	14.68	14.23	5.53	6.24	2.46	1.31	.59
3900.0	15.02	17.96	14.82	14.31	5.54	6.43	2.34	1.27	.58
4000.0	14.69	17.90	14.42	13.93	5.42	6.26	2.25	1.34	.56
4100.0	14.83	17.89	14.50	14.02	5.46	6.33	2.23	1.32	.57
4200.0	15.08	17.72	14.73	14.06	5.42	6.43	2.20	1.25	.56
4300.0	15.25	17.60	14.94	14.15	5.44	6.54	2.17	1.19	.56
4400.0	15.65	17.54	15.39	14.38	5.53	6.69	2.16	1.12	.57
4500.0	15.69	17.42	15.40	14.29	5.39	6.77	2.12	1.11	.56

REFL PLANES: 4.25 3.97 TRAN LIN: 8.22

Fig. 2—Computer printout showing *S* parameters for HFET 2201.

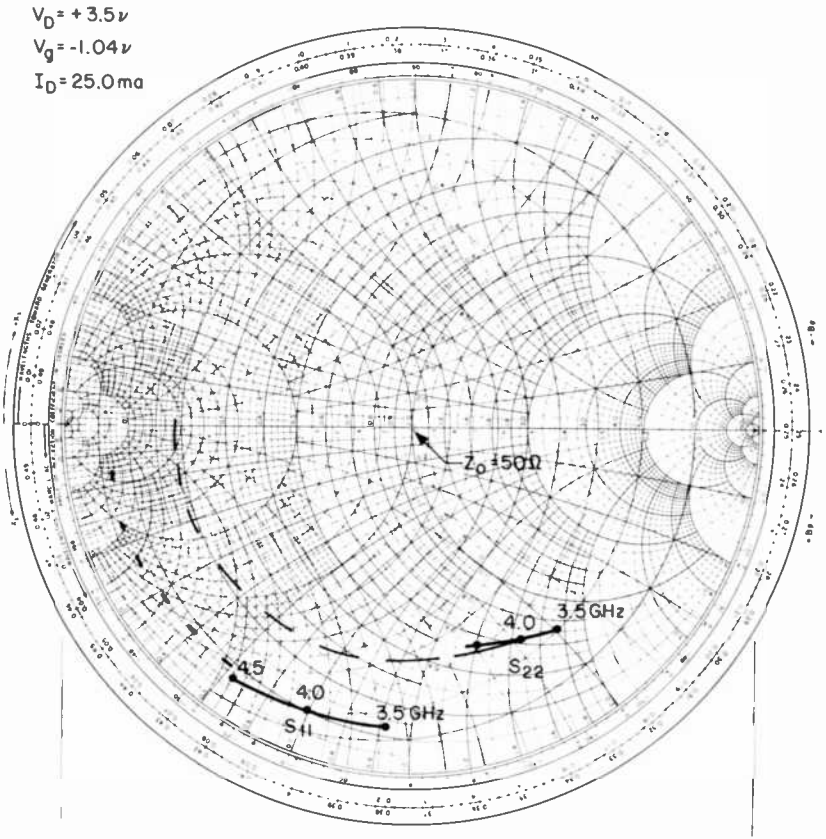

Fig. 3—Input and output (S_{11} and S_{22}) reflection coefficients for HFET 2201.

2.1 Low-Noise FET Amplifier Stages

The first two stages of the amplifier utilize Hewlett-Packard HFET-2201 FETs as the active device. These are specified with a 1.2-dB noise figure and associated gain of greater than 14 dB at 4.0 GHz. Since our performance specification requires 13-dB gain from each of the first two stages, it was possible to use the identical design in each of the first two stages. This results in two obvious manufacturing benefits: lower parts count and interchangeability of the first two stages. The required gain was obtained from these devices across the entire 500 MHz band. The overall amplifier noise power is essentially determined by the first stage. Meeting the amplifier requirement of noise power plus spurious signal of −10 dB in any 10-MHz bandwidth was accomplished without the need to sacrifice performance from these stages.

FREQ	GAIN PH X	1.000DB	FLATNESS X	1.000DB	S11,1.EC X	1.000<	S22,0.EC X	1.000<
3.500	11.726	61.11	.000	.00	.680	-81.25	.312	-75.71
3.600	12.380	31.69	.654	.65	.630	-117.73	.226	-116.44
3.700	12.421	2.96	.695	.04	.585	-153.56	.173	-156.03
3.800	12.367	-25.81	.695	-.05	.551	170.14	.174	160.37
3.900	12.286	-49.65	.695	-.08	.568	142.78	.173	131.03
4.000	12.179	-83.56	.695	-.11	.510	98.12	.175	80.11
4.100	12.313	-168.91	.695	.14	.493	66.09	.177	30.30
4.200	12.364	-137.70	.695	.05	.476	24.13	.193	8.29
4.300	12.318	-164.75	.695	-.05	.479	-16.78	.210	-32.56
4.400	11.950	165.49	.695	-.37	.540	-62.39	.253	-71.86

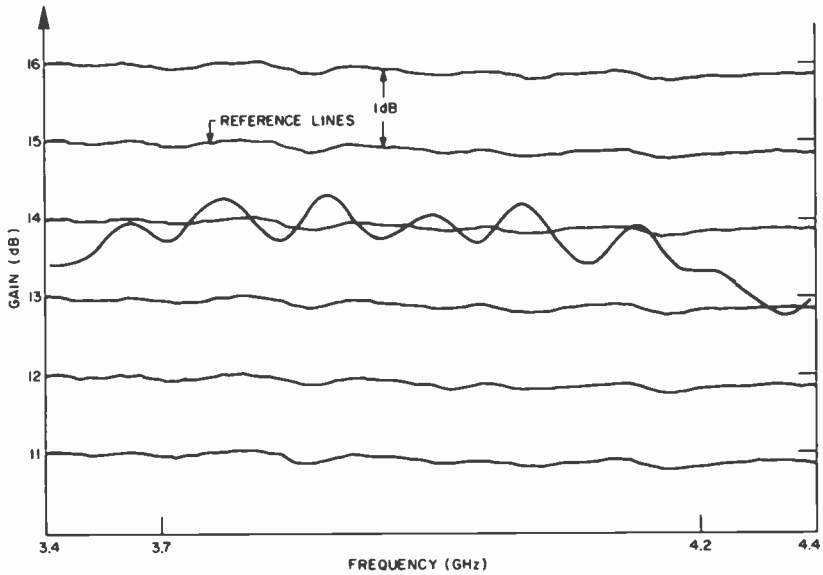

Fig. 4—Computer printout and curves showing swept gain response of completed amplifier.

The first step in the design of the low-noise amplifier stages was the measurement of the small signal S-parameters. These S-parameter measurements were performed at the dc operating point of the active amplifier. A number of devices were measured at this operating point to determine the range in S-parameters to be expected when a large number of amplifiers were to be built during the manufacturing phase. A sample of the computer output for the S-parameters for a Hewlett-Packard HFET-2201 FET is shown in Fig. 2. The operating point of these stages was determined to be a drain-to-source voltage of 3.5 V and a drain current that is approximately 20% of the saturated drain current. The gate bias was adjusted to control the drain current. A sample of the data for the input (S_{11}) and output (S_{22}) reflection coefficients is shown in Fig. 3. Fig. 4(a) shows the actual computer printout and 4(b) shows the swept gain response of the completed amplifier.

Table 1—Comparison of COSMIC-S Versus Actual Results for HFET-2201

Frequency (GHz)	Gain (dB)	
	COSMIC-S	Actual
3.7	12.4	13.8
3.8	12.3	13.7
3.9	12.3	13.8
4.0	12.2	14.2
4.1	12.3	13.9
4.2	12.4	13.5

A comparison of test results obtained from an HFET-2201 stage with the predicted results from the CAD program is shown in Table 1. The differences between the two sets of data can be attributed to the variations in S-parameters between devices. This slight variation, which is present even for devices in the same lot, poses no problem in the overall amplifier performance.

2.2 Linear Amplifiers

The third and fourth stages are linear amplifiers that require high efficiency and sufficient output power to drive the power stages. The proper selection of devices for these stages was necessary to obtain the required output power without gain compression. The devices selected for use in these stages were Fujitsu type FLC-02 and FLC-08 GaAs FETs. These devices are capable of providing output powers of 200 mW and 630 mW, respectively, at the 1-dB gain compression point while providing the required power-added efficiency at 4.0 GHz.

The selection of the Fujitsu devices for use in the linear amplifier stages reduced the qualification requirements for the overall amplifier since they are generically the same device that is used in the power stage of the amplifier. This fact allows the driver-stage FETs to be qualified on the basis of similarity, eliminating the need for life testing of those FETs. This will be further discussed in the reliability section of this paper.

Table 2—Comparison of COSMIC-S Versus Actual Results for FLC-02

Frequency (GHz)	Gain (dB)	
	COSMIC-S	Actual
3.7	12.0	11.0
3.8	11.9	11.1
3.9	11.9	11.2
4.0	11.9	11.5
4.1	11.8	11.2
4.2	11.7	11.8

The design procedure used for the linear amplifier stages was identical to that used for the low-noise stages. The small signal S-parameter measurements were performed, a preliminary matching circuit was designed, and the matching circuits were then optimized using computer simulation. A comparison of the predicted performance versus actual test data for the FLC-02 is shown in Table 2. The test results show reasonable agreement with predicted results.

Large-signal design procedures were not required for these stages because they are operated in the linear region. Large-signal design techniques were required for the power stages of the amplifier in order to provide 8.5 W of output power with the best possible efficiency.

2.3 Power Stage

The block diagram of the power output stage is shown in Fig. 5. The output from the driver stage is split equally by an interdigitated hybrid power coupler. This is used to drive a balanced amplifier consisting of two identical FLC-15 amplifiers in each of its arms. The output power from each of these amplifiers is again split to drive identical FLC-30 amplifiers, and the output of these four amplifiers is combined by a series of interdigitated hybrid power couplers to produce the 8.5 W of output power. Since the FET amplifiers in each arm of the hybrid couplers are similar, the input and output VSWRs are determined by the interdigi-

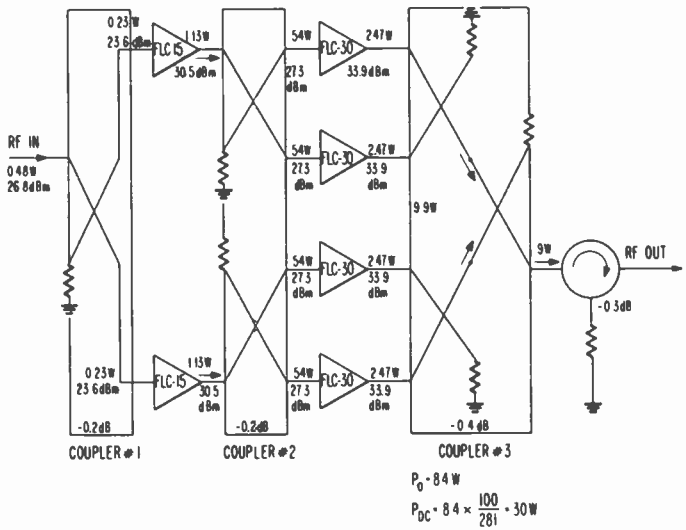

Fig. 5—Block diagram of power output stage.

tated couplers. Significant advantages in parts count and interchangeability are obtained by the use of four identical FLC-30 and two identical FLC-15 amplifiers in the output power stage.

The design goals for the power stages were to achieve high saturated rf output power with high efficiency, good linearity, and minimal rf gate current. The power and efficiency of the last two stages were optimized by matching the input of the FET for maximum small-signal gain. The ouput impedance of the FET was matched using our automatic load-pull system to determine the optimal impedance for output power, efficiency, linearity, and minimum rf gate current. The load-pull system, a unique instrument developed by RCA, is controlled by a HP RTE 2100 special-purpose computer. Both the RTE computer and the network-analyzer computer can communicate with one another, thereby greatly enhancing the design and optimization capability of the equipment.

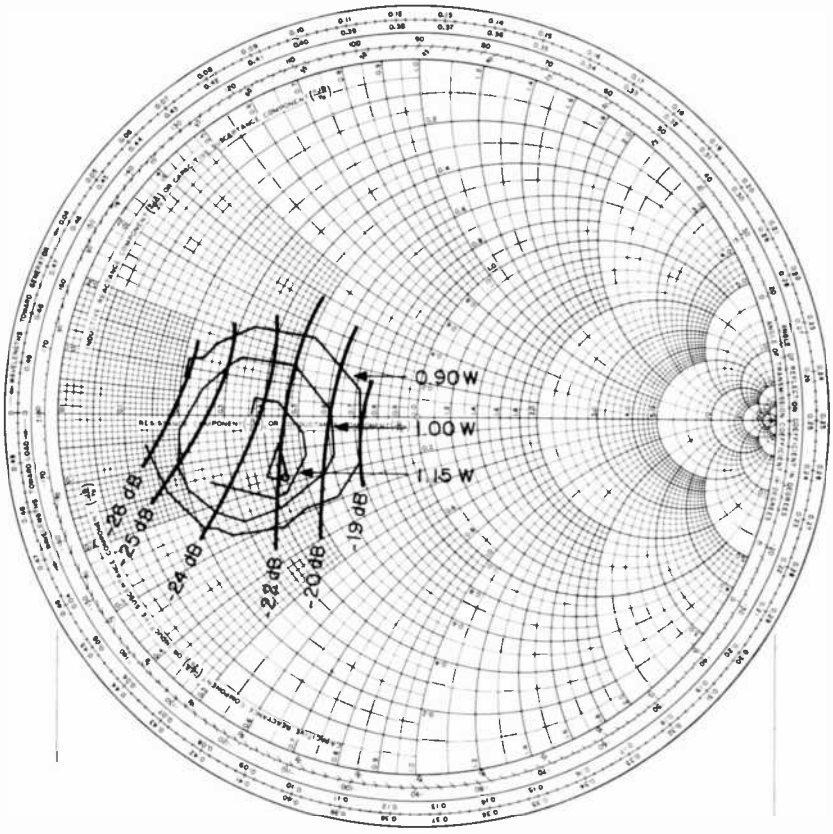

Fig. 6—Intermodulation and power contours for a Fujitsu FLC-30.

The power stage consists of four amplifiers, paralleled by means of quadrature interdigitated couplers. This arrangement is well known for its advantages in combining the output power of two amplifiers while maintaining isolation and low VSWR at the input port.

The procedure used for the circuit design of the amplifier can be outlined as follows. The ouput circuit, simulated on a network analysis computer program, is optimized to present to the FET an impedance corresponding to the previously determined load impedance for best output power and low intermodulation distortion over the operating bandwidth. The active device, characterized by means of its S-parameters, is then added to the optimized output circuit. The input circuit is then computer-optimized for high and constant gain over the operating bandwidth. This computer-aided design procedure resulted in an amplifier having nearly optimum power and intermodulation distortion over the operating bandwidth while still maintaining high and constant gain.

The intermodulation and power contours for a Fujitsu FLC-30 device are shown in Fig. 6. The load impedance for optimum intermodulation performance was critical. It can be seen, for instance, that although more than one value of load impedances provides the same output power, these impedances produce intermodulation distortions (IMD) varying by more than 7 dB. Therefore, the design procedure, which permitted a choice

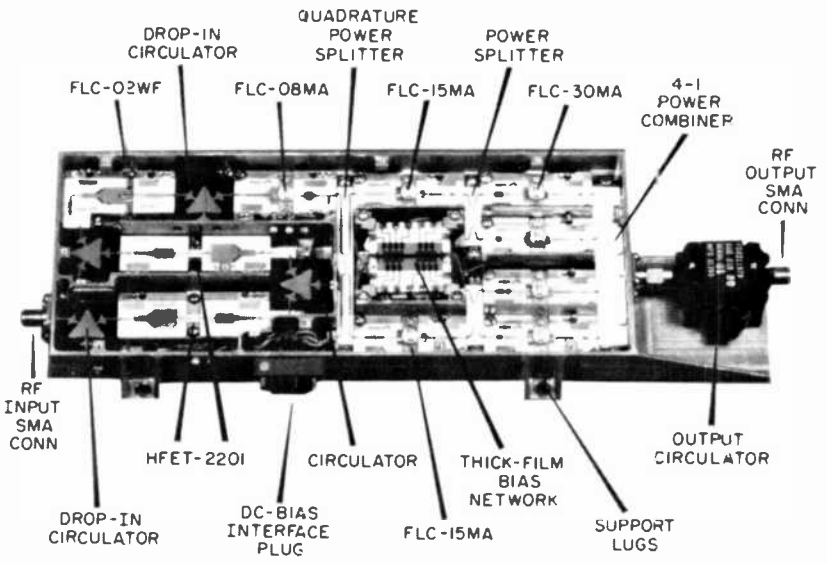

Fig. 7—Solid-state power amplifier.

Table 3—Summary of RF Requirements and Performance for Two Engineering Models

Performance Characteristic	Specified Values	Engineering Models Unit #1	Unit #2
1. Type I	3.7–3.9 GHz		Type I
Type II	3.85–4.05 GHz		
Type III	4.0–4.2 GHz	Type III	
2. High-Power Operating-Point Power Output Minimums (Watts)	8.5 (EOL)	8.50	8.71
3. Gain at High-Power Operating Point (dB)	50–53	52.5–53.0	55.5
4. Small-Signal Gain (dB)	Typically 3–4 dB greater	55.0–56.0	59.0
5. Small-Signal-Gain Flatness (Any Channel) (dB p-p)	0.25	0.80	0.50
6. Small-Signal-Gain Slope (Any Channel) (dB/MHz)	±0.010	±0.02	±0.02
7. Small-Signal Gain Stability (Over Full Temp. Range) (dB p-p)	1.3	1.50	0.55
8. Level of IM Output Relative to Carrier Input Levels (dB):			
−3	−13	−13	−13
−10	−24	−23	−24
−17	−32	−34	−36
9. Harmonics Power Relative to Fundamental (Under Full Power) (dB)			
2nd Harmonic	−12	~60	~60
3rd Harmonic	−21	~70	~70
10. Input VSWR	1.25	1.23	1.25
Output VSWR	1.15	1.09	1.08
11. Group Delay (Any Channel):			
Variations ns p-p	0.5	0.25	0.83
Slope $(\Delta\tau/\Delta f)$ηs/10 MHz	0.1	0.04	0.23
12. Phase Shift in Degrees for Input Drive Level of Carrier Below Operating Point of			
0 dB	22°	5.2°	20.0°
−3 dB	17°	8.0°	14.0°
−6 dB	14°	7.0°	11.0°
−10 dB	7°	4.0°	4.5°
13. AM/PM Conversion (°/dB)	2.0	1.40	1.70
14. AM/PM Transfer (°/dB) With Level of Unmodulated Carrier Relative to Modulated Carrier of:			
−20 dB	3.0	2.65	—
0 dB	2.0	1.50	—
15. Max. Dissipation Over Range of No Drive to Operating-Point Drive (Watts)	27	23.36	25.30
16. Max. Weight (lbs)	1.0	1.0	0.81
17. Max. Size* (in^3)	20	15.68	15.68

* Excluding output isolator.

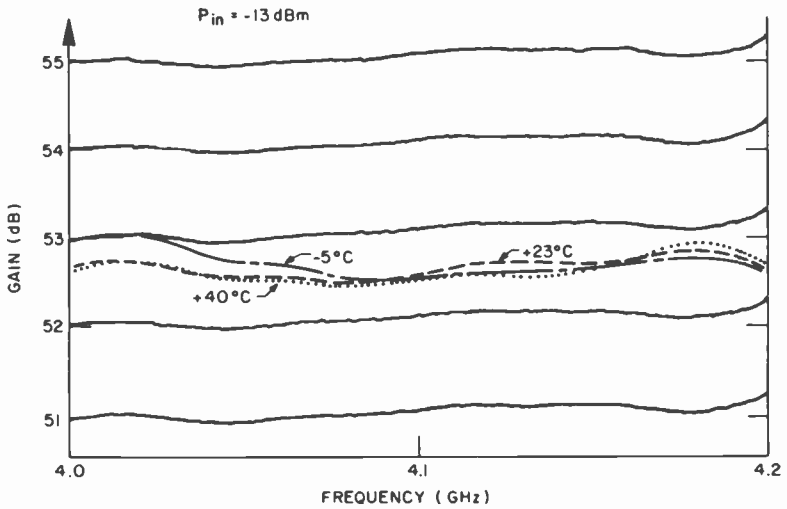

Fig. 8—Amplifier operating gain over 200-MHz frequency band (4.0 to 4.2 GHz) showing effectiveness of temperature compensation network.

of the optimum load impedance for low intermodulation performance, had to be accurate. It also had to account for the variation in the IMD with rf input power.

The design procedure is described here largely by making reference to the measured performance at the center frequency. The contours of

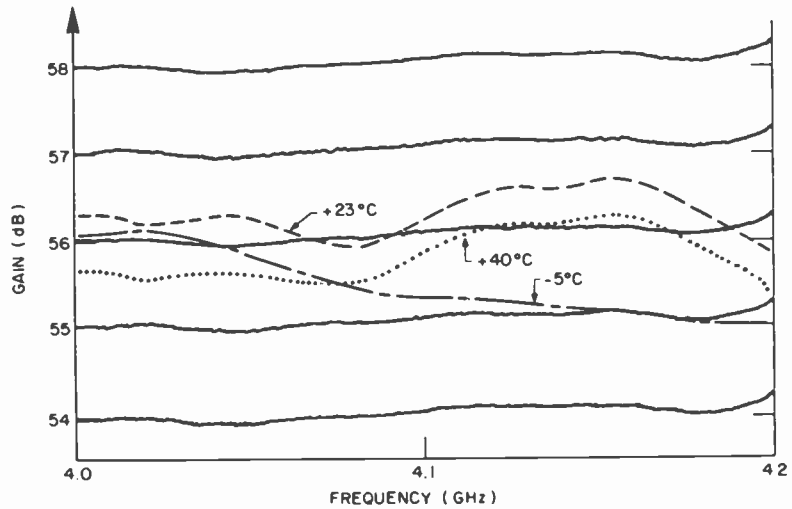

Fig. 9—Amplifier small-signal gain.

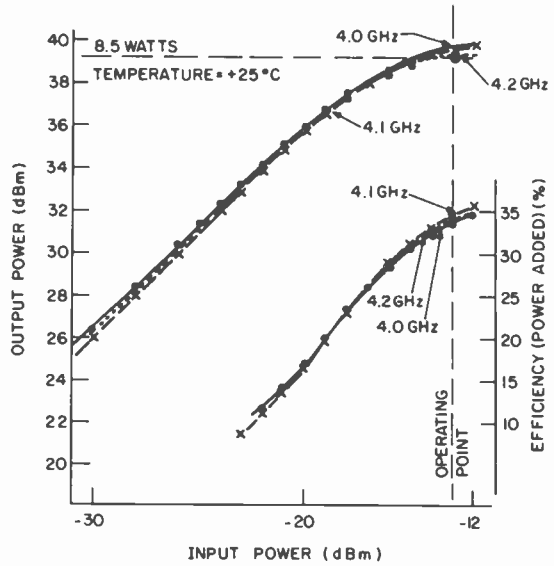

Fig. 10—Amplifier output power and efficiency for ambient temperature of +25°C.

Fig. 6, for instance, represent the output power and the intermodulation distortion as a function of the load impedance. The input power was 500 mW and the frequency was 4.00 GHz. One can see by inspection that,

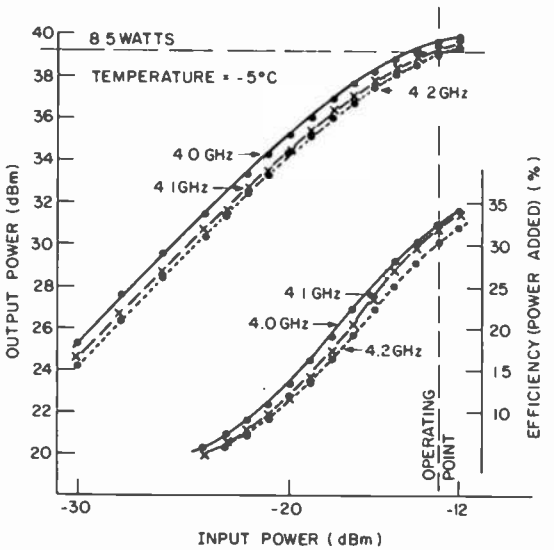

Fig. 11—Amplifier output power and efficiency for ambient temperature of −5°C.

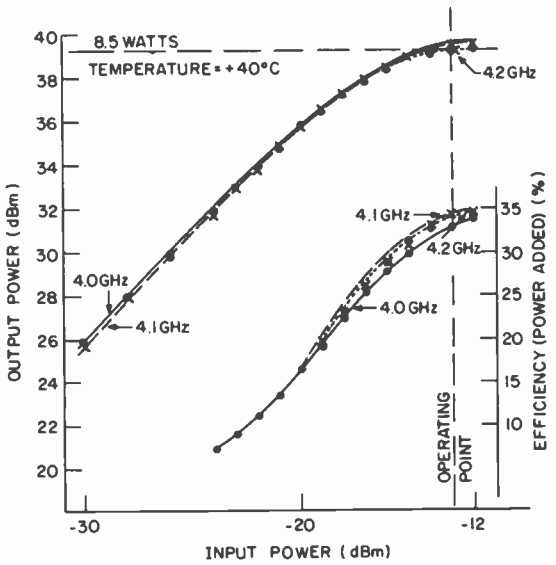

Fig. 12—Amplifier output power and efficiency for ambient temperature of +40°C.

along a line of constant intermodulation, the best load impedance is defined by the point "closest" to the center of the power contours, since this load would provide the maximum output power for a given value of C/I. This condition can be defined more precisely by stating that the

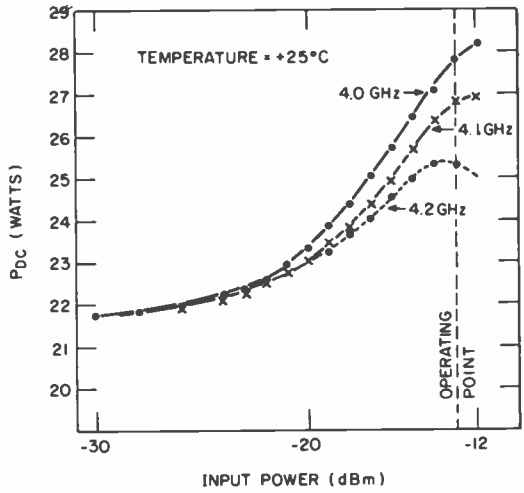

Fig. 13—Required dc input power versus rf input power for +25°C ambient.

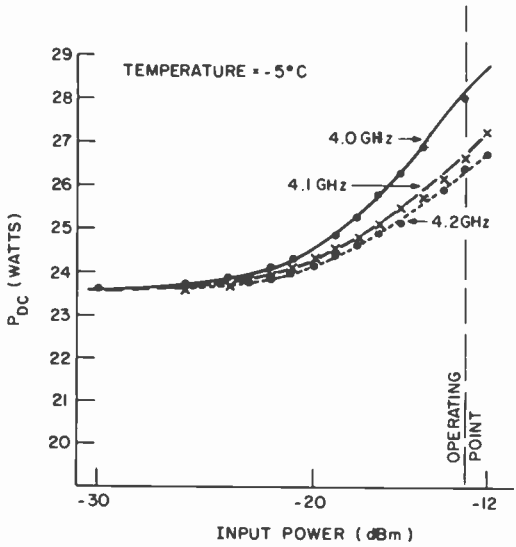

Fig. 14—Required dc input power versus rf input power for −5°C ambient.

optimum point is the tangent point between the C/I contour and one of the power contours.

This same design technique was then applied at different frequencies and different power levels, resulting in an optimum load impedance for the required frequency band and drive level.

To ensure a low VSWR at the output, an isolator is used along with

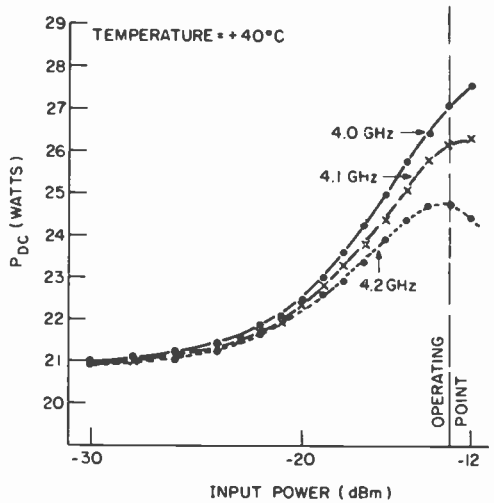

Fig. 15—Required dc input power versus rf input power for +40°C ambient.

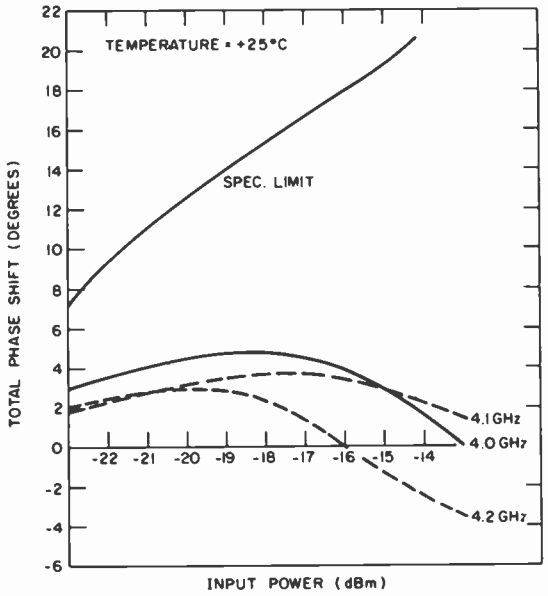

Fig. 16—Total phase shift corresponding to +25°C ambient.

the hybrid. The termination used for the output isolator is a high-power type, so that in the event of an open circuit in the load, it can handle the total rf power of the amplifier without causing damage.

2.4 Test and Evaluation

Table 3 shows a comparison between the specifications for the 8.5 W SSPA and the test results of two units. It is believed that the test results of the SSPA are the best reported to date.

Fig. 7 is a photograph of the solid-state amplifier. Fig. 8 shows the amplifier operating gain across the 200-MHz frequency band from 4.0 to 4.2 GHz. The gain is 52.75 ± 0.25 dB at the rated rf input power of −13 dBM. The amplifier has a built-in temperature compensation network. The gain varies by less than ±0.12 dB under an ambient temperature change from −5 to +40°C. The amplifier small signal gain is shown in Fig. 9. The small signal gain is 55.75 dB ± 0.75 dB for all temperature (−5 to +40°C) over the 4.0 to 4.2 GHz band. Figs. 10 to 12 are the amplifier output power and efficiency for ambient temperatures of +25, −5 and +40°C, respectively. The output is in excess of 8.5 Watt across the 4.0 to 4.2 band for any temperature from −5 to +40°C. The rf-to-dc conversion efficiency is between 30% and 35%. The required dc input

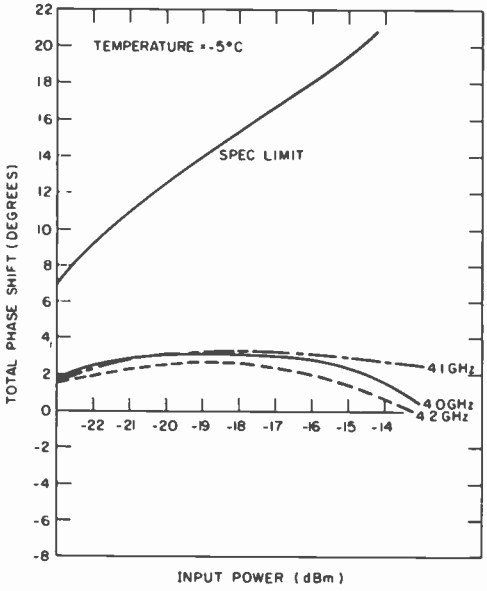

Fig. 17—Total phase shift corresponding to −5°C ambient.

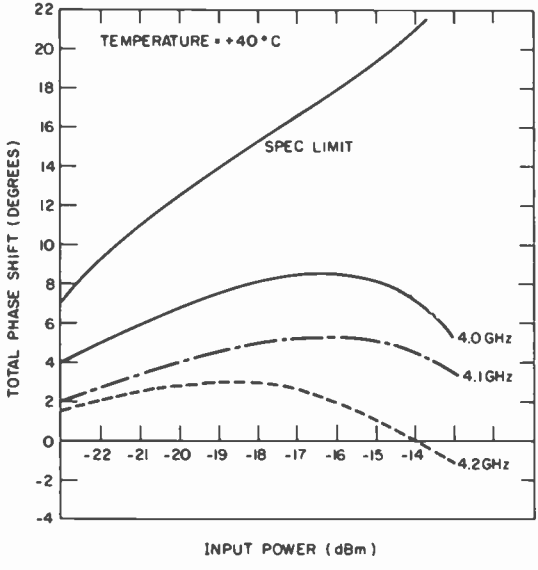

Fig. 18—Total phase shift corresponding to +40°C ambient.

power as a function of rf input power is shown in Figs. 13 to 15 for +25, −5 and +40°C ambient, respectively. Since the power stages of the amplifier are in a class AB mode, the required dc input power varies from about 21.7 W for small signal conditions to 27.8 W for the full drive condition. Figs. 16 to 18 show the total phase shift corresponding to the 3 ambient temperatures. The maximum phase shift is 8.5° under all the designed operating conditions. Except for the amplifier efficiency at full saturation, the performance of the SSPA surpasses that of a comparable TWTA in every respect. The capability and advantage of an SSPA over a TWTA is thus clearly demonstrated.

3. Reliability

In the development of the 8.5-W SSPA, particular attention has been given to the reliability of the components and techniques used in the construction. A committment was made to use space-qualified components and assembly techniques in all phases of the program. This resulted in early identification of problems during design and assembly of the breadboard amplifiers and resulted in changes that enhanced the reliability of the final model of the amplifier.

The primary reliability effort focused on life-testing the Fujitsu (FLC-30) devices, which are used in the output stage of the amplifier. A decision was made to life test the FLC-30 devices as 2.5 W amplifier modules. In effect, the life test would qualify the entire amplifier module for space use. Four of those modules in parallel comprise the output stage of the amplifier.

The qualification of the devices proceeded in three stages. Initially, commercially available devices were tested at a single elevated temperature to characterize the performance of the devices and to establish failure modes and mechanisms. This was followed by a step stress test to evaluate the temperature limitations of both the devices and the amplifier module components. The third stage, still in progress, consists of a two-temperature accelerated rf life test to determine the activation energy and failure mechanisms of flight-type amplifier modules and devices.

3.1 Initial Life Test Studies on Commercial Grade FETs

After a survey of GaAs FET performance characteristics by the rf design group, the Fujitsu series of power devices (FLC-02, 08, 15, 30) were chosen as the most likely candidates for use in the SSPA. This family of devices are identical in geometry and fabrication. An rf life test using

FLC-30 devices was chosen as the means to qualify these devices. Based on a thermal and electrical stress analysis, these devices would be the hottest running devices in the SSPA (100°C channel temperature at a spacecraft temperature of 45°C) and would have the greatest power density (power/unit active area). Because of these two conditions, it was decided to life test the FLC-30 devices and qualify the FLC-15, -08, -02 devices on the basis of similarity with appropriate derating based on drain voltage, rf input power, and operating channel temperature.

(a) FLC-30 MM Lifetest

The qualification of the Fujitsu devices proceded in three steps, initial life test studies, stress tests, and the flight model life test. Initially, twenty-four commercial grade FETs were purchased from Fujitsu, Inc. and characterized extensively at room temperature. These devices consisted of sixteen FLC-30 MM and eight FLS-50 MM transistors. The purpose of this initial test was (1) to provide experience in the handling, assembling as amplifiers, and testing of Fujitsu devices, and (2) to identify the failure modes of these devices. This information served as a basis for establishing specifications and screening procedures for the flight-qualified FETs.

These devices were commercial grade (not super-high-reliability grade) and purchased to an initial RCA specification. The salient portion of this specification was a 168 hour dc burn-in at an estimated channel temperature of 175°C. The received devices were characterized in a test fixture provided by Fujitsu, Inc., and this data was compared with data accompanying the devices. This was done to establish our confidence in the repeatability of device data for future orders. The parameters measured during this characterization were transconductance, pinch-off voltage, saturated drain current, gate breakdown voltage, and drain resistance. Another initial concern was the effect on device characteristics due to temperature extremes reached during their assembly as amplifiers. To determine this effect, the parameters were remeasured after the amplifiers were assembled. The results of these characterizations indicated that (1) the Fujitsu data was repeatable and (2) assembly techniques were valid and produced no changes in the device characteristics. Of some twenty-eight devices initially assembled, only one was rejected after assembly because of a significant decrease in the gate breakdown voltage.

The initial amplifier consisted of a gold-plated brass pallet with end blocks and 25-mil thick alumina matching circuits 1 × 1 inch in size. The rf lines were 25-mil-wide with ceramic dc blocking capacitors soldered into the circuit. The rf choke lines through which the dc bias was applied

Table 4—Lifetest of FLC-30 MM Devices at 200°C (V_{DS} = 10 V, I_{DS} = 0.5 A, P_{in} = 1.0 W)

Device Failure Time (Hrs)	Cause
300	
370	Gracefull drop in output
660	Power >0.5 dB
1150	Mechanical Failure
1700	Catastrophic short
2379	
2608	Gracefull drop in output
2800	Power >0.5 dB

were wire-bound nichrome wire soldered near the dc blocking capacitors and to the rf bypass capacitors on the side of the pallet.

Eight of the FLC-30 MM and eight of the FLC-50 MM devices were tested at a channel temperature of approximately 200°C and eight of the FLC-30 MM devices were to be tested at a channel temperature of 225°C.

The FLC-30 MM FETs were tested at 200°C for approximately 2800 hours until the last device failed. The failure criteria during this test was a 0.5 dB drop in power measured at 4.0 GHz. The conditions of the test were V_{DS} = 10.0 volts, I_{DS} = 0.5 amps, and P_{in} = 1.0 watt. The first

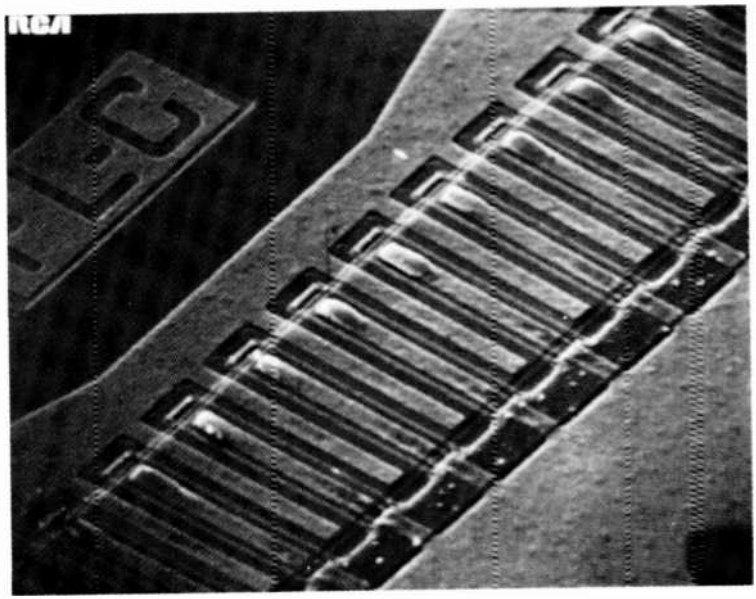

Fig. 19—Initial lifetest transistor with source-drain electromigration.

failure occurred at 300 hours. A complete listing of failure times and causes is shown in Table 4. This data indicated a rather large percentage of infant mortality failures.

The three early failures were characterized by a large increase in the gate leakage current after the first 100 hours of testing. This gate leakage current increased with additional testing until at failure it was in the milliampere range. The longer lasting devices did not show this behavior. All of the failures up to 2379 hours showed severe metal migration in the source and drain fingers as shown in Fig. 19. The gate stripes, on the other hand, appeared to be intact. The last two failures, in addition to the source-drain migration, showed gate stripe migration as shown in Fig. 20. Two of the early failures were analyzed at the Naval Research Laboratories using a micro-spot Auger technique. This allows material analysis of spot sizes as small as 2000 Å. In addition to a build-up of gold at the end of the source fingers, a significant amount of gallium and to a lesser extent, arsenic were also present on the metal buildups (Fig. 19). Etching away of the surface material revealed that gold had spread laterally as well as vertically into the gallium-arsenide. Thus, a complex migration-diffusion process had occurred in the source finger. Analysis

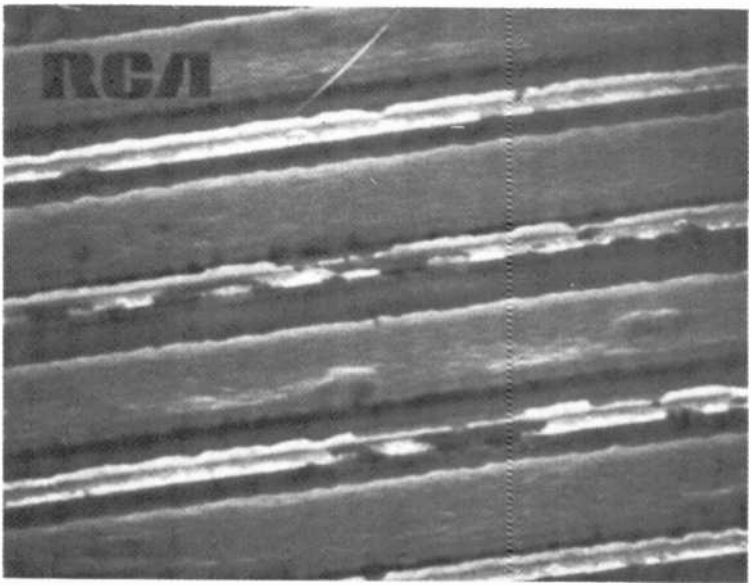

Fig. 20—Initial lifetest transistor with gate degradation (removed from test at 2500 hours).

of the gate region of these devices showed only aluminum, with no other materials present.

The second set of FLC-30 devices, which were tested at a channel temperature of 225°C, all failed catastrophically within minutes when they were brought to the test temperature. The failures were caused by an increase in gate current until gate control was lost; which resulted in thermal runway caused by the drain current increasing to its saturation limit.

(b) FLS-50 MM Lifetest

The FLS-50 MM devices were tested at a channel temperature of approximately 200°C with V_{DS} = 10.0 volts, I_{DS} = 0.8 A, and P_{in} = 1.0 watt. Of the eight devices tested, one shorted immediately after the rf was turned on at test temperature. The second failed within the first 100 hours. A third failed catastrophically at 1700 hours during rf measurements. The remaining five devices operated until 2100 hours when they were lost to an overheating condition of the hotplate. The devices that operated for 2100 hours showed no degradation in their output power over this time. A SEM analysis of these five devices showed much less electromigration in the source fingers than was present in the FLC-30 devices. One area in which the device test conditions differed was that of input rf power per unit gate width. The geometry of the FLC-30 and FLS-50 devices is quite similar. The only difference is the total gate width of the device; the FLC-30 device width is 7.28 mm, while that of the FLS-50 is 10.4 mm which is 40% wider. For equal rf input powers, the power density in the FLS-50 would be less than that in the FLC-30. The low rf power density results in lower instantaneous voltage along the gate of the FLS-50 devices and possibly lower instantaneous drain currents that might lead to reduced migration effects.

(c) Lifetest Redesign

To insure reliability in the test itself and to eliminate catastrophic failure owing to extraneous power supply malfunctions, a number of protective features were incorporated in the second lifetest stations. Fig. 21 is a representation of a lifetest station. The devices are heated on a hotplate under control of a Love temperature monitor. In addition to the built-in fail-safe features of this monitor, an over-temperature shut-off is attached in series with the Love monitor. In the event of an over-temperature condition, the hotplate is disconnected from the line voltage and

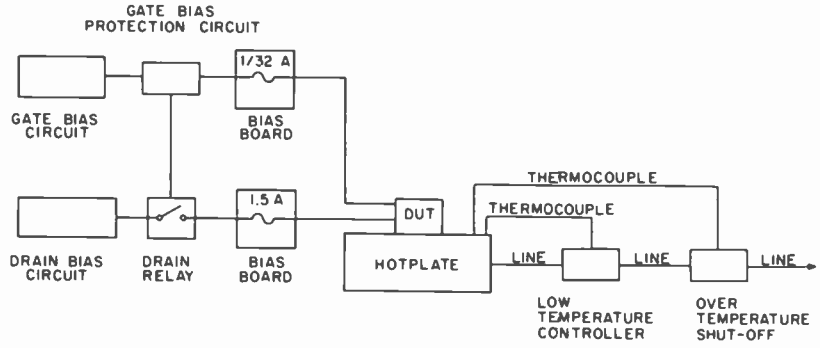

Fig. 21—Protective features of FLC-30 MA lifetest station.

must be manually restored. To prevent loss of gate supply with the drain on, the drain bias line is latched to the gate supply as shown in Fig. 22. In the event that gate bias fails, the drain switch will disengage. A six-volt battery will maintain the gate bias during this period.

Perhaps the most important change made as a result of the previous tests was to reduce the bias voltage and rf drive of the FLC-30 devices in the new SSPA design. It was felt that the reduction of the input rf power from 1.0 W to 0.56 W would significantly enhance the life of these devices based on our comparison of the power density in the FLC-30 and FLS-50 devices. Because the instantaneous drain voltage may swing to twice V_{DS} and Fujitsu was initially unwilling to test their devices beyond a V_{DS} of 18.0 V, the drain voltage in the SSPA design was reduced to 8.5 V.

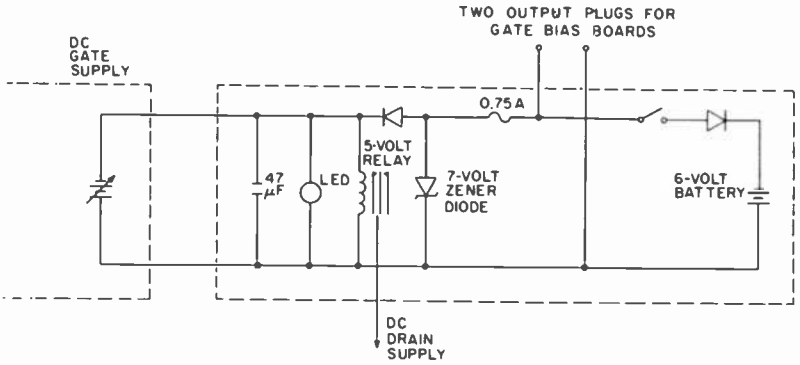

Fig. 22—Gate-bias protection circuit.

Table 5—Stress Test Data

Condition	P_{out} (dBm) for Four Devices			
	#159	#509	#491	#487
0 hour data for P_{in} = 27.5 dBm, T_{case} = 50°C	33.86	33.27	33.17	33.11
After 150°C test for 48 hours	33.95	33.45	33.04	32.93
After 165°C test for 48 hours	34.05	33.63	33.03	32.90
After 175°C test for 48 hours	34.06	33.83	32.81	33.05

3.2 Lifetest on Flight Grade FETs

(a) Stress Test

Before attempting the full flight model lifetest, it was decided to stress test four amplifier modules to verify assembly techniques. The amplifiers were stressed successfully for 48 hour intervals at the hotplate temperatures shown in Table 5, with no significant adverse effects to either the power output or the amplifier components. These amplifiers and subsequent lifetest amplifiers included a 10-mil-wide gold ribbon drain-bias strap as additional protection against bias-line burn-out during testing.

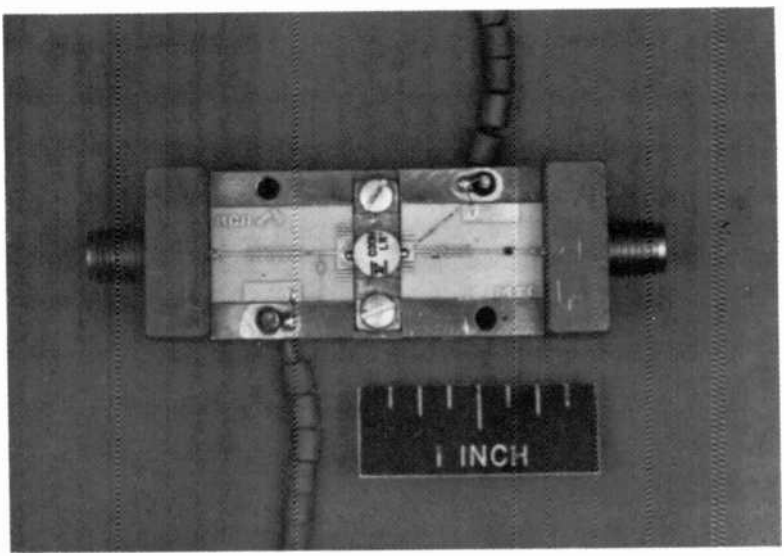

Fig. 23—Phase II lifetest amplifier module.

(b) FLC-30 MA Lifetest

The second lifetest consisted of the accelerated temperature testing of an additional twenty-nine FLC-30 MA hermetically sealed devices as 2.5 watt amplifier modules. These devices were assembled as amplifiers using space-qualified techniques subject to review and inspection by the RCA Reliability and Quality Assurance Department. Fig. 23 shows an FLC-30 MA device assembled as a lifetest amplifier. A schematic of the amplifier components along with the bias circuit is shown in Fig. 24. In effect, we qualified the amplifier module for space use. This represents a more stringent condition than simply testing devices in drop-in test fixtures. The unique feature of this test is that the individual lifetest amplifier modules are identical to those used in the flight module SSPA.

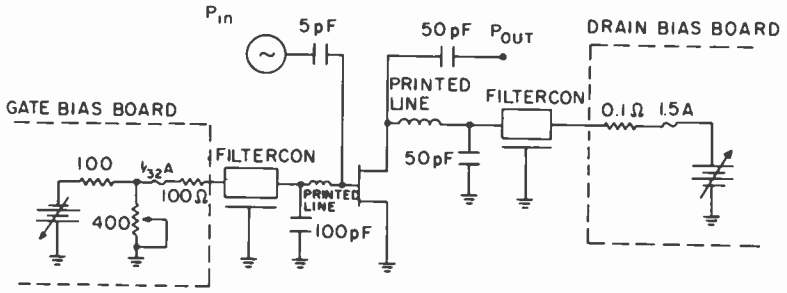

Fig. 24—FLC-30 MA bias circuit.

The lifetest conditions are shown in Table 6. The test flow diagram for the lifetest mentioned in Sec. 3.1(a) is shown in Fig. 25. After mounting in the lifetest fixture, the dc parameters were measured. The devices were then biased to 9.0 V and 500 mA under rf drive. The temperature of the test fixture was raised to the operating level and the drain current was adjusted in the range 425 to 500 mA ($\sim$1/2 I_{DSS}) to bring the channel temperature to the desired level. The devices were then returned to room temperature and the rf parameters (P_{OUT}, I_{DS}, I_G, and

Table 6—Flight-Model Lifetest

Channel Temperature	190°C	215°C
Number of Devices	19	10
RF Drive (4.0 GHz)	27.5 dBm	
Drain Voltage	9.0 V	
Drain Current	425 to 500 mA	

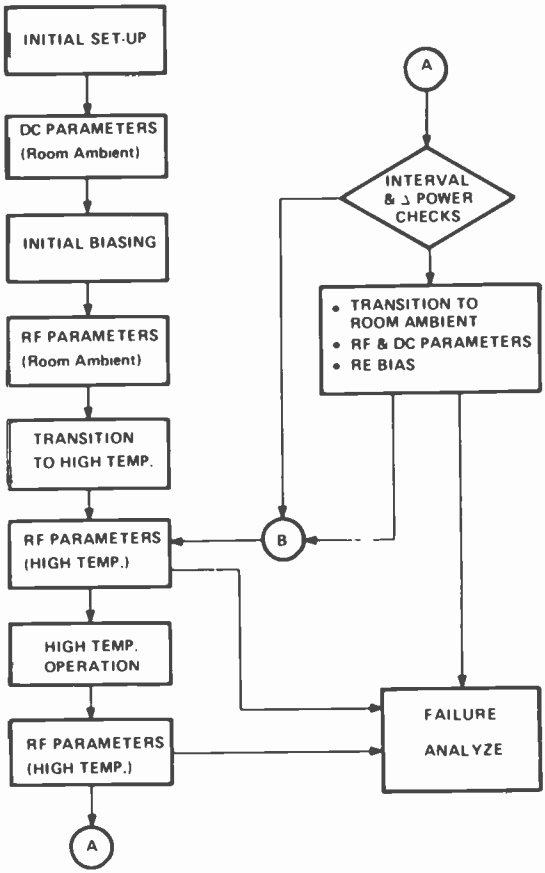

Fig. 25—Test flow chart.

V_G) were measured at input power levels of 0, 23.5, 25.5, 27.5, and 28.5 dBm. The test schedule is as follows: every 168 hours, the rf parameters are measured at test temperature; every 504 hours, the dc and rf parameters are measured at room temperature.

(c) FLC-30 MA Life test Results

To date, we have accumulated over 1×10^5 device-hours at elevated temperatures. Conforming with SSPA system requirements, the amplifier failure criterion has been determined to be 0.3 dB drop in gain. Two devices have failed as measured by this criterion. One device on test at 190°C failed at 2403 hours, and a second device on test at 215°C failed

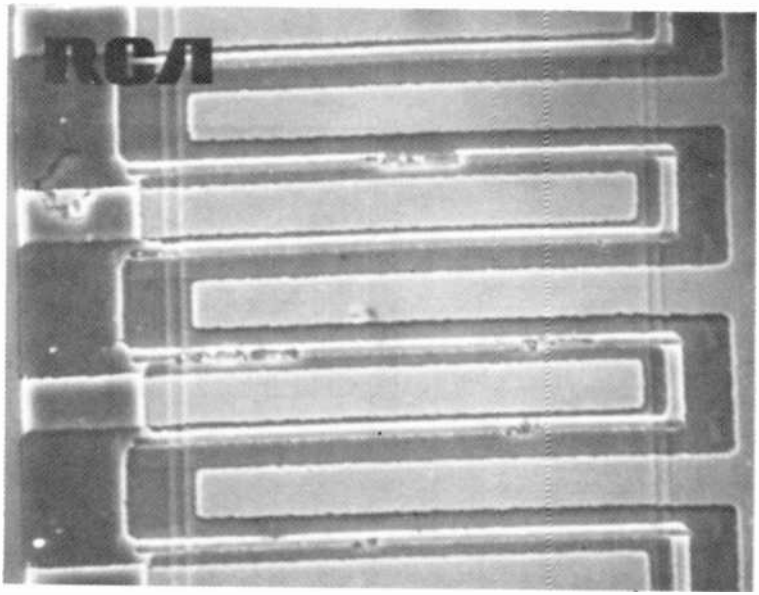

Fig. 26—Failed device removed from 190°C test at 2403 hours. Severe voiding observed in gate stripes.

at 1416 hours. The failure mode is graceful in nature and the amplifier continues to operate at reduced gain.

The device that failed at 2403 hours is shown in Fig. 26. The source–drain region shows little evidence of electromigration effects, but the gate regions show voiding, probably caused by migration of the aluminum gate material. It would appear, based solely on visual evidence, that this device failed due to gate and not source–drain migration problems.

A third device, on test at 215°C, failed at 2197 hours due to a solder contact problem. The device is shown in Fig. 27. Like the failure at 2403 hours on the 190°C test, this device has severe gate problems, but unlike that device, there is clear visual evidence of significant source–drain migration, which would indicate a possible mixed failure mechanism. Although this particular device shows both gate and source–drain migration effects, the electrical performance had not degraded until the solder connection failed. As more failures are analyzed, we should be able to establish either gate or source–drain migration as the dominant failure mechanism.

There is a basic difficulty in making statistical reliability predictions with only two data points. Because of the obvious need to make some

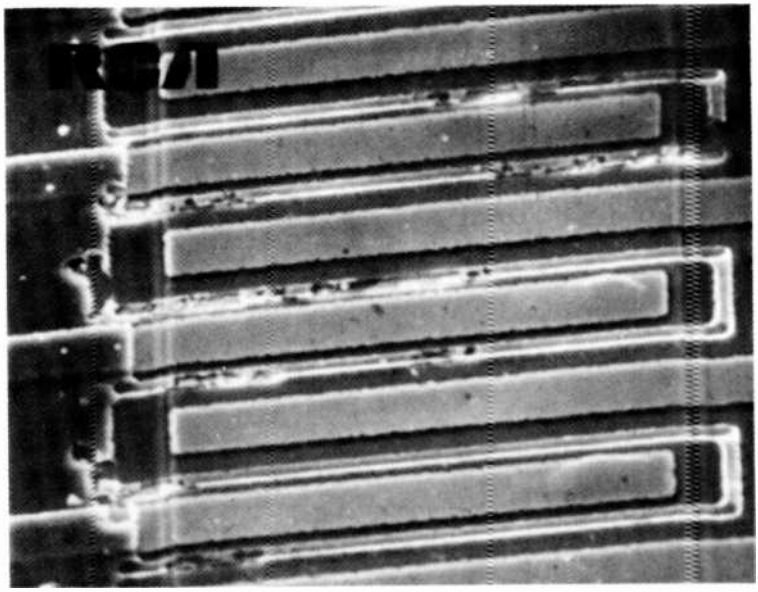

Fig. 27—Failed device removed from 215°C lifetest at 2197 hours due to solder failure. Device met electrical specifications prior to solder failure. Note both gate and source-drain migration.

estimate of the life of these devices, which have already operated for more than 3000 hrs at a test temperature of 190°C, we have made several assumptions that must await the conclusion of the lifetest to be confirmed or refuted. The risk in this type of exercise can be minimized by making those assumptions as conservative as possible. A computer program has been developed (FETANLY) that requires the assumption of three parameters to make an estimate of life based on one failure point: the activation energy, the failure rate distribution, and the standard deviation of the population. With this program, device test hours are transformed to device operating point hours by the choice of a multiplication factor uniquely defined by the activation energy (assumption 1). The operating point temperature is of course defined by system requirements. At the operating temperature, the device operating hours are fitted to a log-normal distribution (assumption 2) with a standard deviation (assumption 3) which characterizes the distribution. The computer program then fits the failure point to a log-normal failure distribution with a probability of 60% or 90%, depending on the selection of the operator. This failure distribution is then integrated to obtain an average failure rate over the ten year mission life.

Table 7—DC Parameters Measured During Radiation Tests

rads(Si)	V_{DS}* volts	I_{DS}* amps	V_G* volts	I_{DSS} amps	g_m amp/volt	V_p volts	Date
Device 1							
0	9.0	0.5	−1.64	1.22	417	−3.15	25/2/80
1×10^5	9.0	0.5	−1.62	1.22	417	−3.11	25/2/80
2×10^6	9.0	0.5	−1.63	1.22	417	−3.11	26/2/80
4×10^6	9.0	0.5	−1.63	1.23	417	−3.11	27/2/80
6×10^6	9.0	0.5	−1.63	1.22	417	−3.09	28/2/80
8×10^6	9.0	0.5	−1.63	1.21	417	−3.09	29/2/80
Device 2							
0	9.0	0.5	−1.19	1.05	435	−2.70	26/2/80
1×10^5	9.0	0.5	−1.19				
2×10^6	9.0	0.5	−1.19	1.05	435	−2.68	27/2/80
4×10^6	9.0	0.5	−1.18	1.05	435	−2.65	28/2/80
6×10^6	9.0	0.5	−1.18	1.04	435	−2.65	29/2/80

* DC operating point during gamma exposure.
Gamma ray exposure source—C_0^{60} 1×10^5 rad/hr.

This calculation was carried out for the FLC-30 MA devices based on the initial failure which occurred at 2403 hours. The standard deviation chosen was $\sigma = 1.0$ which is a conservative number for a well controlled semiconductor processes. The calculation was made for an activation energy of 0.9 eV, and gave 4 and 15 fits for the 60% and 90% confidence levels, respectively. These calculations are for devices operating at a spacecraft temperature of 45°C.

(d) Radiation Tests

Two FLC-30 MA devices assembled as SSPA amplifiers were subjected to gamma radiation at the Ft. Monmouth radiation test facility. They were biased at 9.0 volts and 500 mA during the radiation exposure. The exposure rate was 1×10^5 rad/hr (Si). The device dc parameters (g_m, V_p, I_{DSS}) were recorded every 20 hours with the radiation source off. Additionally, prior to testing and after the final exposure, the P_{in}–P_{out} characteristics were measured for both devices at 4.0 GHz.

The dc parameters measured during the course of the test are shown in Table 7. The only observable change was a slight decrease in pinch-off voltage. Although there appears to be a downward trend, the changes are very close to the measurement accuracy of the meters employed. The P_{in}–P_{out} characteristics for device #2 are shown in Fig. 28. There was

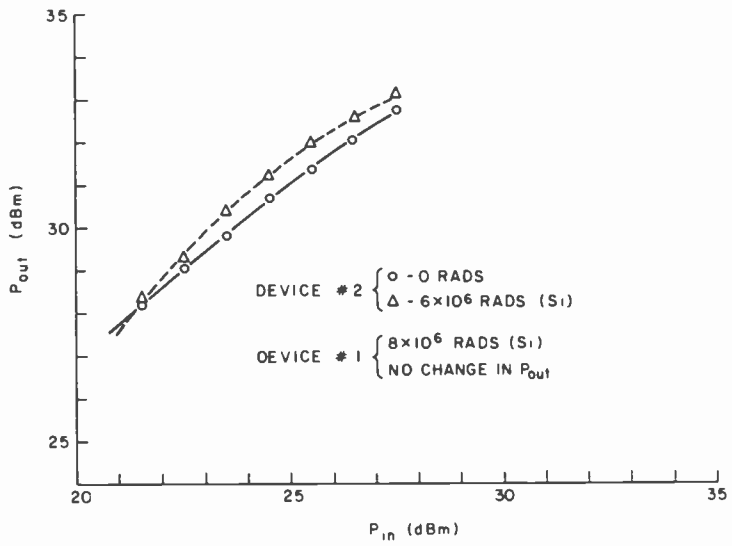

Fig. 28—Radiation test results.

a minor increase in the output power after the radiation exposure. Device #1 showed no change in the P_{in}–P_{out} characteristic after irradiation.

The maximum expected radiation dose with 50 mil aluminum shielding during a 10-year satcom mission is 7×10^6 rads(Si). Based on this projection and the radiation testing, the FLC-30 MA devices should not be adversely affected by radiation during the planned mission life.

3.3 Summary and Conclusion for Test Results

During the initial phase of the SSPA development, it was felt that the GaAs FET device reliability was not well established. Extensive tests were then began to understand the failure modes and failure mechanisms of these devices in order to qualify the SSPA for space use.

As a result of the initial test, a gate weakness which occurred early in device life was revealed in several of the devices. The device specification was then rewritten to screen out these failures. The approach appears to have been successful as we have observed no early failures of this type for the flight type devices. Design changes were also made in the bias network of the SSPA to reduce feedback effects caused by an increase in gate current during life.

A comparison of data from the FLC-30 MM and FLS-50 MM tests resulted in reducing the input drive level of these devices by nearly fifty percent. This change and the reduction in the drain voltage from 10 to 8.5 volts were prompted by reliability considerations.

A preliminary estimate of the life of these devices based on the ongoing tests predicts an average failure rate over ten years of 15 fits or lower, depending on the activation energy. These numbers are acceptable for spacecraft use.

It is estimated that the probability of having 24 channels available for use at the end of 10 years is 0.83 for the SSPA; a comparable TWT amplifier would have a corresponding probability of 0.36.

The dominant failure mechanism for these devices has not yet been established. Failure analysis of devices from the previous and ongoing life test show both drain-source and gate degradation in these devices. In particular, analysis of two failed devices from the second test shows source-drain migration may not be as important as gate migration in degrading the electrical performance of these devices.

Acknowledgment:

The authors wish to express their appreciation for the strong support and encouragement from F. Sterzer, K. Powers, and P. Wright. This work

was carried out in close cooperation with AED personnel including J. Keigler, J. Hawley, F. Drago, and N. LaPrade in engineering design, and V. Monshaw and M. Plesher in the reliability evaluation. Thanks are also due to M. Cummings, R. Menna, K. McEwan, and K. Pinkerton for their assistance in the testing and assembly of the amplifier.

Patents Issued to RCA Inventors—Second Quarter 1980

April

A. A. Ahmed Temperature Compensating Comparator (4,198,581)
A. A. Ahmed Integrated Injection Logic with Floating Reinjectors (4,199,776)
G. A. Alphonse and W. C. Saunders, Jr. Anti-Reflective Acoustic Wavefront Refraction Element (4,197,921)
C. H. Anderson and L. S. Cosentino Modulator Structure for a Flat Panel Display Device (4,199,705)
R. L. Angle CCD Multiple Channel Network (4,199,691)
A. R. Balaban and S. A. Steckler Frequency Divider Circuit (4,200,811)
B. B. Baptiste Method of Fabricating MNOS Transistors Having Implanted Channels (4,196,507)
H. R. Beelitz and D. R. Preslar Method of Integrating Semiconductor Components (4,199,860)
B. F. Bowman Reflectarray Antenna (4,198,640)
D. E. Carlson Article and Device Having an Amorphous Silicon Containing a Halogen and Method of Fabrication (4,196,438)
D. E. Carlson Amorphous Silicon Schottky Barrier Solar Cells Incorporating a Thin Insulating Layer and Thin Doped Layer (4,200,473)
P. S. Carnt, E. A. Rutishauser, and J. Schiess Encoding and Transcoding Apparatus for VideoDisc Systems (4,200,881)
J. Craft Intercarrier Sound System (4,199,787)
A. G. Dingwall Buried Contact Configuration for CMOS/SOS Integrated Circuits (4,196,443)
F. L. Dixon, L. P. Fox, and E. G. Trachman Wiping Apparatus and Method for a High-Density Information Record (4,198,060)
K. Y. Eng Redundancy System with Eight Devices for Five Channels (4,198,611)
R. W. Engstrom and A. F. McDonie Bi-Alkali Telluride Photocathode (4,196,257)
R. D. Faulkner Electron Discharge Device Including an Electron Emissive Electrode Having an Undulating Cross-Sectional Contour (30,249)
J. J. Gibson Rotating Field Polarization Antenna System (4,198,641)
S. T. Hsu MNOS Memory Device (4,198,252)
S. T. Hsu Method of Making a Planar Semiconductor on Insulating Substrate Device Utilizing the Deposition of a Dual Dielectric Layer Between Device Islands (4,199,384)
K. C. Hudson Defect Detection and Plotting System (4,197,011)
R. H. Hughes CRT Generating Three Inline Beams and Having Shunts for Weakening Center Beam Horizontal Magnetic Deflection and Strengthening Vertical Deflection (4,196,370)
A. C. Ipri Method of Fabricating a Narrow Base-Width Bipolar Device and the Product Thereof (4,200,878)
T. Kamprath Method of Fabricating MNOS Transistors Having Implanted Channels (4,197,630)
S. A. Keneman Electron Multiplier Input Electron Optics (4,199,702)
H. P. Kleinknecht and W. A. Bosenberg Optically Testing the Lateral Dimensions of a Pattern (4,200,396)
R. S. Mezrich and D. H. Vilkomerson Ultrasonic Wave Energy Electronic B-Scan Imaging Apparatus (4,197,749)
A. Month and T. E. Benner Pick-Up Tube Having Bias Lighting and Controls Therefor (4,196,372)
R. C. Palmer Recording/Playback Apparatus Facilitating Track Skip Detection (4,198,658)
R. P. Parker D.C. Gain Controlled Amplifier (4,198,652)
F. R. Ragland, Jr. Deflection Yoke Assembly Including a Beam Positioning Magnet Arrangement (4,198,614)
W. Rosnowski and J. M. Neilson Method of Diffusing Aluminum into Monocrystalline Silicon (4,199,386)
E. A. Rutishauser Overload Protection Circuit for Video Amplifiers (4,197,558)
O. H. Schade, Jr. Extended-Drain MOS Mirrors (4,199,733)
G. L. Schnable and A. W. Fisher Method of Chemically Vapor-Depositing a Low-Stress Glass Layer (4,196,232)
R. D. Scott Apparatus for Developing Photographic Images on an Emulsion Coated Film (4,198,145)
I. Spetgang and J. J. Brennan Magnetic Tape Rotary Headwheel Assembly with Venting Means (4,196,457)
F. Sterzer Hyperthermia Applicator (4,197,860)
L. A. Torrington VideoDisc Player (4,196,906)
A. V. Tuma, W. H. Groeneweg, and L. A. Harwood Brightness Control Circuit Employing a Closed Control Loop (4,197,557)

C. C. Turner Fixture for Holding a Faceplate and a Funnel of a CRT During Sealing (4,200,274)
D. H. Vilkomerson and R. S. Mezrich Pulse-Echo Ultrasonic Wave-Energy Imaging System Incorporating High-Angular Velocity Oscillated Transducer (4,197,751)
P. K. Weimer Solid State Image Sensor (4,200,892)
C. E. Weitzel and A. M. Goodman Insulated Gate Field Effect Silicon-On-Sapphire Transistor and Method of Making Same (4,199,773)
C. P. Wu Pulsed Laser Irradiation for Reducing Resistivity of a Doped Polycrystalline Silicon Film (4,198,246)

May

A. A. Ahmed Temperature-Sensitive Control Circuits (4,204,133)
F. Aschwanden Tuning Circuit with Provisions for Reducing Pulse Width Jitter (4,204,173)
T. J. Christopher and T. H. Lin FM Signal Demodulator with Defect Detection (4,203,134)
C. F. Coleman and M. C. Stewart RF Connector Assembly Including Mounting Apparatus for a Washer-Like Capacitor (4,202,594)
W. F. Dietz Side Pincushion Correction System (30,271)
L. A. Goodman Transistor Using Liquid Crystal (4,204,217)
T. M. Gurley Television Picture Compressor (4,204,227)
L. A. Harwood, R. L. Shanley, 2nd, and E. J. Wittmann Predictable Automatic Brightness Control Circuit in a Video Signal Image Reproducing System (4,203,131)
F. Z. Hawrylo Method of Epitaxially Deposited Cadmium Sulfide (4,203,785)
H. Khajezadeh Semiconductor Integrated Circuit Device (4,202,006)
R. D. Larrabee Power Transfer Apparatus (4,204,147)
P. Loeb and I. P. Magasiny Movement Detecting Apparatus and Method (4,203,063)
E. J. Nossen Code Correlator Loop Using Arithmetic Synthesizer (4,203,002)
L. S. Onyshkevych Inductance Fabricated on a Metal Base Printed Circuit Board (4,201,965)
L. S. Onyshkevych Method and Apparatus for Trimming Resistors (4,201,970)
R. W. Paglione Coaxial Applicator for Microwave Hyperthermia (4,204,549)
W. F. Reichert and H. Huang Semiconductor Device Having Grid for Plating Contacts (4,202,001)
E. A. Rutishauser Dual Standard VideoDisc Player (4,204,220)
O. H. Schade, Jr. Long-Tailed-Pair Connections of MOSFET's Operated in Sub-Threshold Region (4,201,947)
J. H. Scott, Jr. and A. C. Ipri Method of Fabricating Improved Short Channel MOS Devices Utilizing Selective Etching and Counterdoping of Polycrystalline Silicon (4,201,603)
R. L. Shanley, 2nd Predictably Biased Kinescope Driver Arrangement in a Video Signal Processing System (4,204,221)
J. L. Smith Color Purity Adjusting Method (4,201,932)
D. L. Staebler Updateable Optical Storage Medium (4,202,928)
D. L. Staebler Laser Beam Apparatus and Method for Analyzing Solar Cells (4,205,265)
E. M. Sutphin, Jr. Filter Which Tracks Changing Frequency of Input Signal (4,204,171)
J. R. Zuber and H. Foxman Method of Stripping Photoresist (4,202,703)
B. Zuk Circuits for Producing Sequentially Spaced Pulses (4,201,927)

June

R. F. Abt Pre-Processing Apparatus for FM Stereo Overshoot Elimination (4,207,526)
R. F. Abt Pre-Processing Apparatus for FM Stereo Overshoot Elimination (4,207,527)
W. E. Babcock Switching Regulator with Reduced Inrush Current (4,207,516)
A. G. Dingwall Circuit for Limiting Voltage Differential in Differential Amplifiers (4,206,418)
A. G. Dingwall and R. G. Stewart Precharge Circuit for Memory Array (4,208,730)
R. A. Dischert and W. J. Cosgrove System for Increasing the Sharpness in a Television Picture (4,209,801)
G. Forster Cathode Ray Tube Arc-Over Protection (4,207,493)
R. J. Giger Surge Protection of Full-Wave Rectifier by Biased Ionization Tube (4,207,603)
J. Goel Temperature Compensation Circuit (4,207,538)
I. Gorog and A. H. Firester Optical Recording with Track Drop Compensation (4,206,477)
L. A. Harwood Automatic Kinescope Bias Control Circuit (4,207,592)
L. A. Harwood Stabilized Automatic Brightness Control Network in a Video Signal Processing System Including an Automatic Kinescope Beam Current Limiter (4,209,808)
D. C. Herrmann and L. J. Bazin Low Pass Filter with Remotely Controllable Rise Time (4,206,474)
T. T. Hitch Mercury Vapor Leaching from Microelectronic Substrates (4,207,138)
N. S. Klein Mounting for Solar Cell (4,209,347)
P. A. Levine Reduction of Sparkle Noise in CCD Imagers (4,206,372)

D. L. Matthies, R. M. Mehalso, and G. Kaganowicz Metallized VideoDisc Having an Insulating Layer Thereon (4,206,256)
S. Miko and P. R. Mullis Magnetic Switching Regulator for a Deflection Circuit (4,209,731)
A. Miller Waveguide Method for Determining Stress at the Convex Surface of a Body (4,207,000)
S. V. Naimpally and T. D. Yost Combined Phase Shift and Filter Network in a Color Video Signal Processing System Employing Dynamic Flesh Tone Control (4,207.590)
E. J. Nossen Digitized Phase Modulating Means (4,206,423)
E. J. Nossen Digitized Phase Modulating Means (4,206,424)
E. J. Nossen Digitized Frequency Synthesizer (4,206,425)
L. P. Orchard Food Product Extrusion Apparatus (4,205,415)
R. P. Parker Gated Automatic Beam Current Limiter in a Video Signal Processing System (4,207,591)
W. A. Perlich Frequency Signal Splitting Circuit (4,207,532)
L. R. Rockett, Jr. CCD A-to-D Converter (4,206,446)
D. L. Ross Novel Ortho-Quinone Diazide Photoresist Sensitizers (4,207,107)
L. E. Smith Regulated Deflection Circuit (4,209,732)
F. R. Stave VideoDisc Player Having Record Side Identification Apparatus (4,206,926)
L. A. Torrington Record Side Identification Apparatus for VideoDisc Player (4,205,853)
J. W. Tuska and A. D. Robbi Impedance Measuring Circuit (4,206,648)
L. C. Upadhyayula Exclusive OR Circuit (4,207,476)
P. K. Weimer CCD with Differently Doped Substrate Regions Beneath a Common Electrode (4,206,371)
J. A. Weisbecker and P. K. Baltzer Color Display Using Auxiliary Memory for Color Information (4,206,457)
H. A. Wittlinger Current Amplifier (30,297)

AUTHORS

Liston Abbott received his engineering education at City University of New York and Brooklyn Polytechnic Institute, and has over 24 years of experience in the analysis, development, and design of communications systems. Mr. Abbott is a member of the technical staff of RCA Laboratories and is currently working on video quality and capacity improvements in satellite transmission systems. He was involved in the development of the Alaskan Bush TV program, the two-TV-channel-per-transponder system used by RCA Americom for transmission between Los Angeles and Alaska, a four-TV-channel-per-transponder demonstration system, and a two-video/five-high-quality-audio/teletext transmission system via a single transponder into small earth stations. Mr. Abbott is also involved in research and development of video and audio signal processing systems for noise reduction and security and in systems and equipment evaluations for RCA Americom.

Mr. Abbott has several patents in the field of communications systems and received an RCA Laboratories Achievement Award for the development of techniques that double the television transmission capacity of satellites.

Alfonse Acampora received his B.E.E. (magna cum laude) in 1957, and his M.E.E. on a research fellowship in 1959, from the Polytechnic Institute of Brooklyn. Following graduation, he joined the RCA Advanced Communications Laboratory in New York City, where he was engaged in the development of military communications systems. Mr. Acampora contributed in the areas of multiplexed voice/data, modem development, digital data, and signal demodulation techniques. From 1968 to 1970, Mr. Acampora was with the General Telephone and Electronics Research Laboratory in Bayside, N.Y. He headed a program to apply orthoferrite domain (bubble memory) technology to the system design of distributed logic and memory architectures. In 1970, Mr. Acampora re-joined RCA at the Global Communications facility. He received the David Sarnoff Outstanding Achievement Award in 1973 for his work in narrowband video systems. As Staff Engineer to the Vice President of Operations, Mr. Acampora had major responsibilities in the planning of high speed data and other wideband communications systems, including the utilization of international satellite systems and the inauguration of communications with the Peoples Republic of China. Since 1978, Mr. Acampora has been involved in both digital and analog signal processing systems, video bandwidth compression, and satellite technology at RCA Laboratories.

Mr. Acampora is a member of IEEE, The Society of Sigma Xi, Tau Beta Pi, and Etu Kappa Nu.

Russell R. Barton studied at Princeton University under an RCA Merit Scholarship, receiving a B.S.E.E. with honors in 1973. While an undergraduate, he studied the feasibility of electric cars powered by conventional lead-acid batteries, and conducted electric vehicle tests for ESB. He received Masters and Ph.D. degrees in Operations Research from Cornell University in 1975 and 1978, respectively. From 1975 to 1978 he worked as a consultant on operations research problems for the Departments of Justice, Transportation, Labor, and the Army. His doctoral thesis was a study of statistical failure rate techniques applied to the analysis of exoffender behavior. In 1978, he joined RCA Laboratories where he has worked on a variety of projects, including VideoDisc testing, satellite reliability analysis, organizational effectiveness, and decomposition solutions for large network problems.

Dr. Barton is a member of Eta Kappa Nu, Sigma Xi, the Operations Research Society of America, and the American Statistical Association.

Guy Ward Beakley received his B.E. degree from Vanderbilt University in 1964 and his M.S., M.Phil. and Ph.D. degrees from Yale University in 1965, 1968, and 1970, respectively. He joined the RCA David Sarnoff Research Center in Princeton, N.J., in 1969. From 1970 to 1972 he worked on problems in computer speech recognition and speaker identification. From 1973 to 1974 his major interest were probabilistic reliability and quality control. During this time, he received an RCA Laboratories Achievement Award for a team effort leading to a better understanding of systems factors affecting color television reliability. In March 1974, he presented a briefing to the U.S. and Alaskan Departments of Interior on the reliability of the communication system for the Alaskan Pipeline. In 1975, Dr. Beakley led an effort in analog and digital television transmission systems. One application of this work is transmission of television by satellite to small, inexpensive earth stations. In 1976 Dr. Beakley was appointed head of Image Processing Research in the Communications Research Laboratory, where he established a digital video processing laboratory for data compression, noise reduction, and picture compression.

Dr. Beakley joined Scientific-Atlanta, Inc. in 1977 as manager of engineering for the Satellite Communications Division. In 1978 he was appointed general manager of that Division. In 1980 he was named director of research and development for Scientific-Atlanta, Inc., a job that encompasses all divisions of the company.

Walter H. Braun received the Bachelor of Electrical Engineering degree and the Master of Engineering in Electrical Engineering from Rensselaer Polytechnic Institute, Troy, N.Y., in 1967 and 1968, respectively, and was awarded the Master of Business Administration in June of 1980 from Rutgers University. He is presently Director of Systems & Advanced Technology Engineering for RCA American Communications, Inc. Employed by RCA since December of 1972 he has been actively involved in all technical aspects of the development of RCA's Domestic Satellite Communications System. Prior to this he served on active duty with the U.S. Air Force from 1968 until his discharge with the rank of Captain in 1972 with responsibilities for development, test and procurement of tactical military communications systems.

Brian R. Dornan received a B.S. degree with honors in Electrical Engineering from Newark College of Engineering, in 1973, and an M.S. degree in Electrical Engineering at New Jersey Institute of Technology (formerly Newark College of Engineering) in 1979. Since joining RCA in 1968, Mr. Dornan has worked on microwave tubes and active solid-state microwave devices. This includes extensive work on voltage-controlled oscillators, linearizers, laser modulators, and amplifiers. Mr. Dornan is currently working on microwave FET amplifiers for use on the SATCOM satellite program.

Marvin Freeling received the B.A. degree in Physics from New York University in 1953 and an M.S. degree in Applied Physics from Harvard University in 1954. In 1954 he joined the Technical Staff at Bell Telephone Laboratories where he worked on the design and development of reflex klystrons for radio-relay systems. Mr. Freeling joined RCA in 1957, engaged in the design and development of traveling-wave tubes for electronic countermeasure systems and for communication systems. In 1963, he received the RCA Electronic Components and Devices Engineering Achievement Award for participation in the design and development of the traveling-wave tube for Relay, RCA's first communication satellite. Mr. Freeling later joined RCA Americom in 1974. He has since been engaged in communications systems studies and design for RCA's Satcom satellites. He is also responsible for technical support of RCA Americom's legal department in dealings with governmental regulatory agencies, such as the FCC. Mr. Freeling has received a U.S. Patent as the co-inventor of recirculation memory system having a diplexed feedback loop.

Allan A. Guida received the B.S. degree from the City College of New York in 1957, and the M.S. and Ph.D. degrees from the Polytechnic Institute of Brooklyn, New York, in 1961 and 1968, respectively, all in Electrical Engineering. At ITT Laboratories, where he was employed from 1957 to 1965, he worked in the Electronic Countermeasures, Avionics, and Satellite Communications Laboratories. He joined RCA Astro Electronics Division in 1967 and worked on applications of Gunn and avalanche diodes and digital magnetic recording systems. He has worked on directional couplers, the phase-locked loop, delay modulation, spectrum analyzers, and maximum likelihood estimation. In 1971, Dr. Guida received the Outstanding Achievement Award from RCA Laboratories for work done in the area of digital magnetic recording systems. Dr. Guida's most recent work (1974 to present) has been connected with the RCA satellite communications system. He has prepared numerous computer programs for satellite communications including programs to calculate link budgets, intermodulation distortion, signal-to-noise ratios for TV transmission, and optimization of transponder usage.

Carl Hubert received his B.S. in Engineering from the State University of New York at Stony Brook in 1970, and his M.S. in Space Mechanics from Cornell University in 1973. In 1975, after two additional years of graduate study, he left Cornell to join the Guidance and Control Group at RCA Astro Electronics. He completed his doctoral dissertation while employed by RCA, and he was recently awarded his Ph.D. in Space Mechanics from Cornell University. At Astro Electronics, Dr. Hubert has worked on the dynamics and control of various communications, scientific, meteorological, and military satellites. In addition to attitude maneuvers, his work has addressed problems such as appendage deployment and the control of spacecraft with flexible structures.

Dr. Hubert is a member of the American Institute of Aeronautics and Astronautics.

Ho-Chung Huang received his B.S. degree from National Taiwan University, Taiwan, Republic of China, in 1959, and his M.S. and Ph.D. degrees from Cornell University in 1965 and 1967, respectively. As a graduate student at Cornell, Dr. Huang discovered the hybrid mode of transferred-electron devices. From 1967 to 1969, he was a Senior Physicist with Monsanto Company in St. Louis, Missouri, where he was engaged in the research and development of the transferred-electron oscillators operating in the hybrid mode and LSA mode. Dr. Huang joined RCA in 1969. Since then he has been heavily engaged in the device fabrication technology, device physics, and device circuit interaction. He initiated the GaAs IMPATT program at RCA and proposed a high-low junction IMPATT structure for the improvement of dc-to-rf conversion efficiency. In parallel to the design and fabrication of GaAs IMPATTs, he was also responsible for the fabrication of Si and GaAs electron-beam semiconductor (EBS) diodes and multioctave $LiNbO_3$/spinel acoustic-delay lines. In 1975, he was a team leader responsible for the development of GaAs FETs.

Dr. Huang is presently Head of Microwave Processing Technology in the Microwave Technology Center of RCA Laboratories. He has the responsibility for the modeling and processing technology of microwave devices. Dr. Huang is a member of IEEE.

Krishnamurthy Jonnalagadda received his B.Sc. in Physics from the Osmania University, India, in 1963; his B.E. (1967) and M.E. (1969) in Power Systems from the Indian Institute of Science, Bangalore, India; and his Ph.D. (1972) from the Clarkson College in the area of Statistical Theory of Communication. He taught at the Indian Institute of Science and Clarkson College in the years 1973–1978, where he also conducted research in the areas of interference in digital communications, digital filters, and information theory. He joined RCA Laboratories, Princeton, N.J., in 1978. His areas of work include voice and video communication through satellites and signal processing in the VideoDisc system.

Dr. Jonnalagadda is a member of Eta Kappa Nu, IEEE, and Sigma Xi.

Gerald S. Kaplan received his B.S.E.E. from City College, New York, N.Y., in 1962, and his M.S.E.E. from Princeton University, Princeton, N.J., in 1964. As a member of the Advanced Technology Group at RCA Americom, Mr. Kaplan has investigated various techniques to improve the utilization of RCA Americom's communications resources (both satellite and terrestrial). These investigations encompassed areas including analog, digital, video, audio, fiber optics, compandors, TDMA and broadcast technology. He has interfaced with technology and business planning groups and has served to guide and coordinate the efforts of RCA Americom and RCA Laboratories on collaborative projects involving advanced microwave and satellite communication systems. Mr. Kaplan had responsibility for the installation and demonstration of a new transmission technique that allows a doubling of the video transmission capability for terrestrial microwave systems and participated in and guided the development effort for this program. Prior to joining RCA Americom, Mr. Kaplan at RCA Laboratories investigated various problems in electromagnetic and communication theory. Some projects included the acquisition and analysis of X band and 1 GHz propagation data in urban environments; studies of the effects of atmospheric phenomona, including rain, on satellite-earth X-band communication links; and the study of point-to-point microwave and millimeter wave communication systems. Mr. Kaplan was a major contributor to the design of an electronic-signpost

automatic-vehicle-monitoring (AVM) system for the location and tracking of motor vehicles in urban areas and has also worked in the field of automotive collision avoidance radars.

Mr. Kaplan is a member of Eta Kappa Nu and Tau Beta Pi.

Kevin Kelly received his B.S.E.E. from Villanova University in 1976. In August of 1976 he joined RCA Laboratories in Princeton, N.J. Since then he has worked in the Communication Systems Research Laboratory on techniques for increasing the video transmission capacity of both satellite and terrestrial microwave links.

Richard J. Klensch received the B.S.E.E. degree from the University of Illinois in 1951. He did graduate work in the Electrical Engineering Department of Princeton University from 1952 to 1958. Mr. Klensch joined RCA Laboratories in 1952 and performed research in the areas of high-resolution radar systems and infrared detection devices. From 1954 to 1956, he served in the U.S. Army as a radar instructor, returning to the RCA Laboratories in 1956. Subsequently, he did research in the areas of microwave scanning antennas, time division multiplex systems, digital and analog communications, and color television. In 1961, he participated in research leading to an advanced Naval Communications System, continuing this effort until 1966. From 1966 until 1971, he did research in new electronic half-tone generation techniques and CRT display systems. This was followed by two years of research leading to the development and demonstration of a Harmonic Radar Automobile Collision Avoidance System. During this period a Microwave Automatic Vehicle-Identification System was also developed and demonstrated. From late 1973 to early 1975, Mr. Klensch was involved in color television systems research. Since then he has been doing research in satellite and terrestrial audio and video communications techniques. In 1975 he received an RCA Laboratories Achievement Award. He is a member of Sigma Xi and a senior member of the IEEE.

Visvaldis Mangulis received the B.S. degree in Physics from Brooklyn College in 1956 and the M.S. degree in Physics from New York University in 1958. In 1956 he joined TRG, Inc., which later became a division of Control Data Corp. As Head of the Applied Mathematics Section he developed radiation theory for the largest surface ship sonar array ever attempted (the conformal/planar array). From 1968 to 1970 he worked as a Senior Staff Consultant for Computer Applications, Inc. In 1970 he became one of the founders of Questek, Inc. As Vice-President he participated in the design and execution of an extensive simulation experiment to evaluate the effects of human factors on the ability of pilots to detect approaching aircraft with the aid of a Pilot Warning Instrument. The statistical analysis of the experiment consisted of one of the largest factorial designs ever done. He joined RCA in 1975 at the Missile and Surface Radar Division, Moorestown, N.J. He developed a theory of the effects of obstructions on the performance of a radar system. In 1978 he transferred to the RCA Laboratories in Princeton, N.J., where he has been engaged in research on radar and communications.

Mr. Mangulis is the author or the *Handbook of Series for Scientists and Engineers*. He is a member of IEEE, the American Physical Society, the Acoustical Society of America, and Phi Beta Kappa. He is listed in American Men and Women of Science and in Who's Who in the East.

Paul F. Pelka graduated from RCA Institutes in 1956 with a diploma in Electronic Technology. He joined RCA that same year in the Microwave Device and Technology Group in Harrison, N.J., where he worked on various development programs including traveling-wave tubes and backward-wave, tunnel-diode, and transferred-electron oscillators. In 1966 he was promoted to Supervisor and was in charge of a production group to build frequency multipliers for the Apollo program. In 1969 he helped establish a Solid State Technology Center in Harrison. He also worked with materials and processes to develop hyperabrupt and transferred-electron diodes by the use of GaAs. In 1975 Mr. Pelka was transferred to RCA Laboratories in Princeton, N.J., where he worked on processing and packaging hyperabrupt, transferred-electron diodes and GaAs-FETs.

In 1979 he was promoted to Associate Member of Technical Staff. He is currently responsible for diode pilot production and thin-film technology within the Microwave Technology Center.

William T. Rowse attended Plymouth College, England, where he was awarded Intermediate City and Guilds of London Certificate in Telecommunications in 1958. He completed his studies and graduated from Cheltenham College, England, being awarded the Final City and Guilds of London Certificate in Telecommunications in 1965. After serving in the Royal Air Force and the Ministry of Defence (Air), London, from 1958 to 1971, he joined Cable and Wireless, Ltd., London, where he worked on the installation of the Barbados Satellite Earth Station. He subsequently joined RCA Global Communications, working on the installation of RCA's first earth stations at Valley Forge, Point Reyes, Los Angeles, and Thule, Greenland. He later became a senior member of the engineering staff responsible for the design and installation of the RCA cable TV transmission system at Valley Forge and Leader, Implementation Engineering, responsible for the design and installation of Government Digital earth stations. He joined RCA Americom in 1976, as Program Manager, Tiros-N. In his present position as Manager, Technical Programs, Government Services, Mr. Rowse is responsible for technical sufficiency of government programs and provides technical support to Government Marketing.

Gary J. Saulnier received a B.S.E.E. (summa cum laude) from Rensselaer Polytechnic Institute in 1980, winning the J. Erik Jonsson Award for the highest academic average in his class. During the summer of 1978, he joined RCA Laboratories as a co-op student, working on the development of low-power-consumption deflection circuitry. The summers of 1979 and 1980 he spent with the Transmission Technology Group, contributing to the development and implementation of systems for 2-for-1 satellite video. Mr. Saulnier is continuing his studies at R.P.I. in the fall of 1980 funded by a Rensselaer Scholar Fellowship.

He is a member of IEEE and Eta Kappa Nu Societies.

Leonard Schiff received the B.S.E.E. degree, magna cum laude, from City College of New York in 1960, the M.S.E.E. degree from New York University in 1962, and the Ph.D. degree in Electrical Engineering from the Polytechnic Institute of Brooklyn, New York, in 1968. From 1960 to 1967 he was employed by Bell Laboratories. There he participated in the development of the #1 ESS Switching System, including device development of the "ferreed" cross-point, design of the central processor, and support of Western Electric personnel in placing the system on-line. Dr. Schiff later contributed to the design of the experimental #1 ESS-ADF, a large store-and-forward message switch. His work was largely concerned with the design, analysis, and construction of the basic software architecture. On joining RCA Laboratories in 1967, Dr. Schiff worked on the analysis of a variety of communications systems, both analog and digital, and on traffic and queueing systems. Many of these projects were in support of cellular mobile radio systems, especially techniques for making these systems more spectrally efficient and more efficient in their traffic-carrying capacity. His work on both mobile radio systems and automatic vehicle location systems has military as well as commercial applications.

Dr. Schiff is presently Head of the Communications Analysis Research group. His recent work has been in support of the development and operation of various satellite communications systems. He has been devising cost-effective methods of terrestrial interconnect and tradeoff studies for various methods of multiple access to the satellite. Dr. Schiff is a member of Eta Kappa Nu, Tau Beta Pi, Sigma Xi, and IEEE.

Walter Slusark received the B.A. and B.S. degrees in Electrical Engineering from Rutgers University in 1969. He received the M.S. and Ph.D. degrees from Rutgers in 1972 and 1976, respectively. Supported by the National Science Foundation, he investigated the optical and structural properties of thin Au-Cr films for his Master's thesis. His Ph.D. thesis dealt with the dielectric, transport, and switching properties of the transition metal oxide Nb_2O_5. Dr. Slusark joined the ITT Electro-Physics Laboratory in 1976 and engaged in the research and development of charge-coupled devices and their application to analog signal processing. In 1977, Dr. Slusark joined RCA Laboratories where he has been concerned with GaAs-FET fabrication technology and its influence on device reliability. He is also responsible for a program of accelerated stress testing and failure analysis of GaAs-FET devices at the Microwave Technology Center.

Dr. Slusark is a member of IEEE, AVS, and Sigma Xi.

Dr. Harold Staras has had over 30 years of professional experience in research and development in areas relating to propagation, antennas, and telecommunications. He played an instrumental role in the development of troposcatter in the 1950s. In the 60s, he directed a group that developed a total-system concept for a complex, computer driven, spectrum efficient mobile radio system which included a subsystem for locating and tracking vehicles as they moved through heavily built up urban areas.

At present, Dr. Staras is a Staff Scientist involved in satellite communication studies at both C-Band and K-Band in support of RCA's communications satellite programs. He has performed communication traffic analysis for satellite links, assessed the relative performance of different modulation techniques for different types of traffic (voice, hi-fi, data, TV) and carried out cost-benefit analyses involving tradeoffs between earth station costs (and performance) and satellite traffic capacity. Recent studies included electronic mail service, adaptive satellite antenna arrays and time com-

pression of color information on video signals in order to improve the SNR in TV transmission.

Dr. Staras has numerous publications to his name and is the co-inventor on two issued patents. During 1961–62, he was a Guggenheim Fellow and visiting professor at the Technion-Israel Institute of Technology. He is also a member of several study groups of the CCIR and URSI and has served on several government-industry advisory committees. On several occasions, he was a U.S. delegate to international meetings of these bodies.

Herbert J. Wolkstein joined RCA Microwave Operations in 1955 after seven years as Project Engineer in the Research Laboratories of National Union Electric Corporation where he worked on the design of special-purpose beam-deflection and high-speed computer-switching tubes. In 1958, he became Engineering Leader and in 1961, Manager, TWT Design and Development. In 1964, as Manager of Microwave Advanced Product Development, Mr. Wolkstein directed a group in advanced development and applications work on TWTs and solid-state devices. In 1972, he was named Manager of the Advanced Programs and Application Engineering Group. He held that position until 1975, when he joined the Microwave Technology Center, RCA Laboratories, Princeton, N.J. In his present position of Manager, Space and Countermeasure Programs, Mr. Wolkstein is engaged in the development and applications of solid-state microwave devices and subsystems.

Mr. Wolkstein has been awarded ten patents in the electron-tube and solid-state fields. He is a member of IEEE's Professional Group on Electron Devices and Professional Group on Microwave Theory and Techniques.

You-Sun Wu received his B.S. degree from National Taiwan University, Taiwan, Republic of China, in 1967 and his M.S. and D.Sc. degrees from Washington University, St. Louis, MO, in 1970 and 1972, respectively. As a graduate student, he studied Gunn-effect oscillator and ferrite devices such as phase-shifters, circulators, and isolators. From 1972 to 1973, he was a Research Associate at Cornell University, working on very broadband impedance matching networks. From 1973 to 1979, he was with the Central Research Laboratory of Texas Instruments, Dallas, Tex., where he engaged in the research and development of high-power silicon bipolar transistors. He helped develop a silicon bipolar transistor which by the use of electron-beam lithography achieved a 2-W output power at 10 GHz. A high-power X-band bipolar transistor amplifier and VCO were developed.

Since 1979, Dr. Wu has been with RCA Laboratories, Princeton, N.J., working on the 4-GHz, 8.5-W SATCOM FET amplifier design. He is also working on high-power FET device modeling as well as fabrication. Dr. Wu is a member of IEEE.